



Número: 299/2003  
UNIVERSIDADE ESTADUAL DE CAMPINAS

INSTITUTO DE GEOCIÊNCIAS

PÓS-GRADUAÇÃO EM CIÊNCIAS  
ÁREA DE METALOGÊNESE

FERNANDO HENRIQUE BUCCO TALLARICO

O CINTURÃO CUPRO-AURÍFERO DE CARAJÁS, BRASIL

Tese apresentada ao Instituto de Geociências como parte dos requisitos para obtenção do título de Doutor em Ciências, área de Metalogênese.

Orientador: Prof. Dr. Bernardino Ribeiro de Figueiredo

Este exemplar corresponde à redação final da tese defendida por Fernando Henrique Bucco Tallarico e aprovada pelo Comitê de Julgamento em 29/08/2003

B. Figueiredo  
ORIENTADOR

200334563

CAMPINAS - SÃO PAULO

Agosto - 2003

UNIDADE	<i>PL</i>
Nº CHAMADA	T144c
V	EX
TOMBO	BC/56540
PROC.	16124/03
C	<input type="checkbox"/>
D	<input checked="" type="checkbox"/>
PREÇO	28,00
DATA	12/11/03
Nº CPD	

FICHA CATALOGRÁFICA ELABORADA PELA  
BIBLIOTECA DO IG - UNICAMP

CR00192031-1

550 0 305288

Tallarico, Fernando Henrique Bucco  
T144c      O cinturão cupro-aurífero de Carajás, Brasil / Fernando Henrique  
                Bucco Tallarico.- Campinas,SP.: [s.n.], 2003.

Orientador: Bernardino Ribeiro de Figueiredo  
Tese (doutorado), Universidade Estadual de Campinas, Instituto de  
Geociências.

1. Geologia econômica – Carajás, Serra dos (PA). 2. Minas e  
recursos minerais – Carajás, Serra dos (PA). I. Figueiredo Bernardino  
Ribeiro de. II. Universidade Estadual de Campinas, Instituto de  
Geociências. III. Título.



UNIVERSIDADE ESTADUAL DE CAMPINAS  
INSTITUTO DE GEOCIÊNCIAS  
PÓS-GRADUAÇÃO EM GEOCIÊNCIAS  
ÁREA DE METALOGÊNESE

AUTOR: FERNANDO HENRIQUE BUCCO TALLARICO

ORIENTADOR: Prof. Dr. Bernardino Ribeiro de Figueiredo

Aprovada em: 29/08/2003

**EXAMINADORES:**

**Prof. Dr. Bernardino Ribeiro de Figueiredo**

**Prof. Dr. Alfonso Schrank**

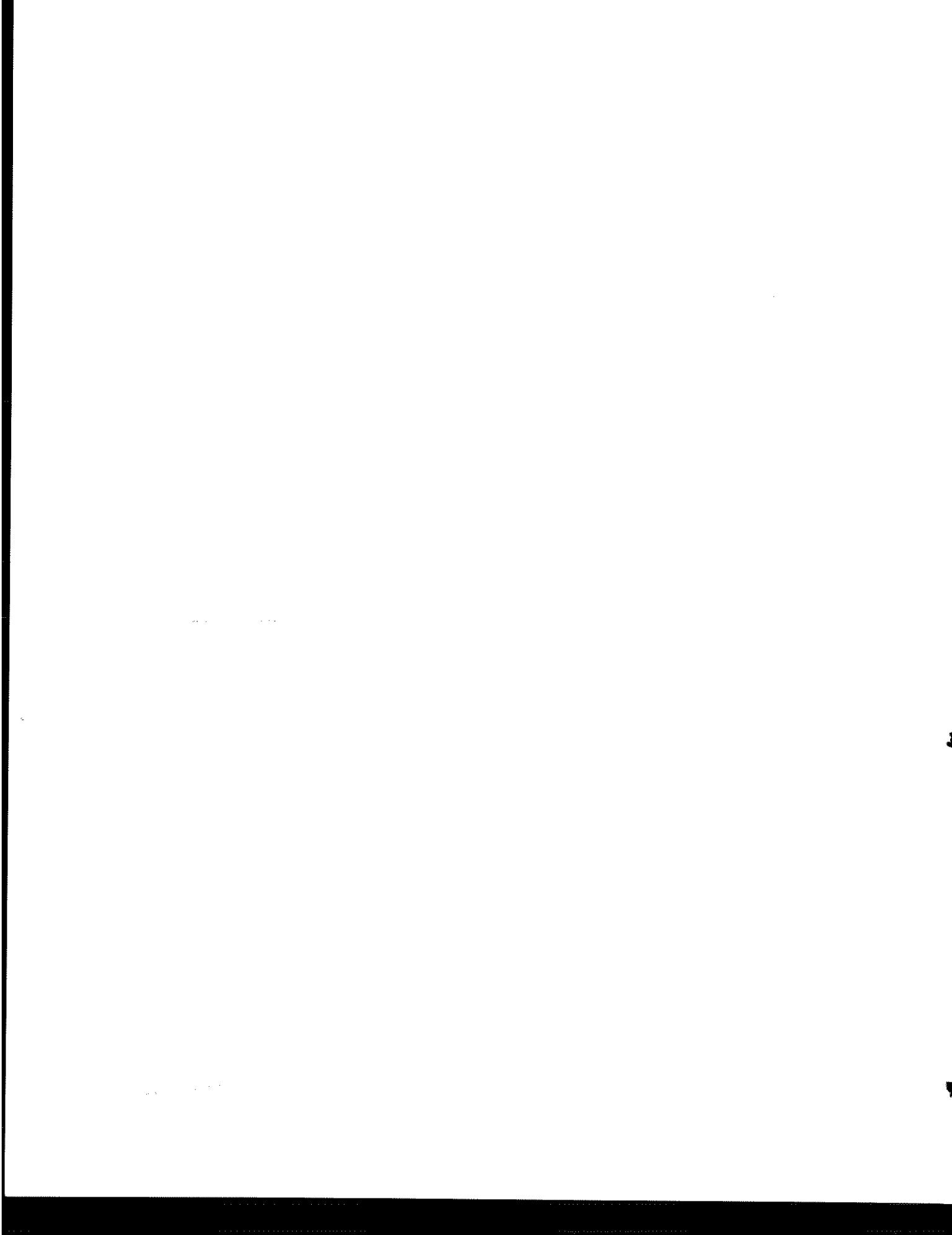
**Prof. Dr. Carlos Roberto de Souza Filho**

**Prof. Dr. Marcel Auguste Dardenne**

**Prof. Dr. Jean Michel Lafon**

Bernardino Ribeiro de Figueiredo - Presidente  
Alfonso Schrank  
Carlos Roberto de Souza Filho  
Marcel Auguste Dardenne  
Jean Michel Lafon

Campinas, 29 de agosto de 2003





**UNICAMP**

**UNIVERSIDADE ESTADUAL DE CAMPINAS/  
INSTITUTO DE GEOCIÊNCIAS**

**PÓS-GRADUAÇÃO EM GEOCIÊNCIAS  
ÁREA DE METALOGÊNESE**

## **O CINTURÃO CUPRO-AURÍFERO DE CARAJÁS, BRASIL**

### **RESUMO**

### **TESE DE DOUTORADO**

**Fernando Henrique Bucco Tallarico**

A presente tese trata da geologia, caracterização de minérios e geocronologia U-Pb SHRIMP dos depósitos cupro-auríferos de Igarapé Bahia, Breves e Cento e Dezoito, e ainda da geologia e metalogênese do depósito de Au-Pd-Pt de Serra Pelada. Os resultados mostram que ocorreram no Cinturão Cupro-Aurífero de Carajás ao menos dois eventos metalogenéticos distintos, um no Neoarqueano (~2,57 Ga) representado pelo depósito de Fe-óxido Cu-Au-(U-ETR) de Igarapé Bahia e outro no Paleoproterozóico (~1,88 Ga) tipificado pelo depósito de Cu-Au-(W-Bi-Sn) de Breves. Os resultados do depósito Cento e Dezoito sugerem que este seja um depósito híbrido derivado da superposição de eventos neoarqueanos e paleoproterozóicos. A excepcional vocação metalogenética da região inicia-se no Arqueano com o desenvolvimento de um rift continental onde se deu a acumulação de ferro, e possivelmente cobre, singenético. Neste ambiente ocorreu também a formação de depósitos de Pt-Pd associados a complexos máficos-ultramáficos. A precoce cratonização da região e sua complexa história tectônica, que registra múltiplos eventos de transtensão associados a magmatismo, permitiram a formação ainda no Neoarqueano de depósitos do tipo Fe-óxido Cu-Au-(U-ETR). Durante o Paleoproterozóico a região experimentou um novo episódio transtensional que permitiu o alojamento de diversos granitos do tipo-A, aos quais se associam os depósitos do tipo Cu-Au-(W-Bi-Sn). Desta justaposição de eventos resulta um quadro metalogenético complexo que inclui uma diversidade de depósitos minerais, alguns dos quais exóticos. Um exemplo é o depósito Serra Pelada que representa um caso único na região de mineralização de Au-Pd-Pt alojada em rochas meta-sedimentares.





UNIVERSIDADE ESTADUAL DE CAMPINAS/  
INSTITUTO DE GEOCIÊNCIAS

PÓS-GRADUAÇÃO EM GEOCIÊNCIAS  
ÁREA DE METALOGÊNESE

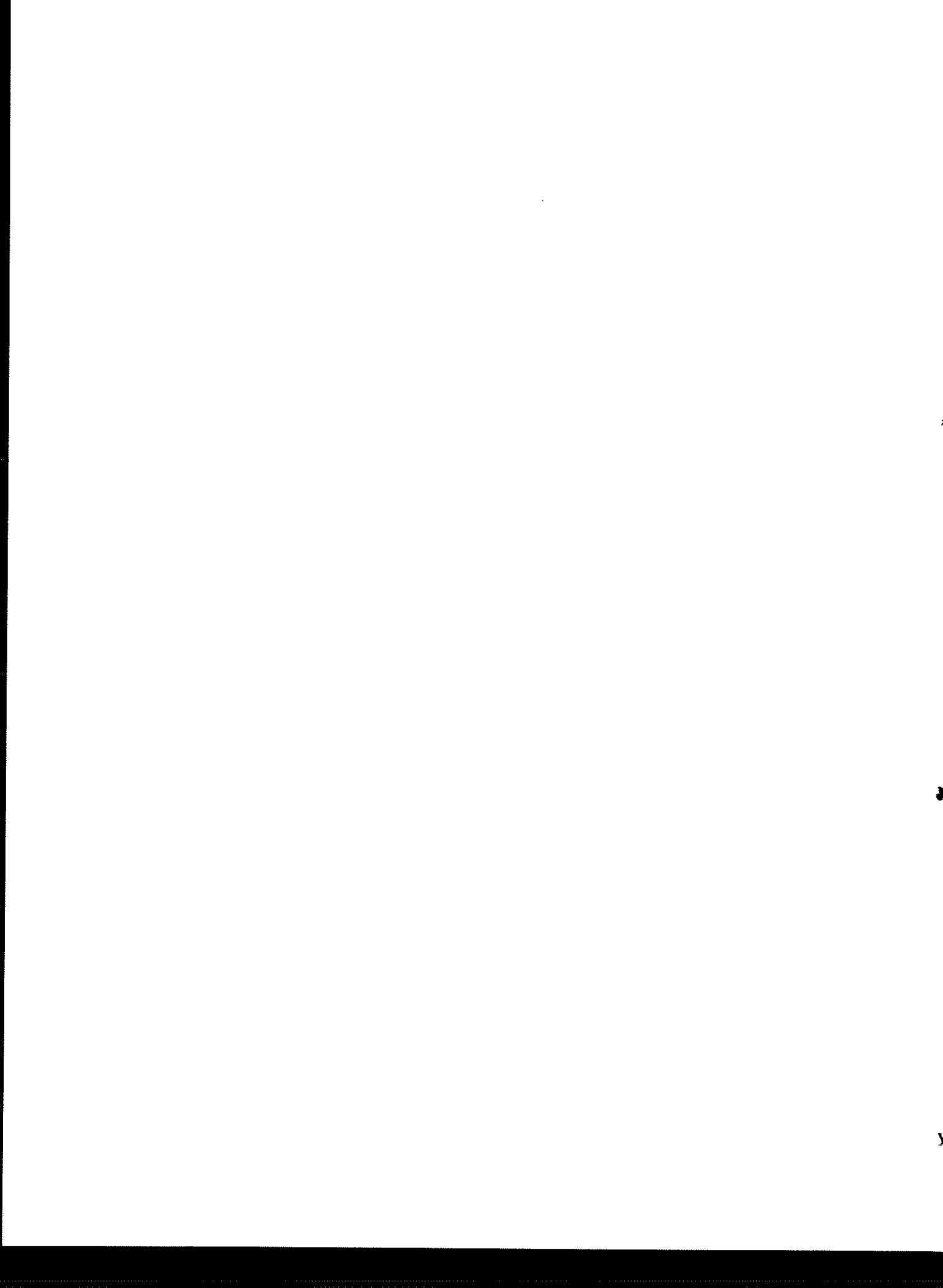
## THE CARAJÁS COPPER-GOLD BELT, BRAZIL

### ABSTRACT

### Ph.D. THESIS

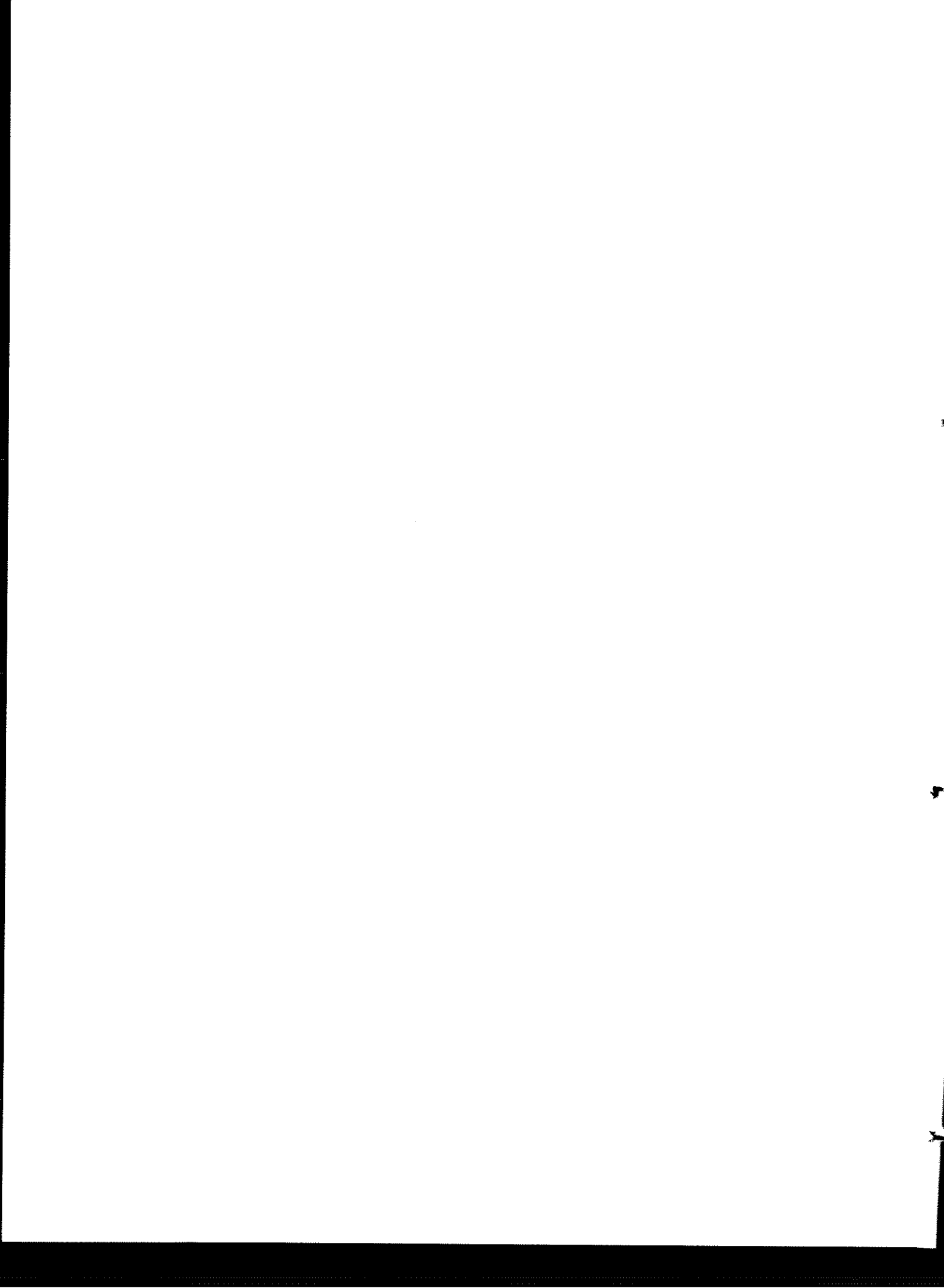
**Fernando Henrique Bucco Tallarico**

This research addresses the geology, ore assemblages and SHRIMP U-Pb geochronology of the Igarapé Bahia, Breves and Cento e Dezoito copper-gold deposits, and the geology and metallogenesis of the Serra Pelada Au-Pd-Pt deposit. The data indicate that two temporally distinct metallogenetic events occurred in the Carajás Copper-Gold Belt, one Neoarchean (~2.57 Ga) represented by the Igarapé Bahia Fe-oxide Cu-Au-(U-REE) deposit, and other Paleoproterozoic (~1.88 Ga) represented by the Breves Cu-Au-(W-Bi-Sn) deposit. The results suggest that Cento e Dezoito is possibly a hybrid deposit resulting from the interplay of Neoarchean and Paleoproterozoic ore forming processes. The metallogenesis of the belt initiates in the Archean with the development of a continental rift where syngenetic iron, and possibly copper, were accumulated. This environment also favored the formation of Pt-Pd deposits associated with layered mafic-ultramafic intrusions. The early cratonization and the complex tectonic history of the Carajás Copper-Gold Belt, that includes multiple transtensional events, allowed the formation of Fe-oxide Cu-Au-(U-REE) during the Neoarchean. During the Paleoproterozoic the belt underwent other transtensional episode that favored the ascent of several A-type granites to which Cu-Au-(W-Bi-Sn) deposits are associated. The juxtaposition of these distinct metallogenetic events resulted in a complex scenario that includes a variety of ore deposits some of which exotic, as for example the Serra Pelada Au-Pd-Pt deposit, a unique case of Au-Pd-Pt deposit hosted by meta-sedimentary rocks.



“Where an ore deposit has been found, it can be expected to find others of similar type under analogous conditions, because most ore deposits tend to occur gregariously”

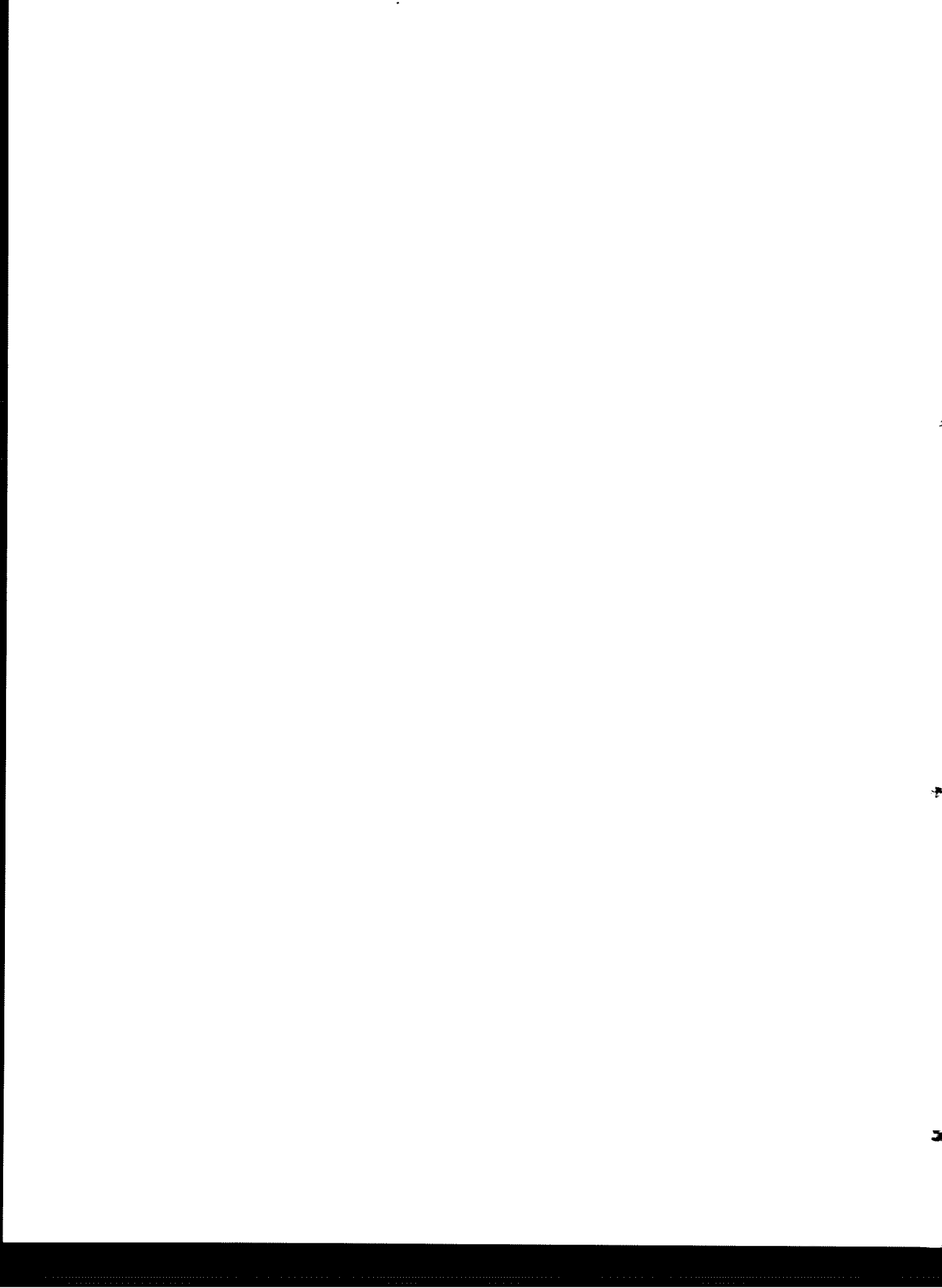
Cotta (1859)



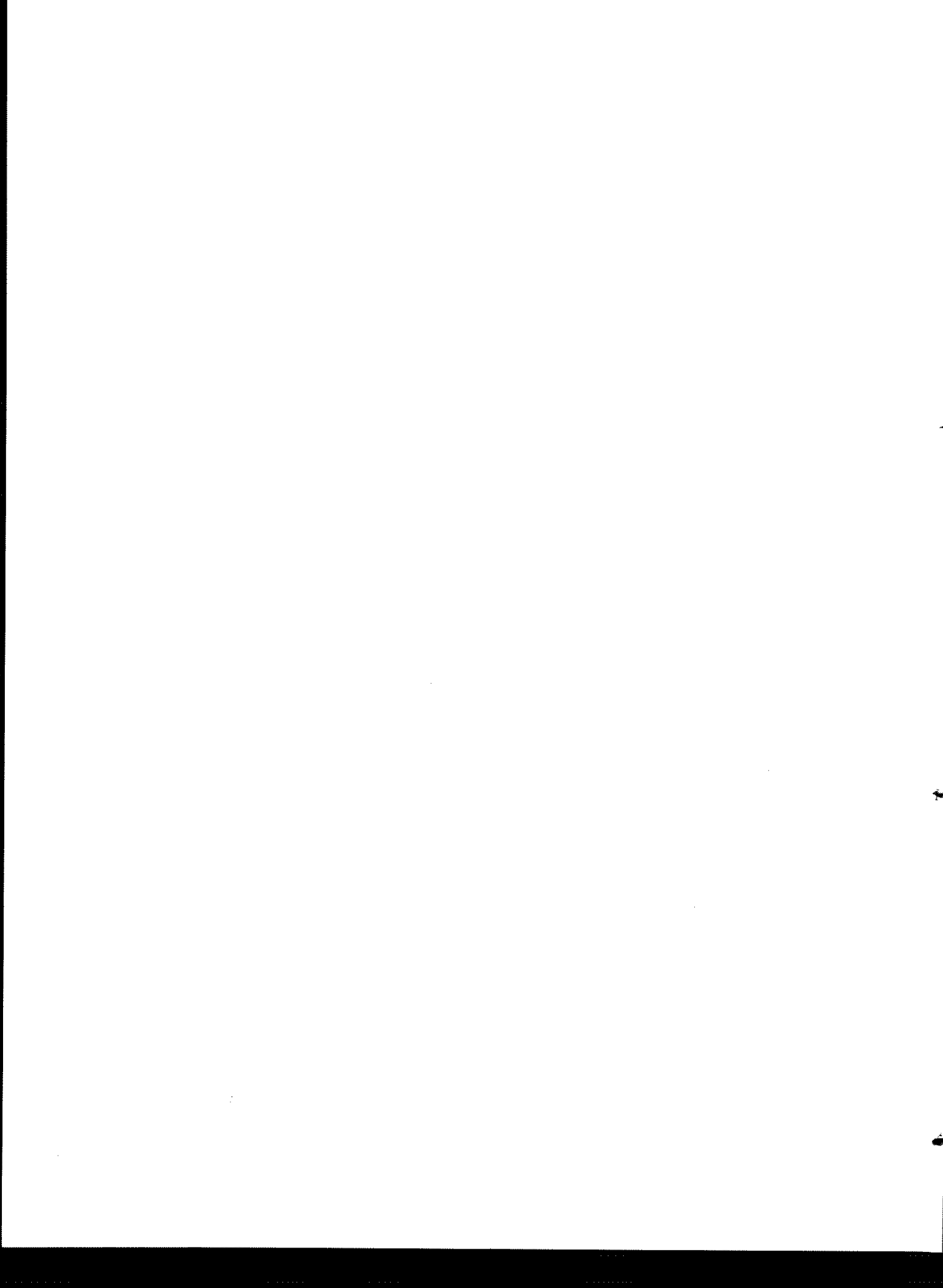
## Agradecimentos

Extero meus sinceros agradecimentos a todas as pessoas e instituições que direta ou indiretamente tornaram possível a realização desta pesquisa. Expresso especiais votos de agradecimentos para:

- O meu orientador Prof. Bernardino R. Figueiredo pelo excepcional apoio e motivação durante a pesquisa.
- A todo o *staff* do Instituto de Geociências da UNICAMP pelo constante apoio no decorrer da pesquisa.
- A Companhia Vale do Rio Doce (CVRD) e a Rio Doce Mineração e Geologia (DOCEGEO) pelo acesso aos depósitos estudados e a dados de sua propriedade, bem como pelo suporte durante os trabalhos de campo e laboratório.
- Os geólogos José Luzimar Rego e Alfredo Rossetto Nunes pelo apoio durante a pesquisa dos depósitos de Breves e Igarapé Bahia.
- O geólogo Marcelo Andrade Cavalcanti de Albuquerque pelo apoio durante a pesquisa do depósito Cento e Dezoito.
- Os geólogos Carlos Henrique Cravo Costa e Cláudio Rodrigues Coimbra pelo suporte durante os trabalhos no depósito de Serra Pelada.
- A Dra. Jéssica Beatriz Carvalho Tallarico pelo suporte durante os trabalhos de microssonda eletrônica, difração de raios-X e microscopia ótica e eletrônica nos laboratórios do Centro de Desenvolvimento Mineral da CVRD.
- O Centro de Desenvolvimento de Tecnologia Nuclear, e em particular ao geólogo Walter de Brito, pelo apoio logístico e acesso ao laboratório de separação de minerais.
- Aos Professores Dr. Colombo Celso Gaeta Tassinari e Dra. Marly Babisnki pelo importante apoio durante os trabalhos de concentração de minerais e análises isotópicas dos sistemas Sr-Sr e Pb-Pb no Centro de Pesquisas Geocronológicas da Universidade de São Paulo.
- O Prof. Maurício Carneiro pelo suporte durante a preparação de amostras na Universidade Federal de Ouro Preto.



- O Dr. Neal J. McNaughton e Dr. Ian R. Fletcher do Centre for Global Metallogeny (CGM) da Universidade de Western Australia (UWA) pela orientação e suporte durante as análises isotópicas pelo método SHRIMP.
- O Prof. David I. Groves pelo apoio e orientação durante o estágio no CGM/UWA e posterior confecção de artigos.
- A Sra. Marion Marshall do Departamento de Geologia e Geofísica da UWA pelo apoio durante a preparação de amostras para geocronologia SHRIMP.
- O Prof. Brendan J. Griffin e a Sra. Sharon Platten do Centre for Microscopy and Microanalysis da UWA pelo apoio e orientação durante a etapa de microscopia eletrônica.
- A Fundação de Amparo a Pesquisa do Estado de São Paulo (FAPESP) pela bolsa de doutorado #98/14401-5.
- Ao Prof. Dr. Roberto Perez Xavier e a geóloga Ana Maria Dreher, membros do projeto “Evolução e origem de fluidos e metais no depósito de Cu-Au de Igarapé Bahia, Província Mineral de Carajás, PA: implicações para o modelo genético (Processo FAPESP #99/03058-0), pelo suporte financeiro e também pelas importantes discussões metalogenéticas.
- A Society of Economic Geologists Foundation pelo apoio financeiro através da Hugh E. McKinstry Grant no ano de 2000.
- Aos Professores Dr. Alfonso Schrank, Dr. Carlos Roberto de Souza e Dr. Marcel Auguste Dardenne pelas importantes observações feitas no exame de qualificação que resultaram numa melhora significativa do manuscrito inicial da tese.
- Aos editores e revisores da Revista Brasileira de Geologia, Mineralium Deposita e Economic Geology pelas críticas e sugestões que em muito contribuíram para a melhoria dos artigos referentes a esta tese.



## Índice

1. Introdução.....	1
2. Geologia regional e depósitos minerais associados.....	1
3. Materiais e métodos.....	7
4. Resultados.....	8
5. Modelo metalogenético regional.....	13
6. Referências.....	24

**ANEXO 1 – O método SHRIMP**

**ANEXO 2 – The Igarapé Bahia Cu-Au mineralization, Carajás Province.**

**ANEXO 3 – The occurrence of ilvaite in the Igarapé Bahia Cu-Au deposit, Carajás Province, Brazil.**

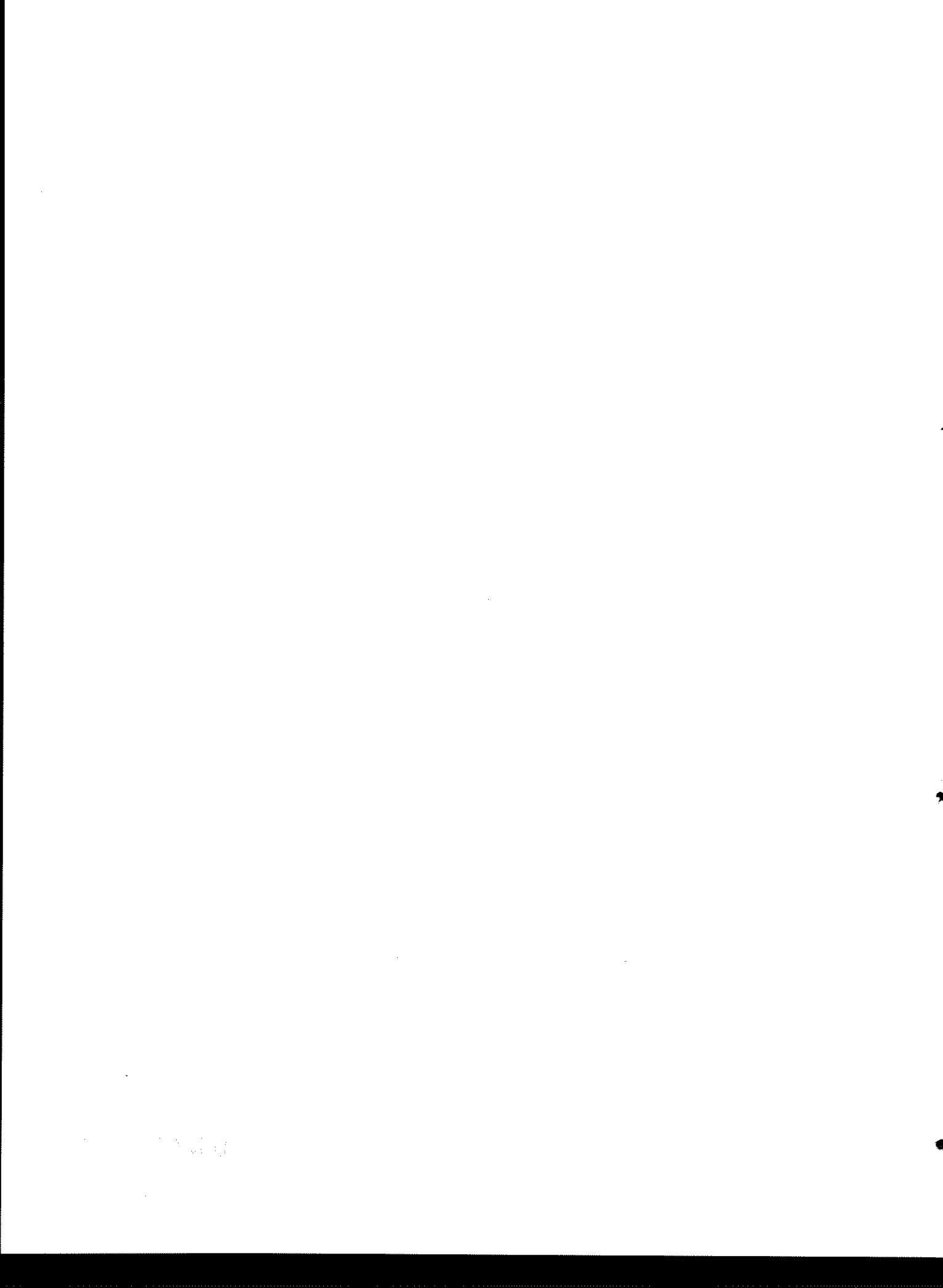
**ANEXO 4 – Geology and SHRIMP geochronology of the Igarapé Bahia Fe-oxide Cu-Au-(U-REE) mineralisation, Carajás copper-gold belt, Brazil: an Archean (2.57 Ga) Olympic Dam-Type deposit.**

**ANEXO 5 – Geological and SHRIMP II U-Pb constraints on the age and origin of the Breves Cu-Au-(W-Bi-Sn) deposit, Carajás, Brazil.**

**ANEXO 6 – Geologia e geocronologia SHRIMP II do depósito de Cu-Au Cento e Dezoito, Carajás, Brasil**

**ANEXO 7 – Report to the Society of Economic Geologists Foundation, Inc., Hugh E. McKinstry Grant for year 2000 - Pb-Pb Isotopic Results.**

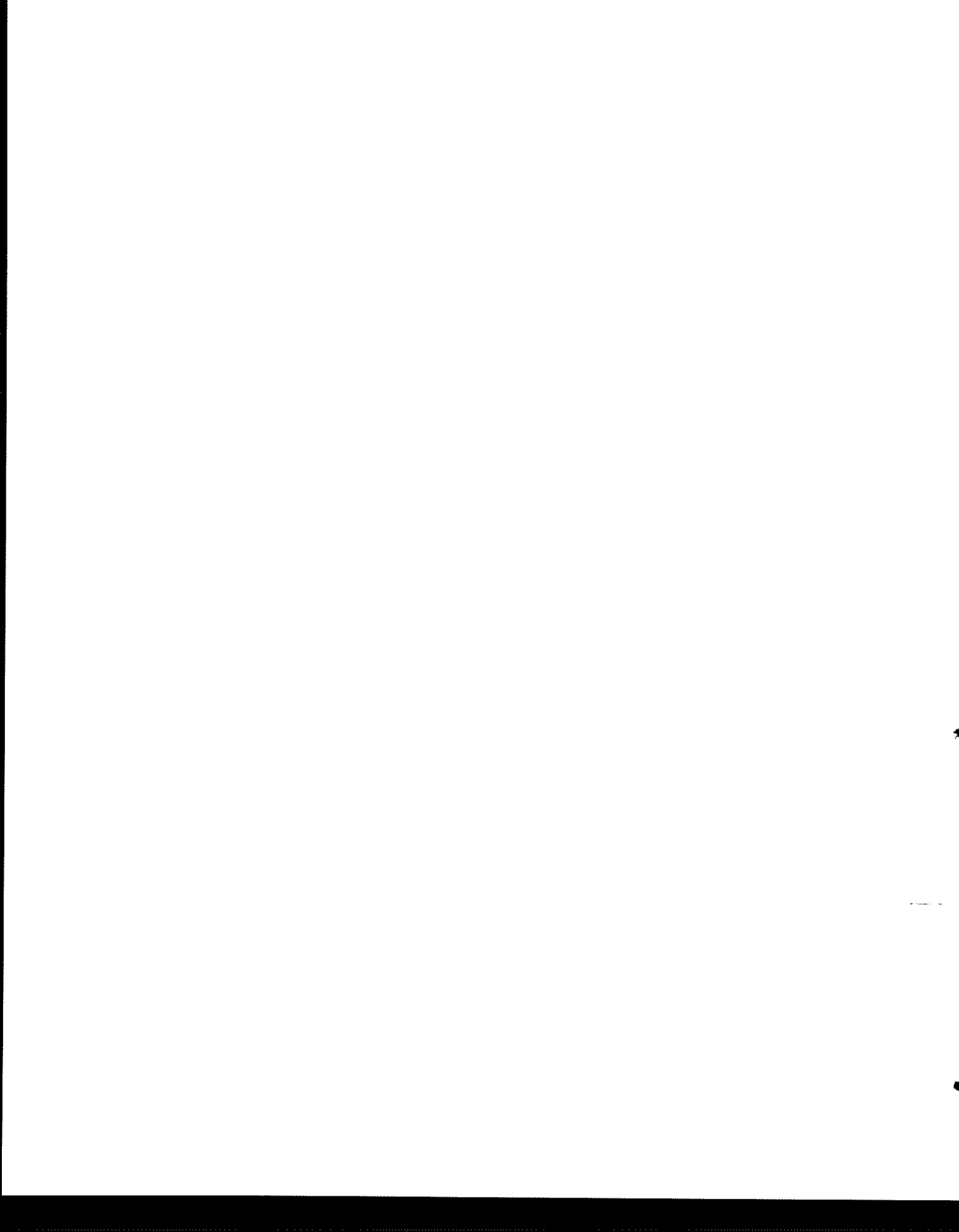
**ANEXO 8 – The Serra Leste sediment-hosted Au-(Pd-Pt) mineralization, Carajás Province**



## **Lista de Figuras**

**Figura 1.** Mapa geológico simplificado do Cinturão Cupro-Aurífero de Carajás mostrando a distribuição dos principais depósitos do tipo Fe-óxido Cu-Au-(U-ETR) e Cu-Au-(W-Bi-Sn). Encontram-se também representados os depósitos gigantes de ferro, o depósito de Au-Pd-Pt de Serra Pelada e o depósito de Pd-Pt de Luanga.

**Figura 2.** Síntese metalogenética regional do Cinturão Cupro-Aurífero de Carajás, relacionando o controle estrutural na ascensão de magmas e formação dos depósitos de Fe-óxido Cu-Au-(U-ETR) neoarqueanos e Cu-Au-(W-Bi-Sn) paleoproterozóicos. Encontram-se também representados os depósitos gigantes de ferro, o depósito de Pt-Pd de Luanga e o depósito de Au-Pd-Pt de Serra Pelada para ilustrar o conceito de permanência de metais no cinturão.



## **Lista de Tabelas**

**Tabela 1.** Resumo das idades  $^{207}\text{Pb}/^{206}\text{Pb}$ , pelo método SHRIMP, do depósito de Cu-Au-(U-ETR) de Igarapé Bahia.

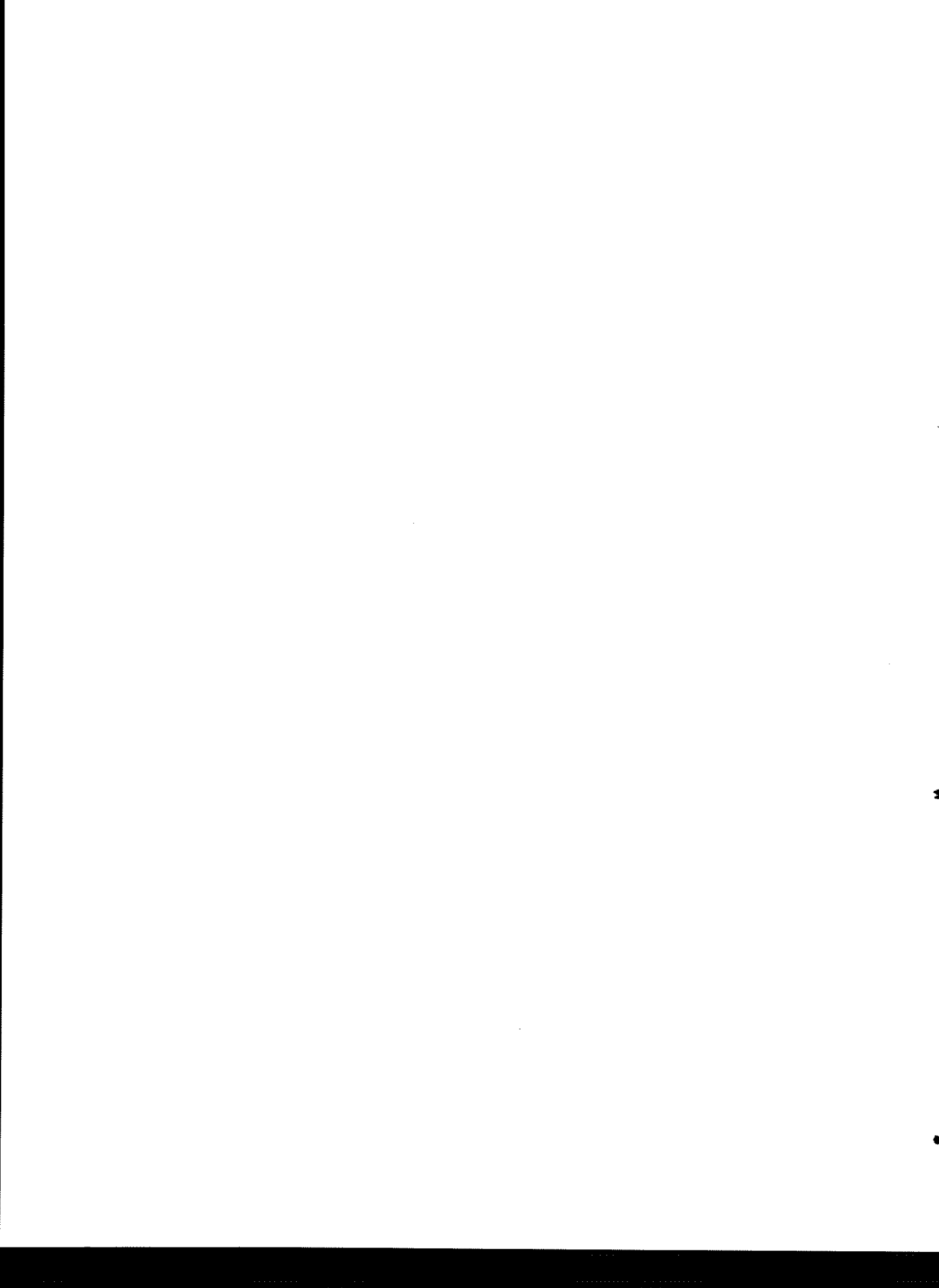
**Tabela 2.** Resumo das idades  $^{207}\text{Pb}/^{206}\text{Pb}$ , pelo método SHRIMP, do depósito de Cu-Au-(W-Bi-Sn) de Breves.

**Tabela 3.** Resumo das idades  $^{207}\text{Pb}/^{206}\text{Pb}$ , pelo método SHRIMP, do depósito de Cu-(Au) Cento e Dezoito.

**Tabela 4.** Quadro comparativo das alterações hidrotermais e paragêneses de minério dos depósitos de Cu-Au de Salobo, Igarapé Bahia, Cento e Dezoito, Águas Claras e Breves.

**Tabela 5.** Resumo dos dados geocronológicos relacionados ao evento magmático-hidrotermal neoarqueano (~2,57 Ga) no Cinturão Cupro-Aurífero de Carajás.

**Tabela 6.** Resumo dos principais atributos geológicos dos depósitos do tipo Fe-óxido Cu-Au-(U-ETR) e Cu-Au-(W-Bi-Sn) do Cinturão Cupro-Aurífero de Carajás.



## **1. Introdução**

A Província Mineral de Carajás, localizada no sul do estado do Pará (Fig. 1), é um dos mais promissores distritos minerais da atualidade, motivo pelo qual vem recebendo, desde a última década, investimentos maciços das principais empresas de exploração mineral do mundo.

A presente tese de doutorado trata da geologia, caracterização de minérios e geocronologia U-Pb SHRIMP II de três depósitos de Cu-Au de Carajás, que ocorrem em situações estratigráficas diferenciadas. Foram selecionados os depósitos de (i) Igarapé Bahia que é alojado por rochas meta-vulcanossedimentares; (ii) Breves que está encaixado em rochas meta-sedimentares; e (iii) Cento e Dezoito que é hospedado em parte por rochas intrusivas de composição tonalítica. O depósito de Au-Pd-Pt de Serra Pelada também foi abordado sucintamente. Esta seleção objetivou a geração de dados que subsidiasssem a avaliação dos modelos genéticos existentes e a proposição de um modelo metalogenético regional para os depósitos de Cu-Au de Carajás.

## **2. Geologia regional e depósitos minerais associados**

O Cinturão Cupro-Aurífero de Carajás (Figura 1) situa-se na porção sudoeste do Craton Amazônico, sendo limitado a leste pela faixa de dobramentos Araguaia de idade neoproterozóica, e a oeste por rochas supra-crustais paleoproterozóicas do Supergrupo Uatumã (Docegeo 1988; Araújo e Maia 1991; Tassinari e Macambira 1999). A sul é balizado pelo contato com o Bloco Rio Maria, uma unidade tectônica mais antiga que inclui tipicamente terrenos do tipo granito-*greenstone* (Docegeo 1988; Huhn et al. 1988). A norte o cinturão é limitado principalmente pelo sistema de falhas transcorrentes Salobo-Cinzento, sendo parcialmente coberto por sedimentos paleozóicos e cenozóicos da Bacia Amazônica (Pinheiro e Holdsworth 1997).

O embasamento do cinturão inclui principalmente gnaisses e migmatitos integrantes do Complexo Xingu e o ortogranulitos do Complexo Pium. Dados recentes de geocronologia SHRIMP, conduzidos por Pidgeon et al. (2000), forneceram idades de  $3002 \pm 14$  Ma para os núcleos, e  $2859 \pm 9$  Ma para as bordas de zircões extraídos de edembergítos de fácies

granulito que compõe o Complexo Pium. Os resultados foram interpretados pelos autores como representativos das idades de cristalização e metamorfismo, respectivamente. Estes dados concordam com datações U-Pb convencionais, realizadas por Machado et al. (1991), em zircões extraídos de gnaisses e migmatitos do Complexo Xingu, que forneceram idade de  $2859 \pm 2$  Ma para o metamorfismo e migmatização da assembléia de embasamento.

Regionalmente o padrão de deformação das rochas do embasamento define um complexo sistema de falhas transcorrentes sub-verticais, com orientação geral E-W, denominado de Zona de Cisalhamento Itacaiúnas. Este sistema de falhas representa um clássico exemplo de herança tectônica tendo sido reativado diversas vezes desde o Arqueano até o Proterozóico (Pinheiro e Holdsworth 1997; Holdsworth e Pinheiro 2000). Assim, o aqui definido Cinturão Cupro-Aurífero de Carajás comprehende um domínio metálico da crosta continental, estruturalmente balizado pela Zona de Cisalhamento Itacaiúnas, onde ocorre uma excepcional concentração de depósitos de Cu-Au circunscritos por rochas supra-crustais de idade arquena.

As seqüências meta-vulcanossedimentares de Carajás, reunidas no Supergrupo Itacaiúnas, incluem rochas de grau metamórfico variado. Na porção norte do cinturão ocorrem rochas intensamente deformadas e metamorfisadas em fácies anfibolito alto a granulito do Grupo Igarapé Salobo, enquanto na sua porção central ocorrem rochas muito pouco deformadas e de baixo grau metamórfico dos Grupos Grão Pará e Igarapé Bahia (Docegeo 1988). A acumulação destas seqüências supra-crustais foi determinada por vários autores em ~2.75 Ga (e.g. Wirth et al. 1986; Machado et al. 1991; Trendall et al. 1998). O Grupo Grão Pará é a unidade vulcanosedimentar dominante do cinturão, incluindo rochas meta-vulcânicas com expressivas intercalações de formação ferrífera bandada onde são encontrados depósitos gigantes de minério de ferro tais como o de Serra Norte, Serra Leste e Serra de São Felix que totalizam recursos de 17,3 bilhões de toneladas de minério com teores da ordem de 66 % Fe (Tolbert et al. 1971). Segundo Gibbs et al. (1986) e Olszewski et al. (1989), a estratigrafia, natureza geoquímica e assinatura isotópica Sm-Nd das rochas do Grupo Grão Pará, indicam que esta seqüência meta-vulcanosedimentar se formou em ambiente de rift intra-continental durante o Arqueano.

As unidades anteriores são recobertas por uma sucessão de arenitos e siltitos, depositados em ambiente marinho raso com incursões fluviais, da Formação Águas Claras

(Nogueira et al. 1994, 2000). A idade mínima desta Formação foi proposta por Dias et al. (1996) em  $2645 \pm 12$  Ma, obtida pelo método U-Pb convencional, em zircões extraídos de sill gabróico intrusivo na seqüência sedimentar. Trendall et al. (1998) obtiveram uma idade de  $2681 \pm 5$  Ma, pelo método U-Pb SHRIMP, em amostras de arenito contendo zircões supostamente sin vulcânicos. Com base nestes resultados, Trendall et al. (1998) inferiram que a Formação Águas Claras representaria a unidade de topo, derivada de acumulação contínua, da “bacia Grão Pará” que teria durado menos que 100 Ma.

O Cinturão Cupro-Aurífero de Carajás alojou diversos pulsos de magmatismo que variam em idade e composição. As intrusões arqueanas compreendem granitos e dioritos da Suite Plaquê ( $2736 \pm 24$  Ma, Avelar et al. 1999), o Granito Planalto ( $2747 \pm 2$  Ma, Huhn et al. 1999a) e o diorito Cristalino ( $2738 \pm 6$  Ma, Huhn et al. 1999b). Ocorrem também granitos alcalinos neoarqueanos tais como o Granito “Old Salobo” ( $2573 \pm 2$  Ma, Machado et al. 1991) e o Granito Itacaiúnas ( $2560 \pm 37$  Ma, Souza et al. 1996). Durante o Paleoproterozóico o cinturão foi palco de novo episódio magmático que compreendeu a formação de vários plutons graníticos tais como o Granito Central de Carajás ( $1880 \pm 2$  Ma, Machado et al. 1991) e o Granito Cigano ( $1883 \pm 3$  Ma, Machado et al. 1991). Os últimos fazem parte do que é considerada uma das mais extensas províncias anorogênicas do mundo (e.g. Santos et al. 2001), que se estende a oeste por vasta porção do Craton Amazônico, merecendo destaque por hospedar expressivos depósitos de estanho aos quais associam-se ocorrências menos significativas de F, Zr, ETR, Y e W (Issler e Lima 1987; Dall’Agnol et al. 1993; Dall’Agnol et al. 1994).

Além dos depósitos gigantes de ferro e manganês, ocorrem na região vários depósitos de Cu-Au que coletivamente compõe o Cinturão Cupro-Aurífero de Carajás. Os depósitos mais comuns do cinturão são aqueles caracterizados pela associação metálica Fe-óxido Cu-Au-(U-ETR), que tipicamente apresentam tonelagem de classe mundial ( $> 200$  Mt). Os exemplos mais significativos deste grupo de depósitos são: Salobo com recursos de 994 Mt @ 0,94 % Cu e 0,52 g/t Au (Farias e Saueressig 1982; Vieira et al 1988; Lindenmayer 1990), Igarapé Bahia com recursos de 219 Mt @ 1,4 % Cu e 0,86 g/t Au (Ferreira Filho 1985; Almada 1998; Tazava 1999; Soares et al. 1999; Tallarico 2000), Sossego com recursos de 355 Mt @ 1,1 % Cu e 0,28 g/t Au (Cordeiro 1999; Lancaster et al. 2000), Cristalino com recursos de 500 Mt @ 1,0 % Cu e 0,3 g/t Au (Huhn et al. 1999b)

e Cento e Dezoito com recursos de 170 Mt @ 1,0 % Cu e 0,3 g/t Au (Rigon et al. 2000). O cinturão inclui também um segundo conjunto de depósitos cupro-auríferos que se caracterizam por apresentar uma tonelagem menos expressiva (até 50 Mt) e pela associação metálica Cu-Au-(W-Bi-Sn). Exemplos deste grupo de depósitos são: Águas Claras com recursos de 9,5 Mt de minério oxidado @ 2,43 g/t Au (Soares et al. 1994; Silva e Villas 1998), e Breves com recursos de 50 Mt @ 1,22% Cu, 0,75 g/t Au, 2,4 g/t Ag, 1200 g/t W, 70 g/t Sn, 175 g/t Mo e 75 g/t Bi.

Igarapé Bahia é um dos depósitos mais intensamente estudados da classe Fe-óxido Cu-Au-(U-ETR). A mineralização consiste de uma série de corpos de brecha, ricos em calcopirita, que ocorrem no contato entre rochas meta-vulcânicas e meta-sedimentares. O fato da mineralização ser hospedada em uma seqüência meta-vulcanossedimentar motivou alguns autores a relacionar sua gênese a processos singenéticos (tipo Besshi) arqueanos (e.g. Ferreira Filho 1985; Almada 1999). Por outro lado, o diagnóstico enriquecimento em U e ETR, e a configuração circular dos corpos de minério, encorajou outros autores a propor modelos hidrotermais-magmáticos, relacionados à intrusão de granitos paleoproterozóicos (e.g. Lindendenmayer et al. 1998), ou modelos multi-estágio envolvendo a superposição de processos arqueanos e paleoproterozóicos (Ribeiro 1989; Mousgeot, 1996). Alternativamente, as similaridades paragenéticas com o depósito australiano de Olympic Dam, levou uma série de autores a propor um modelo epigenético associado a um componente magnético alcalino de idade desconhecida (e.g. Huhn e Nascimento 1996, Tallarico 1996; Tallarico et al. 1998; Oliveira et. al. 1998; Tazava 1999; Soares et al. 1999). Esta controvérsia não se restringe ao depósito de Igarapé Bahia, e de forma genérica sintetiza a polêmica em torno da gênese dos depósitos de Fe-óxido Cu-Au-(U-ETR) do Cinturão Cupro-Aurífero de Carajás.

Os depósitos do grupo Cu-Au-(W-Bi-Sn) são, até a presente data, muito mais escassos. O exemplo mais conhecido é o depósito de Águas Claras, que consiste de corpos sulfetados tabulares hospedados em rochas sedimentares da Formação Águas Claras. As relações de campo indicam claramente uma mineralização de caráter epigenético, alojada em zonas tectonicamente ativas. A presença de minerais como cassiterita e wolframita, e a proximidade com o Granito Central de Carajás, serviram de argumento para relacionar a mineralização ao magmatismo granítico de idade paleoproterozóica (e.g. Soares et al. 1994;

Silva e Villas 1998), porém ainda não foram reconhecidos no depósito corpos graníticos intrusivos. O segundo exemplo do grupo Cu-Au-(W-Bi-Sn) é o depósito de Breves que foi recentemente descoberto pela Companhia Vale do Rio Doce. O depósito também é hospedado em arenitos e siltitos da Formação Águas Claras, porém em Breves, a relação genética com corpos intrusivos é óbvia, pois a mineralização associa-se a um greisen situado na zona apical de um complexo granítico.

O cenário exposto suscita alguns questionamentos. Quais são as idades das mineralizações de Fe-óxido Cu-Au-(U-ETR) e Cu-Au-(W-Bi-Sn)? Existe algum vínculo genético entre estes dois grupos de depósitos, ou estes derivam de eventos metalogenéticos distintos? Torna-se evidente que estas incertezas decorrem em parte da escassez de dados geocronológicos robustos que permitam circunscrever as idades destas mineralizações. Esta tese de doutorado vem preencher parte destas lacunas pois identifica os atributos geológicos e determina as idades de depósitos representativos dos grupos Fe-óxido Cu-Au-(U-ETR) e Cu-Au-(W-Bi-Sn), e finalmente propõe um modelo metalogenético regional para o Cinturão Cupro-Aurífero de Carajás.

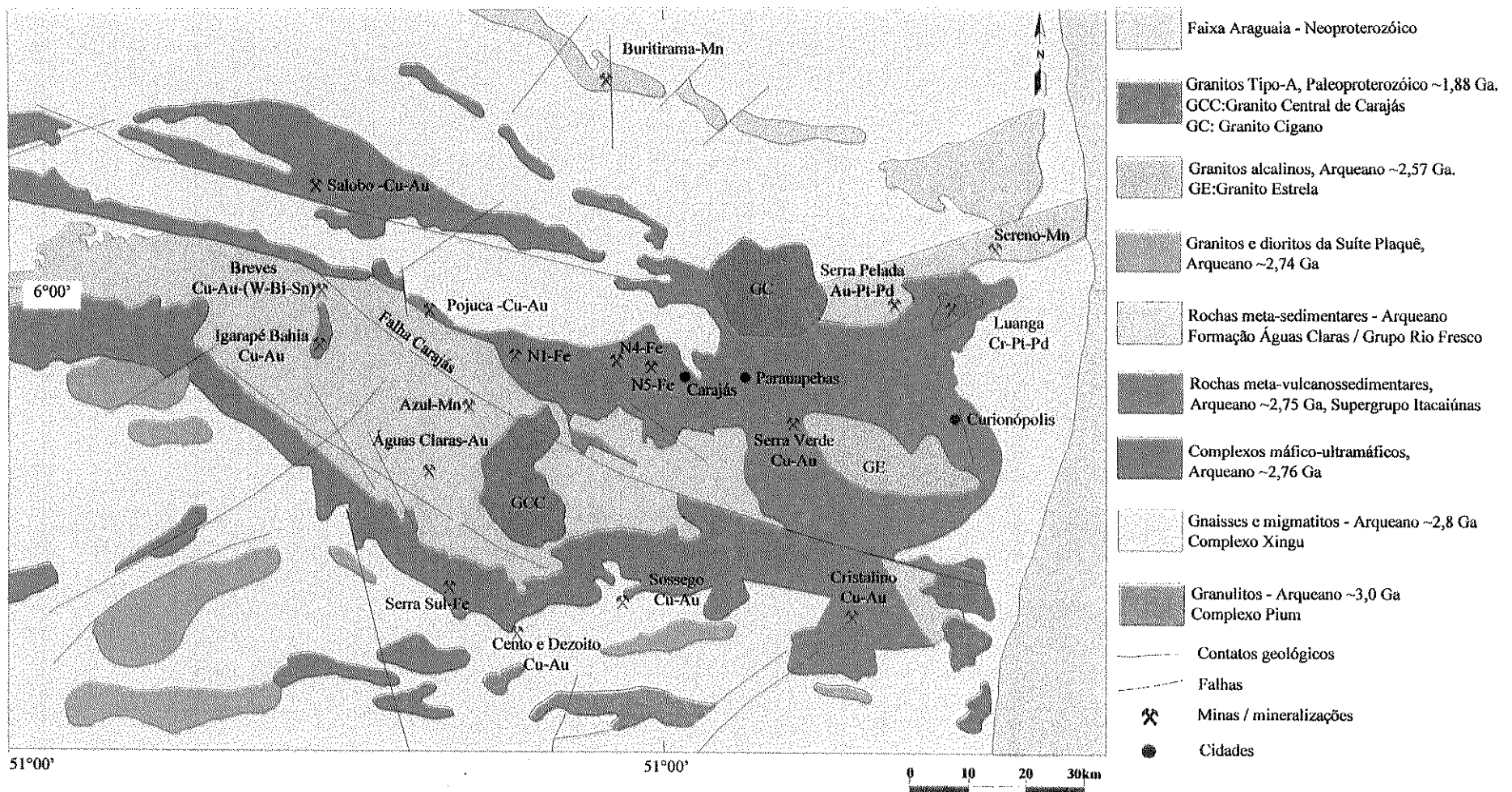


**Figura 1.** Mapa geológico simplificado do Cinturão Cupro-Aurífero de Carajás mostrando a distribuição dos principais depósitos do tipo Fe-óxido Cu-Au-(U-ETR) e Cu-A-(W-Bi-Sn). Encontram-se também representados os depósitos gigantes de ferro, o depósito de Au-Pd-Pt de Serra Pelada e o depósito de Pd-Pt de Luanga.

### **3. Materiais e métodos**

Os depósitos estudados nesta tese foram visitados em duas etapas de campo. Os trabalhos concentraram-se em produzir dados descritivos da geologia dos depósitos e principalmente do(s) modo(s) de ocorrência dos minérios de Cu-Au. Além da observação em superfície, retratada em mapas, foram descritos e amostrados vários furos de sondagem rotativa que permitiram a construção de seções geológicas verticais.

As atividades de laboratório inicialmente concentraram-se na produção de dados mineralógicos e petrográficos, obtidos por meio de difração de raios-x, microscopia ótica e eletrônica e também microanálises qualitativas e quantitativa de minerais via espectrometria dispersão de energia e comprimento de onda, respectivamente. Estes dados foram utilizados principalmente na caracterização dos minérios, descrição de suas assembleias minerais e diferentes paragêneses envolvidas, bem como determinação dos elementos e minerais traços associados. Também a caracterização dos diferentes estilos de alteração hidrotermal mereceu especial atenção. Em seguida os equilíbrios minerais e os dados de termometria de clorita (Cathelineau 1988) foram utilizados para modelar os parâmetros termodinâmicos dos sistemas hidrotermais estudados, por meio de diagramas petrogenéticos disponíveis na literatura.

A etapa seguinte envolveu a preparação de amostra seguida de análises isotópicas de minerais selecionados. Foram extraídos e concentradas amostras de calcopirita, carbonato e magnetita para a produção de dados Pb-Pb e Sr-Sr. Foram também produzidas amostras de zircão, monazita e xenotíma para geocronologia U-Pb pelo método SHRIMP II, cujos detalhes metodológicos encontram-se disponíveis no ANEXO 1.

## 4. Resultados

### 4.1. Depósito de Fe-óxido Cu-Au-(U-ETR) de Igarapé Bahia

Os resultados obtidos no depósito de Igarapé Bahia estão expostos em três artigos, disponíveis em anexo e listados a seguir:

- ANEXO 2: *The Igarapé Bahia Cu-Au mineralization, Carajás Province*. Este artigo foi publicado na Revista Brasileira de Geociências (RBG) e trata do modelo descritivo do depósito, abordando a geologia e geoquímica de rochas e minerais.
- ANEXO 3: *The occurrence of ilvaite in the Igarapé Bahia Cu-Au deposit, Carajás Province, Brazil*. Trata-se de um artigo publicado na RBG, cujo texto descreve a ocorrência inédita do mineral ilvaita no Brasil. A ilvaita é um mineral extremamente raro e a sua identificação no depósito de Igarapé Bahia representa a primeira ocorrência documentada no Brasil e a 14<sup>a</sup> no mundo.
- ANEXO 4: *Geology and SHRIMP geochronology of the Igarapé Bahia Fe-oxide Cu-Au-(U-REE) mineralisation, Carajás copper-gold belt, Brazil: an Archean (2.57 Ga) Olympic Dan-Type deposit*. Trata-se de um manuscrito completo submetido e aprovado pelo corpo editorial da revista Economic Geology, encontrando-se em fase final de revisão. O texto retoma os aspectos descritivos da geologia e da geoquímica do depósito, porém focaliza principalmente os resultados geocronológicos obtidos via SHRIMP e dados de  $^{87}\text{Sr}$ - $^{86}\text{Sr}$  determinados em carbonato.

No depósito de Fe-óxido Cu-Au-(U-ETR) de Igarapé Bahia foram datadas, pelo método SHRIMP, as seguintes rochas: (a) rochas vulcânicas da lapa que representam a encaixante imediata do minério, (b) o minério primário de Cu-Au e (c) diques de diabásio que cortam o minério e suas rochas hospedeiras. Os resultados encontram-se resumidos na Tabela 1.

Foram obtidos resultados inéditos e de grande relevância metalogenética. A idade  $^{207}\text{Pb}/^{206}\text{Pb}$  de  $2751 \pm 42$  Ma para as rochas vulcânicas encaixantes, apesar da baixa precisão, concorda com o quadro geológico regional uma vez que o Grupo Igarapé Bahia encontra-se circunscrito ao Grupo Grão Pará que foi repetidamente datado em  $\sim 2.75$  Ga (e.g. Gibbs et al. 1986; Olszewski et al. 1989; Machado et al. 1991), devendo representar uma variação faciológica desta bacia. A idade  $^{207}\text{Pb}/^{206}\text{Pb}$  de  $2575 \pm 12$  Ma obtida em monazitas do minério claramente revela o caráter epigenético da mineralização, que se formou aproximadamente 176 Ma após a acumulação da seqüência vulcanossedimentar hospedeira. Finalmente a idade  $^{207}\text{Pb}/^{206}\text{Pb}$  máxima de  $2579 \pm 7$  Ma para os diques que cortam a mineralização, está de acordo com as idades SHRIMP obtidas para a mineralização e rochas hospedeiras, e é compatível com as evidências de campo.

As razões  $^{87}\text{Sr}-^{86}\text{Sr}$  obtidas em carbonato da matriz de brechas mineralizadas e de veios são altamente radiogênicas (0,7138 a 0,7553) e indicam derivação a partir da crosta continental. Os valores são inconsistentes com a composição isotópica da água do mar no Arqueano (Veizer e Compstron 1976) e diferem da razão  $^{87}\text{Sr}-^{86}\text{Sr}$  inicial das rochas metavulcânicas do Grupo Grão Pará ( $0,7057 \pm 0,0010$ ) determinada por Gibbs et al. (1986). O amplo intervalo de variação e o caráter altamente radiogênico das razões  $^{87}\text{Sr}-^{86}\text{Sr}$  dos carbonatos de Igarapé Bahia, sugerem derivação a partir de múltiplas fontes crustais. Esta interpretação é coerente com a origem epigenética da mineralização conforme indicam os resultados geocronológicos.

**Tabela 1.** Resumo das idades  $^{207}\text{Pb}/^{206}\text{Pb}$ , pelo método SHRIMP, do depósito de Cu-Au-(U-ETR) de Igarapé Bahia.

Amostra (mineral datado)	Rocha	Idade (Ma)	Erro (Ma)	Evento Datado
UWA-B36A e UWA-B21D (xenocristais de zircão)	Dique de Diabasio	2579	$\pm 7$	Idade máxima de intrusão do dique
UWA-B34 (monazita)	Brecha magnetítica mineralizada a Cu-Au	2575	$\pm 12$	Atividade hidrotermal e deposição do minério
UWA-B18C e UWA-B18D (zircão magmático)	Rocha meta-vulcânica encaixante	2751	$\pm 42$	Idade de cristalização

#### 4.2. Depósito de Cu-Au-(W-Bi-Sn) de Breves

Os resultados obtidos no depósito de Breves estão descritos no manuscrito:

- ANEXO 5: *Geological and SHRIMP II U-Pb constraints on the age and origin of the Breves Cu-Au-(W-Bi-Sn) deposit, Carajás, Brazil.* Este manuscrito foi aceito para publicação no periódico Mineralium Deposita. O texto aborda os aspectos descritivos da geologia e da geoquímica do depósito e concentra-se em documentar um conjunto de idades radiométricas que foram utilizadas para a elaboração de um modelo genético.

No depósito de Breves foram datadas os seguintes litotipos: (a) granito, (b) episienito e (c) veios tardios que cortam a mineralização e o complexo granítico subjacente. Os resultados (Tabela 2) foram suficientes para circunscrever precisamente a idade de formação do minério, uma vez que as idades do complexo granítico ( $1880 \pm 9$  Ma a  $1878 \pm 8$  Ma) e dos veios que cortam o greisen ( $1872 \pm 7$  Ma) são concordantes dentro do erro analítico.

Estes resultados são extremamente relevantes e inéditos, pois esta é a primeira mineralização de Cu-Au de Carajás, que tem sua gênese inquestionavelmente associada ao magmatismo anorogênico paleoproterozóico.

Tabela 2. Resumo das idades  $^{207}\text{Pb}/^{206}\text{Pb}$ , pelo método SHRIMP, do depósito de Cu-Au-(W-Bi-Sn) de Breves.

Amostra (mineral datado)	Rocha	Idade (Ma)	Erro (Ma)	Evento datado
UWA-B40A/B/C (xenotima e monazita)	Veios cortando o graisen	1872	$\pm 7$	Atividade hidrotermal tardia / idade mínima de formação de minério
UWA-B09A (zircão)	Granito	1878	$\pm 8$	Cristalização magmática
UWA-B30A (zircão)	Episienito	1880	$\pm 9$	Cristalização magmática

#### *4.3. Depósito de Cu-(Au) Cento e Dezoito*

Os resultados obtidos no depósito Cento e Dezoito estão sendo documentados no manuscrito:

- ANEXO 6: *Geologia e geocronologia SHRIMP II do depósito de Cu-Au Cento e Dezoito, Carajás, Brasil.* O texto inclui dados geológicos e geocronológicos inéditos referentes ao depósito Cento e Dezoito, que aparentemente trata-se de um depósito com características híbridas.

No depósito Cento e Dezoito foram datadas as seguintes rochas: (a) tonalito que representa a hospedeira imediata da mineralização, (b) diques de composição dacítica a riolítica que cortam o tonalito, (c) xenotima extraída de amostra composta de minério maciço de Cu-Au, e (d) xenotima extraída de veios de quartzo + calcopirita que cortam o minério maciço. Os resultados geocronológicos encontram-se resumidos na Tabela 3.

Zircões extraídos do tonalito encaixante forneceram uma idade  $^{207}\text{Pb}/^{206}\text{Pb}$  de  $2743 \pm 3$  Ma, que é cronocorrelata aos granitos e dioritos arqueanos da Suíte Plaquê que foram datados por vários autores em  $\sim 2,74$  Ga (e.g. Huhn et al. 1999a). Resultados inéditos foram obtidos nos diques de composição dacítica e riolítica que forneceram idades  $^{207}\text{Pb}/^{206}\text{Pb}$  de  $2645 \pm 9$  Ma e  $2654 \pm 9$  Ma respectivamente. Este evento magmático de  $\sim 2.65$  Ga é presentemente pouco conhecido na região de Carajás, tendo sido publicada apenas uma única idade de  $2645 \pm 12$  Ma em zircões extraídos de um dique de gábro que corta a Formação Águas Claras (Dias et al. 1996).

Na tentativa de se circunscrever a idade da mineralização foram preparadas duas amostras para geocronologia. A primeira consiste de uma amostra composta de minério maciço de Cu-Au, rica em calcopirita em equilíbrio com hematita, que foi britada e a partir da qual foram concentrados cristais de xenotima. A segunda consiste de cristais de xenotima, de veios quartzo + calcopirita que cortam o minério maciço, que foram extraídos a partir de lâmina delgada. As amostras forneceram idades  $^{207}\text{Pb}/^{206}\text{Pb}$  Proterozóicas de  $1869 \pm 7$  Ma e  $1868 \pm 7$  para minério maciço e veios respectivamente. Os resultados indicam a atuação de um evento hidrotermal correlato ao observado no depósito de Breves.

Porém, dado o fato da amostra de minério maciço ter sido preparada pelo método convencional de concentração, os cristais datados podem derivar de veios portadores de xenotima que cortam o minério. Assim, assume-se que no depósito de Cu-Au Cento e Dezoito foi determinada apenas a idade do último episódio formador de minério, que é representado pelos veios de quartzo + calcopirita  $\pm$  xenotima. O minério maciço que é cortado pelos veios de quarto + calcopirita e se caracteriza pela associação Fe-óxido + calcopirita não foi diretamente datado.

Tabela 3. Resumo das idades  $^{207}\text{Pb}/^{206}\text{Pb}$ , pelo método SHRIMP, do depósito de Cu-(Au) Cento e Dezoito.

<b>Amostra (mineral datado)</b>	<b>Rocha</b>	<b>Idade (Ma)</b>	<b>Erro (Ma)</b>	<b>Evento Datado</b>
UWA-B35 (xenotima)	Veios de quartzo + calcopirita	1868	$\pm 7$	Alteração hidrotermal tardia
UWA-B36D (xenotima)	Minério maciço de Cu-Au	1869	$\pm 7$	Alteração hidrotermal precoce
UWA-B21A (zircão magmático)	Dique de riolito	2654	$\pm 9$	Idade de cristalização
UWA-B21B (zircão magmático)	Dique de dacito	2645	$\pm 9$	Idade de cristalização
UWA-B30C (zircão magmático)	Tonalito	2743	$\pm 3$	Idade de cristalização

## **5. Modelo metalogenético regional**

Os resultados obtidos no depósito de Igarapé Bahia e Breves mostram que no Cinturão Cupro-Aurífero de Carajás ocorreram ao menos dois eventos metalogenéticos distintos. Os eventos formadores de minério de Cu-Au no Neoarqueno (~2,57 Ga) e no Paleoproterozóico (~1,88 Ga) apresentam estilos de alteração hidrotermal, paragêneses, associações metálicas e tonelagens muito distintas.

O evento metalogenético neoarqueano se caracteriza por gerar depósitos de Cu-Au de classe mundial (> 200 Mt) que apresentam as seguintes características comuns: (a) intenso Fe-metassomatismo levando a formação de fayalita, grunerita e/ou Fe-óxidos (magnetita e hematita), (b) intensa carbonatação com formação preferencialmente de siderita, (c) paragêneses metálicas pobres em enxofre (calcopirita, bornita e calcocita primária), (d) sistemas hidrotermais relativamente pobres em quartzo, (e) forte enriquecimento em elementos terras raras leves, com concentrações de La e Ce aproximadamente quatro ordens de grandeza superiores aos valores condrícticos, e (d) diagnóstico enriquecimento em U e Co (Tabela 4).

A idade  $^{207}\text{Pb}/^{206}\text{Pb}$  SHRIMP de  $2575 \pm 12$  Ma definida em cristais de monazita da matriz das brechas mineralizadas de Igarapé Bahia é concordante dentro do erro analítico com idades  $^{207}\text{Pb}/^{206}\text{Pb}$  convencionais obtidas em zircão extraídos dos granitos neoarqueanos Old Salobo (Machado et al. 1991) e Itacaiúnas (Souza et al. 1996). Idades equivalentes também foram obtidas utilizando-se o sistema Rb-Sr em amostras de rocha total do Granito Itacaiúnas (Montalvão et al. 1984) e do Complexo Granítico Estrela (Barros e Barbey 1998), refletindo possivelmente a idade de resfriamento destas intrusões. Estes dados indicam que os processos hidrotermais que resultaram na formação do minério de Igarapé Bahia são temporalmente relacionados a intrusão dos granitos neoarqueanos de Carajás (Tabela 5). A idade Rb-Sr de  $2577 \pm 72$  Ma determinada em amostra de rocha total da lapa do minério de Igarapé Bahia por Ferreira Filho (1985), fornece suporte adicional a este modelo pois denota superposição de atividade termal ~170 Ma após a acumulação da seqüência vulcano-sedimentar. Dados recentes de Re-Os em amostras de molibdenita dos depósitos de Salobo (Réquia e Fontboté 2001) e Serra Verde (Marschik et al. 2001) comprovam que o evento metalogenético de ~2,57 Ga tem expressão regional.

O sistema hidrotermal de Igarapé Bahia caracteriza-se pela alta salinidade, elevada temperatura, baixa atividade de enxofre e alta fugacidade de oxigênio (ANEXOS 2 e 4). Os dados de isótopos estáveis (Oliveira et al. 1998, Tazava 1999) e de inclusões fluidas (Ribeiro 1989, Lindenmayer et al. 1998) indicam participação importante de fluidos magmáticos. Estas evidências concordam com os dados geocronológicos obtidos neste trabalho os quais indicam que o minério de Igarapé Bahia é epigenético e temporalmente correlato à intrusão de granitos neoarquenos.

Os resultados geocronológicos obtidos no depósito de Breves comprovam claramente a existência de um segundo evento metalogenético no Cinturão Cupro-Aurífero de Carajás. Este evento caracteriza-se por gerar depósitos de menor tonelagem (até 50 Mt) com paragêneses de minério enriquecidas em quartzo, relativamente redutoras, ricas em enxofre e sem óxidos de Fe, às quais se associam concentrações sub-econômicas de Bi, Sn e W (Tabela 4). O conjunto de idades  $^{207}\text{Pb}/^{206}\text{Pb}$  SHRIMP do complexo granítico de Breves ( $1878 \pm 8$  Ma e  $1880 \pm 9$  Ma) e de veios tardíos a pós-mineralização ( $1872 \pm 7$  Ma) permitem correlacionar o depósito ao magmatismo anorogênico de  $\sim 1,88$  Ga que não se restringiu somente a região de Carajás estendendo-se a oeste em uma vasta porção do Craton Amazônico.

Dada a evidência de dois eventos metalogenéticos distintos no Cinturão Cupro-Aurífero de Carajás, há a possibilidade de existirem na região depósitos híbridos resultantes da superposição de eventos neoarqueanos e paleoproterozóicos. O depósito Cento e Dezoito é um potencial exemplo, pois inclui atributos análogos aos do depósito neoarqueano de Igarapé Bahia, como a ocorrência de minério maciço, relativamente oxidado e pobre em enxofre, porém também portando vénulas com a associação quartzo + calcopirita  $\pm$  xenotima, similar a do depósito paleoproterozóico de Breves. Além da idade  $^{207}\text{Pb}/^{206}\text{Pb}$  SHRIMP de  $1868 \pm 7$  da xenotima, extraída de veios de quartzo, a ocorrência de fragmentos de calcopirita  $\pm$  bornita  $\pm$  Fe-óxidos soldados por matrix rica em quartzo é coerente com a sugestão de um modelo multi-estágio para o depósito Cento e Dezoito.

O Cinturão Cupro-Aurífero de Carajás experimentou um longa história tectônica, que registra vários episódios de reativação com magmatismo associado (Figura 2). De acordo com Pinheiro e Holdsworth (1997) e Holdsworth e Pinheiro (2000), o primeiro evento tectônico foi uma transpressão sinistral dúctil desenvolvida em condições de alta

temperatura, que teria ocorrido em ~2,8 Ga e afetando as rochas do embasamento (Complexos Xingu e Pium). Em ~2,75 Ga a região foi submetida a um período de dilatação que permitiu a acumulação, em ambiente de rift, das seqüências vulcanossedimentares do Supergrupo Itacaiúnas. Por volta de 2,65 Ga, o cinturão participou de um episódio de transtensão destral que provocou o abatimento das unidades anteriores e permitiu a ascensão passiva de diques de composição gabróica, riolítica e dacítica. Durante o Neoarqueano (~2,57 Ga) a região foi submetida a transtensão destral rúptil que condicionou o alojamento de magmas graníticos alcalinos (e.g. Granito Old Salobo, Granito Itacaiúnas). No Paleoproterozóico (~1,88 Ga) novamente a região foi submetida a transtensão rúptil sinistral que controlou a intrusão de diversos batólitos de granito tipo-A (e.g. Granito Central de Carajás, Granito Cigano).

Um aspecto particular do Cinturão Cupro-Aurífero de Carajás é a ausência de uma série de depósitos minerais que characteristicamente associam-se aos terrenos arqueanos. Os terrenos tipo *greenstone* arqueanos são conhecidos por conter depósitos do tipo VMS (Barrie e Hannington 1999; Large 1992; Slack 1993), depósitos de níquel sulfetado associados a komatiitos (Salomon e Groves 2000) e depósitos orogênicos de ouro (Groves 1993; Goldfarb e Groves al. 2001). O quadro metalogenético distinto, aliado à ausência de derrames ultramáficos nas seqüências meta-vulcanosedimentares, indicam que o Cinturão Cupro-Aurífero de Carajás é um terreno arqueano particular que não compartilha as feições geológicas e metalogenéticas dos clássicos terrenos tipo *greenstone*.

Os aspectos geológicos e geoquímicos das rochas do Grupo Grão Pará (Gibbs et al. 1986) indicam que a região de Carajás encontrava-se estabilizada no Neoarqueano quando se deu a acumulação em ambiente de rift intracontinental da pilha vulcanosedimentar. O Cinturão Cupro-Aurífero de Carajás experimentou no Neoarqueano uma evolução geológica que denuncia crescente cratonização, representando juntamente com as seqüências de Ventersdorp no Craton do Kaapvaal e Fortescue no Cráton de Pilbara (Nelson et al. 1999) raros exemplos onde o limite Arqueano-Proterozóico foi diacrônico.

Assim, enquanto nos terrenos tipo *greenstone*, predominantes no Arqueano, vigoravam processos geológicos de formação de crosta continental juvenil, a região de Carajás constituía um bloco crustal estabilizado que precocemente experimentava processos ensiálicos de rifteamento. O adelgaçamento da crosta continental derivou possivelmente da

interação desta com material mantélico ascendente e convectivo. Os magmas gerados nesta etapa potencialmente se acumularam na base da crosta provocando *underplating*, tendo também ascendido, através de falhas, aos níveis crustais rasos para originar câmaras magmáticas diferenciadas, ou ainda se extravasado para compor as seqüências vulcanossedimentares do Supergrupo Itacaiúnas (Figura 2).

A acumulação de seqüências vulcanossedimentares de ambiente rift no Neoarqueano (~2,75 Ga) introduz um metalotecto importante ao Cinturão Cupro-Aurífero de Carajás, pois estas sucessões tem vocação para gerar concentrações, não necessariamente econômicas, de cobre. Dados recentes de Pb-Pb em calcopirita e ouro do depósito de Igarapé Bahia, produzidos por Toro (2002), indicam uma história prolongada de acumulação de cobre e ouro, que teria se iniciado em ~2,75 Ga durante a deposição das seqüências vulcanossedimentares do Supergrupo Itacaiúnas. É também neste ambiente que ocorre significativa acumulação de ferro exalativo, que posteriormente deu origem aos gigantes depósitos supergênicos de Carajás.

Outro metalotecto importante é também adicionado ao cinturão durante a evolução do rift continental. As contrapartes plutônicas das sucessões vulcânicas cristalizam-se em profundidade dando origem a corpos máficos-ultramáficos acamados. O complexo Luanga é o exemplo mais conhecido de Carajás, e hospeda concentrações econômicas de elementos do grupo da platina (EGP) associados a sulfetos e à cromita (Suita e Nilson 1988). A evidência reafirma o ambiente de rift continental, pois a precipitação tanto de sulfetos quanto de cromita, as quais associam-se EGP, depende fundamentalmente de processos de contaminação crustal (Naldrett 1989), motivo pelo qual todos os depósitos econômicos de EGP do mundo ocorrerem em ambiente continental.

A precoce estabilidade do Cinturão Cupro-Aurífero de Carajás e sua complexa história tectônica, que registra múltiplos eventos de transtensão associados a magmatismo, permitiu a formação ainda no Neoarqueano de depósitos de Cu-Au-(U-ETR), que em outras partes do mundo characteristicamente se associam a terrenos Proterozóicos (Hitzman et al. 1992). Em ~2,57 Ga magmas graníticos ascenderam a níveis crustais rasos ao longo de zonas de dilatação de falhas reativadas. Em condições epicrustais desenvolveram-se sistemas hidrotermais-magmáticos oriundos da persistente circulação e mistura de fluidos magmáticos e meteóricos, conforme denunciam os dados de inclusões fluidas e isótopos

estáveis (Ribeiro 1989; Lindenmayer et al. 1998; Oliveira et al. 1998; Tazava 1999). Tanto os dados de Sr-Sr obtidos em carbonatos (ANEXO 4) quanto os dados de Pb-Pb obtidos em magnetita, siderita e calcopirita (ANEXO 7) de Igarapé Bahia revelam razões altamente radiogênicas que necessariamente sugerem fontes com longa residência crustal. Portanto, estas razões concordam com o modelo proposto pois indicam que o Sr e o Pb incorporados nestes sistemas hidrotermais derivam da crosta continental.

Eventualmente, os depósitos de Fe-óxido Cu-Au-(U-ETR) de Carajás se especializam em virtude de condicionantes locais em depósitos proximais, como possivelmente o do Sossego onde a relação com corpos graníticos intrusivos é óbvia, e em depósitos distais e estruturalmente controlados, como o do Igarapé Bahia, onde esta relação não é tão evidente.

O cobre e o ouro acumulado nestes depósitos pode simplesmente ter derivado dos sistemas graníticos correspondentes, entretanto, é provável que estes depósitos tenham se beneficiado do enriquecimento prévio destes metais ocorrido durante a formação da seqüências vulcanossedimentares do Supergrupo Itacaiúnas (cf. Toro 2002). O fato dos depósitos de Fe-óxido Cu-Au-(U-ETR) de Carajás estarem circunscritos a seqüências vulcanosedimentares aparentemente reforça a hipótese. Um aspecto obscuro na gênese destes depósitos é sua associação metálica. Elementos incompatíveis como U e ETR, de reconhecida filiação ácida, coexistem com elementos como Co e Ni. O depósito de Igarapé Bahia inclui minerais como uraninita, monazita, cobaltita e siegenita associados ao minério. O fato, aparentemente paradoxal, poderia estar relacionado ao *underplating* por magmas maficos ocorrido durante o desenvolvimento do rift. Este material basáltico portador de elementos compatíveis como Co e Ni e alojado na base da crosta poderia contaminar os posteriores pulsos magmáticos.

Durante o Paleoproterozóico (~1,88 Ga) a região experimentou um novo episódio tectônico de extensão que permitiu o alojamento de diversos granitos anorogênicos, aos quais associam-se os depósitos do tipo Cu-Au-(W-Bi-Sn). Novamente parece ter havido especialização destes depósitos em função de aspectos locais, dando origem a depósitos proximais, como o de Breves, onde a relação com a fonte intrusiva é inquestionável, e a depósitos distais como possivelmente o de Águas Claras, onde a relação é obscura. Diferentemente dos demais depósitos associados a granitos Proterozóicos no Cráton

Amazônico que são mineralizados a Sn, os de Carajás são distintamente enriquecidos em Cu-Au, contendo Sn como subproduto. Tal diferença pode novamente estar associada a permanência de metalotectos. Assim, é possível que mais uma vez os magmas ascendentes tenham incorporado metais não só das seqüências meta-vulcanossedimentares como também dos depósitos neoarqueanos.

Uma aspecto marcante da metalogênese regional é o aparente condicionante estratigráfico. Enquanto os depósitos paleoproterozóicos (~1,88 Ga) do tipo Cu-Au-(W-Bi-Sn) de Carajás são encaixados em rochas meta-sedimentares da Formação Águas Claras, os depósitos neoarqueanos (~2,57 Ga) do tipo Fe-óxido Cu-Au-(U-ETR) são hospedados em rochas meta-vulcanosedimentares do Supergrupo Itacaiúnas. A julgar pela idade mínima de  $2645 \pm 12$  Ma para Formação Águas Claras, determinada por Dias et al. (1996), não haveria restrição estratigráfica. Porém, salienta-se que esta a idade provém de determinações em cristais de zircão extraídos de um dique de gábrico que corta as rochas meta-sedimentares. A exemplo dos diques básicos de Igarapé Bahia, onde concluiu-se que os zircões coletados representavam xenocristais, é possível que a idade proposta como mínima para a Formação Águas Claras, retrate a idade de xenocristais incorporados durante a ascensão do dique. Assim, considera-se que a unidade estratigráfica em questão não tenha sido ainda precisamente datada. As evidências de campo sugerem que os depósitos do Cinturão Cupro-Aurífero de Carajás possam ser subdivididos em depósitos pré- e pós-Águas Claras (Figura 2).

Desta superposição de eventos resulta um quadro metalogenético complexo que inclui uma diversidade de depósitos minerais, alguns dos quais bastante exóticos. Um exemplo é o depósito de Serra Pelada (ANEXO 8) que representa um caso único em Carajás de mineralização de Au-Pd-Pt alojada em rochas meta-sedimentares. As relações de campo e as características do sistema hidrotermal indicam que a mineralização é epigenética, e provavelmente relacionada a fluidos salinos, oxidantes e ácidos. Mais uma vez a herança e permanência de metalotectos parece ter influenciado a gênese deste depósito, pois as soluções hidrotermais foram capazes de coletar EGP de rochas maficas-ultramáficas que ocorrem nas adjacências do depósito (Complexo Luanga) e depositá-los nas rochas meta-sedimentares do Grupo Rio Fresco / Formação Águas Claras. A julgar pela natureza das rochas encaixantes é possível que o depósito de Serra Pelada seja

paleoproterozóico estando incluído no conjunto pós-Águas Claras. Todavia, existem inúmeras incertezas relacionadas à gênese deste depósito que vão desde a exata definição da natureza dos fluidos até a idade da mineralização.

A despeito das inúmeras incertezas ainda relacionadas a metalogêneses de Carajás, que poderão ser endereçadas em trabalhos futuros, a principal contribuição desta pesquisa foi a identificação de dois eventos metalogenéticos distintos no Cinturão Cupro-Aurífero de Carajás (Tabela 6). O reconhecimento de uma série de atributos geológicos, geoquímicos e isotópicos distintivos entre os depósitos neoarquenos (~2,57 Ga) de Fe-óxido Cu-Au-(U-ETR) e paleoproterozóicos (~1,88 Ga) de Cu-Au-(W-Bi-Sn) de Carajás, e ainda de um provável controle estratigráfico que identifica estes depósitos respectivamente como pré- e pós-Águas Claras, dão margem a interessantes desdobramentos prospectivos que vão desde a seleção de áreas baseada em critérios geológicos e/ou geofísicos até as assinaturas geoquímicas esperadas em amostras de solo e sedimento de corrente.

**Tabela 4.** Quadro comparativo das alterações hidrotermais e paragêneses de minério dos depósitos de Cu-Au de Salobo, Igarapé Bahia, Cento e Dezoito, Águas Claras e Breves.

Depósito	Salobo	Igarapé Bahia	Cento e Dezoito	Águas Claras	Breves
Tipo	Fe-óxido Cu-Au-(U-ETR)	Fe-óxido Cu-Au-(U-ETR)	Híbrido ?	Cu-Au-(W-Bi-Sn)	Cu-Au-(W-Bi-Sn)
Idade	~2,5 Ga	~2,57 Ga	~1.87 Ga (fase tardia)	?	~1.88 Ga
Tonelagem	994 Mt	219 Mt	170 Mt	9,5 Mt	50 Mt
Teor	0,94%Cu; 0,52 g/t Au	1,4%Cu; 0,86 g/t Au	1,0%Cu; 0,3 g/t Au	2,43 g/t Au (minério supergênico)	1,22%Cu; 0,75g/tAu; 2,4g/tAg; 1200g/tW; 70g/tSn; 175g/tMo; 75g/tBi
Rochas encaixantes	Rochas meta-vulcanossedimentares de alto grau	Rochas meta-vulcanossedimentares de baixo grau	Diorito, riolito, dacito, rochas meta-vulcânicas	Meta-arenitos, meta-siltitos	Granito, meta-arenito
Alteração Hidrotermal	Cloritação, K-Fe-metassomatismo	Cloritação, carbonatação, K-Fe-metassomatismo	Cloritação, carbonatação, K-Fe-metassomatismo	Silicificação, veios de quartzo, cloritação, sericitização, turmalinização, caulinitização	Graisen (quartzo + muscovita ± clorita) e veios de quartzo
Cu-Fe-sulfetos (outros sulfetos)	Calcopirita + bornita ± calcocita	Calcopirita ± bornita	Calcopirita ± bornita	Calcopirita + pirita + pirrotita (galena, esfalerita, tenantita)	Calcopirita + pirita + pirrotita
Au-Ag	Au nativo	Au nativo (~12% Ag), hessita, muthmannita	Ag nativa	Au nativo (~25% Ag)	Au nativo (~24% Ag)
W-Bi-Sn	-	-	-	Wolframita, ferbelita, cassiterita, bismutinita, stanita	Ferberita, bismutinita, Bi nativo, cassiterita
Óxidos e silicatos de Fe	Grunerita, faialita, magnetita	Grunerita, magnetita	Magnetita ± hematita	Rara magnetita ± hematita	-
U-Th	Uraninita	Uraninita, uranofano, thorita, thorianita	Thorita	-	-
F-Cl	Fluorita	Fluorita, escapolita, ferropirosmalita	Fluorita	-	Fluorita
ETR-P	Allanita e apatita	Allanita, parisita, bastnásita, monazita, apatita	Y-tritomita, Y-synchysita, xenotima, monazita, apatita	Apatita	Monazita, xenotima
Mo	Molibdenita	Molibdenita	-	-	-
As-Co	Co-pentlandita, cobaltita, saflorita	Cobaltita	-	Arsenopirita	Arsenopirita (~12% Co)
Ganga	Biotita, almandina, quartzo, clorita, grenalita	Siderita, biotita, clorita, stilpnometano, turmalina	Quartzo, clorita, biotita, K-Feldspato, muscovita, stilpnometano, albite, calcita	Abundante quartzo, clorita, turmalina, sericitá, caulinita	Abundante quartzo, muscovita, clorita, turmalina
Referências	Lindenmayer 1990; Figueiredo et al. 1994; Réquia e Xavier 1995; Réquia e Fontboté 2001	Este trabalho (Anexos 2 a 4)	Este trabalho (Anexo 6)	Soares et al. 1994; Silva e Villas 1998	Este trabalho (Anexo 5)

**Tabela 5.** Resumo dos dados geocronológicos relacionados ao evento magmático-hidrotermal neoarqueano (~2,57 Ga) no Cinturão Cupro-Aurífero de Carajás.

Rocha	Idade (Ma)	Método	Material Datado	Evento Datado	Referência
Minério de Cu-Au de Igarapé Bahia	$2575 \pm 12$	U-Pb <sup>1</sup>	monazita	alteração hidrotermal e formação de minério	Este trabalho (ANEXO 4)
Granito Old Salobo	$2573 \pm 2$	U-Pb <sup>2</sup>	zircão	cristalização magnética	Machado et al. (1991)
Granito Itacaiúnas	$2560 \pm 37$	U-Pb <sup>2</sup>	zircão	cristalização magnética	Souza et al. (1996)
Granito Itacaiúnas	$2480 \pm 40$	Rb-Sr	rocha total	idade de resfriamento da intrusão	Montalvão et al. (1984)
Complexo Granítico Estrela	$2527 \pm 34$	Rb-Sr	rocha total	idade de resfriamento da intrusão	Barros e Barbey (1998)
Rocha meta-vulcânica encaixante do minério de Igarapé Bahia	$2577 \pm 72$	Rb-Sr	rocha total	atividade termal	Ferreira Filho (1985)
Minério de Cu-Au do depósito Salobo	$\sim 2550$	Re-Os	molibdenita	atividade hidrotermal e formação de minério	Réquia e Fontboté (2001)
Minério de Cu-Au do depósito Serra Verde	$2609 \pm 13$	Re-Os	molibdenita	atividade hidrotermal e formação de minério	Marschik et al (2001)

1: datação U-Pb pelo método SHRIMP, 2: datação U-Pb convencional.

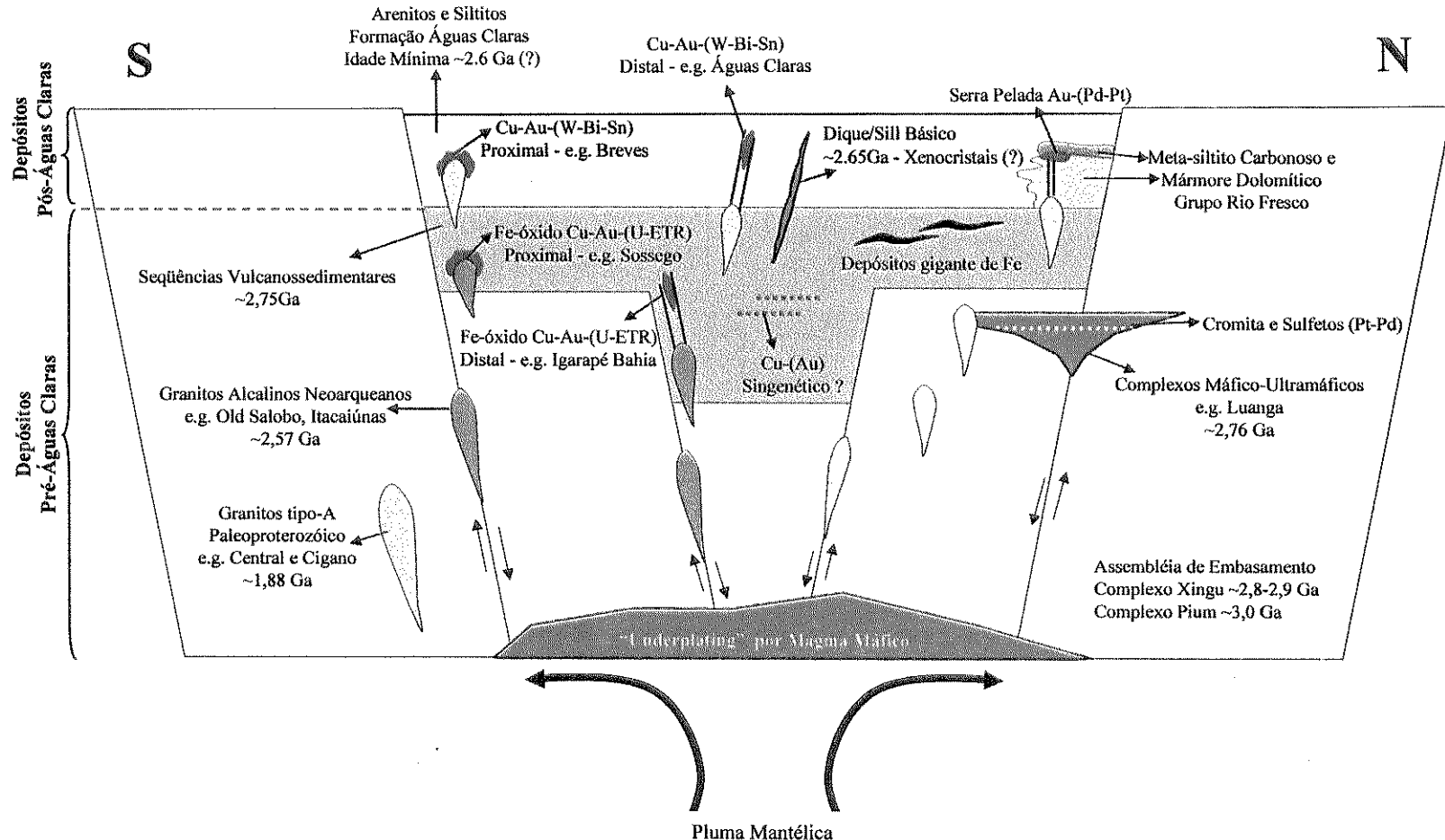


**Figura 2.** Síntese metalogenética regional do Cinturão Cupro-Aurífero de Carajás, relacionando o controle estrutural na ascensão de magmas e formação dos depósitos de Fe-óxido Cu-Au-(U-ETR) neoarqueanos e Cu-Au-(W-Bi-Sn) paleoproterozóicos. Encontram-se também representados os depósitos gigantes de ferro, o depósito de Pt-Pd de Luanga e o depósito de Au-Pd-Pt de Serra Pelada para ilustrar o conceito de permanência de metais no cinturão.

**Tabela 6.** Resumo dos principais atributos geológicos dos depósitos do tipo Fe-óxido Cu-Au-(U-ETR) e Cu-Au-(W-Bi-Sn) do Cinturão Cupro-Aurífero de Carajás.

Tipo de depósito	Fe-óxido Cu-Au-(U-ETR)	Cu-Au-(W-Bi-Sn)
Idade	~2,57 Ga	~1,88 Ga
$fO_2$	Oxidado (magnetita $\pm$ hematita)	Reduzido (pirrotita)
$a_{\Sigma S}$	Pobre em enxofre (calcopirita + bornita + calcocita primária)	Enriquecido em enxofre (pirrotita + pirita + calcopirita)
$SiO_2$	Pobre em quartzo	Abundantes veios de quartzo
Morfologia do minério	Corpos tabulares de brecha estruturalmente controlados	Corpos tabulares em zonas de falha e <i>ore shell</i> (greisen) em zonas de cúpula
Minerais de ETR	Monazita abundante Xenotima rara	Xenotima abundante Monazita rara
F-Cl	Sistema hidrotermal rico em F (fluorita) e Cl (ferropirosmalita, escapolita, Cl-apatita)	Sistema hidrotermal rico em F (fluorita)
Alteração Hidrotermal	Carbonatação (siderita), Cloritização (Fe-clorita), Fe-metassomatismo (grunerita, faialita, magnetita, hematita)	Carbonatação incipiente (veios contendo calcita), graisen (quartzo + muscovita $\pm$ clorita), veios de quartzo com textura em pente
Tonelagem	Depósitos maiores que 200 Mt até 1 bilhão de toneladas	Os depósitos conhecidos não ultrapassam 50 Mt

## 6. Referências

- Almada, M.C.O. 1998. O Corpo Acampamento Sul do depósito Bahia, Carajás: características geológicas e fluidos hidrotermais. Tese de Mestrado (inédito), Belém, Brasil, Universidade Federal do Pará, 99 p.
- Araújo, O.J.B. e Maia, R.G.N. 1991. Serra dos Carajás, folha SB.22-Z-A, Estado do Pará. Brasília, Programa Levantamentos Geológicos Básicos do Brasil, DNPM, 136 p.
- Avelar, V.G.; Lafon, J.M.; Correia, F.C.Jr.; Macambira, B.E.M. 1999. O magmatismo arqueano da região de Tucumã, Província Mineral de Carajás, Amazônia Oriental, Brasil: novos dados geocronológicos. Rev Bras Geociênc 29:453-460.
- Barrie, C.T. e Hannington, M.D. 1999. Classification of volcanic-associated massive sulfide deposits based on host-rock composition: In: Barrie, C.T. and Hannington (ed.) Volcanic-associated massive sulfide deposits: processes and examples in modern and ancient settings. Reviews in Economic Geology, vol. 8, 1-11 p.
- Barros, C.E.M. e Barbey, P. 1998. A importância da granitogênese tardi-arqueana (2.5Ga) na evolução tectono-metamórfica da Província Mineral de Carajás – O Complexo Granítico Estrela e sua auréola de contato. Revista Brasileira de Geociências, 28(4): 513-522.
- Cathelineau M. 1988. Cation site occupancy in chlorites and illites as a function of temperature. Clay Minerals, 23:471-485.
- Cordeiro, A.A.C.. 1999. Pesquisa mineral: panorama atual da CVRD na Amazônia. VI Simpósio de Geologia da Amazônia, 80-83 p.
- Dall'Agnol, R.; Teixeira, N.P.; Magalhães, M.S. 1993. Diagnostic features of the tin-specialized anorogenic granites of the Eastern Amazonian Region. Anais da Academia Brasileira de Ciência 65: 33-50.
- Dall'Agnol, R.; Lafon, J.M.; Macambira, M.J.B. 1994. Proterozoic anorogenic magmatism in the Central Amazonian Province, Amazonian Craton: geochronological, petrological and geochemical aspects. Min Petrol 50: 113-138.

- Dias, G.S.; Macambira, M.J.B.; Dall'Agnol, R.; Soares, A.D.V.; Barros, C.E.M. 1996. Datação de zircões de *sill* de metagabro: comprovação da idade arqueana da Formação Águas Claras, Carajás, Pará. V Simpósio de Geologia da Amazônia, 376-379 p.
- DOCEGEO - Rio Doce Geologia e Mineração S.A. 1988. Província Mineral de Carajás. Litoestratigrafia e principais depósitos minerais. In: SBG, Congresso Brasileiro de Geologia, 35, Belém, Anexo aos Anais, 165 pp
- Farias, N.R. e Saueressig, R. 1982. Jazida de cobre Salobo 3A. Simpósio de Geologia da Amazônia, I. 1982. Belém, Anais, pp 61-73.
- Ferreira Filho, C.F. 1985. Geologia e mineralizações sulfetadas do Prospecto Bahia, Província Mineral de Carajás. Tese de Mestrado (inédito), Brasília, Brasil, Universidade de Brasília, 112 p.
- Figueiredo, B.R.; Réquia, K.C.M.; Xavier, R.P. 1994. Post-depositional changes in the Salobo ore deposit, Carajás Mineral Province, northern Brazil. Comunicaciones, 45:23-32.
- Gibbs, A.K.; Wirth, K.R.; Hirata, W.K; Olszewski, W.J. 1986. Age and composition os the Grão Pará Group volcanics, Serra dos Carajás. Revista Brasileira de Geociências, 16(2): 201-211.
- Goldfarb, R.J. e Groves, D.I. 2001. Orogenic gold deposits and geological time: a global synthesis. Ore Geology Reviews, 18: 1-75.
- Groves, D.I. 1993. The crustal continuum model for late-Archean lode-gold deposits of the Yilgarn Block, Western Australia. Mineralium Deposita, 28: 366-374.
- Hitzman, M.W.; Oreskes, N.; Einaudi, M.T. 1992. Geological characteristics and tectonic setting of Proterozoic iron oxide (Cu-U-Au-REE) deposits. Precambrian Research, 58: 241-287.
- Holdsworth, R.E. e Pinheiro, R.V.L. 2000. The anatomy of shallow-crustal transpressional structures: insights from the Archean Carajás fault zone, Amazon, Brazil. Journal of Structural Geology, 22: 1105-1123.
- Huhn, S.R.B. e Nascimento, J.A.S., 1996, São os depósitos cupríferos de Carajás do tipo Cu-Au-U-ETR?: In: Marcondes & Angélica (eds.) Contribuições à Geologia da Amazônia, p.143-160.

- Huhn, S.R.B.; Macambira, M.J.B.; Dall'Agnol, R. 1999a. Geologia e geocronologia Pb/Pb do granito alcalino Arqueano Planalto, Região da Serra do Rabo, Carajás - PA. VI Simpósio de Geologia da Amazônia, 463-466 p.
- Huhn, S.R.B; Santos, A.B.S.; Amaral, A.F.; Ledsham, E.J.; Gouvea, J.L.; Martins, L.P.; Montalvão, R.G.M; Costa, V.G. 1988. O terreno “granito greenstone” da região de Rio Maria - Sul do Pará. XXXV Cong Bras Geol, Anais, 3: pp 1438-1452
- Huhn, S.R.B.; Souza, C.I.J.; Albuquerque, M.C.; Leal, E.D.; Brustolin, V. 1999b. Descoberta do depósito Cu(Au) Cristalino: geologia e mineralização associada – Região da Serra do Rabo – Carajás – PA. VI Simpósio de Geologia da Amazônia, 140-143 P.
- Issler, R.S. e Lima, M.I.C. 1987. Amazonic Craton (Brazil) granitogenesis and its relation to geotectonic units. Revista Brasileira de Geociências, 17(4): 426-441.
- Lancaster Oliveira, J.A.; Fanton, J.; Almeida, A.J.; Leveille, R.A.; Vieira, S. 2000. Discovery and geology of the Sossego copper-gold deposit, Carajás District, Pará State, Brazil. 31 International Geological Congress, [abstracts].
- Large, R.R. 1992. Australian volcanic-hosted massive sulfide deposits: features, styles, and genetic model. Economic Geology, 87: 471-510.
- Lindenmayer, Z.G. 1990. Salobo Sequence, Carajás, Brazil: geology, geochemistry and metamorphism. Tese de Doutorado (inédita), London, Canada, University of Western Ontario, 407 p.
- Lindenmayer, Z.G.; Ronchi, L.H.; Laux, J.H. 1998. Geologia e geoquímica da mineralização de Cu-Au primária da mina de Au do Igarapé Bahia, Serra dos Carajás. Revista Brasileira de Geociências, 28(3): 257-268.
- Machado, N.; Lindenmayer, Z; Krogh, T.E.; Lindenmayer, D. 1991. U-Pb geochronology of Archean magmatism and basement reactivation in the Carajás area, Amazon Shield, Brazil. Precambrian Research, 49: 329-354
- Marschik, R.; Mathur, R.; Spangenberg, J.E.; Ruiz, J. Leveille, R.A.; Almeida, A.J. 2001. The Serra Verde Cu-Mo-Au deposit, Carajás Mineral Province, Pará State, Brazil. Geological Society of America Annual Meeting, Abstracts, vol. 33 No.6.

- Montalvão, R.G.M; Tassinari, C.C.G.; Bezerra, P.E.L. 1984. Geocronologia dos granitóides e gnaisses das regiões do Rio Maria, Fazenda Mata Geral e Rio Itacaiunas, Sul do Pará (Distrito Carajás-Cumaru). XXXIII Congresso Brasileiro de Geologia, 2757-2766 p.
- Muogeot, R.; Respaut, J.P.; Briquel, L.; Ledru, P.; Milesi, P.; Lerouge, C.; Marcoux, E.; Huhn, S.R.B.; Macambira, M.J.B. 1996. Isotope Geochemistry constrains for Cu, Au mineralizations and evolution of the Carajás Province (Pará, Brazil). XXXIX Congresso Brasileiro de Geologia, 321-324 p.
- Naldrett, A.J. 1989. Stratiform PGE deposits in layered intrusions. Reviews in Economic Geology, vol. 4, 135-166 p.
- Nelson, D.R.; Trendall, A.F.; Altermann, W. 1999. Chronological correlations between the Pilbara and Kaapvaal cratons. Precambrian Research, 97: 165-189.
- Nogueira, A.C.R.; Truckenbrod, W.; Costa, J.B.S.; Pinheiro, R.V.L. 1994. Análise faciológica e estrutural da Formação Águas Claras, Pré-Cambriano da Serra dos Carajás. In: 4 Simpósio de Geologia da Amazônia, Belém, Resumos Expandidos, SBG, pp 363-364.
- Nogueira, A.C.R.; Truckenbrod, W.; Pinheiro, R.V.L. 2000. Storm and tide-dominated siliciclastic deposits of the Archean Águas Claras Formation, Serra dos Carajás, Brazil. In: 31 International Geological Congress, Rio de Janeiro, Abstracts.
- Oliveira, C.G.; Tazava, E.; Tallarico, F.H.B.; Santos, R.V.; Gomes, C. 1998. Gênese do depósito de Au-Cu-(U-ETR) de Igarapé Bahia, Província Mineral de Carajás. XL Congresso Brasileiro de Geologia, 137 p.
- Olszewski, W.J.; Wirth, K.R.; Gibbs, A.K.; Gaudette, H.E. 1989. The age, origin and tectonics of the Grão Pará Group and associated rocks, Serra dos Carajás, Brazil: Archean continental volcanism and rifting. Precambrian Research, 42: 229-254.
- Pidgeon, R.T.; Macambira, M.J.B.; Lafon, J.M. 2000. Th-U-Pb isotopic systems and internal structures of complex zircons from enderbite from the Pium Complex, Carajás Province, Brazil: evidence for ages of granulite facies metamorphism and protolith of the enderbite. Chem Geol 166: 157-171

- Pinheiro, R.V.L. e Holdsworth, R.E. 1997. Reactivation of Archean strike-slip fault systems, Amazon region, Brazil. *Journal of the Geological Society*, 154: 99-103.
- Réquia, K.C.M. e Fontboté, L. 2001. The Salobo iron oxide copper-gold hydrothermal system, Carajás Mineral Province, Brazil. *Geological Society of America Annual Meeting, Abstracts*, vol. 33 No.6.
- Réquia, K.C.M. e Xavier, R.P. 1995. Fases fluidas na evolução metamórfica do depósito polimetálico de Salobo, Província Mineral de Carajás, Pará. *Revista da Escola de Minas*, 49(2):117-122.
- Ribeiro, A.M.R. 1989. Estudo geoquímico do sistema hidrotermal relacionado à mineralização cuprífera da Área Bahia, Serra dos Carajás, Pará. Tese de Mestrado (inédito), Belém, Brasil, Universidade Federal do Pará, 134 p.
- Rigon, J.C.; Munaro, P.; Santos, L.A.; Nascimento, J.A.S.; Barreira, C.F. 2000. The Alvo 118 copper-gold deposit: geology and mineralization, Serra dos Carajás, Pará: 31 International Geological Congress, Abstracts.
- Salomon, M. e Groves, D.I. 2000. The geology and origin of Australia's mineral deposits. Centre for Ore Deposit Research and Centre for Global Metallogeny, Publication No. 32, 1002 p.
- Santos J.O.S.; Groves, D.I.; Hartmann, L.A.; Moura, M.A.; McNaughton, N.J. 2001 Gold deposits of the Tapajós and Alta Floresta Domains, Tapajós-Parima orogenic belt, Amazon Craton, Brazil. *Mineralium Deposita* 36(3/4): 278-299.
- Silva, C.M.G. e Villas, R.N. 1998. The Águas Claras Cu-sulfide ± Au deposit, Carajás Region, Pará, Brazil: geological setting, wall-rock alteration and mineralizing fluids. *Revista Brasileira de Geociências*, 28(3): 315-326.
- Slack, J.F. 1993. Descriptive and grade-tonnage models for Besshi-type massive sulphide deposits. In: Kirkham, R.V.; Sinclair, W.D.; Thrope, R.I.; Duke, J.M (ed.). *Mineral Deposit Modeling*. Geological Association of Canada, Special Paper 40, 343-371 p.
- Soares A.D.V.; Santos, A.B.; Vieira, E.A.; Bella, V.M.; Martins, L.P.B. 1994. Área Águas Claras: contexto geológico e mineralizações. 4 Simpósio de Geologia da Amazônia, 379-382 p.

- Soares, A.D.V.; Ronzê, P.C.; Santos, M.G.S.; Leal, E.D.; Barreira, C.F. 1999. Geologia e mineralizações do depósito de Cu-Au Alemão – Província Mineral de Carajás (PA): VI Simpósio de Geologia da Amazônia, 144-147 p.
- Souza, S.R.B.; Macambira, M.J.B.; Scheller, J. 1996. Novos dados geocronológicos para os granitos deformados do Rio Itacaiunas (Serra dos Carajás, PA); implicações estratigráficas. V Simpósio de Geologia da Amazônia, 380-383 p.
- Suita M.F.T e Nilson, A.A. 1988. Geologia do Complexo Máfico-Ultramáfico Luanga (Província Mineral de Carajás, Pará) e das unidades encaixantes. XXXV Congresso Brasileiro de Geologia, 6: 2813-2823.
- Tallarico, F.H.B. 1996. Projeto de revisão do modelo geológico da mina de Igarapé Bahia – petrografia, química mineral e litogeoquímica. Relatório interno da Companhia Vale do Rio Doce (inédito), 57 p.
- Tallarico, F.H.B.; Oliveira, C.G.; Figueiredo, B.R. 2000. The Igarapé Bahia Cu-Au mineralization, Carajás Province. Revista Brasileira de Geociências, 30: 230-233.
- Tallarico, F.H.B.; Rego, J.L.; Oliveira, C.G. 1998. A mineralização de Au-Cu de Igarapé Bahia – Carajás: um depósito da classe óxido de Fe (Cu-U-Au-ETR). XL Congresso Brasileiro de Geologia, 116 p.
- Tassinari, C.C.G. e Macambira, M.J.B. 1999. Geochronological provinces of the Amazonian Craton. *Episodes* 22(3): 174-182
- Tazava, E. 1999. Mineralização de Au-Cu-(±ETR-U) associada às brechas hidrotermais do depósito de Igarapé Bahia, Província Mineral de Carajás, PA. Tese de Mestrado (inédito), Ouro Preto, Brasil, Universidade Federal de Ouro Preto, 81 p.
- Toro, M.A.G. 2002. Geocronologia e geoquímica isotópica dos depósitos de Cu-Au Igarapé Bahia e Gameleira, Província Mineral de Carajás (PA), Brasil. Tese de Doutorado (inédito), Belém, Brasil, Universidade Federal do Pará, 214p.
- Trendall, A.F.; Basei, M.A.S.; Laeter, J.R.; Nelson, D.R. 1998 SHRIMP zircon U-Pb constraints on the age of the Carajás formation, Grão Pará Group, Amazon Craton. *J S Am Earth Sci* 11(3): 265-277.
- Tolbert, G.E.; Tremaine, J.W.; Melcher, G.C.; Gomes, C.B. 1971. The recently discovered Serra dos Carajás iron deposit, northern Brazil. *Econ Geol* 66: 985-994.

- Veizer, J. e Compston, W. 1976.  $^{87}\text{Sr}/^{86}\text{Sr}$  in Precambrian carbonates as an index of crustal evolution. *Geochimica et Cosmochimica Acta*, 40: 905-914.
- Vieira, E.A.P.; Saueressig, R.; Siqueira, J.B.; Silva, E.R.P.; Rego, J.L.; Castro, F.D.C. 1988, Caracterização geológica da jazida polimetálica do Salobo 3A – reavaliação. XXXV Congresso Brasileiro de Geologia, 97-111 p.
- Wirth, K.R.; Gibbs, A.K.; Olszewski, W.J. Jr. 1986. U-Pb ages of zircons from the Grão Pará and Serra dos Carajás granite, Pará, Brazil. *Rev Bras Geociênc* 16:195-200.

## **ANEXO 1**

O método SHRIMP



## O método SHRIMP

### *Seleção de amostras*

Os depósitos de Igarapé Bahia, Breves e Cento e Dezoito foram visitados e documentados durante duas etapas de campo. Após a primeira etapa de campo foram conduzidos nos laboratórios da UNICAMP uma série de estudos de petrografia e geoquímica mineral e de rocha que tiveram como objetivo caracterizar as rochas encaixantes e minérios dos depósitos estudados. Estes estudos subsidiaram a seleção das rochas e minerais adequados aos trabalhos de geocronologia. A segunda etapa de campo foi conduzida como o propósito específico de coletar amostras para a geocronologia.

Através dos estudos petrográficos dos depósitos concluiu-se que as rochas encaixantes e minérios continham zircão e ETR-fosfatos (monazita e xenotima) respectivamente. Estes minerais são adequados à determinação de idades radiométricas pelo método U-Th-Pb, porém o reduzido tamanho dos cristais de monazita e xenotima ( $\leq 50 \mu\text{m}$ ) não favorecia a utilização de espctrômetros convencionais. Assim, optou-se pela utilização da técnica SHRIMP (Sensitive High Resolution Ion Microprobe) que permite a realização de análises isotópicas do sistema U-Th-Pb em áreas de até  $7 \mu\text{m}$ . A pesquisa contou portanto com um estágio no Centre for Global Metallogeny da Universidade de Western Australia para a condução das análises isotópicas pelo método SHRIMP.

### *Preparação de amostras para geocronologia SHRIMP*

As amostras de zircão foram concentradas de forma tradicional uma vez que dispunha-se de uma quantidade apreciável de amostra original ( $> 20 \text{ kg}$ ) e os cristais de zircão eram relativamente abundantes e de tamanho razoável. Após o desmonte da amostra original, os minerais pesados foram concentrados via bateia e posteriormente trabalhados em separador magnético para eliminação de minerais como clorita e siderita que apresentam alta susceptibilidade magnética. As frações não magnéticas foram ainda tratadas em iodeto de metileno para a remoção de fases indesejadas. Ocasionalmente foi necessário o tratamento em ácido nítrico para a remoção de sulfetos. Os concentrados finais foram então

examinados ao estereomicroscópio para a seleção e coleta dos cristais de zircão a serem analisados. Os cristais selecionados foram montados, juntamente com os padrões, numa seção polida de grãos que seguiu para o SHRIMP. Todos as amostras de zircão desta pesquisa e uma amostra de xenotima do minério de Cu-(Au) do depósito Cento e Dezoito (UWA-B36D) foram preparadas adotando esta rotina (Fig. 1A).

A concentração de xenotima e monazita, a partir de amostras de minério, revelou-se inviável adotando-se a mesma rota empregada nas amostras de zircão. O principal motivo foi o reduzido tamanho dos cristais ETR-fosfato ( $\leq 50 \mu\text{m}$ ) que não apresentavam liberação adequada mesmo quando as amostras eram reduzidas a frações granulométricas bastante finas (-100#). A solução foi adotar uma rotina alternativa e inédita de preparação de amostras. Os cristais de ETR-fostatos foram identificados e selecionados em lâminas delgadas e seções polidas de minério utilizando-se o microscópio eletrônico de varredura (MEV). Após a seleção dos cristais desejados, áreas de aproximadamente 2 milímetros de diâmetro foram recortadas das lâminas e seções polidas utilizando-se uma pequena broca diamantada (Figura 2A). Estes pequenos discos contendo os minerais de interesse foram então montados, juntamente com os padrões, numa seção polida que seguiu para o SHRIMP. O procedimento é extremamente laborioso, porém permitiu o perfeito controle petrográfico dos cristais datados. Todas as amostras de monazita e as demais amostras xenotima desta pesquisa seguiram este procedimento de preparação.

As seções polidas contendo grãos ou discos recortados de lâminas e/ou seções polidas, foram cuidadosamente documentadas através de uma série de imagens óticas e eletrônicas. Inicialmente foram preparados mapas das seções polidas que foram utilizados na navegação tanto no MEV quanto no SHRIMP (Figuras 1B e 2B). Estes mapas consistem de mosaicos de fotomicrografias produzidas em microscópio ótico convencional utilizando-se um aumento de 20x. Em seguida os mapas foram divididos em quadros que foram ampliados por meio de fotomicrografias com luz transmitida e refletida ou fotomosaicos no MEV com a finalidade de se obter maior detalhe na navegação (Figuras 1C e 2C).

A última etapa na preparação das amostras foi a documentação dos grãos selecionados para análise num MEV ambiental (com câmara de baixo vácuo) utilizando-se detectores de *back-scattering electrons* (BSE), *secondary electrons* (SE), e *cathodoluminescence* (CL). A utilização do MEV ambiental além de agilizar os trabalhos de microscopia pelo fato de

dispensar a metalização das preparações e não requerer estabelecimento de alto vácuo, permitiu também a aquisição de imagens de *charge-induced contrast* (CC). O CC é uma técnica recente e baseia-se no contraste de carga elétrica na superfície dos cristais decorrente de imperfeições cristalográficas, zoneamentos químicos e/ou microfraturas (Griffin 2000). Este tipo de imagem somente pode ser obtido num MEV ambiental uma vez que o contraste de carga que gera a imagem é produzido pelas moléculas de H<sub>2</sub>O que pressurizam a câmara do microscópio.

As imagens de CL (Figura 1D) foram utilizadas para identificar zonas com diferentes concentrações de urânio. Zonas com teores muito elevados de urânio são indesejáveis, pois geralmente estão fortemente metamictizadas havendo perda de chumbo. As imagens de SE/CC foram extremamente úteis para se identificar microfraturas nos cristais (Figura 1E). Estas também são regiões que devem ser evitadas pois há acumulo de chumbo comum, indesejável nos trabalhos de geocronologia. As imagens de BSE (Figura 1F e 2D) foram utilizadas para identificar zonações ou diferenças de composição nos cristais, que poderiam ter algum significado geológico.

#### *Análises isotópicas pelo método SHRIMP*

O SHRIMP é uma microssonda iônica de alta resolução com a qual é possível se dosar diferentes isótopos (*cf.* Williams 1998). Na Figura 3 tem-se um diagrama esquemático do equipamento ilustrando seus principais componentes. A fonte de excitação da amostra é um feixe de íons de oxigênio (feixe primário), que é focalizado na amostra por uma série de lentes eletromagnéticas. Ao atingir a amostra o feixe primário tem um diâmetro entre 7 e 20 µm a depender do arranjo analítico, e um ângulo de incidência de 45° com a amostra. No *sputtering pit*, ou “sítio de análise”, átomos do mineral sob investigação são extraídos, ionizados e acelerados em direção à unidade de contagem, constituindo assim um feixe de íons secundário. Após a extração, o feixe secundário passa por um analisador eletrostático que tem a função de filtrar as diferentes partículas pela sua energia cinética, uma vez que os isótopos mais pesados tem maior inércia. A seguir os íons passam por um campo magnético que influencia a trajetória dos diferentes isótopos. Os isótopos mais

pesados posicionam-se na parte externa do arco e os mais leves na sua porção interna. Finalmente uma unidade de contagem faz a leitura dos diferentes isótopos.

O fato do feixe de íons primário SHRIMP possuir um diâmetro da ordem de dezenas de  $\mu\text{m}$ , possibilitou a realização de análises com grande resolução espacial. Os sítios de análise foram selecionados em zonas de alto contraste de CL, i.e., zonas com concentrações moderadas de urânio, evitando-se portanto as porções metamictizadas onde poderia ter havido perda de chumbo. As porções do cristal que apresentavam microfraturas também foram evitadas pois potencialmente poderiam conter chumbo comum. Com isso a qualidade dos dados analíticos foi otimizada. A grande resolução espacial também possibilitou a realização de múltiplas análises em um mesmo cristal, permitindo a identificação de eventuais núcleos herdados (xenocróstais) e bordas epitaxiais mais jovens em cristais de zircão. Outro benefício foi a possibilidade de realizar datações *in situ* de diminutos cristais de monazita e xenotima nos discos extraídos das lâminas e seções polidas.

O SHRIMP além de proporcionar grande resolução espacial, possui também uma resolução espectral da ordem de 5000, i.e., pode discriminar dois feixes de íons que diferem entre si por 1:5000 unidades de massa atômica, o que é suficiente para resolver a maioria das interferências isobáricas. A sensibilidade da unidade de contagem é de aproximadamente 20 cps/seg/ppm/nA, o que é excepcionalmente elevado em comparação com outros equipamentos similares. O benefício da sensibilidade do equipamento se traduz na estatística de contagem que é otimizada. Como o erro associado à medida é aproximadamente igual a  $n^{1/2}$  (onde  $n$  = número de contagens), quanto maior a sensibilidade, maior é o número de contagens e por decorrência menor o erro associado a medida. Estas características asseguraram a geração de uma acervo de dados geocronológicos de ótima qualidade.

Após a etapa analítica, os dados foram reduzidos e sua qualidade é testada. O primeiro critério de qualidade adotado foi a concentração de urânio, que em geral não pode exceder 300 ppm para zircões arqueanos. O segundo critério observado foi a discordância das razões U/Pb em relação à concórdia, que não pode ser superior a 5%. O terceiro critério foi a presença de chumbo comum, diagnosticada pela intensidade do isótopo  $^{204}\text{Pb}$ . A quantidade de chumbo comum é expressa pela função  $f_{206}$  (onde  $f_{206} =$

$^{206}\text{Pb}_{\text{comum}}/^{206}\text{Pb}_{\text{total}}$ ) que deve ser inferior a 1%. O último critério de qualidade foi o MSWD (*mean square width distance*) que é uma medida estatística do alinhamento dos dados na reta que intercepta a concórdia. O MSWD deve ser menor ou igual a  $[1 + (2/f)^{1/2}]$ , onde  $f$  = número de análises – 2. De maneira geral, dados de qualidade internacional devem apresentar um MSWD menor do que 2. Foram utilizados nos cálculos das idades somente as análises que obedeciam estes critérios de qualidade. O resultado foi a produção de um conjunto de idades radiométricas de alta precisão com erros muito satisfatórios.

### *Referências*

- Griffin, B.J. 2000. Charge contrast imaging of material growth and defects in environmental scanning electron microscopy – linking electron emission and cathodoluminescence. *Scanning*, 22: 234-242.
- Williams, I.S. 1998. U-Th-Pb geochronology by ion microprobe. In: McKibben M.A., Shanks III; W.C., Ridley I. (ed.). Application of microanalytical techniques to understanding mineralizing processes. *Reviews in Economic Geology* vol. 7: 1-35 p.

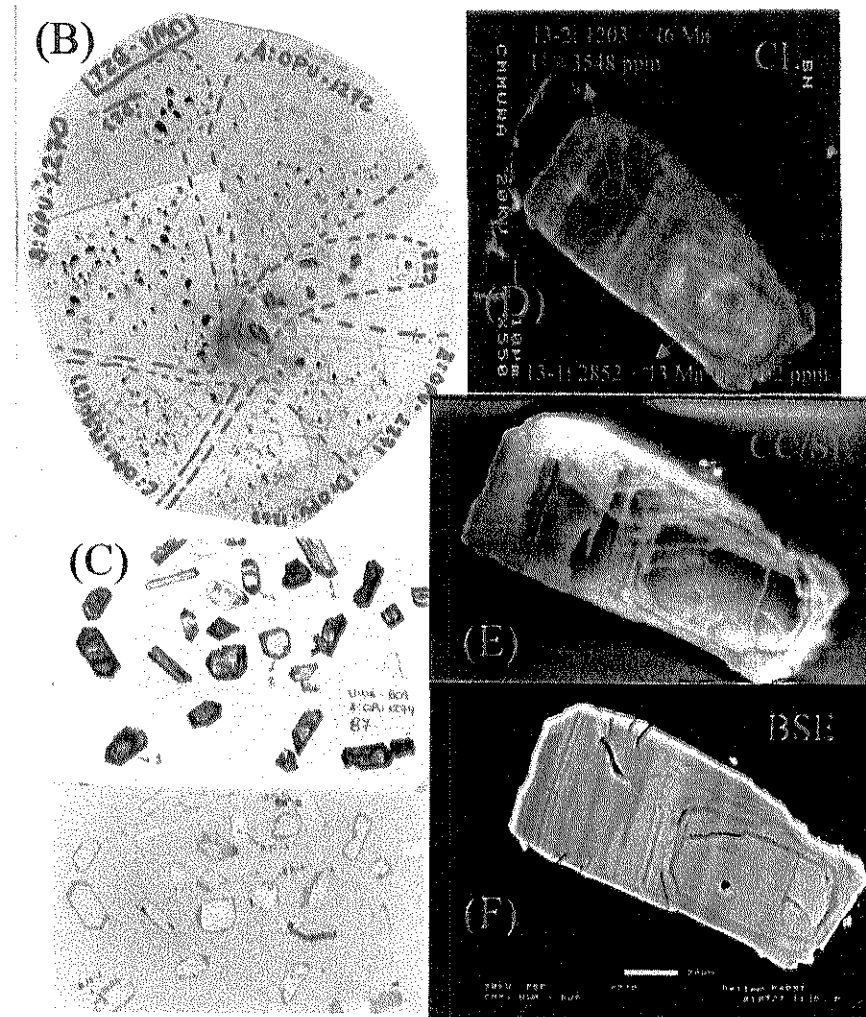
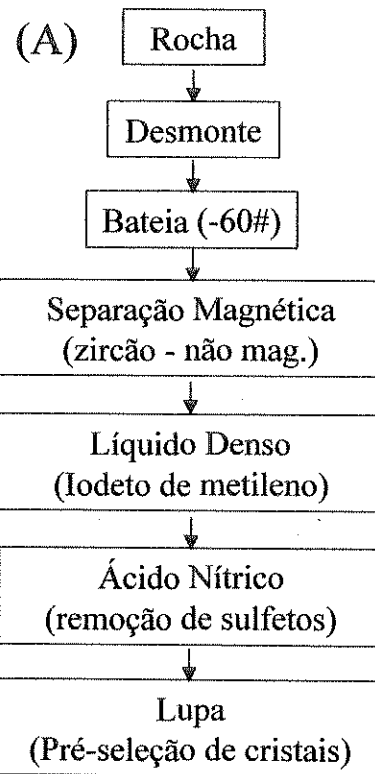


**Figura 1.** Quadro esquemático da preparação convencional de amostras para geocronologia SHRIMP. A: fluxograma de concentração do mineral de interesse. B: mapa da seção polida contendo cristais de zircão e o padrão (CZ3). C: fotomicrografias de ampliação dos quadros do mapa utilizando luz transmitida e refletida. D, E e F: imagens de catodoluminescência (CL), *charging contrast* (CC/SE) e elétrons retro-espalhados (BSE), respectivamente, de um mesmo cristal de zircão selecionado para análise (círculos na imagem de CL indicam as áreas analisadas no cristal).

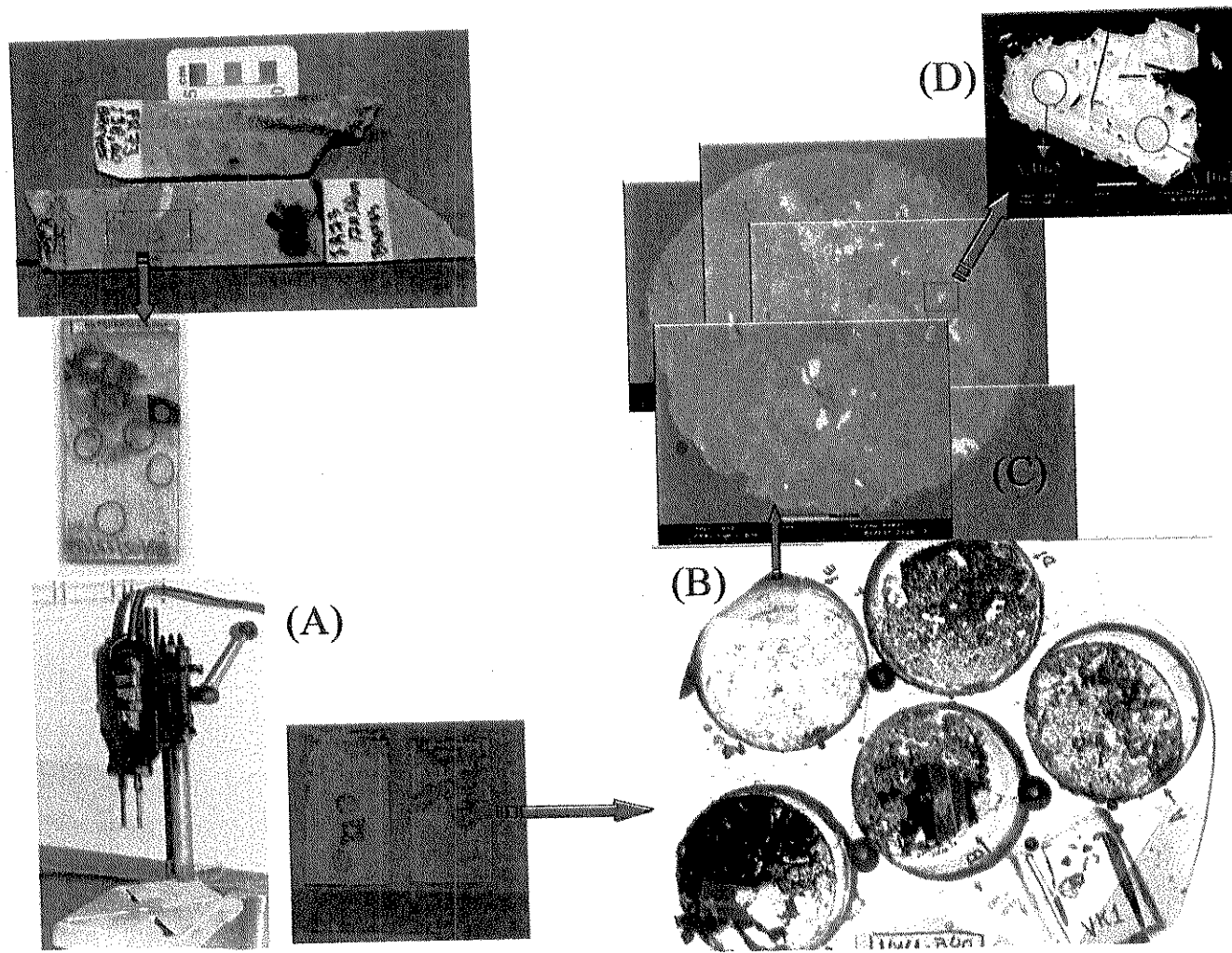


**Figura 2.** Quadro esquemático da preparação de amostras para geocronologia SHRIMP a partir de lâminas e/ou seções polidas. A: seleção e corte de áreas na lâmina delgada contendo minerais de interesse. B: mapa da seção polida montada com os discos e o padrão (VK1). C: fotomosaico dos discos utilizando imagens de elétrons retro-espalhados. D: imagem de elétrons retro-espalhados de detalhe do cristal selecionado para análise (os círculos indicam áreas analisadas no cristal).

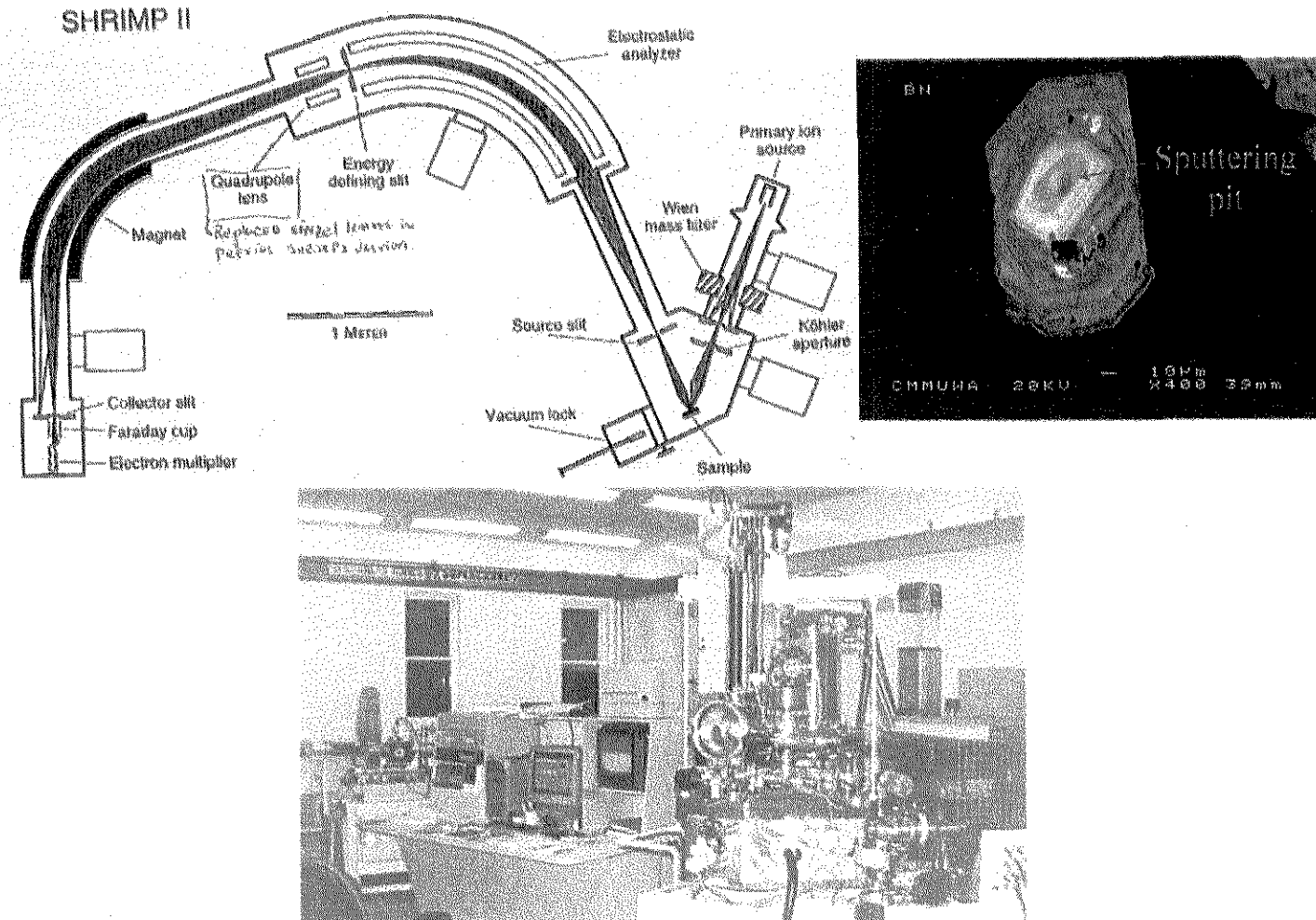


**Figura 3** – Diagrama esquemático da microsonda iônica SHRIMP, extraído de Williams (1988), mostrando os principais componentes de sua ótica iônica e a trajetória dos feixes de íons primário e secundário. No canto superior direito um detalhe do “sputtering pit”, ou sítio de análise, para ilustrar a capacidade de resolução espacial do equipamento. Na porção inferior uma fotografia do laboratório de SHRIMP da Curtin University of Technology que é operado em associação com o Centre for Global Metallogeney da Universidade de Western Australia.

## **ANEXO 2**

The Igarapé Bahia Cu-Au mineralization, Carajás Province



# THE IGARAPÉ BAHIA CU-AU MINERALIZATION, CARAJÁS PROVINCE

FERNANDO HENRIQUE BUCCO TALLARICO<sup>1</sup>, CLAUDINEI GOUVEIA DE OLIVEIRA<sup>2</sup>  
AND BERNARDINO RIBEIRO FIGUEIREDO<sup>1</sup>

**ABSTRACT** The Igarapé Bahia Cu-Au mineralization is hosted by an Archean, low-grade metavolcano-sedimentary sequence. The orebodies define an ellipsoidal structure and are associated with subvertical breccia units located at the contact between two distinct units of the host sequence. Mineralized breccias include fragments of both footwall and hanging wall, which are cemented by variable amounts of chlorite, siderite, magnetite, chalcopyrite, K-bearing phases and minor U-REE-minerals. Quartz diorite dikes that disrupt the host rocks show a variety of textures, ranging from weakly altered granophytic terms to intensely venuelated and brecciated rocks. Hydrothermal alteration of dikes includes propylitization, potassification and local albitization. Based on ore petrology and geochemical data (major elements, REE, oxygen and carbon stable isotopes) it is proposed that the progressive interaction of a hot saline and acid, deep-seated fluid with a low-temperature less saline and oxidizing meteoric solutions is the most likely depositional mechanism of the Igarapé Bahia mineralization. The resemblance of the alteration styles of mineralized breccias and dioritic dikes suggest that both have interacted with the same hydrothermal fluid. Thus, the dioritic dikes could have been the source of heat and of magmatic fluids during the final stages of epicrustal emplacement.

**Keywords:** Carajás Province, Igarapé Bahia, copper, gold, uranium, rare earth elements

**INTRODUCTION** The Carajás Basin (Itacaiúnas Supergroup) is located in northern Brazil, on the eastern border of the Archean Amazon Craton (Docegeo 1988) (Fig. 1). Basement rocks consist of gneiss and migmatite of the Xingú Complex (*ca.* 2.8 Ga - Machado *et al.* 1991) and the E-W-trending orthogranulites of the Pium Complex (*ca.* 3.0 Ga - Rodrigues *et al.* 1992). The Carajás Basin includes metavolcano-sedimentary rocks, of different metamorphic grades, deposited during Late Archean time (*ca.* 2.75 Ga - Machado *et al.* 1991). Sandstone and siltstone of a marine environment (Águas Claras Formation - Araújo and Maia 1991), overlie these rocks. The Carajás Basin was intruded by granitic magmas of distinct ages and compositions. Archean intrusions include granites and diorites of the Plaqué Suite (*ca.* 2.74 Ga - Huhn *et al.* 1999) and younger alkaline granites (*ca.* 2.5 Ga) such as the Estrela Complex (Barros *et al.* 1992) and the Old Salobo Granite (Machado *et al.* 1991). Paleoproterozoic intrusions (*ca.* 1.88 Ga - Machado *et al.* 1991) include several anorogenic granitic plutons (e.g. Central Carajás Granite, Cigano Granite).

A striking feature of the Carajás Basin is the large number of Cu-Au mineralizations that are stratigraphically and tectonically related. These are collectively known as the Carajás Copper-Gold Belt, including the Igarapé Bahia Deposit. The proposed genetic models for

the Igarapé Bahia Deposit are: (a) syngenetic, volcanic-associated or Besshi-type deposits (e.g. Ferreira Filho 1985, Almada 1998), (b) hydrothermal Fe-oxide Cu-Au-(U-REE) mineralization (e.g. Huhn 1996, Tallarico 1996, Tazava 1999), (c) epigenetic mineralization related to anorogenic Proterozoic granitic plutons (e.g. Lindenmayer *et al.* 1998) and (d) multistage genesis involving remobilization of primary Archean mineralization during Proterozoic time (e.g. Ribeiro 1989).

The purpose of this work is to present the diagnostic geological attributes, i.e. the descriptive model (Barton 1993) of the Igarapé Bahia primary mineralization. The present study includes the results of fieldwork, petrography, geochemistry (including REE, oxygen and carbon stable isotopes) and mineralogical investigation by XRD, SEM and EMPA. Finally, the data are modelled to investigate the fluid constraints and discuss the genetic alternatives.

**GEOLOGY OF THE IGARAPÉ BAHIA DEPOSIT** The Igarapé Bahia Group The Igarapé Bahia Deposit is hosted by metavolcano-sedimentary rocks with very low-grade hydrothermal-metamorphic assemblages (Igarapé Bahia Group). Ductile deformation is absent and primary structures and textures are usually preserved. Volcanic rocks including aphanitic, vesicular and microporphyratic

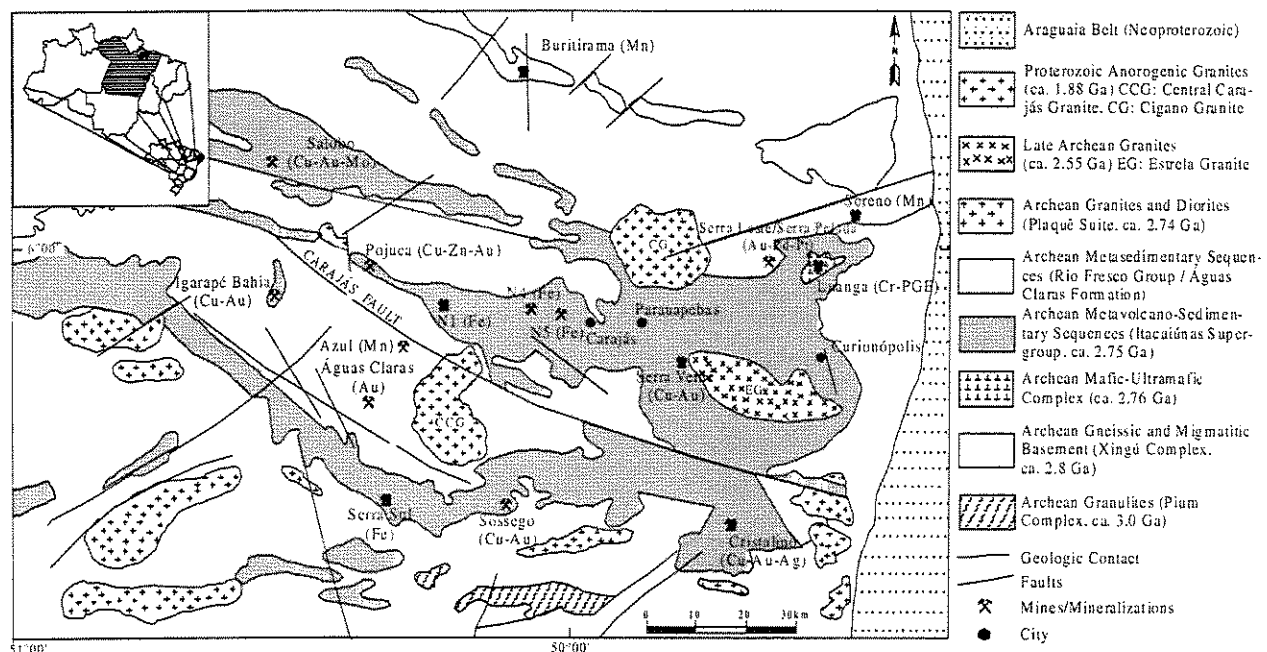


Figure 1-Simplified geological map of the Carajás Copper-Gold Belt (based on Docegeo 1988, Araújo and Maia 1991, Barros and Barbey 1998).

1 - Instituto de Geociências, Universidade Estadual de Campinas, Cx. Postal 6152, 13083-970, Campinas, SP. fernando@ige.unicamp.br, berna@ige.unicamp.br.

2 - Instituto de Geociências, Universidade de Brasília, Campus Universitário Darcy Ribeiro, Asa Norte, 70910-900, Brasília, DF. gouveia@unb.br.

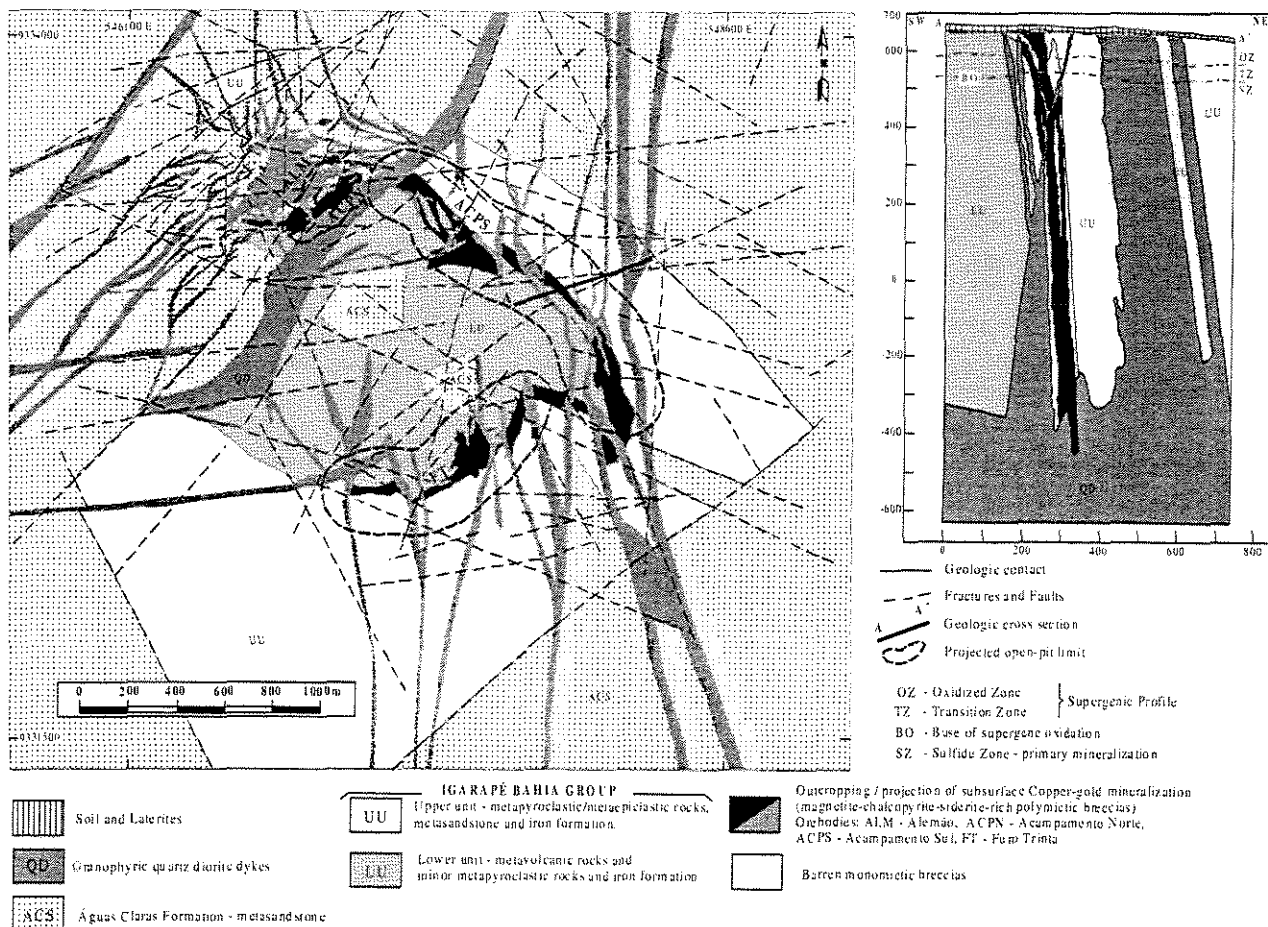


Figure 2-Geological map of the Igarapé Bahia Copper-Gold mineralization and geological cross section A-A' through the Acampamento Sul Orebody (modified from CVRD/DOCEGEO 1996, unpublished).

varieties, and minor crystal tuffs and ironstones dominate the lower unit. The upper unit is composed of lithic tuffs, crystal tuffs, laminated epiclastics, ironstone, epiclastic conglomerates and sandstone (Fig. 2).

These rocks display extensive hydrothermal alteration. Primary phases are completely replaced by a mixture of quartz and chlorite. Siderite, chalcopyrite and magnetite occur either disseminated or in veins. Veining of host rocks becomes progressively more intense towards the Cu-Au mineralization, eventually with jigsaw textures and breccia development. Laminated epiclastic rocks exhibit stratabound replacement textures with the development of cm-scale chalcopyrite beds and nodules, both connected to stockwork vein systems. The nodules bent the primary bedding and are also transgressive with respect to lamination.

**Águas Claras Formation** The Igarapé Bahia Group is overlain by sandstone of the Águas Claras Formation. The contact between them is characterized by normal faults. Occasionally the sandstone hosts massive chalcopyrite veins ranging from a few mm up to 1-m thick.

**Quartz diorite dykes** A set of fractures and normal faults control the emplacement of quartz diorite dykes, which disrupt the metavolcano-sedimentary rocks and the Águas Claras sandstone. Zones of intense alteration and veining, where apophyses and contact breccias are common, mark the contact between dykes and the host sequence. Chlorite-rich albite, and concentrations of almandine neoblasts in the host rock locally border the apophyses.

Quartz diorite shows a granophytic texture with primary andesine phenocrysts (An ~ 30 mol%) rimmed by coronas of quartz-albite intergrowth. Matrix includes albite, quartz, and minor K-feldspar and ilmenite. The dykes display hydrothermal alteration of varied intensity. A continuum spectrum including weakly altered to intensely venulated

and brecciated rocks is observed. Primary plagioclase is converted to albite + calcite + chlorite + epidote, and ilmenite is oxidized to rutile + magnetite. Secondary K-feldspar, biotite and muscovite are related to potassic alteration. Quartz diorites also host sulfide minerals (chalcopyrite and rare pyrite, galena, sphalerite and molybdenite) either disseminated or in veins. Uraninite and REE-minerals (monazite, apatite, xenotime, and paratite) are associated with the alteration of the diorite dykes.

**THE COPPER-GOLD MINERALIZATION** The host metavolcano-sedimentary sequence together with the Furo Trinta (FT), Acampamento Sul (ACPS) and Acampamento Norte (ACPN) Orebodies outcrop in a structural window surrounded by the Águas Claras Sandstone. The outcropping orebodies define a semicircular structure at the surface. Although covered by a discordant layer of sandstone, the Alemão (ALM) Orebody also integrates this structure at depth and is connected to the ACPN Orebody by way of normal faults (Soares *et al.* 1999). The orebodies consist of steeply dipping (~75°) Cu-Au-bearing breccias located at the contact zone between the upper (hanging wall) and the lower (footwall) units of the host metavolcano-sedimentary sequence. The orebodies dip outward and the strike is concordant with bedding of host rocks.

**Breccia types, hydrothermal alteration and veins** The Cu-Au breccias are essentially polymictic, thus classification was based on matrix mineralogy leading to the following groups: chlorite breccias, siderite breccias and magnetite breccias. Angular fragments ranging from a few mm to over 20 cm in diameter of both footwall and hanging wall are cemented by variable amounts of hydrothermal matrix. Chlorite breccias and siderite breccias exhibit the same matrix mineralogy but the amounts of these specific minerals are distinct. The matrix is fine-grained and includes Fe-chlorite, siderite, magnetite, chalcopyrite, quartz and minor tourmaline.

Magnetite breccias exhibit a granular matrix of euhedral magnetite in association with Fe-chlorite, Cu-sulfides, siderite, grunerite, quartz, K-feldspar, stilpnomelane, biotite and minor tourmaline, muscovite and fluorite. The association defines a distinctive Fe-(K)-metasomatic zone. Magnetite is stoichiometric and constantly Ti-free.

At the ACPS and FT, mineralization is preferentially related to siderite breccias, while at the ACPN and ALM, it is associated with magnetite breccias. Chlorite breccias broadly occur at the margins of all orebodies and are also mineralized.

Chloritization is the most common and widespread alteration observed. Mg-chlorite ( $50 > mg > 30$ ) is typically associated with calcite, dolomite and quartz in barren and distal altered host rocks, while Fe-chlorite ( $30 > mg > 12$ ) is paragenetic to siderite and magnetite in Cu-Au-bearing breccias ( $mg = 100Mg/[Mg+Fe_{total}]$ , in cation per unit formula). In this work chlorite thermometry (Cathelineau 1988) was calculated for a variety of rocks. The calculated mean temperatures are: 321°C for altered metavolcanic rocks, 339°C for chlorite breccias, 321°C for magnetite breccias, 375°C for siderite breccias, 313°C for altered quartz diorites and 369°C for chalcopyrite nodules from host rocks.

Several vein types crosscut the breccias and the host rocks. Veins are usually discordant to bedding and occasionally exhibit comb structures. The most frequent varieties are: (a) calcite + chalcopyrite  $\pm$  fluorite  $\pm$  stilpnomelane, (b) ankerite  $\pm$  chalcopyrite  $\pm$  gold, (c) siderite + calcite + quartz + chlorite + chalcopyrite, and (d) chalcopyrite  $\pm$  biotite  $\pm$  K-feldspar  $\pm$  tourmaline  $\pm$  REE-minerals. Vein chronology is unknown due to the recurrences and unclear crosscut relations.

**Ore mineralogy** Hypogene copper mineralization consists of chalcopyrite and traces of chalcocite, digenite and covellite that occur as rims on chalcopyrite in grain boundary driven oxidation reactions. Magnetite breccias, unlike other breccias, include chalcopyrite intergrown with bornite, indicating a relatively higher oxidation state of the fluid. Traces of pyrite are observed as inclusions in chalcopyrite as a function of local sulfur excess. The major copper mineralization is juxtaposed to gold mineralization in all orebodies. Additional, sub-economic copper concentration occurs in veins, nodules or disseminated in marginal altered host rocks with negligible gold content. Native gold occur as fine particles, usually between 5 to 20 mm, included in gangue minerals (quartz, siderite and chlorite), chalcopyrite and occasionally in magnetite. Silver is a byproduct occurring as hypogene Au-Ag alloy (up to 12 wt% Ag), hessite ( $Ag_2Te$ ) and argentite/acanthite ( $Ag_2S$ ).

**Supergene alteration and related ore types** At the Igarapé Bahia Deposit weathering is responsible for the development of a thick oxidized profile, where gold and copper are segregated and reconcentrated leading to the formation of different ore-types. The oxidized zone extends from surface to 150-m depth. It constitutes a gold-bearing gossan (total reserves in December 1999 of 18.5 Mt  $\equiv$  1.97 gAu/t) from which approximately 11 t Au per year are mined. Total Au production is ca. 60 t to the present. The gossanous transition zone occurs from 150- to 200-m depth, where supergene solutions have percolated and precipitated metals, originating a secondary Cu-Au ore (9.5 Mt  $\equiv$  2.45 gAu/t, 3.83 wt% Cu). The hypogene Cu-(Au) mineralization (219 Mt  $\equiv$  0.86 gAu/t, 1.4 wt% Cu) occurs beneath 200-m depth.

**Ore Geochemistry** The mineralized breccias contain anomalous concentrations of  $FeO_T$  (25-64 wt%), Cu (0.5-11 wt%), U (28-380 ppm), Au (0.5-15 ppm), Ag (4-52 ppm), Ba (26-200 ppm), F (390-31000 ppm), P (900-6200 ppm) and REE, particularly La (260-2300 ppm) and Ce (450-4400 ppm). Breccias are also enriched in MnO (0.5-3 wt%), CaO (0.5-9 wt%), Mo (50-200 ppm) and Zn (150-450 ppm) relatively to host rocks. The intercorrelated behavior of all these elements suggests a common metasomatic origin and reflects the interplay of Fe-metasomatism, sulfidation, chloritization and carbonate alteration. Traces of barite, fluorite, galena, altaite, sphalerite, molybdenite, uraninite, apatite, monazite, xenotime, bastnasite and parisite as inclusions in chalcopyrite and gangue minerals account for the Ba, F, Pb, Zn, Mo, U, REE and P enrichment. The high manganese content is related to siderite, which contains up to 7 wt% MnO.

The REE-distribution patterns of breccias are similar for different types, and show a strong enrichment in LREE (Fig. 3). Distribution patterns of the metavolcanic rocks, dioritic dikes and breccias show equivalent shape, but the absolute concentrations are quite distinct. Iron formations show a completely distinct pattern. REE minerals are unequivocally related to hydrothermal activity. Thus, rather than

reflecting petrologic information concerning the primary system(s), REE patterns are suitable to monitor the intensity of the hydrothermal alteration. The contrasting La/Lu ratios of host metavolcanic rocks (70-250) and breccias (1000-2500) indicate the preferential concentration of LREE by the hydrothermal solution(s). Additionally, the similarity between the distribution patterns of altered metavolcanic rock, breccias and diorite dikes suggests that these rocks underwent a common alteration process.

Stable isotope analyses were performed in calcite and siderite from veins and matrix of mineralized breccias (Oliveira *et al.* 1998). Carbon isotopes yield a narrow range of  $\delta^{13}C$  (-9.3 to -5.8‰), while oxygen isotopes presented a wider variation of  $\delta^{18}O$  (0.7 to 9.4‰). The results are plotted in Fig. 4, comparatively to other well-known reservoirs.

**DISCUSSION** The results of chlorite geothermometry, that yielded a range between 313-375°C for the Igarapé Bahia hydrothermal system, are in accordance with previous fluid inclusion homogenization temperatures of Ribeiro (1989) and Lindenmayer *et al.* (1998). The equilibrium gold-hessite provides additional support for this thermal range (Markham 1960).

According to the thermodynamic calculations of Mickucki and Ridley (1993), the equilibrium siderite-magnetite-chalcopyrite  $\pm$  bornite, at 300°C and 2 kbar, indicates high  $fO_2$  ( $10^{-29}$  to  $10^{-31}$ ) and low  $a_{SS}$  ( $a_{SS} \sim 10^{-3}$ ) for the Igarapé Bahia hydrothermal system. At greenschist temperatures and high  $CO_2$  content, Fe-oxides equilibrate with siderite instead of minnesotaite/greenalite, with grunerite being stable only at upper greenschist and amphibolite temperatures (Frost 1979). Thus, the equilibrium siderite-magnetite (ACPS and FT) indicates a distinctively high  $CO_2$  content in the fluid in relation to magnetite breccias, while the pair grunerite-magnetite (ALM and ACPN) denotes relatively higher temperatures. The inferred  $CO_2$  enrichment of fluid phases is supported by the fluid inclusion data of Almada (1998) who reported aqueous, aqueous-carbonic and carbonic compositions.

The calculated thermal range coupled with the high  $fO_2$  of the Igarapé Bahia hydrothermal system are consistent with Cu and Au transport via Cl-complexes, which are active in acid, saline and oxidizing fluids (Davidson and Large 1994). In high-temperature, saline and acid solutions, REE and U are complexed preferentially by chloride with or without the competition from fluoride,  $CO_2^{2-}$  or phosphorous species depending on the relative abundance of the ligands (Gieré 1996). These ions were clearly active in Igarapé Bahia and promoted a selective concentration of LREE, only possible under acid to neutral conditions (Gieré 1996).

The narrow range of negative values of  $\delta^{13}C$  together with the indication of high  $fO_2$ , denote a homogeneous deep-seated carbon source from which carbonate minerals were precipitated with limited pH variations. The wider range of  $\delta^{18}O$  values is interpreted as resulting from the mixture of deep-seated solutions with meteoric fluids that respectively account for the high and low  $\delta^{18}O$  values. This fluid mixing hypothesis is in agreement with previous fluid inclusion studies of the Igarapé Bahia hydrothermal system that demonstrated the existence of two distinct groups: (a) 150-430°C and up to 40%  $NaCl_{eq}$  and (b) 100-150°C and ~10%  $NaCl_{eq}$  (e.g. Ribeiro 1989, Lindenmayer *et al.* 1998). Stable isotope and fluid inclusion data, both

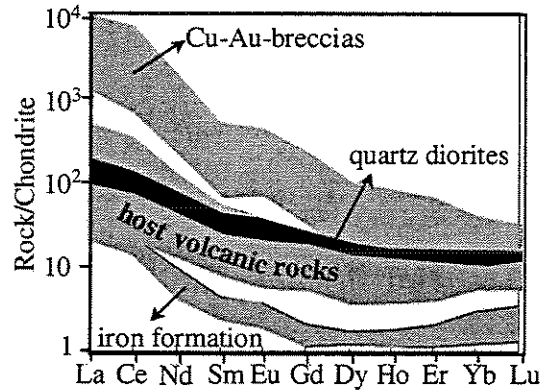


Figure 3-Chondrite normalized REE patterns of mineralized breccia, host metavolcanic rocks and banded iron formations from the Igarapé Bahia Deposit. Chondrite composition according to Evensen *et al.* (1978).

suggest that the progressive interaction of a hot saline and acid magmatic fluid with a low-temperature oxidizing and less saline meteoric solutions is the most likely depositional mechanism of the Igarapé Bahia ore. Persistent fluid mixing over a focused heat source possibly triggered Cu, Au, U and REE deposition through  $fO_2$  and temperature decrease and pH increase.

At deposit scale, primary structures are preserved and ductile elements such as lineation, foliation and satellite folds were not observed. Brittle deformation is extensive and includes fractures and normal faults. Map analysis together with the outward dip of the bedding suggest that the structural framework of the Igarapé Bahia Deposit resulted from pluton emplacement that caused roof uplifting and lateral shoulder of wall rocks along faults. These brittle processes are typically related to near surface plutons (Paterson *et al.* 1991). The resemblance of the alteration styles of mineralized breccias and

dioritic dikes suggest that both have interacted with the same hydrothermal fluid. Thus, the dioritic dikes could have been the source of heat and magmatic fluids during the latest stages of epicrustal emplacement.

The origin of the stratabound morphology of the Igarapé Bahia orebodies remains a matter of debate. One could speculate that it derives from primary exhalative processes or from epigenetic stratabound replacement and brecciation. The brecciation and veining of both footwall and hanging wall, together with the presence of sub-economic chalcopyrite concentrations in the Águas Claras sandstone, suggest an epigenetic origin.

The alteration styles, ore mineralogy and fluid composition of the Igarapé Bahia Deposit are analogous to other intrusion-related hydrothermal Fe-oxide-(Cu-Au-U-REE) deposits (Hitzman *et al.* 1992). On the other hand, the confinement of all known mineralizations of the Carajás Copper-Gold Belt to the Itacaiúnas metavolcano-sedimentary sequences suggests that primary processes could have pre-concentrated metals. Thus, a multi-stage genesis involving the superposition of Archean exhalative processes and further hydrothermal-magmatic activity seems plausible. Mellito (1998) documented a similar process at Salobo, where Archean syngenetic mineralization was reconcentrated during the Late Archean time due to tectonic and magmatic activity.

The composition of the dikes favors an Archean age for the magmatic activity at Igarapé Bahia, since the dioritic magmatism in the region is bracketed within the interval of 2.55 to 2.74 Ga. Additional support is provided by the Rb-Sr bulk-rock age of  $2.577 \pm 2$  Ma of the Igarapé Bahia host metavolcanic rocks (Ferreira Filho 1985). This age is inconsistent with the minimum age of ca. 2.6 Ga of the overlying Águas Claras Sandstone (Dias *et al.* 1996), and may indicate thermal resetting of the Sr isotopic system during the emplacement of Late Archean (ca. 2.55 Ga) intrusions.

**Acknowledgments** To the Companhia Vale do Rio Doce for the permission to publish their private data. The authors are thankful to all the geologists of the Igarapé Bahia mine, especially José Luzimar Rego for enthusiastic discussions during fieldwork. We acknowledge the referees of RBG and also all the anonymous reviewers that improved our original manuscript. We are also indebted to FAPESP (Fundação de Amparo à Pesquisa do Estado de São Paulo) for the grants #98/14401-5 and #99/03058-0. We are thankful to the Multi User SEM laboratory (IG-UNICAMP) funded by FAPESP grant #95/06401-7.

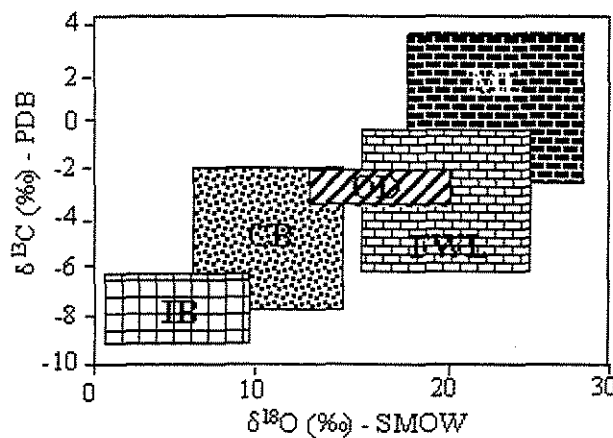


Figure 4 -  $\delta^{13}\text{C}$  vs.  $\delta^{18}\text{O}$  diagram showing the isotopic composition of siderite and calcite from the Igarapé Bahia mineralization (IB), relative to carbonatites (CB), the Olympic Dam mineralization (OD), freshwater limestone (FWL) and marine limestone (ML). Fields for CB, OD, FWL and ML after Oreskes and Einaudi (1992).

- Almeida M.C.O. 1998. *O corpo Acampamento Sul do depósito Bahia, Carajás: características geológicas e fluidos hidrotermais*. Centro de Geociências, UFFPA, Belém, MSc Dissertation, 99p.
- Araújo O.J.B., Maia R.G.N. 1991. *Serra dos Carajás, folha SB.22-Z-A, Estado do Pará*. Brasília, DNPM, 136p. (Programa Levantamentos Geológicos Básicos do Brasil)
- Barros C.E.M., Barberi P. 1998. A importância da granitogênese tardí-arqueana (2.5 Ga) na evolução tectono-metamórfica da Província Mineral de Carajás - Complexo Granítico Estrela e sua auróea de contato. *Revista Brasileira de Geociências*, 28:513-522
- Barros C.E.M., Dall'Agnol R., Lafon J.M., Teixeira N.P., Ribeiro J.W. 1992. Geologia e geocronologia Rb-Sr do Gnaiss Estrela, Curionópolis, PA. *Boletim do Museu Paraense Emílio Goeldi, Ciências da Terra*, 4:83-104
- Barton P.B. 1993. Problems and opportunities for mineral deposit models. In: R.V. Kirkham; W.D. Sinclair; R.I. Thrope; J.M. Duke (eds.) *Mineral Deposit Modeling*. Geological Association of Canada, Special Paper 40, 7-13
- Cathelineau M. 1988. Cation site occupancy in chlorites and illites as a function of temperature. *Clay Minerals*, 23:471-485
- Davidson G.J., Large R.R. 1994. Gold metallogeny and the copper-gold association of Australian Proterozoic. *Mineral Deposit*, 29:208-223
- Dias G.S., Macambira M.J.B., Dall'Agnol R., Soares A.D.V., Barros C.E.M. 1996. Datação de zircões de sills de metagabbro: comprovação da idade arqueana da Formação Águas Claras, Carajás, PA. In: SBG, Simpósio de Geologia da Amazônia, 5, Belém, Resumos Expandidos, 376-379
- DOCEGEO (Río Doce Geologia e Mineração S.A.). 1988. Província Mineral de Carajás. Litoestratigrafia e principais depósitos minerais. In: SBG, Congresso Brasileiro de Geologia, 35, Belém, Anexo aos Anais, 165p.
- Evensen N.M., Hamilton P.J., O'Nions R.K. 1978. Rare-earth abundance in chondritic meteorites. *Geochim. Cosmochim. Acta*, 42:1199-1212
- Ferreira Filho, C.F. 1985. *Geologia e mineralizações sulfetadas do Prospective Bahia, Província Mineral de Carajás*. Instituto de Geociências, Universidade de Brasília, Brasília, MSc Dissertation, 112p.
- Frost B.R. 1979. Metamorphism of iron-formation: paragenesis in the system Fe-Si-C-O-H. *Economic Geology*, 74:775-785
- Gieré R. 1996. Formation of rare earth minerals in hydrothermal systems. In: A.P. Jones; F. Wall; C.T. Williams (eds.) *Rare Earth Minerals*. London, Chapman & Hall, 105-150
- Hitzman M.W., Oreskes N., Einaudi M.T. 1992. Geological characteristics and tectonic setting of Proterozoic iron oxide (Cu-Au-U-REE) deposits. *Precambrian Research*, 58:241-287
- Huhn S.R.B. 1996. São os depósitos cupíferos de Carajás do tipo Cu-Au-U-ETR? In: SBG, Simpósio de Geologia da Amazônia, 5, Belém, Resumos Expandidos, 140-143
- Huhn S.R.B., Macambira M.J.B., Dall'Agnol R. 1999. Geologia e geocronologia Pb-Pb do granito alcalino Arqueano Planalto, Região da Serra do Rabo, Carajás - PA. In: SBG, Simpósio de Geologia da Amazônia, 6, Manaus, Resumos Expandidos, 463-466
- Lindenmayer Z.G.; Ronchi, L.H.; Laux, J.H. 1998. Geologia e geoquímica da mineralização de Cu-Au primária da mina de Au do Igarapé Bahia, Serra dos Carajás. *Revista Brasileira de Geociências*, 28:257-268
- Machado N., Lindenmayer Z., Krogh T.E., Lindenmayer D. 1991. U-Pb geochronology of Archean magmatism and basement reactivation in the Carajás area, Amazon Shield, Brazil. *Precambrian Research*, 49:329-354
- Markham N.L. 1960. Synthetic and natural phases in the system Au-Ag-Tc, Part I. *Economic Geology*, 55:1148-1178
- Mellito K.M. 1998. Aplicações dos sistemas Rb-Sr, Pb-Pb e Sm-Nd no depósito polimetálico do Salobo 3A, Província Mineral de Carajás, Pará. Inst. Geociências, USP, São Paulo, MSc Dissertation, 113p.
- Mikucki E.J. & Ridley J.R. 1993. The hydrothermal fluids of Archean lode-gold deposits at different metamorphic grades: compositional constraints from ore and wallrock alteration assemblages. *Mineral Deposit*, 28:469-481
- Oliveira C.G., Tazava E., Tallarico F.H.B., Santos R.V., Gomes C. 1998. Gênese do depósito de Au-Cu-(U-ETR) de Igarapé Bahia, Província Mineral de Carajás. In: SBG, Congresso Brasileiro de Geologia, 40, Belo Horizonte, Anais, 137
- Oreskes N. & Einaudi, M.T. 1992. Origin of hydrothermal fluids at Olympic Dam: preliminary results from fluid inclusions and stable isotopes. *Economic Geology*, 87:64-90
- Paterson S.R., Vernon R.H., Fowler T.K. 1991. Aureole tectonics. In: D.M. Kerrick (ed.) *Contact Metamorphism*. Min. Soc. America, Reviews in Mineralogy, Volume 26, 673-722
- Ribeiro A.M.R. 1989. Estudo geoquímico do sistema hidrotermal relacionado à mineralização cupífera da Área Bahia, Serra dos Carajás, PA. Centro de Geociências, UFFPA, Belém, MSc Dissertation, 134p.
- Rodrigues E.S., Lafon J.M., Scheller T. 1992. Geocronologia Pb-Pb da Província Mineral de Carajás: primeiros resultados. In: SBG, Congresso Brasileiro de Geologia, 37, São Paulo, Resumos Expandidos, 2:183-184
- Soares A.D.V., Ronzé P.C., Santos M.G.S., Leal E.D., Barreira C.F. 1999. Geologia e mineralizações do depósito de Cu-Au Alemão - Província Mineral de Carajás (PA). SBG, Simpósio de Geologia da Amazônia, 6, Manaus, Anais, 144-147
- Tallarico F.H.B. 1996. Projeto de revisão do modelo geológico da mina de Igarapé Bahia: petrografia, química mineral e litogeocronologia. Belo Horizonte, CVRD (relatório interno), 57p.
- Tazava E. 1999. Mineralização de Au-Cu-(±ETR-U) associada às brechas hidrotermais do depósito de Igarapé Bahia, Província Mineral de Carajás, PA. Dep. Geologia, UFOP, Ouro Preto, MSc Dissertation, 81p.

### **ANEXO 3**

The occurrence of ilvaite in the Igarapé Bahia Cu-Au deposit, Carajás Province, Brazil



# OCCURRENCE OF ILVAITE IN THE IGARAPÉ BAHIA Cu-Au DEPOSIT, CARAJÁS PROVINCE, BRAZIL

FERNANDO HENRIQUE BUCCO TALLARICO<sup>1</sup>

**ABSTRACT** This paper describes the first known occurrence of the mineral ilvaite in Brazil. The mineral is sited in the matrix of magnetite-rich breccias and stockwork veins of the Igarapé Bahia Cu-Au deposit. Electron microprobe analysis (EMPA) of the Igarapé Bahia ilvaite reveals the following composition: Ca<sub>0.96</sub>Fe<sup>2+</sup><sub>0.04</sub>Fe<sup>3+</sup><sub>0.01</sub>Si<sub>1.00</sub>O<sub>4</sub>(OH) and X-ray diffraction (XRD) data indicate a structure compatible with the monoclinic polymorph ( $a_0=13.032$  Å,  $b_0=8.810$  Å,  $c_0=5.850$  Å and  $\alpha=90.254^\circ$ ). It is suggested that ilvaite crystallized from hydrothermal solutions, at a temperature range of 300–350°C, under conditions of high  $\text{H}_2\text{O}$  and low sulfur activity. The formation of ilvaite is tentatively related to the reaction magnetite + calcite + quartz +  $\text{H}_2\text{O} = \text{ilvaite} + \text{CO}_2 + \text{O}_2$ .

**Keywords:** ilvaite, Igarapé Bahia, Cu-Au deposit, Carajás

**INTRODUCTION** Ilvaite was named after its discovery locality, on the Rio Marina, Elba (Latin Ilva) Italy (Blackburn & Dennen 1997). This rare Ca-Fe-silicate occurs typically as a late stage mineral in Ca-Fe-Si-skarns related to the intrusion of granodiorite, quartz diorite, monogranite and granite (e.g. Shannon 1918, Plimer & Ashley 1978, Gauthier & Albankis 1981, Gole 1981, Kwak 1983, Pesquera & Velasco 1986). Ilvaite also occurs as a product of deuteric or hydrothermal alteration of basalt, dolerite and quartz diorites (e.g. Baker 1953, Naslund 1983, Barton & Van Bergen 1984, Wise & Moller 1990). Less commonly, the mineral is related to low-grade retrometamorphic reactions of ultramafic rocks (Agata & Adachi 1995). Desborough & Amos (1961) report the occurrence of magmatic ilvaite related to the latest stages of gabbro crystallization. This paper describes the mode of occurrence, mineralogical association, chemical composition and crystal structure of ilvaite from the Igarapé Bahia Cu-Au deposit, which is the first reported occurrence of the mineral in Brazil.

**GEOLOGICAL SETTING** A remarkable feature of the Carajás region is the clustering of a large number of world-class (> 200 Mt) Fe-oxide Cu-Au-(U-REE) deposits (e.g. Salobo, Cristalino, Igarapé Bahia, Sossego) that are collectively known as the Carajás Copper-Gold Belt. The Igarapé Bahia deposit, with total reserves of 219 Mt @ 1.4% Cu and 0.86 g/t Au, is perhaps the best documented deposit of the belt (e.g. Tallarico *et al.* 2000 and references therein).

A low-grade metavolcano-sedimentary sequence (Igarapé Bahia/Grão Pará Group), which includes a variety of volcanic, pyroclastic and epiclastic rocks and minor ironstones, hosts the Igarapé Bahia mineralization. Sandstones that formed in a shallow marine environment (Águas Claras Formation) overlie

the former unit. A set of radial fractures and faults control the emplacement of quartz diorite and diabase dikes, which disrupt the metavolcano-sedimentary rocks and the Águas Claras sandstone.

The ore bodies define an ellipsoidal structure at surface and are associated sub-vertical breccia units. The ore-bearing with breccias include fragments of both footwall and hanging wall that are cemented by variable amounts of chlorite, siderite, magnetite, chalcopyrite and minor uraninite and REE-minerals.

**OCCURRENCE OF ILVAITE** Ilvaite is a rare mineral in the Igarapé Bahia deposit, and was recognized in the matrix of magnetite-rich breccias and veins that crosscut the former. The magnetite breccia include angular fragments (up to 6 cm in diameter) of banded iron formation and altered volcanic rocks. These fragments are welded by a fine-grained isotropic matrix that includes magnetite (8-33%), stilpnomelane (15-40%), chlorite (1-17%), amphibole (5-13%), tourmaline (1-3%), quartz (1-23%), calcite (1-20%), sericite (1-6%) and minor amounts of biotite, apatite, monazite, uraninite, fluorite, epidote and ilvaite. Matrix mineralogy also includes chalcopyrite (1-20%) in equilibrium with bornite (1-6%), and traces of cobaltite. Hessite (Ag<sub>2</sub>Te) and native gold particles (3-50 µm) occur in the matrix of magnetite breccias as inclusions in gangue minerals, chalcopyrite and bornite.

Stockwork veins, which range from a few millimeters up to 4 cm width, crosscut the magnetite breccias. Vein mineralogy includes calcite (40-50%), chalcopyrite (10-30%), magnetite (5-15%), ilvaite (1-10%), quartz (5-10%), fluorite (up to 5%) and tourmaline (up to 5%).

Ilvaite occurs in both breccia matrix and veins as subhedral

<sup>1</sup> Instituto de Geociências, Universidade Estadual de Campinas, Caixa Postal 6152, 13.083-970, Campinas, SP, Brazil. e-mail: fernando@ige.unicamp.br

crystals ranging from 50µm to 0.5cm. Ilvaite frequently contains inclusions of magnetite, suggesting that it originated from the alteration of the later. Rare sheelite crystals also occur as inclusions in ilvaite, with hematite commonly occurring as rims on, or filling fractures in ilvaite.

**X-RAY CRYSTALLOGRAPHY** Ilvaite was examined in a Philips-X'Pert X-ray diffractometer with a θ-θ goniometer. Analytical conditions were: CuK $\alpha_1$  radiation (graphite

monochromator), 40kV accelerating voltage, 55mA current, 5°-75° angular range (2θ), 0.04° step size and 0.5 second/step counting rate. The fifty-four measured X-ray reflections show a very good agreement with the Powder Diffraction File (PDF) - Set 25-149, for monoclinic ilvaite (Table 1). Least-square refinement of the X-ray reflections, assuming monoclinic constrains, yield the following unit cell parameters:  $a_0 = 13.032 \text{ \AA}$ ,  $b_0 = 8.810 \text{ \AA}$ ,  $c_0 = 5.850 \text{ \AA}$  and  $\alpha = 90.254^\circ$ .

Table 1 - X-ray powder diffraction data of ilvaite from Igaraپ Bahia.

Igarapé Bahia Ilvaite		PDF 25-149		Igarapé Bahia Ilvaite		PDF 25-149	
d (Å)	I/I <sub>0</sub>	d (Å)	I/I <sub>0</sub>	d (Å)	I/I <sub>0</sub>	d (Å)	I/I <sub>0</sub>
7,279	100	7.305	70	1,907	23	1,902	17
6,494	47	6.518	18	1,894	17	1,896	
4,870	8	4,887	10	-	-	1,861	2
4,565	17	4,575	16	-	-	1,848	5
4,169	10	4,172	6	1,855	10	1,846	4
3,889	32	3,984	35	-	-	1,824	3
3,392	8	3,397	14	1,817	5	1,819	3
3,253	45	3,255	55	-	-	1,768	5
-	-	3,237	4	-	-	1,760	5
3,089	14	3,091	18	1,742	14	1,744	20
-	-	3,053	2	1,712	19	1,713	30
2,927	11	2,928	18	1,706	10	1,701	2
2,864	50	2,865	70	1,699	5	1,687	2
2,838	94	2,849	95	1,677	9	1,677	10
-	-	2,840		1,672	28	1,673	13
-	-	2,737	19	-	-	1,671	15
-	-	2,730	20	-	-	1,649	2
-	-	2,721	70	1,631	18	1,633	10
2,713	98	2,714		-	-	1,630	10
2,674	82	2,676	100	-	-	1,624	20
2,614	21	2,617	35	-	-	1,619	20
2,571	14	2,572	20	1,610	52	1,613	10
2,550	16	2,558	19	1,607	34	1,599	8
-	-	2,552		1,575	8	1,578	5
2,495	20	2,496	19	-	-	1,576	
2,436	36	2,438	35	-	-	1,565	5
-	-	2,432		-	-	1,562	6
2,384	11	2,392	25	-	-	1,545	3
-	-	2,385		1,525	21	1,526	22
2,346	16	2,343	30	1,501	16	1,500	35
2,333	23	2,336		1,495	13	1,497	
2,280	4	2,297	3	1,470	24	1,471	20
2,243	1	2,245	5	-	-	1,469	25
2,201	13	2,203	2	1,464	36	1,463	60
2,182	21	2,179	55	-	-	1,458	35
2,169	47	2,171	55	1,426	13	1,426	16
-	-	2,128	10	-	-	1,423	12
-	-	2,121		-	-	1,419	22
2,118	36	2,116	50	-	-	1,415	8
2,108	34	2,109		1,389	5	1,389	4
2,084	18	2,085	20	-	-	1,379	2
1,963	23	1,963	35	-	-	1,376	4
1,956	27	1,953	14	1,366	8	1,366	24
-	-	1,947	17				

Table 2 – Representative microprobe analysis of ilvaite and paragenetic chlorite from magnetite breccias of the Igarapé Bahia Cu-Au deposit.

Ilvaite (wt%)		Chlorite (wt%)			
Core	Rim	1	2	3	4
SiO <sub>2</sub>	29.02	29.47	24.79	22.94	25.37
TiO <sub>2</sub>	0.08	0.01	0.11	0.04	0.12
Al <sub>2</sub> O <sub>3</sub> *	0.01	0.00	19.73	15.04	18.86
Fe <sub>2</sub> O <sub>3</sub> *	19.50	19.55	0.00	0.00	0.00
FeO	34.44	34.43	38.78	33.2	36.5
MgO	0.11	0.10	5.45	5.17	6.61
CaO	13.73	13.13	0.01	3.42	0.08
MnO	0.97	1.01	0.15	0.14	0.12
Na <sub>2</sub> O	0.00	0.00	0.30	0.59	0.28
K <sub>2</sub> O	0.00	0.00	0.00	0.00	0.00
F	0.07	0.00	n.a.	n.a.	n.a.
Cl	0.01	0.02	n.a.	n.a.	n.a.
H <sub>2</sub> O*	2.16	2.20	10.75	10.67	10.86
Total	100.11	99.93	100.07	91.21	98.80
O=F=Cl	0.03	0.00	0.00	0.00	0.00
Total	100.07	99.92	100.07	91.21	98.80
# cations per 9 (O,OH)		# cations per 14 (O,OH)			
Si	1.98	2.01	2.76	2.86	2.84
Ti	0.00	0.00	0.01	0.00	0.01
Al	0.00	0.00	2.59	2.21	2.49
Fe <sup>3+</sup>	1.00	1.00	0.00	0.00	0.00
Fe <sup>2+</sup>	1.96	1.96	3.61	3.46	3.42
Mg	0.01	0.01	0.91	0.96	1.10
Ca	1.00	0.96	0.00	0.46	0.01
Mn	0.06	0.06	0.01	0.01	0.01
Na	0.00	0.00	0.06	0.14	0.06
K	0.00	0.00	0.00	0.00	0.00
F	0.02	0.00	-	-	-
Cl	0.00	0.00	-	-	-
OH	0.98	1.00	7.99	8.00	8.00
T(°C)**	-	-	336.43	305.70	311.90
					314.63

\* Fe<sub>2</sub>O<sub>3</sub> and H<sub>2</sub>O calculated from charge balance

\*\* Chlorite-geothermometer (Cathelineau 1988)

n.a. - not analyzed

**MINERAL CHEMISTRY** Chemical analyses of minerals were collected on a JEOL-JCXA-733 microprobe, with the following analytical conditions: 15kV accelerating voltage, 15.10<sup>-9</sup>A current and calibration using natural and synthetic standards. EMPA data of ilvaite reveals a near-stoichiometric composition,  $\text{Ca}_{0.96}\text{Fe}^{2+}_{1.96}\text{Fe}^{3+}_{1.00}\text{Si}_{2.01}\text{O}_8(\text{OH})$ , with low manganese content ( $\text{MnO} \sim 1\text{wt\%}$ ) (Table 2). Chlorite from the matrix of magnetite breccias is typically Fe<sup>2+</sup>-rich ( $\text{FeO}_{34-38\text{wt\%}}$ ) and yields, through calculations of the Cathelineau (1988) geothermometer, a temperature range between 305-336°C for the hydrothermal system.

**DISCUSSION** According to Gustafson (1973), at high fluid pressures, ilvaite is stable below approximately 470°C and over a wide range of  $f\text{O}_2$ . The mode of occurrence of the Igarapé Bahia ilvaite, together with the temperature estimate given by chlorite-geothermometry, suggests that the mineral formed under hydrothermal conditions at temperatures possibly between 300-350°C. The presence of coexisting magnetite and chalcopyrite in equilibrium with bornite denotes an oxidized and sulfur-poor hydrothermal system. The presence of magnetite inclusions in ilvaite, coupled with the occurrence of paragenetic quartz and calcite, suggest that ilvaite could have formed through the reaction magnetite + calcite + quartz + H<sub>2</sub>O = ilvaite + CO<sub>2</sub> + O<sub>2</sub> (Barton and Bergen, 1984). The excess oxygen released from this reaction could be responsible for the precipitation of hematite in fractures, or as rims on ilvaite.

**Acknowledgments** To the Companhia Vale do Rio Doce for support during fieldwork and access to the EMPA and DRX laboratories. To FAPESP (Fundação de Amparo à Pesquisa do Estado de São Paulo) for grants #98/14401-5 and #99/03058-0. I am thankful to the Multi User SEM laboratory (IG-UNICAMP) funded by FAPESP grant #95/06401-7. To Dr. Bernardino R. Figueiredo, Dr. David I. Groves, and to the reviewers of RBG for their suggestions to the original.

## References

- Agata T. & Adachi M. 1995. Ilvaite from serpentinitized peridotite in the Asama igneous complex, Mikabu greenstone belt, Sambagawa metamorphic terrain, central Japan. *Min. Mag.*, **59**:489-496
- Baker G. 1953. Ilvaite and prehnite in micropegmatitic diorite, Southeast Papua. *Am. Mineral.*, **38**:840-844
- Barton M. and Van Bergen M.J. 1984. Secondary ilvaite in a dolerite dyke from Rogaland, SW Norway. *Mineral. Mag.*, **48**:449-456
- Blackburn W.H. & Dennen W.H. 1997. Encyclopedia of mineral names. The Canadian Mineralogist, Special Publication #1. *Mineral. Assoc. Can.*, 360p.
- Cathelineau M. 1988. Cation site occupancy in chlorites and illites as a function of temperature. *Clay Minerals*, **23**: 471-485
- Desborough G.A. & Amos D.H. 1961. Ilvaite: a late magmatic occurrence in gabbro of Missouri. *Am. Mineral.*, **46**:1509-1511
- Gauthier G. & Albandakis N. 1991. Minerals of the Seriphos karn, Greece. *The Mineral. Rec.*, **22**:303-308.
- Gole M.J. 1981. Ca-Fe-Si skarns containing babingtonite: first known occurrence in Australia. *Can. Mineral.*, **19**:269-277
- Gustafson W.I. 1974. The stability of andradite, hedbergite, and related minerals in the system Ca-Fe-Si-O-H. *J. Petrol.*, **15**:455-496
- Kwak T.A.P. 1983. The geology and geochemistry of the zoned, Sn-W-F-Be skarns at Mt. Lindsay, Tasmania, Australia. *Econ. Geol.*, **78**:1440-1465
- Nauslund H.R., Hughes J.M., Birnie R.W. 1983. Ilvaite, an alteration product replacing olivine in the Skaergaard intrusion. *Am. Mineral.*, **68**:1004-1008
- Pesquera A. & Velasco F. 1986. An occurrence of ilvaite layers in the Cinco Villas metassomatic rocks, Western Pyrenees (Spain). *Mineral. Mag.*, **50**:653-656
- Plimer I.R. & Ashley P.M. 1978. Manganese ilvaite from Broken Hill, N.S.W. and Bar Bar, Queensland, Australia. *Mineral. Mag.*, **42**:85-88

Shannon E.V. 1918. On the occurrence of ilvaite in the South Mountain District, Owyhee County, Idaho. *Am. J. Sci.*, **45**:118-125

Tallarico F.H.B., Oliveira C.G., Figueiredo B.R. 2000 The Igarapé Bahia Cu-Au mineralization, Carajás Province. *Rev. Bras. Geoc.*, **30**:230-233

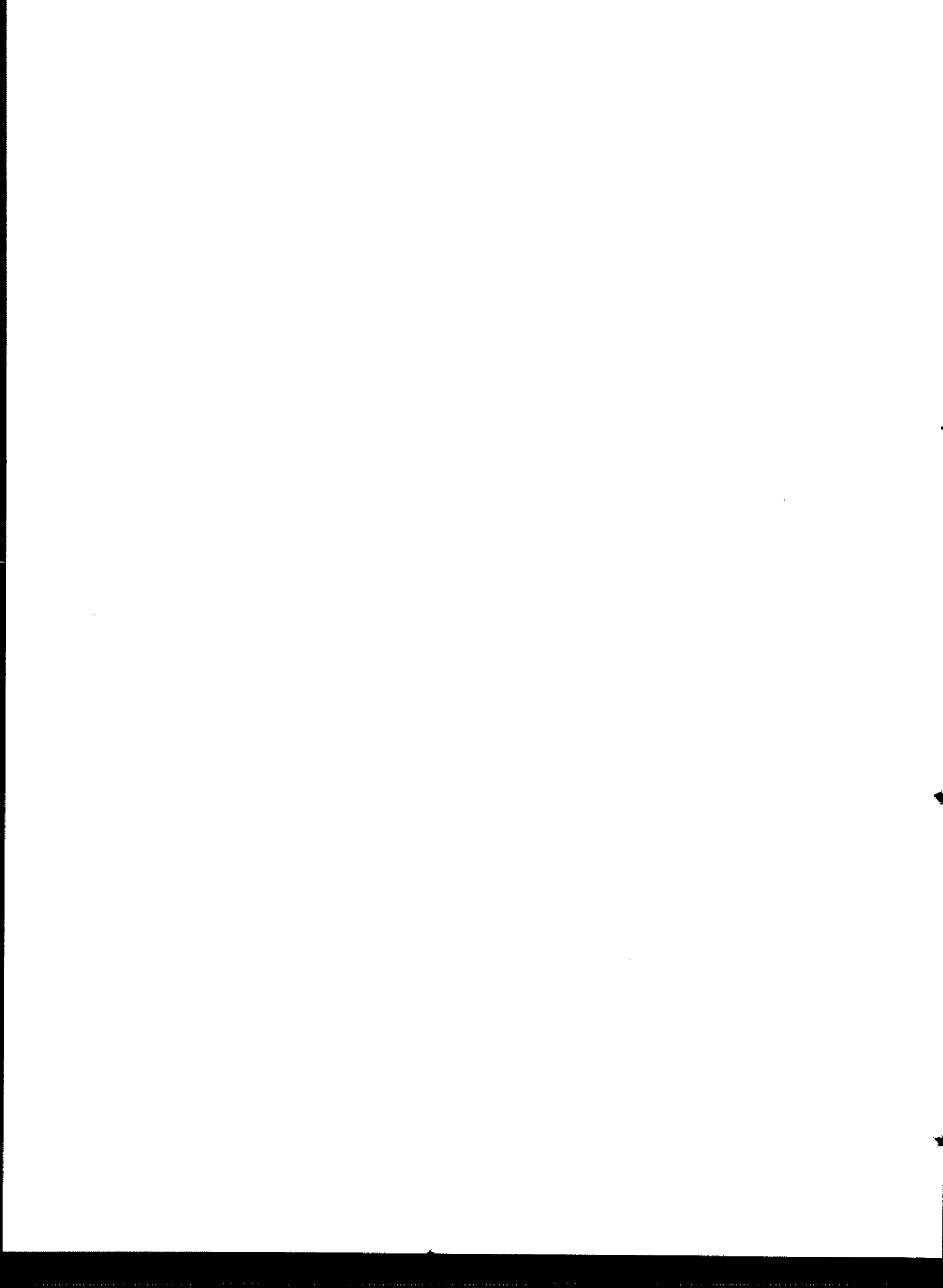
Wise W.S. & Moller W.P. 1990. Occurrence of Ca-Fe-silicate

minerals with zeolites in basalt cavities at Bombay, India. *Europ. J. Mineral.*, **2**:875-883

Manuscrito NB-42  
Recebido em 15 de fevereiro de 2002  
Revisão do autor em 22 de março de 2002  
Revisão aceita em 31 de março de 2002

#### **ANEXO 4**

Geology and SHRIMP geochronology of the Igarapé Bahia Fe-oxide Cu-Au-(U-REE)  
mineralisation, Carajás copper-gold belt, Brazil: an Archean (2.57 Ga) Olympic Dan-Type  
deposit



**Geology and SHRIMP II U-Pb Geochronology of the Igarapé Bahia Fe-oxide Cu-Au-(U-REE)**

**Mineralisation, Carajás Copper-Gold Belt, Brazil: an Archean (2.57 Ga) Olympic Dam-Type Deposit**

FERNANDO H. B. TALLARICO, Instituto de Geociências, Universidade Estadual de Campinas, Caixa Postal 6152, 13.083-970, Campinas, SP, Brazil, fernando@ige.unicamp.br.

BERNARDINO R. FIGUEIREDO, Instituto de Geociências, Universidade Estadual de Campinas, Caixa Postal 6152, 13.083-970, Campinas, SP, Brazil.

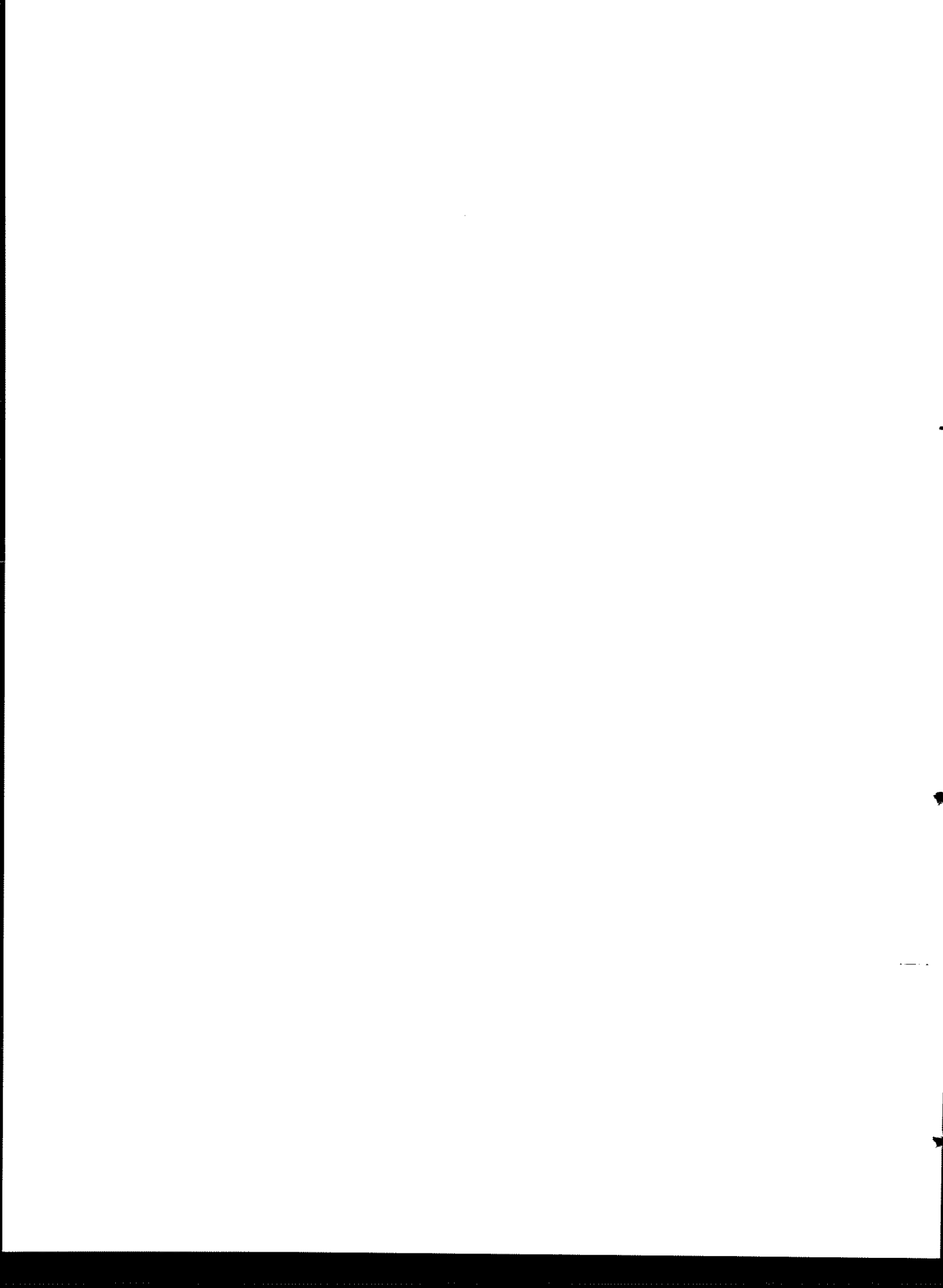
DAVID I. GROVES, Centre for Global Metallogeny, Department of Geology & Geophysics, University of Western Australia, 35 Stirling Highway, Crawley WA 6009, Australia.

NEAL J. MCNAUGHTON, Centre for Global Metallogeny, Department of Geology & Geophysics, University of Western Australia, 35 Stirling Highway, Crawley WA 6009, Australia.

IAN R. FLETCHER, Centre for Global Metallogeny, Department of Geology & Geophysics, University of Western Australia, 35 Stirling Highway, Crawley WA 6009, Australia.

JOSÉ L. REGO, Companhia Vale do Rio Doce, Caixa Postal 51, Serra dos Carajás, 68.516-000, Parauapebas, PA, Brazil.

Abstract .....	1
Introduction.....	2
Regional geology and metallogeny.....	4
Geology of the Igarapé Bahia Fe-oxide Cu-Au-(U-REE) deposit.....	7
Geochemistry.....	10
Sampling and analytical procedures for SHRIMP II analysis.....	11
SHRIMP II U-Pb results.....	12
Strontium isotopic composition of carbonate minerals.....	14
Deposit and genetic model for the Igarapé Bahia Fe-oxide Cu-Au-(U-REE) mineralization.....	15
Discussion.....	17
Acknowledgments.....	19
References.....	19
Tables (1 to 7) .....	29
Figures (1 to 15) .....	37



# **Geology and SHRIMP II U-Pb Geochronology of the Igarapé Bahia Fe-oxide Cu-Au-(U-REE) Mineralisation, Carajás Copper-Gold Belt, Brazil: an Archean (2.57 Ga) Olympic Dam-Type Deposit**

**FERNANDO H. B. TALLARICO<sup>1,2</sup>, BERNARDINO R. FIGUEIREDO<sup>1</sup>,**

*1. Instituto de Geociências, Universidade Estadual de Campinas, Caixa Postal 6152, 13.083-970, Campinas, SP, Brazil*

**DAVID I. GROVES<sup>2</sup>, NEAL J. MCNAUGHTON<sup>2</sup>, IAN R. FLETCHER<sup>2</sup>**

*2. Centre for Global Metallogeny, Department of Geology & Geophysics, University of Western Australia,  
35 Stirling Highway, Crawley WA 6009, Australia*

**AND JOSÉ L. REGO<sup>3</sup>**

*3. Companhia Vale do Rio Doce, Caixa Postal 51, Serra dos Carajás, 68.516-000, Parauapebas, PA, Brazil*

## **Abstract**

A striking feature of the Carajás region is the clustering of a variety of Cu-Au deposits. The most abundant in the belt are the world-class (> 200 Mt) Fe-oxide Cu-Au-(U-REE) deposits, that, despite the variety of host rocks and different orebody morphologies, share a series of diagnostic features, such as: (a) intense Fe-metasomatism leading to the formation of grunerite, fayalite and/or Fe-oxides (magnetite and/or hematite), (b) intense carbonate alteration (mainly siderite), (c) sulfur-poor ore paragenesis (chalcopyrite and bornite), (d) quartz-deficient ore systems, (e) extreme LREE enrichment, and (f) enrichment in U and Co. The Igarapé Bahia is perhaps the best documented Fe-oxide Cu-Au-(U-REE) deposit of the belt, containing about 219 Mt @ 1.4 % Cu and 0.86 g/t Au. The Cu-Au ore consist of steeply dipping breccia bodies that are hosted by hydrothermally altered metavolcano-sedimentary rocks.

SHRIMP II zircon dating of the host metavolcanic rocks gives a  $^{207}\text{Pb}/^{206}\text{Pb}$  age of  $2751 \pm 42$  Ma. This result is sufficient to correlate the Igarapé Bahia volcano-sedimentary sequence to the Grão Pará volcanic

rocks that are consistently dated at ca. 2.75 Ga by various authors. The *in situ* SHRIMP II dating of monazite, from the matrix of ore-bearing magnetite breccias, gives a  $^{207}\text{Pb}/^{206}\text{Pb}$  age of  $2575 \pm 12$  Ma. The result confirms the epigenetic nature of the mineralisation, and places it  $\sim 175$  Ma after accumulation of the host volcano-sedimentary sequence. The SHRIMP II dating of zircon xenocrysts recovered from crosscutting diabase dikes indicate a maximum  $^{207}\text{Pb}/^{206}\text{Pb}$  age of  $2579 \pm 7$  Ma, consistent with field evidence and the SHRIMP II ages of the ore and host rocks.

The  $2575 \pm 12$  Ma U-Pb in monazite SHRIMP II age of the Igarapé Bahia mineralisation is virtually undistinguishable from the conventional  $^{207}\text{Pb}/^{206}\text{Pb}$  ages, previously determined, on zircons from the Archean A-type granites of the Carajás Belt, as for example the Old Salobo Granite and the Itacaiúnas Granite. These data indicate that the mineralisation processes at Igarapé Bahia were temporally related to the A-type Archean granites of the Carajás Belt.

The styles of hydrothermal alteration, mineralogy and geochemistry of the Igarapé Bahia ore, as well as fluid inclusion and stable isotope data, support its classification as a member of the world-class Olympic Dam-type Fe-oxide Cu-Au-(U-REE) deposit group, as previously argued by several authors. The SHRIMP II  $^{207}\text{Pb}/^{206}\text{Pb}$  age of  $2575 \pm 12$  Ma for hydrothermal monazite is important as it clearly defines Igarapé Bahia as the first well-established Archean example of an Olympic Dam-type deposit.

## Introduction

The Carajás Belt is a highly mineralized province, with not only world-class iron and manganese ores (Tolbert et al., 1971; Valarelli et al., 1978; Gibbs and Wirth, 1990), but also a large number of Cu-Au deposits, known collectively as the Carajás Copper-Gold Belt (Fig. 1). There appears to be two distinct types of Cu-Au deposits in the Carajás region. The first group includes Cu-Au-(W-Bi-Sn) deposits that contain quartz veins, and may or may not have associated Fe-oxides, that are genetically related to the cooling of Paleoproterozoic (ca. 1.88 Ga) A-type granites. Representative examples of this deposit-type are the Breves (Tallarico et al. *in press*) and Águas Claras deposits (Soares et al., 1994; Silva and Villas, 1998).

In addition to these, there are several world-class ( $> 200$  Mt) Fe-oxide Cu-Au-(U-REE) deposits, that, despite the variety of host rocks and different orebody morphologies, share a series of diagnostic features, such as: (a) intense Fe-metasomatism leading to the formation of grunerite, fayalite and/or Fe-oxides

(magnetite and/or hematite), (b) intense carbonate alteration, (c) sulfur-poor ore paragenesis (chalcopyrite and bornite), (d) absence of quartz due to silica dissolution, (e) extreme LREE enrichment, and (f) enrichment in U and Co. The most significant Fe-oxide Cu-Au-(U-REE) deposits of the belt are Salobo (Farias and Saueressig, 1982; Vieira et al., 1988; Lindenmayer, 1990), Sossego (Huhn and Nascimento, 1996; Cordeiro, 1999), Cristalino (Cordeiro, 1999; Huhn et al., 1999a), Cento e Dezoto (Rigon et al., 2000) and Igarapé Bahia (Ferreira Filho, 1985; Ribeiro, 1989; Tallarico, 1996; Bocalon, 1997; Tallarico et al., 1998, Almada, 1998; Lindenmayer et al., 1998; Tazava, 1999).

Igarapé Bahia is the only gold deposit presently being mined in the region, and is perhaps the best documented example of the Fe-oxide Cu-Au-(U-REE)-type of the Carajás Belt. The discovery of the deposit began in 1974 when Rio Doce Mineração e Geologia S.A. (Docegeo), the exploration branch of Companhia Vale do Rio Doce (CVRD), located significant copper anomalies in stream sediment samples from the Igarapé Bahia River. During the 1980's, several soil geochemistry surveys and subsequent drilling resulted in the discovery of three outcropping orebodies: Acampamento Norte (ACPN), Acampamento Sul (ACPS) and Furo Trinta (FT). The start-up of the mine was in 1991, with a processing capacity of 80,000 tonnes of ore per month. In 1994, the nominal capacity of the plant was doubled. In 1996, the Alemão orebody (ALM) was located, at a depth of 250 meters, through geological and geophysical modeling of an air-borne magnetic anomaly followed by drilling (Barreira et al., 1999). Total resources of primary ore, including the four orebodies, is of 219 Mt @ 1.4 % Cu and 0.86 g/t Au (Table 1). The original reserve of oxidized gold ore was 15 Mt of high-grade ore @ 5 g/t Au and 14 Mt of low-grade ore @ 1.4 g/t Au. To date, total production of gold is approximately 92 tonnes, derived exclusively from supergene-enriched ore in the oxidized zone.

Previous genetic interpretations for Igarapé Bahia include syngenetic VHMS (Besshi-type) models (e.g., Ferreira Filho, 1985; Almada, 1999), epigenetic hydrothermal-magmatic models, with ore related to Paleoproterozoic (ca. 1.88 Ga) granites (e.g., Lindenmayer et al., 1998), and multistage models that claim an interplay of Archean and Proterozoic processes (e.g., Ribeiro, 1989; Mougeot, 1996). Alternatively, similarities with the Australian Olympic Dam Deposit (Roberts and Hudson, 1983; Oreskes and Einaudi, 1990; Reeve et al., 1990) has encouraged several authors to propose an epigenetic hydrothermal model, related to an alkaline magmatic component of unknown age (Huhn and Nascimento, 1996; Tallarico, 1996; Tallarico et al., 1998; Oliveira et al., 1998; Tazava, 1999; Soares et al., 1999). Uncertainties in interpretation

relate partly to poor exposure of fresh rocks, but mainly due to the absence of robust geochronological data on the ore and host rocks.

The aim of this paper is to provide a brief description of the geology and geochemistry of the Igarapé Bahia deposit, and to put constraints on the age of the mineralisation via SHRIMP II geochronology, so that a much better constrained genetic model can be formulated.

### **Regional Geology and Metallogeny**

The Carajás region (Fig. 1) lies on the eastern portion of the Archean Amazonian Craton, being limited to the east by the Neoproterozoic Araguaia Belt and to the west by overlying Proterozoic sequences (Araújo and Maia, 1991; Docegeo, 1988; Tassinari and Macambira, 1999). To the north, it is concealed by Proterozoic and Cenozoic sedimentary rocks of the Amazon Basin (Pinheiro and Holdsworth, 1997). To the south, it is in contact with the Rio Maria Block (Docegeo, 1988; Huhn et al., 1988), a relatively older, typical granitoid-greenstone terrain that hosts lode-gold deposits, as for example the Sapucaia and Cumaru deposits (Villas and Santos, 2001 and references therein).

Basement rocks consist of gneiss and migmatite of the Xingú Complex and the orthogranulites of the Pium Complex that were metamorphosed at ca. 2.8 Ga (Machado et al., 1991; Rodrigues et al., 1992; Pidgeon et al., 2000). According to Araújo et al. (1988), the Pium Complex represents slabs of infracrustal rocks uplifted through deep shear zones, and could possibly represent the suture zone between the Rio Maria Block and the Carajás Belt. In the Carajás Belt, the basement assemblage defines a broad, steeply-dipping, E-W-trending ductile shear zone, named the Itacaiúnas Shear Zone, that experienced multiple episodes of reactivation during the Archean and Paleoproterozoic (Pinheiro and Holdsworth, 1997; Holdsworth and Pinheiro, 2000).

The Carajás region includes one of the best preserved Archean volcano-sedimentary successions in the world. These rocks, assembled under the Itacaiúnas Supergroup, record different metamorphic grades, ranging from virtually undeformed, low greenschist-facies rocks (Grão Pará Group) in the innermost portions of the belt, to intensely sheared amphibolite/granulite-facies rocks (Salobo Group) at the northern edge of the Itacaiúnas Shear Zone (Docegeo, 1988; Olszewski et al., 1989). Accumulation of the volcanic rocks was determined by various authors to have occurred at ca. 2.75 Ga (e.g., Machado et al., 1991; Trendall et al.,

1998). The Grão Pará Group is the dominant volcano-sedimentary sequence in the Carajás Basin, and includes low-grade metavolcanic rocks that host significant banded-iron formation. These contain the giant iron deposits, such as Serra Norte, Serra Sul, Serra Leste and Serra de São Felix, that contain total resources of 17.3 billion tonnes @ 66% Fe (Tolbert et al., 1971; Gibbs and Wirth, 1990).

Sandstones and siltstones that formed in a shallow marine to fluvial environment (Águas Claras Formation - Nogueira et al., 1994; Nogueira et al., 2000), overlie the former units. A minimum age of  $2645 \pm 12$  Ma for the Águas Claras Formation was determined by Dias et al. (1996) from conventional U-Pb analysis of zircons from cross-cutting gabbro dikes. A SHRIMP II U-Pb age of  $2681 \pm 5$  Ma was determined by Trendall et al. (1998) from a sample of sandstone containing zircons apparently derived from syndepositional volcanism. Based on this result, Trendall et al. (1998) inferred that the Águas Claras Formation could represent the uppermost unit of a continuous accumulation in the “Grão Pará Basin”, that lasted less than 100 million years.

The Carajás region has been intruded by granitic magmas of distinct ages and compositions. Paleoproterozoic intrusions (ca. 1.88 Ga, Machado et al., 1991) include several anorogenic granitic plutons, such as the Central Carajás and Cigano granites. The latter belong to the most extensive A-type Proterozoic Province of the world (e.g., Santos et al. 2001), that covers thousands of square kilometers of the Amazonian Craton. Archean intrusions include granitoids and diorites of the Plaquê Suite (ca. 2.74 Ga – Huhn et al. 1999b) and younger alkaline granitoids (ca. 2.57 Ga), such as the Estrela Complex (Barros et al., 1992; Barros et al., 1997; Barros and Barbey, 1998; Barros et al. 2001), the Old Salobo Granite (Machado et al., 1991) and the Itacaiúnas Granite (Souza et al., 1996). The Estrela Complex is the best documented example of the Archean alkaline granitoids of the Carajás Belt. According to Barros et al. (1997), it consists of a E-W-trending, heterogeneously sheared monzogranitic batholith, that bears a characteristic A-type geochemical signature defined by high  $K_2O+Na_2O$  content, extremely high  $FeO/FeO_t+MgO$  ratio, and elevated Zr, Y and Nb contents. Fabric analysis of the Estrela Complex indicates that magmatic activity was syntectonic to the closure of the Carajás Basin (Barros and Barbey, 1998; Barros et al. 2001).

A striking feature of the Carajás region is the clustering of a variety of Cu-Au deposits. The most abundant in the belt are Fe-oxide Cu-Au-(U-REE) deposits, that are hosted by a variety of rocks and have different orebody morphologies, although most are near-vertical ( $> 75^\circ$ ) breccia bodies. The most significant

examples of this deposit-type are: Salobo with resources of 994 Mt @ 0.94 % Cu and 0.52 g/t Au (Farias and Sauressig, 1982; Vieira et al., 1988; Lindenmayer, 1990), Igarapé Bahia with resources of 219 Mt @ 1.4 % Cu and 0.86 g/t Au (Ferreira Filho, 1985; Almada, 1998; Tazava, 1999; Tallarico, 2000), Sossego with resources of 355 Mt @ 1.1 % Cu and 0.28 g/t Au (Cordeiro, 1999; Lancaster et al., 2000), Cristalino with resources of 500 Mt @ 1.0 % Cu and 0.3 g/t Au (Huhn et al., 1999a) and Cento e Dezoto with resources of 170 Mt @ 1.0 % Cu and 0.3 g/t Au (Rigon et al., 2000).

A second style of Cu-Au deposit is that characterized by a Cu-Au-(W-Bi-Sn) association. This group includes a smaller number of deposits, all of medium to small size, that appear to be genetically related to Proterozoic A-type magmatism. Representative examples are the Águas Claras Cu-Au-(W-Sn) deposit with resources of 9.5 Mt of oxidized ore @ 2.43 g/t Au (Soares et al., 1994; Silva and Villas, 1998), and the Breves Cu-Au-(W-Bi-Sn) deposit with resources of 50 Mt of primary ore @ 1.22% Cu, 0.75 g/t Au, 2.4 g/t Ag, 1200 g/t W, 70 g/t Sn, 175 g/t Mo and 75 g/t Bi (Tallarico et al. in press).

The major question to be resolved in the Carajás Copper-Gold Belt is the relationship between the relatively small (< 50 Mt) Paleoproterozoic (ca. 1.88 Ga) Cu-Au-(W-Bi-Sn) deposits (Tallarico et al. in press) and the world-class (> 200 Mt) Fe-oxide Cu-Au-(U-REE) deposits. One possibility is that they are both related to the ca. 1.88 Ga A-type granites, but a number of the features of the Fe-oxide Cu-Au-(U-REE) deposits make this unlikely because these features are extremely rare or non-existent in the Cu-Au-(W-Bi-Sn) deposit group. These features include: (a) intense Fe-metasomatism leading to the formation of fayalite, grunerite, and/or Fe-oxides (magnetite and/or hematite), (b) the extent of carbonate alteration (mainly siderite), at least in the lower temperature deposits, (c) the S-deficient nature of ore sulfides (chalcocite, bornite, and primary chalcocite), (d) the quartz-deficient nature of the ore systems, (e) the extreme LREE enrichment (approximately  $10^4$  x chondritic values), and (f) enrichment in U and Co. Given the evidence for an alkaline association for Fe-oxide Cu-Au-(U-REE) deposits elsewhere in the world (e.g., Hitzman et al., 1992; Oreskes and Hitzman, 1993; Campbell et al., 1998; Groves and Veilreicher, 2001), it is possible that the iron-oxide Cu-Au-(U-REE) deposits of Carajás are related to 1.88 Ga magmatism, but to more alkaline rocks than the A-type granites (e.g., Kerrich et al. 2000). The other interesting possibility is that they are related to the ca. 2.57 Ga alkaline complexes of the Carajás Belt (e.g., Estrela Complex, Old Salobo Granite), in which case they would represent the oldest known members of the iron-oxide Cu-Au-(U-REE) group worldwide.

This study tests these genetic alternatives via robust SHRIMP II geochronology of host rocks and ore-related minerals at Igarapé Bahia, a typical member of the iron-oxide Cu-Au-(U-REE) deposit group.

### **Geology of the Igarapé Bahia Fe-oxide Cu-Au-(U-REE) Deposit**

The Igarapé Bahia deposit is hosted by a hydrothermally altered metavolcano-sedimentary sequence, the Igarapé Bahia Group. The host sequence, together with the FT, ACPS and ACPN orebodies, crop out in a small structural window within the overlying sandstones of the Águas Claras Formation (Fig. 2). The orebodies define a circular structure at surface, with a shape similar to that of an alkaline ring complex (Fig. 3). The ALM orebody is covered by a 250-m-thick discordant layer of sandstone, and is part of the ACPN orebody which has been faulted out (Soares et al., 1999).

The orebodies consist of steeply dipping ( $\sim 75^\circ$ ) breccia bodies that dip outwards in broad concordance with the strike of the bedding of the host sequence. The ore-bearing breccias are sited at, or close to, the contact zone between two distinct units of the host sequence. The footwall is dominated by volcanic and pyroclastic rocks intercalated with banded iron formations (BIF), whereas the hangingwall includes mainly sedimentary and epiclastic rocks (Fig. 4A and B) and minor BIF and volcanic rocks. The mineralized breccias include fragments of both footwall and hangingwall that are cemented by variable amounts of hydrothermal matrix (Fig. 4C to F).

A set of radial fractures and faults controls the emplacement of quartz diorite and diabase dikes, which disrupt the orebodies, the host volcano-sedimentary sequence, and the Águas Claras sandstone. The quartz diorite dikes display a variety of textures ranging from unaltered granophytic intergrowths to highly altered, veined and/or brecciated rocks, whereas the diabase dikes are texturally monotonous and unaltered.

#### *Supergene alteration and ore types*

At Igarapé Bahia, weathering was responsible for the development of a 200-m-thick supergene profile (Zang and Fyfe, 1993; Angélica, 1996), that initiated the dissolution, segregation and reprecipitation of gold and copper, resulting in the formation of different ore-types (Table 1).

The upper part of the profile includes a gold-bearing gossan that extends to a depth of approximately 150 meters. The gossan is formed mainly of goethite, hematite, gibbsite and kaolinite, and has traces of secondary copper minerals and REE-rich phosphates (florencite, crandalite and rhabdophane).

From 150 to 200 meters there is a transitional zone, where copper-rich supergene solutions precipitated. This copper-gold ore is composed of goethite and hematite, together with abundant secondary copper minerals, such as native copper, chalcocite, digenite, cuprite, malachite, azurite, and pseudomalachite.

The primary copper-gold mineralisation occurs beneath 200 meters, and consists mainly of Fe-chlorite, siderite and magnetite-rich breccias.

#### *Hypogene hydrothermal alteration and breccia-types*

The ore-bearing breccias of Igarapé Bahia are essentially polymictic. Thus their classification is based on matrix mineralogy, leading to the following groups: (a) Fe-chlorite breccias, (b) siderite breccias, and (c) magnetite breccias. The rock fragments display angular to sub-rounded shapes, and diameters that range from a few millimeters up to 20 cm. The fragment/matrix ratio is highly variable, apparently reflecting different fluid/rock ratios.

Magnetite breccias exhibit a granular matrix of euhedral magnetite that is welded by Cu-sulfides (chalcopyrite in equilibrium with bornite), together with minor grunerite, actinolite, minnesotaite, biotite stilpnomelane, K-feldspar, tourmaline, fluorite, siderite, ankerite and uraninite. This mineral assemblage defines a distinctive Fe-(K)-metasomatic zone.

Iron-chlorite breccias and siderite breccias include virtually the same matrix mineralogy, but the percentage of specific minerals is distinct. The matrix is typically fine-grained and includes Fe-chlorite, siderite, magnetite, chalcopyrite and minor tourmaline.

At the ACPS and FT orebodies, the mineralisation is hosted preferentially by siderite breccias, whereas at the ACPN and ALM orebodies, it is associated with magnetite breccias. Iron-chlorite breccias occur at the margins of all orebodies and are also mineralized (Fig. 5).

Chloritization is the most widespread hydrothermal alteration type in the deposit. Chlorite composition shows a diagnostic chemical trend based on the substitution reaction:  $\text{Si}_{\text{IV}}^{4+} + \text{Mg}_{\text{VI}}^{2+} \leftrightarrow \text{Al}_{\text{IV}}^{3+} + \text{Fe}_{\text{VI}}^{3+}$  (Zang & Fyfe, 1995). Mg-chlorite (50>mg>30) is typically associated with calcite and dolomite in

barren and weakly altered distal host rocks, whereas Fe-chlorite ( $30 > mg > 12$ ) is associated with siderite, chalcopyrite and magnetite in the mineralised breccias (Tallarico et al., 2000).

Scanning electron microscopy (SEM) investigation of breccias reveals the presence of the following trace minerals: molybdenite, galena, cobaltite, hessite, altaite, cassiterite, ferberite, scheelite, uraninite, parisite, bastnäsite, allanite, monazite, apatite, and fluorite. The breccia matrix is known also to include chloride-rich minerals such as ferropyrosmalite (Tazava, 1999) and escapolite (Althoff et al., 1994).

Several vein types crosscut the breccias bodies and the host sequence. Veins are discordant to bedding and rarely display comb structures. The most common vein-types are: (a) calcite + chalcopyrite  $\pm$  fluorite  $\pm$  stilpnomelane, (b) ankerite  $\pm$  chalcopyrite  $\pm$  gold, (c) siderite  $\pm$  calcite  $\pm$  chlorite  $\pm$  chalcopyrite, and (d) chalcopyrite  $\pm$  biotite  $\pm$  K-feldspar  $\pm$  tourmaline  $\pm$  REE-minerals. The vein chronology is unclear due to poor exposure and equivocal relationships.

#### *Primary copper-gold mineralisation*

The primary copper mineralisation at Igarapé Bahia is related to the presence of xenomorphic and poikiloblastic chalcopyrite in the matrix of breccias. Rarely, chalcopyrite is rimmed by chalcocite, digenite and covellite due to sub-solidus oxidation reactions along grain boundaries. Magnetite breccias, unlike siderite and Fe-chlorite breccias, have chalcopyrite intergrown with bornite, indicating relatively lower sulfur activity and/or a higher oxidation state of the hydrothermal fluids (Beane and Titley, 1981; Mücki and Ridley, 1993). Rare pyrite occurs as inclusions in chalcopyrite in the more sulfur-rich assemblages.

The major copper mineralisation is juxtaposed against gold mineralisation in all breccia bodies. Additional sub-economic copper concentrations are disseminated, or in veins or nodules, in distal- altered host rocks with negligible gold contents.

Chalcopyrite nodules are hosted by hangingwall laminated sedimentary rocks (Fig. 4A). The nodules both bend the primary bedding and are also transgressive to it. They display a mineralogical zoning, with rims enriched in euhedral Fe-chlorite in association with minor albite and quartz, whereas the cores contain massive chalcopyrite, with inclusions of K-feldspar, cobaltite, thorite, monazite and apatite. Their epigenetic nature is also indicated by the connection of the nodules to veins with the same mineralogy and zoning pattern, that are both discordant and concordant to the sedimentary bedding (Fig. 4A and B). Rarely, rocks

from the hangingwall have stratabound replacement textures with chalcopyrite filling more porous and permeable layer of the laminated rocks.

Native gold occurs in the matrix of breccias as fine-grained particles, normally between 5 and 20  $\mu\text{m}$  diameter, included in gangue minerals (quartz, siderite and chlorite), chalcopyrite and rarely magnetite. Sub-economic concentrations of silver are associated with the gold particles, that can contain up to 12 wt% Ag, or include tellurides (hessite -  $\text{Ag}_2\text{Te}$ ) and sulfides (argentite/acanthite –  $\text{Ag}_2\text{S}$ ).

### Geochemistry

The mineralized breccias contain anomalous concentrations of FeO (25-64 wt%), Cu (0.5-11 wt%), U (28-380 ppm), Au (0.5-15 g/t), Ag (4-52 g/t), Ba (26-200 ppm), F (390-31,000 ppm), P (900-6,200 ppm) and REE, particularly La (260-2,300 ppm) and Ce (450-4,400 ppm) (Fig. 6). The ore-bearing breccias are also enriched in MnO (0.5-3 wt%), CaO (0.5-9 wt%), Mo (50-200 ppm) and Zn (150-450 ppm) relative to the host rocks (Tallarico et al., 2000). The positive correlation between these elements suggests a common metasomatic origin and reflects the interplay of Fe-(K)-metasomatism, sulfidation, chloritization and carbonate alteration. The occurrence of traces of barite, fluorite, galena, altaite, sphalerite, molybdenite, uraninite, apatite, monazite, xenotime, bastnasite and parisite, as inclusions in chalcopyrite and gangue minerals, accounts for the Ba, F, Pb, Zn, Mo, U, REE and P enrichments. The high manganese content is related to siderite, which contains up to 7 wt% MnO.

Iron-chlorite breccias, siderite breccias and magnetite breccias show similar REE distribution patterns (Fig. 7), that are typified by strong LREE enrichment ( $\sim 10^4$  chondritic values). Although the absolute concentrations of REE are quite distinct, the distribution patterns of altered metavolcanic rocks, quartz diorite dikes and mineralized breccias show equivalent shapes, while the BIF display a different pattern. The REE-minerals of the Igarapé Bahia breccias are unequivocally related to hydrothermal alteration. Thus, the REE distribution patterns can be used to monitor the intensity of the hydrothermal alteration. The contrasting La/Lu ratios of the host metavolcanic rocks (70-250) and breccias (1,000-2,500) indicate that the hydrothermal alteration selectively concentrated LREE. The positive correlation between La, Ce, P, Cu and Au assures that minerals enriched in LREE (e.g., monazite) are clearly suitable for dating mineralization-related alteration.

### **Sampling and Analytical Procedures for SHRIMP II Analysis**

The samples selected for SHRIMP II analyses are listed in Table 2. Bulk samples of representative intersections of the host metavolcanic rocks from the footwall (UWA-B18C and UWA-B18D) and diabase dikes (UWA-B21D and UWA-B36A) were collected, and zircons extracted. Zircons from the metavolcanic rocks and from the diabase dikes were concentrated in an attempt to determine their crystallization ages. Samples of hydrothermal monazite (UWA-B34) from the matrix of ore-bearing magnetite breccias were prepared to constrain the age of ore formation.

The separation of zircon samples was carried out at the Universidade Federal de Ouro Preto, Brazil, with final handpicking at the University of Western Australia. After identification of zircons in thin-section, the samples were crushed and a <60# fraction collected, cleaned, and the final selection of zircons hand-picked and mounted in epoxy resin together with chips of the 564 Ma CZ3 standard zircon (Pidgeon et al., 1994; Nelson, 1997). After detailed photography and SEM imaging, the discs were cleaned and coated with high-purity gold.

Uranium-Th-Pb isotope analyses of sectioned single zircons were carried out on the Sensitive High Resolution Ion Microprobe (SHRIMP II) at Curtin University of Technology following the procedures documented by Compston et al. (1986), Williams and Claesson (1987) and Smith et al. (1998). Data were processed using the software package SQUID 1.00 (Ludwig, 2001a).

Monazite SHRIMP II analyses were performed *in situ* on discs and fragments of polished thin sections that were mounted in epoxy mounts. The monazite analyses used two standards (VK1, 488 Ma) both within the same mount and a separate mount. Analytical and data reduction methods for monazite are described by Foster et al. (2000) and Rasmussen et al. (in press).

The uncertainties in the radiogenic Pb isotope ratios are governed principally by ion-counting precision in the isotopes of direct interest and also in  $^{204}\text{Pb}$ , which provides a measure of common Pb. As the  $^{204}\text{Pb}$  content indicated by the analyses of most of the sample zircons is similar to that obtained from the standard zircon analyses, it is assumed that all the Pb came from the gold coat (i.e. Broken Hill galena composition). The data used for age determinations all gave very low common-Pb corrections and are therefore insensitive to the choice of common-Pb composition. All analysis with higher levels of common Pb

have other indications of isotopic disturbance, and the common Pb cannot be assumed to be original, so the choice of composition is necessarily an estimate. The total Pb in each analysis was corrected from common Pb by stripping initial  $^{206}\text{Pb}$ ,  $^{207}\text{Pb}$  and  $^{208}\text{Pb}$  from the measured amounts, using the observed  $^{204}\text{Pb}$ , and Pb from the Broken Hill composition.

Ages are calculated using U decay constants from Jaffey et al. (1971). Unless otherwise stated, analytical uncertainties given in the tables and shown in plots are  $1\sigma$ . The ages from pooled data are weighted means, with uncertainties given as 95% confidence limits. Plots were prepared using ISOPLOT 2.49 (Ludwig, 2001b).

### SHRIMP II U-Pb Results

#### *Host metavolcanic rocks: samples UWA-B18C and UWA-B18D*

Concentration of rock sample UWA-B18D yielded only three zircons out of approximately 8 kg of bulk rock. To test the efficiency of sample preparation techniques, and to increase the number of zircons, a second bulk sample of host metavolcanic rock was prepared. Again the number of zircons was very limited, with only six grains per 24 kg of crushed rock.

The rock samples display an isotropic fabric defined by abundant fine-grained chlorite associated with minor albite and quartz. The primary mineralogy is obliterated by the intense chlorite alteration. The abundance of chlorite and the limited amount of quartz indicate a mafic composition, which is confirmed by previous geochemical investigations of the Igarapé Bahia metavolcanic rocks (e.g., Ferreira Filho, 1985). Thus, the reduced number of zircons recovered is not unexpected, since mafic volcanic rock typically contain limited zircons.

A total of 13 sites were analyzed from the nine zircon grains (Table 3). Only five analyses (C.1-1, C.1-2, D.2-1, D.2-2 e C.6-1) were statistically coherent, yielding a  $^{207}\text{Pb}/^{206}\text{Pb}$  age of  $2751 \pm 42$  Ma, with a MSWD of 18 (Fig. 8). Among the rejected data, two are unquestionably inherited, with  $^{207}\text{Pb}/^{206}\text{Pb}$  ages of ~2864 (C.2-1 and D.1-1), consistent with previously reported ages for the Xingú Complex (e.g., Machado et al. 1991). The remaining data were rejected because of high U content (C.4-1, C.4-2 and C.5-1) and discordance >5% (C.3-1, D.3-1 and C.5-1).

#### *Diabase dikes: samples UWA-B36A and UWA-B21D*

Concentration of sample UWA-B36A yielded a limited quantity of zircons, 22 grains from approximately 31 kg of bulk rock. A second sample was prepared to overcome the limited material for analysis. Sample UWA-B21D yielded 10 zircons out of 40 kg of crushed rock.

A total of 39 spots were analyzed from 32 grains, but no consistent data emerged from the data set. Approximately half of the analyses, mostly from grains with higher U or high  $^{204}\text{Pb}$ , are  $> 5\%$  discordant (Table 4). The majority of the remaining data yield  $^{207}\text{Pb}/^{206}\text{Pb}$  ages that range from ~2889 to 2827 Ma. Spots D.8-3 and A.11-1 yield younger  $^{207}\text{Pb}/^{206}\text{Pb}$  ages of  $2593 \pm 31$  Ma and  $2579 \pm 7$  Ma, respectively. All the analyzed grains display typical corrosion textures, indicating that zircon were not in equilibrium with the host magma, and consequently are interpreted as inherited zircons. Thus, the  $^{207}\text{Pb}/^{206}\text{Pb}$  age of the youngest xenocryst,  $2579 \pm 7$  Ma, is assumed to be the maximum age of intrusion of the host dyke.

#### *Copper-gold bearing magnetite breccia: Sample UWA-B34*

Monazite grains were cut out of thin sections and mounted in epoxy, in order to guarantee high-quality petrographic control on the dated grains. The selected monazite crystals are fine-grained (20 to 40  $\mu\text{m}$ ), and occur in equilibrium with chalcopyrite and magnetite in the matrix of mineralized breccia (Fig. 9).

A total of 18 spots were analyzed from 18 monazite grains from sample UWA-B34 (Table 5). Most of the data fall in a tight cluster near to concordia, with the remainder trending towards the origin, denoting that this is not a simple recent Pb-loss trend (Fig. 10). The main cluster of data appears to be significantly reversely discordant. This is considered to be due to Pb/U calibration offsets because the standard was in a separate mount, and minor defects in the Th- and U-related matrix corrections, once standards have up to 15% Th, leading to a relatively large matrix correction. The tight grouping of the near-concordant data cluster is taken to indicate that the sample is concordant, and thus that the  $^{207}\text{Pb}/^{206}\text{Pb}$  data are reliable. Although not highly precise, the Th/U data are also well grouped, consistent with the sample being well preserved.

By omitting five analyses that are discordant relative to the main cluster (4.3-1, 4.3-2, 5.1-1, 5.1-2 and 7.1-1), a group of 13 analyses remains. Among these, there is one obvious young outlier (6.1-1) that yields a  $^{207}\text{Pb}/^{206}\text{Pb}$  age of  $2519 \pm 19$  Ma. Omitting this analysis gives a weighted mean  $^{207}\text{Pb}/^{206}\text{Pb}$  age of  $2575 \pm 12$  Ma (MSWD = 1.19, n = 12). Spot 2.3-1 is a marginal outlier, and, if rejected, the  $^{207}\text{Pb}/^{206}\text{Pb}$  age of the main

cluster is  $2572 \pm 10$  Ma (MSWD = 0.97, n = 11). Given the number of analysis, and the apparent disturbances of the isotopic system in ~33% of the data set, the rejection of analysis 2.3-1 is not justified, and thus a more conservative  $^{207}\text{Pb}/^{206}\text{Pb}$  age of  $2575 \pm 12$  Ma is assumed.

### Strontium Isotopic Composition of Carbonate Minerals

Eight samples of carbonate minerals from the Igarapé Bahia deposit were concentrated from the matrix of ore-bearing siderite breccias and crosscutting veins to investigate their strontium isotopic composition (Table 6) as a means of constraining fluid source. Preparation of carbonate samples and the subsequent isotopic analysis were carried out at the University of São Paulo, Brazil. Prior to isotopic analysis, X-ray powder diffraction analysis were performed at Companhia Vale do Rio Doce to determine the carbonate specie(s) in each sample.

As the rubidium content of siderite and calcite is negligible, their  $^{87}\text{Sr}/^{86}\text{Sr}$  ratios are assumed to be a reasonable approximation of the initial ratio of the original hydrothermal system from which they crystallized. Samples derived from non-metasomatised mantle (e.g., MORB) have low  $^{87}\text{Sr}/^{86}\text{Sr}$  ratios (~0.702-0.705) as a function of the low Rb/Sr ratio of the source, whereas more differentiated crustal rocks have high  $^{87}\text{Sr}/^{86}\text{Sr}$  ratios (>0.706) due to the incompatible nature of rubidium. The strontium isotopic composition of seawater is a balance between volcanism and continental sedimentation, and shows a composite pattern during geological time (e.g., Faure and Powell, 1972; Veizer and Compston, 1976).

The  $^{87}\text{Sr}/^{86}\text{Sr}$  ratios from the Igarapé Bahia carbonates are highly radiogenic and indicate a crustal derivation (Table 6). These values are inconsistent with the isotopic composition of seawater at ~2.575 Ga (Veizer and Compston 1976) and with the initial  $^{87}\text{Sr}/^{86}\text{Sr}$  ratios of the Grão Pará metavolcanic rocks ( $0.7057 \pm 0.0010$ ) determined by Gibbs et al. (1986). This evidence clearly precludes seawater as a major component of the hydrothermal system, as would be expected in syngenetic VHMS models (e.g., Ferreira Filho, 1985; Almada, 1999). The wide range of highly radiogenic  $^{87}\text{Sr}/^{86}\text{Sr}$  ratios (0.714 to 0.755) of the Igarapé Bahia carbonate minerals suggests multiple crustal sources, consistent with an epigenetic magmatic-hydrothermal origin (Fig. 11). Hydrothermal calcite and tourmaline from the Salobo deposit also show similar  $^{87}\text{Sr}/^{86}\text{Sr}$  ratios (Mellito, 1998), suggesting that highly radiogenic strontium signatures are common to the Fe-oxide Cu-Au deposits of the Carajás Belt.

### **Deposit and Genetic Model for the Igarapé Bahia Fe-oxide Cu-Au-(U-REE) Mineralisation**

The SHRIMP II results reported here are summarized in Table 7. The zircons extracted from the host metavolcanic rocks yield a  $^{207}\text{Pb}/^{206}\text{Pb}$  age of  $2751 \pm 42$  Ma. Although of very low precision, this result is sufficient to correlate the Igarapé Bahia volcano-sedimentary sequence to the Grão Pará volcanic rocks that are consistently dated at ca. 2.75 Ga by various authors (e.g., Gibbs et al., 1986; Wirth et al., 1986; Machado et al., 1991). This result is not unexpected since the so called Igarapé Bahia Group occurs within the domains of the Grão Pará Group, and possibly represents a distinct facies of the Grão Pará Basin.

The positive correlation between the REE, P, Au and Cu, and the evidence of chalcopyrite in equilibrium with REE-minerals in the mineralized breccias, confirms that monazite is genetically related to the precipitation of copper and gold in the Igarapé Bahia deposit. Thus, the *in situ* dating of monazite, from the matrix of ore-bearing magnetite breccias, unequivocally places constraints on the age of ore formation. The SHRIMP II  $^{207}\text{Pb}/^{206}\text{Pb}$  age of  $2575 \pm 12$  Ma for hydrothermal monazite confirms the epigenetic nature of the mineralisation, and places it  $\sim 175$  Ma after accumulation of the host volcano-sedimentary sequence. The data obtained from zircon xenocrysts recovered from the diabase indicate a maximum  $^{207}\text{Pb}/^{206}\text{Pb}$  age of  $2579 \pm 7$  Ma for dike emplacement, consistent with field evidence and the SHRIMP II ages of the ore and host rocks (Fig. 12).

The  $2575 \pm 12$  Ma U-Pb in monazite SHRIMP II age of the Igarapé Bahia mineralisation is virtually undistinguishable from the conventional  $^{207}\text{Pb}/^{206}\text{Pb}$  ages determined on zircons from the Archean A-type granites of the Carajás Belt, as for example the Old Salobo Granite ( $2573 \pm 2$  Ma, Machado et al. 1991) and the Itacaiúnas Granite ( $2560 \pm 37$  Ma, Souza et al. 1996). Similar ages have been also obtained via the Rb-Sr method in bulk samples of the Itacaiúnas Granite ( $2480 \pm 40$  Ma, Montalvão et al. 1984) and the Estrela Complex ( $2527 \pm 34$  Ma, Barros and Barbey 1998), and are possibly related to cooling of these alkaline intrusions. These data indicate that the mineralisation processes at Igarapé Bahia were temporally related to the A-type Archean granites of the Carajás Belt. The Rb-Sr bulk rock age of  $2577 \pm 72$  Ma for the Igarapé Bahia host metavolcanic rocks, determined by Ferreira Filho (1985), provides an additional support to this model since it indicates thermal resetting of strontium isotopes  $\sim 170$  Ma after volcanic accumulation, probably due to the emplacement of an A-type Archean granite or due to the associated mineralisation itself.

The epigenetic nature of the Igarapé Bahia Cu-Au mineralisation is supported by field evidence that includes: (a) the presence of fragments of both footwall and hangingwall in the breccias (Fig. 4C), and (b) the presence of chalcopyrite-rich veins and nodules in the hangingwall rocks (Fig. 4A and B). Additionally, the circular shape of the cluster of breccia bodies (Fig. 3) is similar to that of ring complexes associated with the intrusion of alkaline magmas.

An epigenetic model also is compatible with the characteristics of the Igarapé Bahia hydrothermal system. Chlorite thermometry of the mineralized breccia, determined by Tallarico et al. (2000), indicate a high-temperature hydrothermal system (313-375°C), consistent with the fluid inclusion data of Ribeiro (1989) and Lindenmayer et al. (1998). At these temperatures, the equilibrium assemblage of magnetite + chalcopyrite ± bornite, typical of the Igarapé Bahia breccias, indicates highly oxidized ( $f\text{O}_2 \sim 10^{-29}$  to  $10^{-31}$  atm) and S-poor ( $a_{\text{SS}} \sim 10^{-3}$  atm) ore fluids (Mikucki and Ridley, 1993). The high-temperature and oxidized nature of the Igarapé Bahia ore fluids is consistent with copper and gold transport via Cl-complexes (Figs. 13 and 14) in acid and saline fluids (Davidson and Large 1994). High-temperature, saline and acid solutions can also transport REE and U via Cl-complexes, with or without competing ligands such as fluoride,  $\text{CO}_{2(\text{aq})}$  or phosphorous species, depending upon their relative abundance (Gieré 1996). Mineralogical and geochemical data indicate that all of these ions were active in the Igarapé Bahia ore fluids, and probably promoted selective concentration of LREE, U, Cu and Au.

The stable isotope data of Oliveira et al. (1998) and Tazava (1999), from calcite and siderite in the matrix of mineralized breccias and crosscutting veins from the Igarapé Bahia deposit, yield a narrow range of negative values of  $\delta^{13}\text{C}$  (-9.3 to -5.8 ‰) and a relatively wide variation of  $\delta^{18}\text{O}$  (0.7 to 9.4 ‰; Fig. 15). The extremely negative  $\delta^{13}\text{C}$  values, coupled with the oxidized nature of the Igarapé Bahia hydrothermal system, denote a homogeneous deep-seated carbon source from which carbonate minerals were precipitated within a limited pH range. The wider range of  $\delta^{18}\text{O}$  values is interpreted as resulting from mixing of deep-seated solutions (high of  $\delta^{18}\text{O}$ ) with meteoric fluids (low of  $\delta^{18}\text{O}$ ). This fluid mixing hypothesis is consistent with fluid inclusion studies of the Igarapé Bahia hydrothermal system that indicate the existence of two distinct groups: (a) high-temperature (150-430°C) saline (up to 40% NaCl equivalent) inclusions, and (b) low-temperature (100-150°C) and low-salinity (~10% NaCl equivalent) inclusions (Ribeiro, 1989; Lindenmayer et al., 1998). Thus, stable isotope and fluid inclusion data both suggest that the progressive interaction of a high-

temperature, saline and acid magmatic fluid with low-temperature, oxidized and less saline meteoric solutions is the most likely depositional mechanism for the Igarapé Bahia ore.

The mineralogy, geochemistry, stable isotope composition and thermodynamic data of the Igarapé Bahia ore fluids are consistent with the geochronological evidence for an epigenetic mineralisation. The data suggest that ore formation was related to the emplacement of a suite of Archean (~2.57 Ga) A-type granites, with circulation and mixing of magmatic and meteoric fluids, through a set of ring fractures, triggering the deposition of Cu, Au, U, and REE through  $fO_2$  and temperature decrease and pH increase.

The strontium isotope composition of carbonate minerals from the matrix of mineralized breccias and crosscutting veins in the Igarapé Bahia deposit also are consistent with an epigenetic magmatic-hydrothermal model. The  $^{87}\text{Sr}/^{86}\text{Sr}$  ratios are incompatible with the expected composition of seawater at ~2.57 Ga, and strongly suggest the contribution of multiple radiogenic crustal-sources.

## Discussion

The previously proposed models relating Igarapé Bahia to syngenetic VHMS models (e.g., Ferreira Filho, 1985; Almada, 1999) are negated by the new robust geochronological data. Additionally, the grade-tonnage data of the Igarapé Bahia deposit (219 Mt of primary ore @ 1.4 % Cu and 0.86 g/t Au) would be unusual for the VHMS group, given that most deposits contain < 100 Mt ore (Large, 1992; Slack, 1993; Barrie and Hannington, 1999). The ore paragenesis of the Igarapé Bahia deposit, characterized by the association magnetite + chalcopyrite  $\pm$  bornite with significant amount of U (28-380 ppm), F (390-31,000 ppm), P (900-6,200 ppm), La (260-2,300 ppm) and Ce (450-4,400 ppm), is dramatically distinct from that of VHMS deposits that normally lack significant concentrations of Fe-oxides, typically contain relatively reduced ore sulfides (pyrite in equilibrium with pyrrhotite), and are not known to have anomalous concentrations of U, F, P or REE (Large, 1992; Slack, 1993; Barrie and Hannington, 1999).

The SHRIMP II results reported in this work, together with the mineralogical, geochemical and thermodynamic data for the Igarapé Bahia ore, indicate an epigenetic hydrothermal-magmatic origin, temporally related to the emplacement of Archean (~2.57 Ga) A-type granites of the Carajás Belt.

Iron-oxide Cu-Au-(U-REE) deposits have been recognized as a distinctive ore deposit-type during the last decade (Hitzman et al. 1992; Oreskes and Hitzman, 1993). Representative examples of this group include

the Olympic Dam deposit with resources of 2,000 Mt @ 1.6 % Cu and 0.6 g/t Au (Roberts and Hudson, 1983; Reeve et al., 1990; Hitzman et al. 1992; Cross et al., 1993; Oreskes and Hitzman, 1993) and the Ernest Henry deposit with resources of 167 Mt @ 1.1 % Cu and 0.5 g/t Au (Williams, 1998). These structurally controlled epigenetic deposits share a number of common features, such as: (1) high tonnage (> 100 Mt) and low copper (< 2.0 %) and gold (< 0.8 g/t) grades, (2) abundance of magnetite and/or hematite, (3) oxidized and S-poor ore paragenesis (chalcopyrite, bornite and/or chalcocite), (4) low SiO<sub>2</sub> content of the ore, and (5) metal association of Fe-Cu-Au with anomalous LREE, U, P, and F (Hitzman et al., 1992; Oreskes and Hitzman, 1993; Williams, 1998; Groves and Vielreicher, 2001). Ore fluids are typically high-temperature (200-600°C), extremely saline (as much as 50 wt% NaCl equivalent), acid and oxidizing, with *fO<sub>2</sub>* increasing at shallow levels (Hitzman et al., 1992; Oreskes and Hitzman, 1993; Davidson and Large, 1988). Fluid inclusion and stable isotope data commonly indicate the presence of two distinct fluids: (1) high-temperature saline magmatic fluids, and (2) relatively low-temperature and less saline meteoric fluids (Oreskes and Einaudi, 1992; Oreskes and Hitzman, 1993; Gow et al., 1994; Haynes et al., 1995). Alternatively, connate basinal brines, possibly related to older evaporites, have been suggested as a fluid source (e.g., Barton and Johnson, 1996). Ore deposition is assumed to involve two main episodes of hydrothermal alteration: (1) early high-temperature magnetite-bearing paragenesis related to magmatic fluids, and (2) late-stage, relatively low-temperature paragenesis related to the mixing of magmatic with meteoric fluids, that may convert early magnetite into hematite and trigger Cu-sulfide and gold deposition (Oreskes and Einaudi, 1992).

The styles of hydrothermal alteration, mineralogy and geochemistry of the Igarapé Bahia ore, as well as the fluid inclusion and stable isotope data, support its classification as a member of the world-class Olympic Dam-type Fe-oxide Cu-Au-(U-REE) deposit group, as previously argued by several authors (Huhn and Nascimento, 1996; Tallarico, 1996; Tallarico et al., 1998; Oliveira et al., 1998; Tazava, 1999; Soares et al., 1999). The SHRIMP II <sup>207</sup>Pb/<sup>206</sup>Pb age of 2575 ± 12 Ma for hydrothermal monazite from the matrix of mineralized breccia is important as it clearly defines Igarapé Bahia as the first well-established Archean example of an Olympic Dam-type deposit in the world.

Several other Cu-Au deposits of the Carajás Belt, as for example Salobo, Sossego and Cristalino, share a number of characteristics with the Igarapé Bahia, such as: (a) intense Fe-metasomatism resulting in the formation of grunerite, fayalite and/or Fe-oxides (magnetite and/or hematite), (b) intense carbonate alteration,

(c) sulfur-poor and oxidized ore paragenesis (chalcopyrite and bornite), (d) absence of quartz due to silica dissolution, (e) extreme LREE enrichment and (f) diagnostic enrichment in U and Co. These features suggest that all of these deposits are similar and are genetically related to the intrusion of Archean (ca. 2.57 Ga) Estrela-type alkaline granites in the Carajás Belt.

### Acknowledgments

The authors wish to thank the Companhia Vale do Rio Doce for access to the area, support during field-work, and for access to their electron microprobe laboratory. Ms. Marion Marshall, from the Geology and Geophysics Department of UWA, is thanked for technical assistance with SHRIMP II preparation. The authors are thankful to Professor Brendan J. Griffin and Ms. Sharon Platten, from the Centre for Microscopy and Microanalysis of UWA, for assistance during SEM work. We acknowledge Dr. Maurício Carneiro, from the Geology Department of the Universidade Federal de Ouro Preto, for assistance during sample preparation. We are indebted to the Fundação de Amparo a Pesquisa do Estado de São Paulo (FAPESP) for research grants #98/14401-5 and #99/03058-0. We are also thankful to the Society of Economic Geologist Foundation for financial support through the Hugh E. McKinstry Grant for year 2000.

### References

- Almada, M.C.O., 1998, O Corpo Acampamento Sul do depósito Bahia, Carajás: características geológicas e fluidos hidrotermais: Unpublished Master thesis, Belém, Brazil, Universidade Federal do Pará, 99 p.
- Althoff, A.M.R., Villas, R.N. and Giuliani, G., 1994, A mineralização cuprifera da Área Bahia, Serra dos Carajás (PA): evolução dos fluidos hidrotermais e modelo metalogenético: Geochemica Brasiliense, v. 8(2), p.135-155.
- Araújo, O.J.B., and Maia, R.G.N., 1991, Serra dos Carajás, folha SB.22-Z-A, estado do Pará. Programa levantamentos geológicos básicos do Brasil: Companhia de Pesquisa de Recursos Minerais, 136 p.
- Araújo, O.J.B., Maia, R.G.N., Xafi, J.J.S., and Costa, J.B.S., 1988, A megaestruturação arqueana da folha Serra dos Carajás: VII Congresso Latino-Americano de Geologia, p. 324-333.

Angélica, R.S., 1996, Mineralogia e geoquímica dos gossans e lateritos auríferos na Região de Carajás,

Estado do Pará: os depósitos de Igarapé Bahia e Águas Claras: Unpublished Ph.D. thesis, Belém, Brazil,  
Universidade Federal do Pará, 115 p.

Barreira, C.F., Soares, A.D.V., and Ronzê, P.C., 1999, Descoberta do Depósito Cu-Au Alemão – Província  
Mineral de Carajás (PA): VI Simpósio de Geologia da Amazônia, p. 136-139.

Barrie, C.T., and Hannington, M.D., 1999, Classification of volcanic-associated massive sulfide deposits  
based on host-rock composition: In: Barrie, C.T. and Hannington (ed.) Volcanic-associated massive  
sulfide deposits: processes and examples in modern and ancient settings. REVIEWS IN ECONOMIC  
GEOLOGY, v. 8, p. 1-11.

Barros, C.E.M., and Barbey, P., 1998, A importância da granitogênese tardi-arqueana (2.5Ga) na evolução  
tectono-metamórfica da Província Mineral de Carajás – O Complexo Granítico Estrela e sua auréola de  
contato: Revista Brasileira de Geociências, v. 28(4), p. 513-522.

Barros, C.E.M., Barbey, P., and Boullier, A.M., 2001, Role of magma pressure, tectonic stress and  
crystallization progress in the emplacement of syntectonic granites. The A-type Estrela Granite Complex  
(Carajás Mineral Province, Brazil): Tectonophysics, v. 343, p. 93-109.

Barros, C.E.M., Dall'Agnoll, R., Barbey, P, and Boullier, A.M., 1997, Geochemistry fo the Estrela Complex,  
Carajás region, Brazil: an example of an Archean A-type granite: Journal of South American Earth  
Science, v. 10(3-4), p. 321-330.

Barros, C.E.M., Dall'Agnoll, R., Lafon, J.M., Teixeira, N.P., and Ribeiro, J.W., 1992, Geologia e  
geocronologia Rb-Sr do Gnaiss Estrela, Curionópolis, PA: Boletin do Museu Paraense Emílio Goeldi,  
Ciências da Terra, v. 4, p. 83-104.

Barton, M.D., and Johnson, D.A., 1996, Evaporitic-source model for igneous-related Fe oxide-(REE-Cu-Au-  
U) mineralization: Geology, v. 24(3), p. 259-262.

Beane, R.E., and Titley, S.R., 1981, Porphyry copper deposits Part II. Hydrothermal alteration and  
mineralization: ECONOMIC GEOLOGY, 75<sup>th</sup> Anniversary Volume, p. 235-269.

Bocalon, V.L.S., 1997, Caracterização da mineralização primária de Cu-Au da Mina do Igarapé Bahia,  
Carajás, Pará: Unpublished Master Thesis, São Leopoldo, Brazil, Universidade do Rio dos Sinos, 90 p.

- Campbell, I.H., Compston, D.M., Richards, J.P., Johnson, J.P., and Kent, A.J.R., 1998, Review of the application of isotopic studies to the genesis of Cu-Au mineralisation at Olympic Dam and Au mineralisation at Porgera, Tennant Creek district and Yilgarn Craton: Australian Journal of Earth Sciences, v. 45, p. 201-218.
- Compston, W., Williams, I.S., Campbell, I.H., and Gresham, J.J., 1986, Zircon xenocrysts from the Kambalda volcanics: age constraints and direct evidence for the older continental crust below the Kambalda-Norseman greenstones: Earth and Planetary Science Letters, v. 76, p. 299-311.
- Cordeiro, A.A.C., 1999, Pesquisa mineral: panorama atual da CVRD na Amazônia: VI Simpósio de Geologia da Amazônia, p. 80-83.
- Cross, K.C., Daly, S.J., and Flint, R.B., 1993, Mineralisation associated with the GRV and Hiltaba Suite granitoids: In: Drexel J.F., Preiss W.V. & Parker A.J. (ed.) The Geology of Southern Australia, v. 1, The Precambrian, Geological Survey of Southern Australia, Bulletin 54, 242 p.
- Davidson, G.J., and Large, R.R., 1994, Gold metallogeny and the copper-gold association of Australian Proterozoic: Mineralium Deposita, v. 29, p. 208-223.
- Dias, G.S., Macambira, M.J.B., Dall'Agnol, R., Soares, A.D.V., and Barros, C.E.M., 1996, Datação de zircões de Sill de metagabro: comprovação da idade arqueana da Formação Águas Claras, Carajás, Pará: V Simpósio de Geologia da Amazônia, p. 376-379.
- Docegeo (Rio Doce Geologia e Mineração S.A.), 1988, Província Mineral de Carajás. Litoestratigrafia e principais depósitos minerais: 35 Congresso Brasileiro de Geologia, 165 p.
- Evensen, N.M., Hamilton, P.J., and O'Nions, R.K., 1978, Rare-earth abundances in chondritic meteorites: Geochemica et Cosmochimica Acta, v. 42, p. 1199-1212.
- Farias, N.R., and Saueressig, R., 1982, Jazida de cobre Salobo 3A: I Simpósio de Geologia da Amazônia, p. 61-73.
- Faure, G., and Powell, J.L., 1972, Strontium isotope geology. Mineral, Rocks and Inorganic Materials: Monograph Series of Theoretical and Experimental Studies #5, Springer-Verlag, 188p.
- Ferreira Filho, C.F., 1985, Geologia e mineralizações sulfetadas do Prospecto Bahia, Província Mineral de Carajás: Unpublished Master thesis, Brasília, Brazil, Universidade de Brasília, 112p.

- Foster, G., Kinny, P., Vance, D., Prince, C., and Harris, N., 2000, The significance of monazite U-Th-Pb age data in metamorphic assemblages; a combined study of monazite and garnet chronometry: Earth and Planetary Science Letter, v. 181, p. 327-340.
- Gibbs, A.K., and Wirth, K.R., 1990, Geologic setting of the Serra dos Carajás iron deposits, Brazil: In: Chauvel et al. (eds.). Ancient Banded Iron Formations (Regional Presentations). Atenas, Theophrastus, p. 83-102.
- Gibbs, A.K., Wirthe, K.R., Hirata, W.K., and Olszewski Jr., W.J., 1986, Age and composition of the Grão Pará Group volcanics, Serra dos Carajás: Revista Brasileira de Geociências, v. 16(2), p. 201-211.
- Gieré, R., 1996, Formation of rare earth minerals in hydrothermal systems: In A.P. Jones, F. Wall, C.T. Williams (ed.) Rare Earth Minerals. London, Chapman & Hall, 105-150 p.
- Gow, P.A., Wall, V.J., Oliver, N.H.S., and Valenta, R.K., 1994, Proterozoic iron oxide (Cu-Y-Au-REE) deposits: further evidence of hydrothermal origins: Geology, v. 22, p. 633-636.
- Groves, D.I., and Veilreicher, N.M., 2001, The Phalabowra (Palabora) carbonatite-hosted magnetite-copper sulfide deposit, South Africa: an end-member of the iron-oxide copper-gold-rare earth element deposit group?: Mineral Deposita, v. 36, p. 189-194.
- Haynes, D.W., Cross, K.C., Bills, R.T., and Reed, M.H., 1995, Olympic Dam ore genesis: a fluid-mixing model: ECONOMIC GEOLOGY, v. 90, p. 281-307.
- Hitzman, M.W., Oreskes, N., and Einaudi, M.T., 1992, Geological characteristics and tectonic setting of Proterozoic iron oxide (Cu-U-Au-REE) deposits: Precambrian Research, v. 58, p. 241-287.
- Holdsworth, R.E., and Pinheiro, R.V.L., 2000, The anatomy of shallow-crustal transpressional structures: insights from the Archean Carajás fault zone, Amazon, Brazil: Journal of Structural Geology, v. 22, p. 1105-1123.
- Huhn, S.R.B., and Nascimento, J.A.S., 1996, São os depósitos cupríferos de Carajás do tipo Cu-Au-U-ETR?: In: Marcondes & Angélica (eds.) Contribuições à Geologia da Amazônia, p.143-160.
- Huhn, S.R.B., Santos, A.B.S., Amaral, A.F., Ledsham, E.J., Gougêa, J.L., Martins, L.P., Montalvão, R.G.M., and Costa, V.G., 1988, O terreno “granito greenstone” da região de Rio Maria - Sul do Pará: XXXV Congresso Brasileiro de Geologia, v. 3, p. 1438-1452.

- Huhn, S.R.B., Souza, C.I.J., Albuquerque, M.C., Leal, E.D., and Brustolin, V., 1999a, Descoberta do depósito Cu(Au) Cristalino: geologia e mineralização associada – Região da Serra do Rabo – Carajás – PA: VI Simpósio de Geologia da Amazônia, p. 140-143.
- Huhn, S.R.B., Macambira, M.J.B., and Dall'Agnol, R., 1999b, Geologia e geocronologia Pb/Pb do granito alcalino Arqueano Planalto, Região da Serra do Rabo, Carajás – PA: VI Simpósio de Geologia da Amazônia, p. 463-466.
- Jaffey, A.H., Flynn, K.F., Glendenin, L.E., Bentley, W.C., and Essling, A.M., 1971, Precision measurement of half lives and specific activities of  $^{235}\text{U}$  and  $^{238}\text{U}$ : Physics Reviews v. C4, p. 1889.
- Kerrick, R., Goldfarb, R., Groves, D.I., and Garwin, S., 2000, The geodynamics of world-class gold deposits: characteristics, space-time distribution, and origins. In: Hagemann SG, Brown PE (eds) Gold in 2000. REVIEWS IN ECONOMIC GEOLOGY, v. 13, p. 501-551.
- Lancaster Oliveira, J., Fanton, J., Almeida, A.J., Leveille, R.A., and Vieira, S., 2000, Discovery and geology of the Sossego copper-gold deposit, Carajás District, Pará State, Brazil: 31 International Geological Congress, [abs.].
- Large, R.R., 1992, Australian volcanic-hosted massive sulfide deposits: features, styles, and genetic model: ECONOMIC GEOLOGY, v. 87, p. 471-510.
- Lindenmayer, Z.G., 1990, Salobo Sequence, Carajás, Brazil: Geology, Geochemistry and Metamorphism. Unpublished Ph.D. thesis, London, Canada, University of Western Ontario, 407 p.
- Lindenmayer, Z.G., Ronchi, L.H., and Laux, J.H., 1998, Geologia e geoquímica da mineralização de Cu-Au primária da mina de Au do Igapó Bahia, Serra dos Carajás: Revista Brasileira de Geociências, v. 28(3), p. 257-268.
- Ludwig, K.R., 2001a, SQUID 1.00 – a User's manual: Barkeley Geochronology Centre, Special Publication 2, 17 p.
- Ludwig, K.R., 2001b, User manual for Isoplot/Ex rev. 2.49 – a geochronological toolkit for Microsoft Excel. Barkeley Geochronology Centre, Special Publication 1a, 56 p.
- Machado, N., Lindenmayer, Z., Krogh, T.E., and Lindenmayer, D., 1991, U-Pb geochronology of Archean magmatism and basement reactivation in the Carajás area, Amazon Shield, Brazil: Precambrian Research, v. 49, p. 329-354.

- Mellito, K.M. 1998. Aplicações dos sistemas Rb-Sr, Pb-Pb e Sm-Nd no depósito polimetálico do Salobo 3A, Província Mineral de Carajás, Pará: Unpublished Master thesis, São Paulo, Brazil, Universidade de São Paulo, 90 p.
- Mikucki, E.J., and Ridley, J.R., 1993, The hydrothermal fluids of Archean lode-gold deposits at different metamorphic grades: compositional constraints from ore and wallrock alteration assemblages: *Mineralium Deposita*, v. 28, p. 469-481.
- Montalvão, R.G.M, Tassinari, C.C.G., and Bezerra, P.E.L., 1984, Geocronologia dos granitóides e gnaisses das regiões do Rio Maria, Fazenda Mata Geral e Rio Itacaiunas, Sul do Pará (Distrito Carajás-Cumaru): XXXIII Congresso Brasileiro de Geologia, p. 2757-2766.
- Muogeot, R., Respaut, J.P., Briquel, L., Ledru, P., Milesi, P., Lerouge, C., Marcoux, E., Huhn, S.R.B., and Macambira, M.J.B., 1996, Isotope Geochemistry constrains for Cu, Au mineralizations and evolution of the Carajás Province (Pará, Brazil): XXXIX Congresso Brasileiro de Geologia, p. 321-324.
- Nelson, D.R., 1997, Compilation of SHRIMP U-Pb zircon geochronology data, 1996: Geological Survey of Western Australia, Record 1997/2.
- Nogueira, A.C.R., Truckenbrod, W., Costa, J.B.S., and Pinheiro, R.V.L., 1994, Análise faciológica e estrutural da Formação Águas Claras, Pré-Cambriano da Serra dos Carajás: 4 Simpósio de Geologia da Amazônia, p. 363-364.
- Nogueira, A.C.R., Truckenbrod, W., and Pinheiro, R.V.L., 2000, Storm and tide-dominated siliciclastic deposits of the Archean Águas Claras Formation, Serra dos Carajás, Brazil: 31 International Geological Congress [abs.].
- Oliveira, C.G., Tazava, E., Tallarico, F.H.B., Santos, R.V., and Gomes, C., 1998, Gênese do depósito de Au-Cu-(U-ETR) de Igarapé Bahia, Província Mineral de Carajás: XL Congresso Brasileiro de Geologia, p. 137.
- Olszewski, W.J., Wirth, K.R., Gibbs, A.K., and Gaudette, H.E., 1989, The age, origin, and tectonics of the Grão Pará Group and associated rocks, Serra dos Carajás, Brazil: Archean continental vulcanism and rifting: *Precambrian Research*, v. 42, p. 229-254.
- Oreskes, N., and Einaudi, M.T., 1990, Origin of rare-earth-element-enriched hematite breccias at the Olympic Dam Cu-U-Au-Ag deposit, Roxby Downs, South Australia: *ECONOMIC GEOLOGY*, v. 85: p. 1-28.

- Oreskes, N., and Hitzman, M.W., 1993, A model for the origin of Olympic Dam-type deposits: In: Kirkham, R.V.; Sinclair, W.D.; Thrope, R.I. and Duke, J.M (ed.). Mineral Deposit Modeling. Geological Association of Canada, Special Paper 40, p. 615-633.
- Pidgeon, R.T., Furfaro, D., Kennedy, A.K., and Nemchin, A.A., 1994, Calibration of zircon standards for the Curtin SHRIMP II: Abstracts of the 8<sup>th</sup> International Conference on Geochronology, Cosmochronology and Isotope Geology, Berkeley, USA. U.S. Geological Survey, Circular 1107, p. 251.
- Pidgeon, R.T., Macambira, M.J.B., and Lafon, J.M., 2000, Th-U-Pb isotopic systems and internal structures of complex zircons from enderbite from the Pium Complex, Carajás Province, Brazil: evidence for ages of granulite facies metamorphism and protolith of the enderbite: Chemical Geology, v. 166, p. 157-171.
- Pinheiro, R.V.L., and Holdsworth, R.E., 1997, Reactivation of Archean strike-slip fault systems, Amazon region, Brazil. Journal of the Geological Society, v. 154, p. 99-103.
- Rasmussen, B., Fletcher, I.R., and McNaughton, N.J., (in press) Dating low-grade metamorphism by SHRIMP U-Pb analysis of monazite in shales: Geology.
- Reeve, J.S., Cross, K.C., Smith, R.N., and Oreskes, N., 1990, Olympic Dam copper-uranium-gold-silver deposit. In: Hughes, F.E. (ed.) Geology of the Mineral Deposits of Australia and Papua New Guinea. Melbourne, The Australian Institute of Mining and Metallurgy, p. 1009-1035.
- Ribeiro, A.M.R., 1989, Estudo geoquímico do sistema hidrotermal relacionado à mineralização cuprífera da Área Bahia, Serra dos Carajás, Pará: Unpublished Master thesis, Belém, Brazil, Universidade Federal do Pará, 134 p.
- Rigon, J.C., Munaro, P., Santos, L.A., Nascimento, J.A.S., and Barreira, C.F., 2000, The Alvo 118 copper-gold deposit: geology and mineralization, Serra dos Carajás, Pará: 31 International Geological Congress, [abs.].
- Roberts, D.E., and Hudson, G.R.T., 1983, The Olympic Dam copper-uranium-gold deposit, Roxby Downs, South Australia: ECONOMIC GEOLOGY, v. 78, p. 799-822.
- Rodrigues, E., Lafon, J.M., and Scheller, T., 1992, Geocronologia Pb-Pb da Província Mineral de Carajás: primeiros resultados: XXXVII Congresso Brasileiro de Geologia, v. 1, p. 183-184.

- Santos, J.O.S., Groves, D.I., Hartmann, L.A., Moura, M.A., and McNaughton, N.J., 2001, Gold deposits of the Tapajós and Alta Floresta Domains, Tapajós-Parima orogenic belt, Amazon Craton, Brazil: Mineral Deposita, v. 36(3/4), p. 278-299.
- Silva, C.M.G., and Villas, R.N., 1998, The Águas Claras Cu-sulfide ± Au deposit, Carajás Region, Pará, Brazil: geological setting, wall-rock alteration and mineralizing fluids: Revista Brasileira de Geociências, v. 28(3), p. 315-326.
- Smith, J.B., Barley, M.E., Groves, D.I., Krapez, B., McNaughton, N.J., Bickle, M.J., and Chapman, H.J., 1998, The Scholl Shear zone, West Pilbara: evidence for a domain boundary structure from integrated tectonostratigraphic analyses, SHRIMP U-Pb dating and isotopic and geochemical data of granitoids: Precambrian Research, v. 88, p. 143-171.
- Soares, A.D.V., Ronzê, P.C., Santos, M.G.S., Leal, E.D., and Barreira, C.F., 1999, Geologia e mineralizações do depósito de Cu-Au Alemão – Província Mineral de Carajás (PA): VI Simpósio de Geologia da Amazônia, p. 144-147.
- Soares A.D.V., Santos, A.B., Vieira, E.A., Bella, V.M., and Martins, L.P.B., 1994, Área Águas Claras: contexto geológico e mineralizações. 4 Simpósio de Geologia da Amazônia, p. 379-382.
- Souza, S.R.B., Macambira, M.J.B., and Scheller, J., 1996, Novos dados geocronológicos para os granitos deformados do Rio Itacaiunas (Serra dos Carajás, PA); implicações estratigráficas: V Simpósio de Geologia da Amazônia, p. 380-383.
- Slack, J.F., 1993, Descriptive and grade-tonnage models for Besshi-type massive sulphide deposits: In: Kirkham, R.V.; Sinclair, W.D.; Thrope, R.I. and Duke, J.M (ed.). Mineral Deposit Modeling. Geological Association of Canada, Special Paper 40, p. 343-371.
- Tassinari, C.C.G., and Macambira, M.J.B., 1999, Geochronological provinces of the Amazonian Craton: Episodes, v. 22(3), p. 174-182.
- Tallarico, F.H.B., 1996, Projeto de revisão do modelo geológico da mina de Igarapé Bahia – petrografia, química mineral e litogeoquímica: Companhia Vale do Rio Doce Internal Report, 57 p.
- Tallarico, F.H.B., Oliveira, C.G., and Figueiredo, B.R., 2000, The Igarapé Bahia Cu-Au mineralization, Carajás Province. Revista Brasileira de Geociências, v. 30, p. 230-233.

Tallarico, F.H.B., Rego, J.L., and Oliveira, C.G., 1998, A mineralização de Au-Cu de Igarapé Bahia – Carajás: um depósito da classe óxido de Fe (Cu-U-Au-ETR): XL Congresso Brasileiro de Geologia, p. 116.

Tallarico, F.H.B., McNaughton, N.J., Groves, D.I., Fletcher, I.R., Figueiredo, B.R., Carvalho, J.B., Rego, J.L., and Nunes, A.R., (in press), SHRIMP II U-Pb constraints on the age of the Breves Cu-Au-(W-Bi-Sn) mineralisation: evidence of Paleoproterozoic (1.88 Ga) metallogeny in the Carajás Copper-Gold Belt, Brazil: Mineralium Deposita.

Tazava, E., 1999, Mineralização de Au-Cu-(±ETR-U) associada às brechas hidrotermais do depósito de Igarapé Bahia, Província Mineral de Carajás, PA. Unpublished Master thesis, Ouro Preto, Brazil, Universidade Federal de Ouro Preto, 81 p.

Tolbert, G.E., Tremaine, J.W., Melcher, G.C., and Gomes, C.B., 1971, The recently discovered Serra dos Carajás iron deposit, northern Brazil: ECONOMIC GEOLOGY, v. 66, p. 985-994.

Valarelli, J.V., Bernardeli, A., and Beisiegel, W.R., 1978, Aspectos genéticos do minério de manganês do Azul: XXX Congresso Brasileiro de Geologia, v. 4, p. 1670-1679.

Vieira, E.A.P., Saueressig, R., Siqueira, J.B., Silva, E.R.P., Rego, J.L., and Castro, F.D.C., 1988, Caracterização geológica da jazida polimetálica do Salobo 3A – reavaliação: XXXV Congresso Brasileiro de Geologia, 165p.

Veizer, J., and Compston, W., 1976,  $^{87}\text{Sr}/^{86}\text{Sr}$  in Precambrian carbonates as an index of crustal evolution: Geochimica et Cosmochimica Acta, v. 40, p. 905-914.

Williams, I.S., and Claesson, S., 1987, Isotopic evidence for the Precambrian provenance and Caledonian metamorphism of high grade paragneisses from the Steve Nappes, Scandinavian Caledonides, II. Ion microprobe zircon U-Th-Pb: Contributions to Mineralogy and Petrology, v. 97, p. 205-217.

Williams, P.J., 1998, An introduction to the metallogeny of the McArthur River-Mount Isa-Cloncurry Mineral Provinces: ECONOMIC GEOLOGY, v. 93, p. 1120-1131.

Wirth, K.R., Gibbs, A.K., and Olszewski, W.J., 1986, U-Pb ages of zircons from the Grão-Pará Group and Serra do Carajás Granite, Pará, Brazil: Revista Brasileira de Geociências, v. 16(2), p. 195-200.

Zang, W., and Fyfe, W.S., 1993, A three-stage genetic model for the Igarapé Bahia lateritic gold deposit, Carajás, Brazil: Economic Geology, v. 88, p. 1768-1779.

Zang, W., and Fyfe, W.S., 1996, Chloritization of the hydrothermally altered bedrock at the Igarapé Bahia gold deposit, Carajás, Brazil: Mineralium Deposita, v. 30, p. 30-38.

TABLE 1. Grade-Tonnage Data for the Igarapé Bahia Cu-Au Deposit

Ore Type	Reserve	Grade	Metal Content
Oxidized Ore <sup>1</sup> (Supergene)	15 Mt of high-grade <sup>2</sup> ore 14 Mt of low-grade <sup>3</sup> ore	5 g/t Au 1.4 g/t Au	75 tonnes Au 19.6 tonnes Au
Transitional Ore (Supergene)	9.5 Mt	2.45 g/t Au 3.83 % Cu	23.28 tonnes Au 0.36 Mt Cu
Primary	219 Mt <sup>4</sup>	0.86 g/t Au	188.34 tonnes Au
Mineralisation		1.4 % (Cu)	3.06 Mt Cu

1: Original reserve of oxidized ore. To date, approximately 92 tonnes of Au has been extracted. 2: High-grade ore for carbon-in-pulp processing. 3: Low-grade ore for heap leach processing. 4: Total resources of primary mineralisation including the Acampamento Sul, Acampamento Norte, Furo Trinta and Alemão orebodies.

Abbreviation: Mt = million tonnes.

TABLE 2. Samples from the Igarapé Bahia Fe-oxide Cu-Au-(U-REE) Mineralisation Selected for SHRIMP II Analysis

SHRIMP Mount	Sample-Type (Sample prep. code)	Field Reference (drill hole/depth)	Rock Type	Mineral Analyzed
UWA-B18C	Bulk sample (OPU-1264)	356/317-326m	Host metavolcanic rock (footwall)	Zircon
UWA-B18D	Bulk sample (OPU-1266)	392/381-384m	Host metavolcanic rock (footwall)	Zircon
UWA-B21D	Bulk sample (OPU-1263)	351/420-435m	Diabase dike	Zircon
UWA-B36A	Bulk sample (OPU-1311)	351/421.85-433.34m	Diabase dike	Zircon
UWA-B34	Thin section (FT99C)	332/257-260m	Cu-Au-bearing magnetite breccia	Monazite

TABLE 3.  $^{204}\text{Pb}$  Corrected SHRIMP II Isotopic Data for Zircons from Host Metavolcanic Rock from the Igarapé Bahia Deposit.  
Samples UWA-B18C and UWA-B18D

grain-spot	U (ppm)	Th (ppm)	4f206* (%)	$^{207}\text{Pb}/^{206}\text{Pb}$	$^{206}\text{Pb}/^{238}\text{U}$	$^{207}\text{Pb}/^{235}\text{U}$	$^{208}\text{Pb}/^{232}\text{Th}$	concordance (%)	$^{207}\text{Pb}/^{206}\text{Pb}$ Age (Ma)
C.1-1	178	94	-0.001	$0.1924 \pm 0.4609$	$0.5193 \pm 1.9116$	$13.7742 \pm 1.9664$	$0.1435 \pm 2.1262$	98	$2763 \pm 8$
C.2-1	244	203	0.069	$0.2047 \pm 0.4357$	$0.5087 \pm 1.8704$	$14.3578 \pm 1.9205$	$0.1339 \pm 2.2421$	93	$2864 \pm 7$
C.3-1	299	155	0.057	$0.1232 \pm 0.5234$	$0.3713 \pm 2.0032$	$6.3083 \pm 2.0705$	$0.1030 \pm 2.1597$	102	$2003 \pm 9$
C.4-1	1084	34	0.115	$0.1693 \pm 0.2533$	$0.3398 \pm 1.8109$	$7.9294 \pm 1.8285$	$0.0907 \pm 5.8175$	74	$2550 \pm 4$
C.5-1	1069	62	0.128	$0.1504 \pm 0.3078$	$0.2358 \pm 1.9135$	$4.8916 \pm 1.9381$	$0.1036 \pm 3.1834$	58	$2351 \pm 5$
C.4-2	1844	776	0.119	$0.1443 \pm 0.3123$	$0.1427 \pm 1.8341$	$2.8405 \pm 1.8605$	$0.0439 \pm 1.9316$	38	$2280 \pm 5$
D.1-1	81	98	0.083	$0.2047 \pm 0.9087$	$0.3437 \pm 2.0927$	$9.6990 \pm 2.2815$	$0.0310 \pm 3.5469$	66	$2864 \pm 15$
D.2-1	442	242	0.041	$0.1950 \pm 0.3050$	$0.4606 \pm 1.8213$	$12.3849 \pm 1.8467$	$0.1209 \pm 1.9416$	88	$2785 \pm 5$
D.3-1	454	191	0.182	$0.1769 \pm 0.4904$	$0.2156 \pm 1.8614$	$5.2578 \pm 1.9249$	$0.0380 \pm 2.9856$	48	$2624 \pm 8$
C.5-1	294	65	0.944	$0.1206 \pm 1.1274$	$0.2540 \pm 1.9626$	$4.2226 \pm 2.2633$	$0.0810 \pm 5.1914$	74	$1965 \pm 20$
D.2-2	442	262	0.144	$0.1892 \pm 0.3423$	$0.4236 \pm 1.8220$	$11.0494 \pm 1.8538$	$0.0984 \pm 1.9645$	83	$2735 \pm 6$
C.1-2	148	55	0.092	$0.1901 \pm 0.5340$	$0.5313 \pm 1.9405$	$13.9231 \pm 2.0127$	$0.1411 \pm 2.3496$	100	$2743 \pm 9$
C.6-1	174	58	0.015	$0.1895 \pm 0.4573$	$0.5232 \pm 1.9048$	$13.6733 \pm 1.9589$	$0.1432 \pm 2.1420$	99	$2738 \pm 8$

\* 4f206 (%) =  $^{206}\text{Pb}_{\text{common}}/^{206}\text{Pb}_{\text{Total}}$ , i.e., % of  $^{206}\text{Pb}$  attributed as common Pb. Uncertainties refer to the last digits listed.

TABLE 4.  $^{204}\text{Pb}$  Corrected SHRIMP II Isotopic Data for Zircons from Diabase Dike from the Igarapé Bahia Deposit. Samples UWA-B21D and UWA-B36A

grain-spot	U (ppm)	Th (ppm)	4f206* (%)	$^{207}\text{Pb}/^{206}\text{Pb}$	$^{206}\text{Pb}/^{238}\text{U}$	$^{207}\text{Pb}/^{235}\text{U}$	$^{208}\text{Pb}/^{232}\text{Th}$	concordance (%)	$^{207}\text{Pb}/^{206}\text{Pb}$ Age (Ma)
B36A.1-1	212	151	0.051	$0.2079 \pm 0.4355$	$0.5343 \pm 0.9892$	$15.3153 \pm 1.0809$	$0.1453 \pm 1.2242$	96	$2889 \pm 7$
B36A.2-1	114	55	0.093	$0.2053 \pm 0.5910$	$0.5339 \pm 1.1665$	$15.1157 \pm 1.3077$	$0.1390 \pm 1.9927$	96	$2869 \pm 10$
B36A.3-1	326	172	0.000	$0.2193 \pm 0.3079$	$0.5736 \pm 1.2960$	$17.3423 \pm 1.3320$	$0.1533 \pm 1.4055$	98	$2975 \pm 5$
B36A.4-1	82	55	0.000	$0.2069 \pm 0.6496$	$0.5609 \pm 1.2613$	$16.0019 \pm 1.4188$	$0.1510 \pm 1.6821$	100	$2881 \pm 11$
B36A.5-1	166	85	0.000	$0.1934 \pm 0.6259$	$0.5203 \pm 1.0369$	$13.8708 \pm 1.2112$	$0.1431 \pm 1.5700$	97	$2771 \pm 10$
B36A.6-1	173	144	0.025	$0.2296 \pm 0.5570$	$0.5714 \pm 1.4082$	$18.0932 \pm 1.5143$	$0.1525 \pm 1.5578$	96	$3050 \pm 9$
B36A.7-1	82	74	-0.026	$0.2065 \pm 0.6417$	$0.5600 \pm 1.2800$	$15.9418 \pm 1.4319$	$0.1461 \pm 1.6688$	100	$2878 \pm 10$
B36A.8-1	478	389	0.106	$0.1819 \pm 0.3310$	$0.4349 \pm 0.8535$	$10.9076 \pm 0.9154$	$0.1095 \pm 1.1367$	87	$2670 \pm 5$
B36A.9-1	442	194	0.078	$0.1769 \pm 0.8816$	$0.3321 \pm 1.5642$	$8.0993 \pm 1.7955$	$0.1115 \pm 1.9715$	70	$2624 \pm 15$
B36A.10-1	85	63	0.417	$0.1999 \pm 0.8039$	$0.4640 \pm 1.2757$	$12.7906 \pm 1.5078$	$0.0922 \pm 2.3581$	87	$2826 \pm 13$
B36A.11-1	330	253	0.019	$0.1722 \pm 0.3895$	$0.4427 \pm 0.9196$	$10.5077 \pm 0.9987$	$0.1126 \pm 1.0790$	92	$2579 \pm 7$
B36A.12-1	301	297	0.167	$0.1989 \pm 0.3998$	$0.4842 \pm 0.9165$	$13.2757 \pm 0.9999$	$0.1185 \pm 1.1472$	90	$2817 \pm 7$
B36A.13-1	366	254	0.015	$0.2048 \pm 0.3099$	$0.5524 \pm 0.8971$	$15.5957 \pm 0.9491$	$0.1440 \pm 1.0225$	99	$2864 \pm 5$
B36A.14-1	547	153	0.095	$0.1775 \pm 0.3522$	$0.3648 \pm 0.9235$	$8.9246 \pm 0.9884$	$0.0896 \pm 1.8383$	76	$2629 \pm 6$
B36A.15-1	264	139	0.410	$0.1801 \pm 0.5986$	$0.3566 \pm 1.0163$	$8.8548 \pm 1.1795$	$0.1174 \pm 1.6103$	74	$2654 \pm 10$
B36A.16-1	129	74	0.060	$0.2108 \pm 0.5148$	$0.5658 \pm 1.1280$	$16.4444 \pm 1.2399$	$0.1502 \pm 1.4568$	99	$2912 \pm 8$
B36A.17-1	998	717	1.603	$0.1594 \pm 0.8405$	$0.1630 \pm 0.9839$	$3.5823 \pm 1.2940$	$0.0318 \pm 2.9620$	40	$2449 \pm 14$
B36A.18-1	208	108	0.939	$0.1974 \pm 0.7130$	$0.4356 \pm 0.9819$	$11.8553 \pm 1.2135$	$0.0815 \pm 3.4203$	83	$2805 \pm 12$
B36A.18-2	637	129	0.374	$0.1783 \pm 0.4731$	$0.3062 \pm 0.8286$	$7.5260 \pm 0.9542$	$0.0708 \pm 3.0988$	65	$2637 \pm 8$
B36A.19-1	168	103	0.110	$0.2325 \pm 0.4545$	$0.5929 \pm 1.4169$	$19.0071 \pm 1.4880$	$0.1555 \pm 1.6994$	98	$3069 \pm 7$
B36A.19-2	274	50	0.160	$0.2004 \pm 0.4271$	$0.4779 \pm 0.9282$	$13.2042 \pm 1.0218$	$0.1326 \pm 2.3423$	89	$2829 \pm 7$
B36A.20-1	266	143	0.019	$0.2044 \pm 0.3634$	$0.5666 \pm 0.9321$	$15.9713 \pm 1.0004$	$0.1500 \pm 1.1376$	101	$2862 \pm 6$
B36A.20-2	202	91	0.109	$0.2046 \pm 0.4396$	$0.5534 \pm 1.2325$	$15.6136 \pm 1.3086$	$0.1259 \pm 1.6679$	99	$2864 \pm 7$
B36A.21-1	108	131	-0.025	$0.2044 \pm 0.5823$	$0.5503 \pm 1.1683$	$15.5123 \pm 1.3053$	$0.1488 \pm 1.3732$	99	$2862 \pm 9$
B36A.21-2	260	256	2.767	$0.2001 \pm 1.2721$	$0.3827 \pm 0.9811$	$10.5551 \pm 1.6065$	$0.1396 \pm 2.1999$	74	$2827 \pm 21$
B36A.22-1	229	54	0.035	$0.2042 \pm 0.4151$	$0.5430 \pm 0.9553$	$15.2900 \pm 1.0415$	$0.1486 \pm 1.5310$	98	$2860 \pm 7$
B21D.1-1	175	204	0.178	$0.2080 \pm 0.8645$	$0.5460 \pm 1.9134$	$15.5080 \pm 2.1232$	$0.1009 \pm 2.3976$	97	$2877 \pm 15$
B21D.2-1	29	15	0.895	$0.1922 \pm 2.2737$	$0.5278 \pm 3.5996$	$13.2860 \pm 4.7902$	$0.1193 \pm 9.9392$	101	$2691 \pm 52$
B21D.3-1	794	543	0.390	$0.1815 \pm 0.6702$	$0.2420 \pm 1.5134$	$5.9191 \pm 1.7171$	$0.0411 \pm 2.6132$	53	$2635 \pm 13$
B21D.4-1	1270	701	0.868	$0.1642 \pm 0.7137$	$0.1148 \pm 0.7850$	$2.4555 \pm 1.4074$	$0.0217 \pm 5.1419$	29	$2418 \pm 20$
B21D.5-1	454	28	0.095	$0.2045 \pm 0.5810$	$0.4940 \pm 1.0176$	$13.8574 \pm 1.1873$	$0.1309 \pm 6.5566$	91	$2855 \pm 10$

B21D.6-1	161	110	0.136	$0.2213 \pm 1.0128$	$0.5821 \pm 2.4806$	$17.6385 \pm 2.6886$	$0.1411 \pm 2.9505$	99	$2981 \pm 17$
B21D.7-1	56	62	0.284	$0.2017 \pm 1.5499$	$0.5409 \pm 2.5602$	$14.8129 \pm 3.1038$	$0.1412 \pm 3.6014$	99	$2820 \pm 29$
B21D.8-1	598	540	0.144	$0.1763 \pm 0.6108$	$0.3674 \pm 0.9279$	$8.8540 \pm 1.1355$	$0.0972 \pm 1.2975$	77	$2607 \pm 11$
B21D.8-2	485	411	0.104	$0.1916 \pm 0.5396$	$0.5415 \pm 0.9914$	$14.2191 \pm 1.1434$	$0.1427 \pm 1.2983$	101	$2748 \pm 9$
B21D.8-3	846	9582	1.981	$0.1913 \pm 1.0121$	$0.1784 \pm 0.8754$	$4.1876 \pm 2.0916$	$0.0016 \pm 7.2522$	40	$2593 \pm 31$
B21D.9-1	506	440	0.287	$0.2077 \pm 0.6074$	$0.4126 \pm 1.0886$	$11.6388 \pm 1.3190$	$0.0609 \pm 2.3426$	77	$2868 \pm 12$
B21D.2-2	34	18	1.212	$0.1908 \pm 2.1793$	$0.4970 \pm 5.6575$	$12.1856 \pm 6.3691$	$0.0920 \pm 10.8488$	97	$2653 \pm 48$
B21D.10-1	823	2085	0.165	$0.1369 \pm 0.6574$	$0.3006 \pm 0.8907$	$5.6037 \pm 1.1427$	$0.0779 \pm 1.0652$	78	$2169 \pm 12$

$f_{206}$  (%) =  $^{206}\text{Pb}_{\text{common}} / ^{206}\text{Pb}_{\text{total}}$ , i.e., % of  $^{206}\text{Pb}$  attributed as common Pb. Uncertainties refer to the last digits listed.

TABLE 5.  $^{204}\text{Pb}$  Corrected SHRIMP II Isotopic Data for Monazite from Cu-Au-Bearing Magnetite Breccias from the Igarapé Bahia Deposit. Sample UWA-B34

grain-spot	U			Th			4f206*			concordance			$^{207}\text{Pb}/^{206}\text{Pb}$	
	(ppm)	(ppm)	Th/U	(%)	$^{207}\text{Pb}/^{206}\text{Pb}$	$^{208}\text{Pb}^*/^{206}\text{Pb}$	$^{207}\text{Pb}^*/^{235}\text{U}$	$^{206}\text{Pb}^*/^{238}\text{U}$	$^{208}\text{Pb}/^{232}\text{Th}$	(%)	Age (Ma)			
4.1-1	127	101	0.8	0.055	$0.1715 \pm 21$	$0.210 \pm 7$	$0.5080 \pm 137$	$12.013 \pm 372$	$0.149 \pm 16$	103	$2572 \pm 21$			
4.2-1	526	496	0.9	0.061	$0.1735 \pm 10$	$0.220 \pm 4$	$0.5126 \pm 83$	$12.262 \pm 217$	$0.137 \pm 7$	103	$2592 \pm 10$			
4.4-1	179	267	1.5	0.105	$0.1718 \pm 18$	$0.358 \pm 8$	$0.5364 \pm 131$	$12.706 \pm 350$	$0.143 \pm 10$	107	$2576 \pm 17$			
5.2-1	175	269	1.5	0.100	$0.1698 \pm 18$	$0.376 \pm 8$	$0.5118 \pm 123$	$11.978 \pm 326$	$0.134 \pm 9$	104	$2555 \pm 17$			
5.3-1	177	384	2.2	0.185	$0.1703 \pm 18$	$0.461 \pm 8$	$0.5263 \pm 123$	$12.358 \pm 329$	$0.134 \pm 8$	106	$2561 \pm 18$			
6.2-1	98	395	4.0	0.083	$0.1707 \pm 25$	$0.950 \pm 17$	$0.5167 \pm 176$	$12.159 \pm 468$	$0.139 \pm 8$	105	$2564 \pm 24$			
6.3-1	103	445	4.3	0.000	$0.1703 \pm 19$	$0.952 \pm 16$	$0.5649 \pm 167$	$13.261 \pm 435$	$0.143 \pm 8$	113	$2560 \pm 19$			
7.2-1	142	411	2.9	0.005	$0.1700 \pm 19$	$0.655 \pm 12$	$0.5393 \pm 142$	$12.640 \pm 374$	$0.141 \pm 8$	109	$2557 \pm 19$			
7.3-1	78	306	3.9	0.271	$0.1744 \pm 35$	$0.851 \pm 20$	$0.5218 \pm 204$	$12.545 \pm 573$	$0.140 \pm 10$	104	$2600 \pm 33$			
7.4-1	115	235	2.0	0.050	$0.1723 \pm 22$	$0.495 \pm 11$	$0.5480 \pm 160$	$13.019 \pm 430$	$0.144 \pm 11$	109	$2580 \pm 21$			
8.1-1	92	398	4.3	0.000	$0.1684 \pm 20$	$0.953 \pm 17$	$0.5485 \pm 171$	$12.736 \pm 441$	$0.139 \pm 8$	111	$2542 \pm 20$			
Possible old outlier														
2.3-1	141	224	1.6	0.170	$0.1754 \pm 21$	$0.345 \pm 8$	$0.5327 \pm 140$	$12.886 \pm 388$	$0.142 \pm 16$	105	$2610 \pm 20$			
Young outlier														
6.1-1	130	480	3.7	0.066	$0.1662 \pm 19$	$0.813 \pm 13$	$0.5686 \pm 153$	$13.027 \pm 394$	$0.142 \pm 8$	115	$2519 \pm 19$			
Discordant														
4.3-1	229	301	1.3	0.000	$0.1696 \pm 17$	$0.429 \pm 9$	$0.4417 \pm 103$	$10.327 \pm 271$	$0.133 \pm 12$	92	$2554 \pm 16$			
4.3-2	339	392	1.2	0.000	$0.1709 \pm 17$	$0.362 \pm 7$	$0.4136 \pm 111$	$9.748 \pm 288$	$0.139 \pm 8$	87	$2567 \pm 17$			
5.1-1	760	196	0.3	0.082	$0.1694 \pm 16$	$0.197 \pm 5$	$0.1224 \pm 21$	$2.859 \pm 59$	$0.129 \pm 10$	29	$2552 \pm 16$			
5.1-2	298	172	0.6	0.261	$0.1726 \pm 31$	$0.229 \pm 9$	$0.2505 \pm 68$	$5.960 \pm 203$	$0.120 \pm 14$	56	$2583 \pm 30$			
7.1-1	134	347	2.6	0.000	$0.1443 \pm 30$	$1.027 \pm 24$	$0.3011 \pm 94$	$5.987 \pm 234$	$0.135 \pm 9$	74	$2279 \pm 35$			

4f206 (%) =  $^{206}\text{Pb}_{\text{common}}/^{206}\text{Pb}_{\text{Total}}$ , i.e., % of  $^{206}\text{Pb}$  attributed as common Pb. Uncertainties refer to the last digits listed.

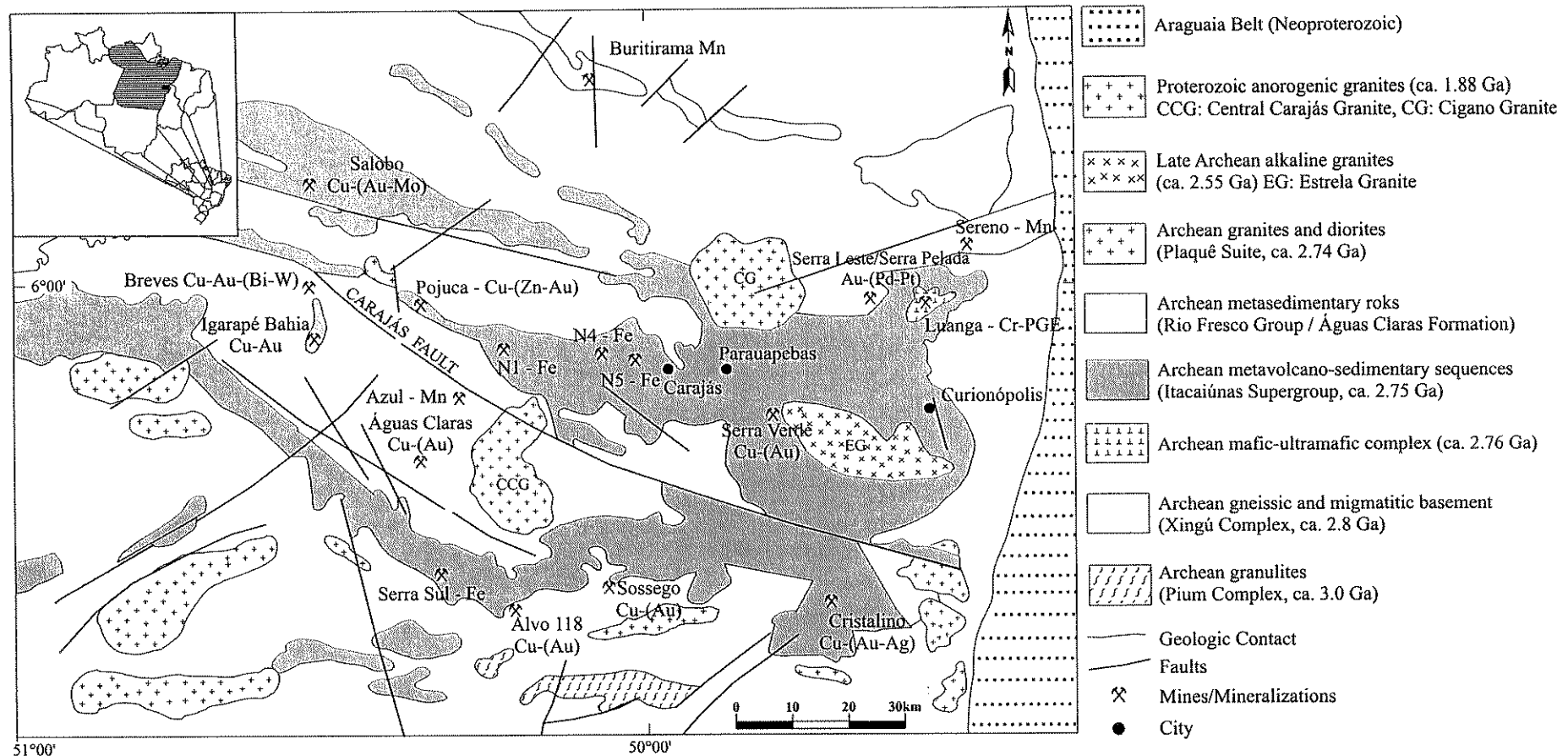
TABLE 6. Strontium Isotopic Composition of Carbonate Minerals from the Igarapé Bahia Deposit.

Field reference (drill hole/depth)	Sample #	Mode of occurrence	XRD*	$^{87}\text{Sr}/^{86}\text{Sr}$	Error ( $\pm$ )
361/189.00m	14436	Siderite $\pm$ quartz vein crosscutting the ACPS orebody	Siderite	0.755264	0.000593
361/195.50m	14437	Siderite vein crosscutting the ACPS orebody	Siderite	0.742402	0.000095
339/88.17m	14440	Siderite from the matrix of ore-bearing siderite breccia (ACPS orebody)	Siderite	0.730052	0.000052
339/101.20m	14441	Siderite from the matrix of ore-bearing siderite breccia (ACPS orebody)	Siderite	0.716341	0.000058
375/1205.55m	14434	Calcite + magnetite vein crosscutting quartz diorite dyke	Calcite	0.728447	0.000095
F10/225.00m	14435	Calcite + chlorite + Ti-magnetite $\pm$ quartz vein crosscutting metavolcanic rocks from the footwall	Calcite	0.717656	0.000072
F12/283.00m	14438	Calcite + chalcopyrite vein crosscutting metavolcanic rocks from the footwall	Calcite	0.713811	0.000036
BHMAG-18/427.40m	14439	Calcite vein crosscutting metavolcanic rocks from the footwall	Calcite	0.720299	0.000017

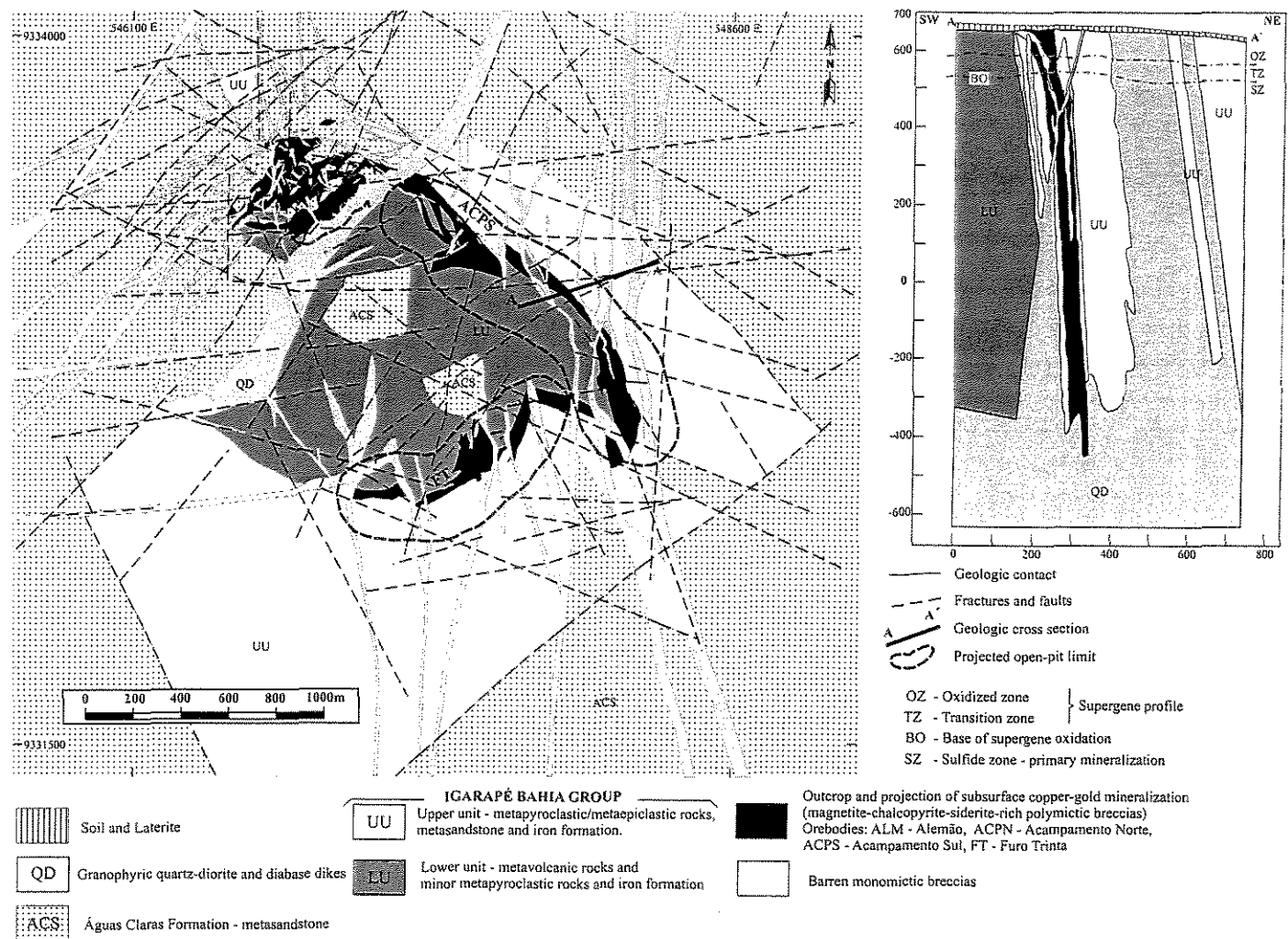
\* XRD: X-ray powder diffraction results using a Philips-X'Pert X-ray diffractometer with a  $\theta\text{-}\theta$  goniometer. Analytical conditions were  $\text{CuK}\alpha_1$  radiation (graphite monochromator), 40kV accelerating voltage, 55mA current,  $5^\circ\text{-}75^\circ$  angular range ( $2\theta$ ),  $0.04^\circ$  step size and 0.5 second/step counting rate.

TABLE 7. Summary Table of SHRIMP II  $^{207}\text{Pb}/^{206}\text{Pb}$  Ages for Igarapé Bahia Cu-Au-(U-REE) Deposit

Sample (mineral dated)	Rock-Type	Age (Ma)	Error (Ma)	Event Dated
UWA-B36A and UWA-B21D (zircon)	Diabase dike	2579	$\pm 7$	Maximum age of dike intrusion
UWA-B34 (monazite)	Cu-Au-bearing magnetite breccia	2575	$\pm 12$	Hydrothermal activity and ore deposition
UWA-B18C and UWA-B18D (zircon)	Host metavolcanic rocks	2751	$\pm 42$	Crystallization of volcanic rocks



**Fig 1** Geological map of the Carajás Copper-Gold Belt, showing the major iron, manganese, Fe-oxide Cu-Au-(U-REE) deposits and the Breves Cu-Au-(W-Bi-Sn) deposit. Simplified from Araújo and Maia (1991), Barros and Barbey (1998) and Docegeo (1988).



**Figure 2** - Geological map of the Igarapé Bahia Cu-Au deposit and geological cross section A-A' through the Acampamento Sul orebody (modified from CVRD/Docegeo 1996 unpublished).

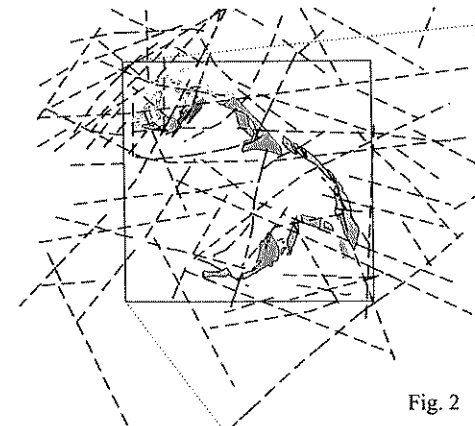


Fig. 2

- Outcroppin copper-gold mineralization
- Projection of subsurface copper-gold mineralization
- 63 Strike and dip of bedding
- Fractures and faults

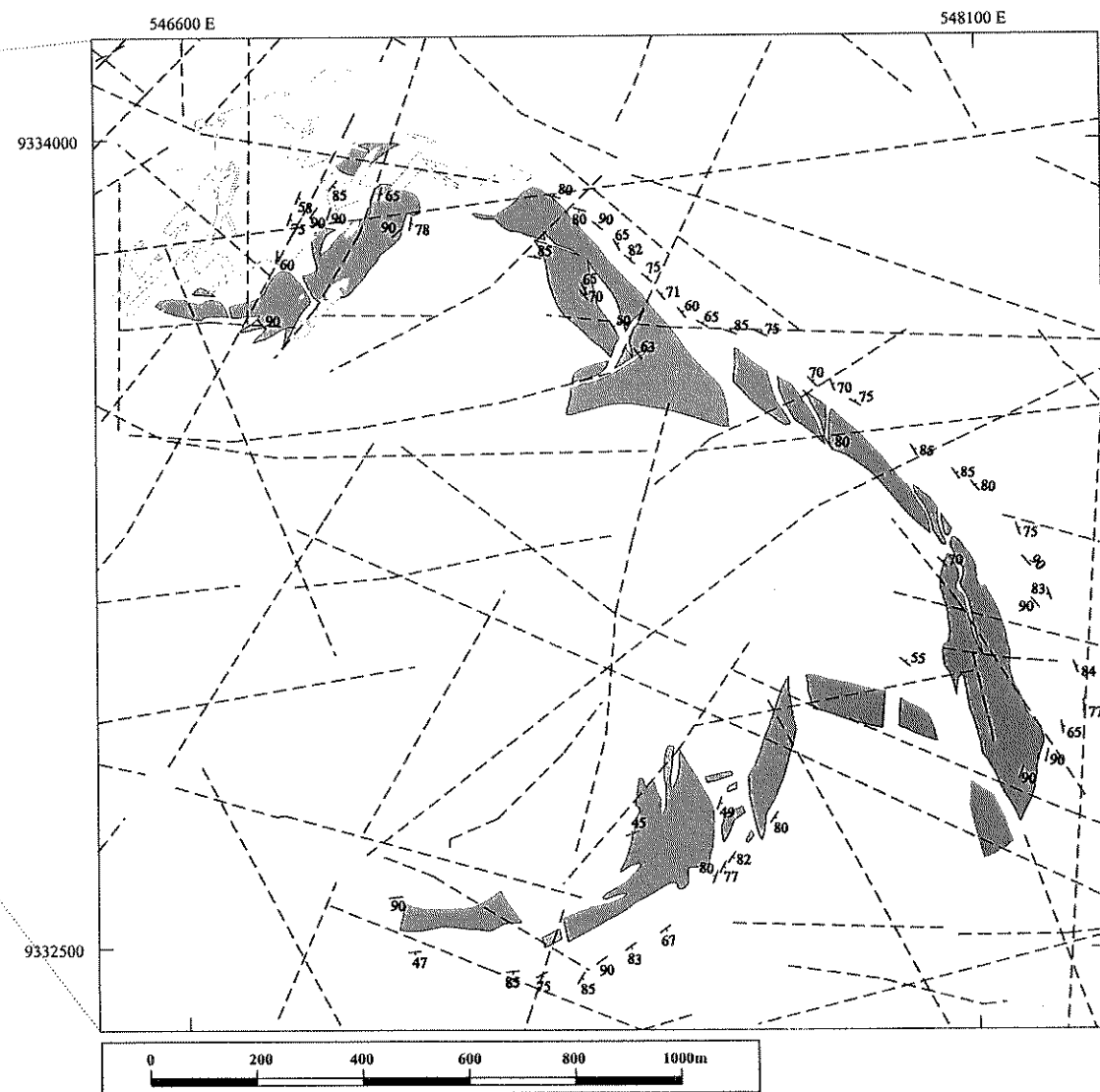


Fig. 3. Structural map of the Igarapé Bahia copper-gold deposit

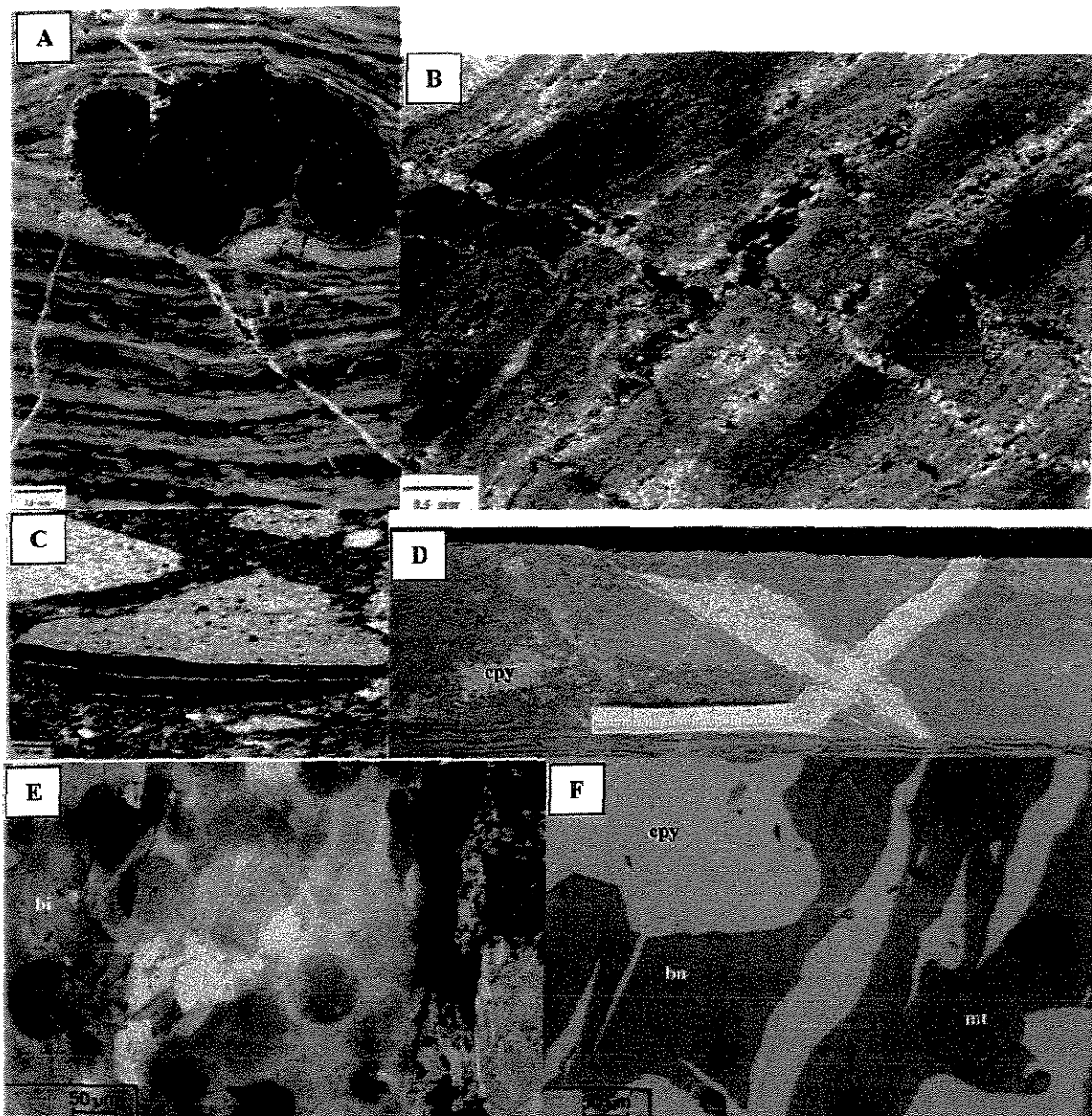


FIG. 4. A. Photomicrograph of a chalcopyrite (cpy) nodule that bends the sedimentary bedding and is connected to discordant veins containing chalcopyrite. Plane-polarized light. 384/141.50m. B. Photomicrograph of a set of discordant and concordant chlorite + chalcopyrite veins crosscutting the sedimentary bedding. Plane-polarized light. 384/141.20m. C. Photomicrograph of a mineralized Fe-chlorite breccia with a fragment of laminated sedimentary rock from the hangingwall welded by a chlorite  $\pm$  magnetite  $\pm$  chalcopyrite matrix. Plane-polarized light. 353/168.70m. D. Magnetite breccia with abundant chalcopyrite (cpy) being crosscut by carbonate veins. BHMAG-003/407.25m. E. Photomicrograph of the matrix of a magnetite breccia with abundant biotite (bi), showing pleochroic halos due to uraninite inclusions. Plane-polarized light. BHMAG-003/407.25m. F: Photomicrograph of the matrix of a magnetite breccia showing the equilibrium between chalcopyrite (cpy), bornite (bn) and magnetite (mt). Reflected light. BHMAG-001/476.00m.

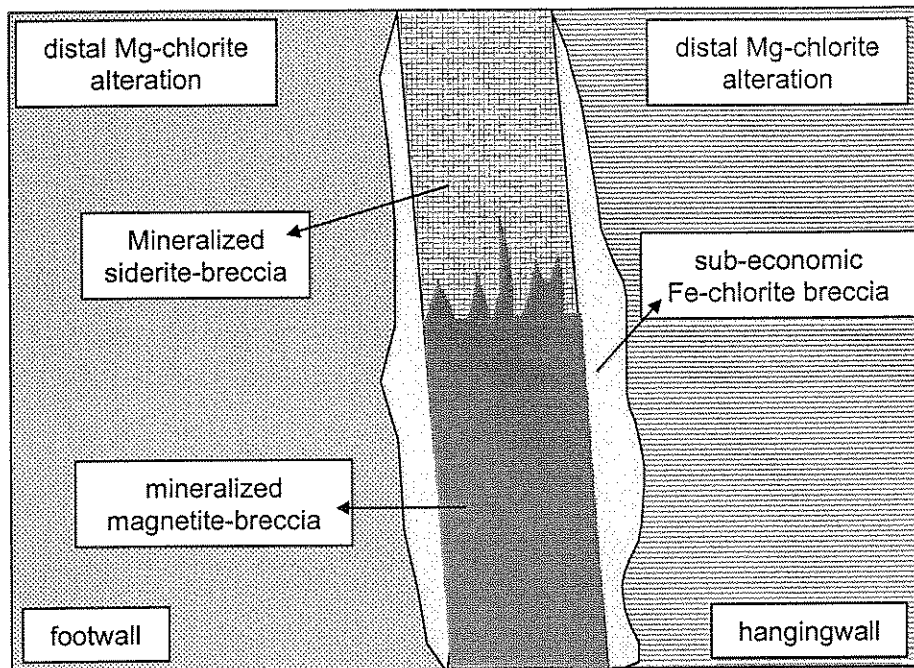


FIG. 5. Idealized distribution of the hydrothermal alteration zones of the Igarapé Bahia Cu-Au-(U-REE) deposit (not to scale).

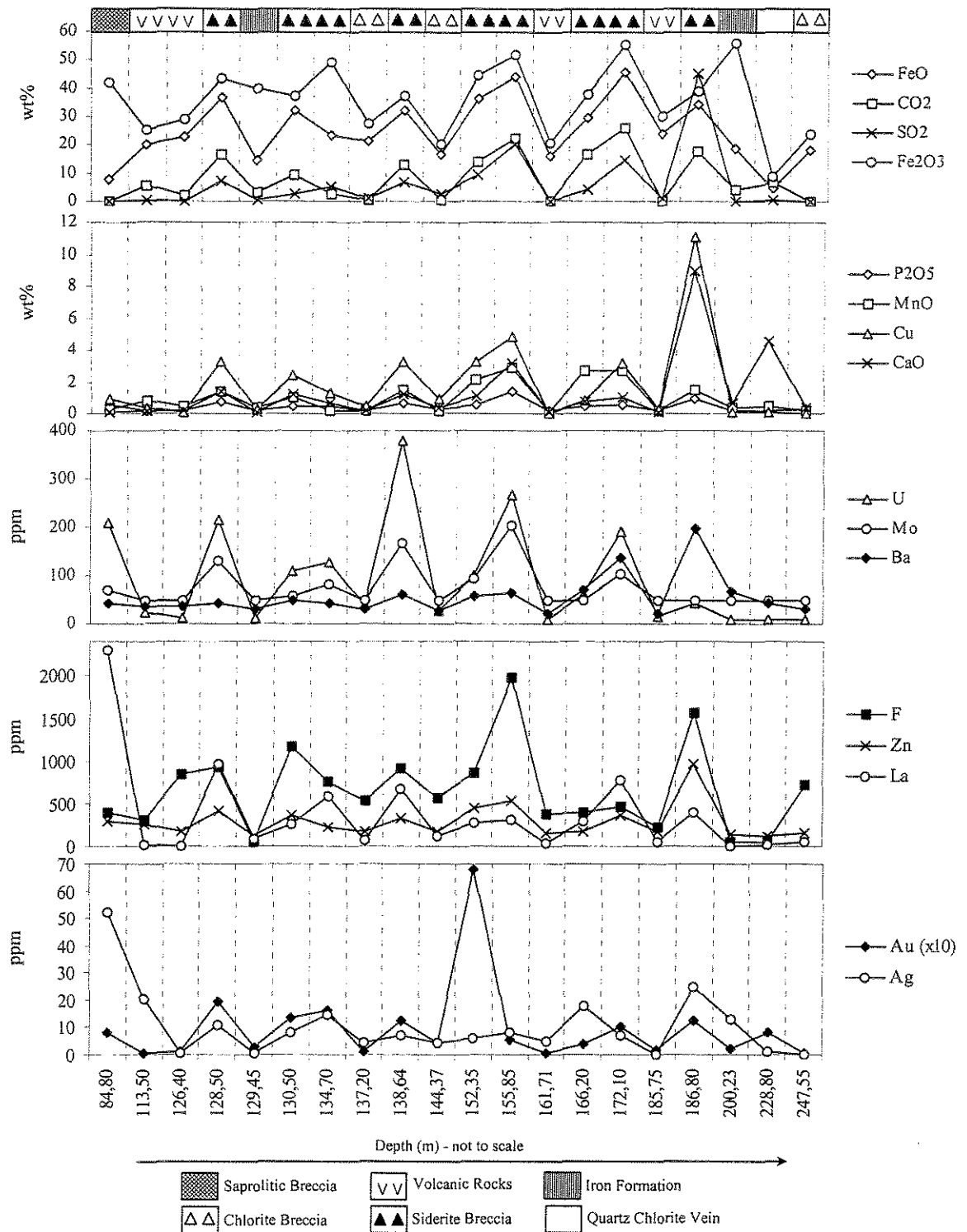


FIG. 6. Geochemical log of drill hole 340 on the Acampamento Sul orebody of the Igarapé Bahia Fe-oxide Cu-Au-(U-REE) deposit, showing the enrichment in  $\text{Fe}^{2+}$ ,  $\text{Fe}^{3+}$ ,  $\text{CO}_2$ ,  $\text{SO}_2$ ,  $\text{P}_2\text{O}_5$ ,  $\text{MnO}$ ,  $\text{Cu}$ ,  $\text{CaO}$ ,  $\text{U}$ ,  $\text{Mo}$ ,  $\text{Ba}$ ,  $\text{F}$ ,  $\text{Zn}$ ,  $\text{La}$ ,  $\text{Au}$  and  $\text{Ag}$  of the chlorite breccia and siderite breccias relatively to the host rocks.

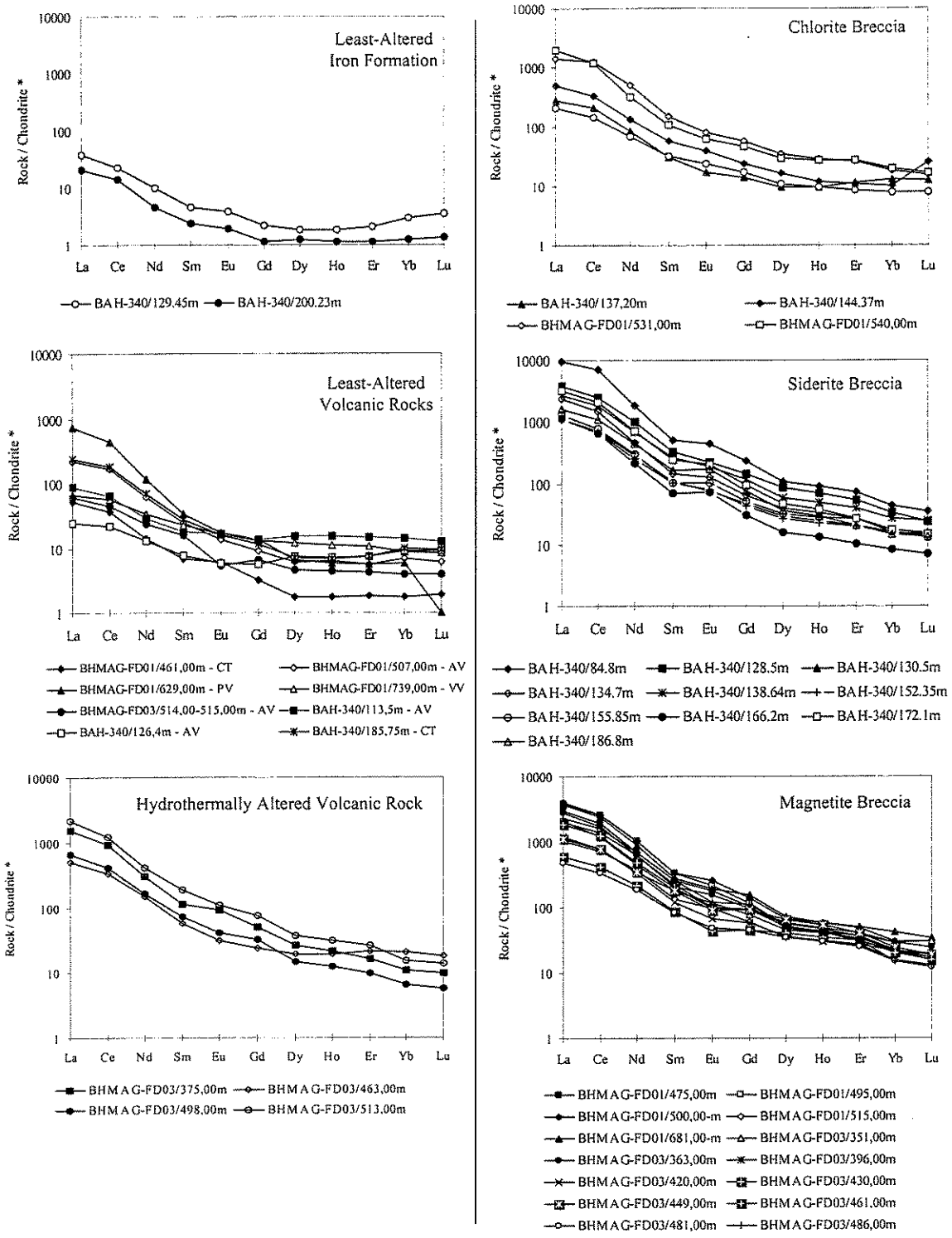


FIG. 7. Representative rare-earth element distribution patterns of host rocks and mineralized breccias from the Igarapé Bahia Fe-oxide Cu-Au-(U-REE) deposit. \* Chondrite composition after Evensen et al. (1978).

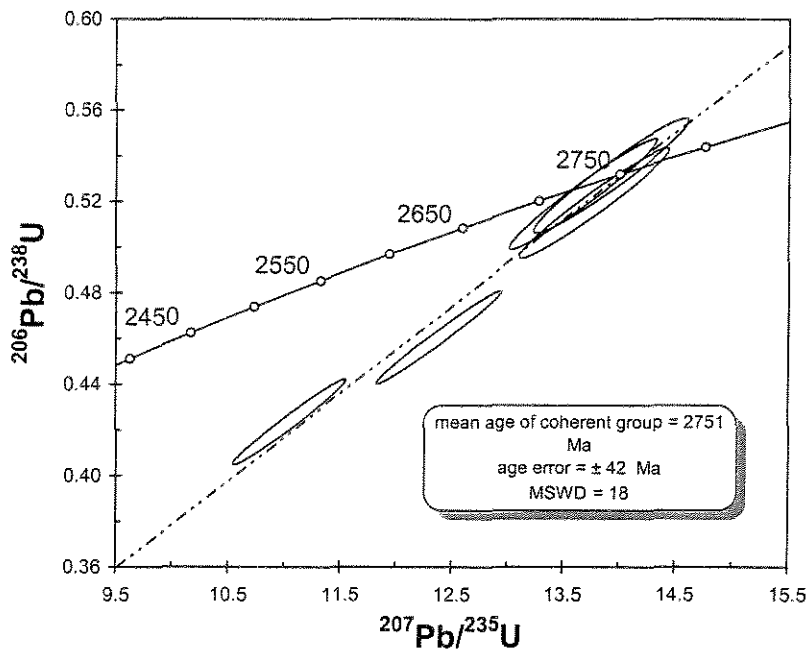


FIG. 8. Concordia plot for SHRIMP II data points from zircons from the host metavolcanic rocks of the Igarapé Bahia Fe-oxide Cu-Au-(U-REE) deposit. Weighted mean  $^{207}\text{Pb}/^{206}\text{Pb}$  age of concordant data is  $2751 \pm 42$  Ma (MSWD = 18). Samples UWA-B18C and UWA-B18D.

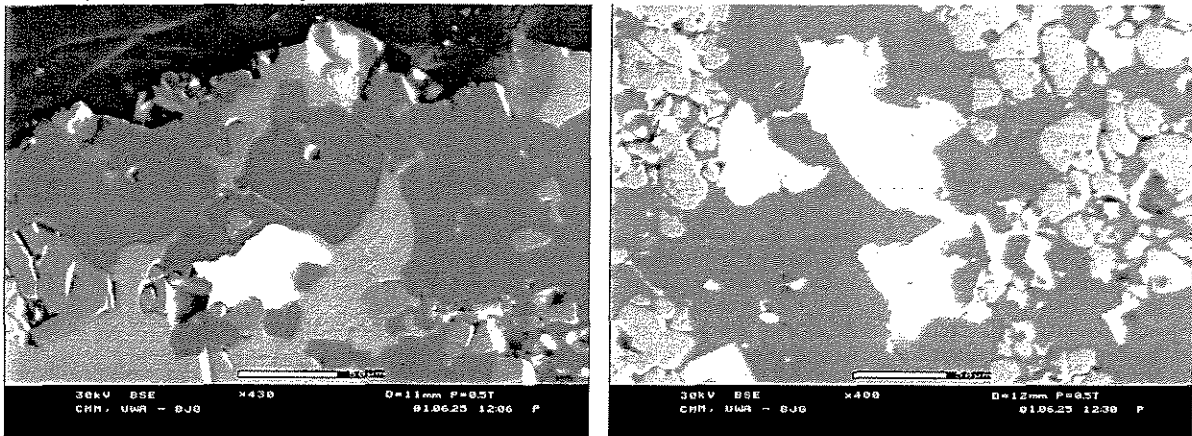


FIG. 9. Representative back-scattering images of sample UWA-B34 showing analyzed monazite grains in equilibrium with chalcopyrite and magnetite in the matrix of ore-bearing breccias of the Igarapé Bahia Fe-oxide Cu-Au-(U-REE) deposit.

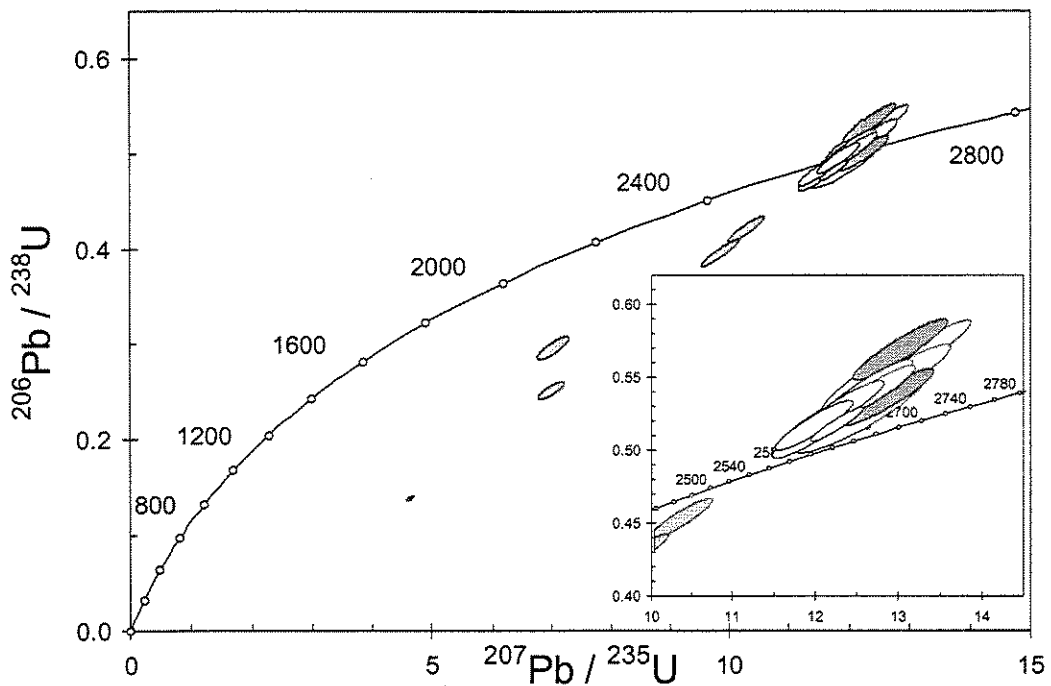


FIG. 10 - Concordia plot for the SHRIMP II data points for monazite from the matrix of mineralized magnetite breccias (sample UWA-B34) of the Igarapé Bahia Fe-oxide Cu-Au-(U-REE) deposit. Weighted mean  $^{207}\text{Pb}/^{206}\text{Pb}$  age of main concordant cluster, shown on the inset, is  $2575 \pm 12$  Ma (MSWD = 1.19).

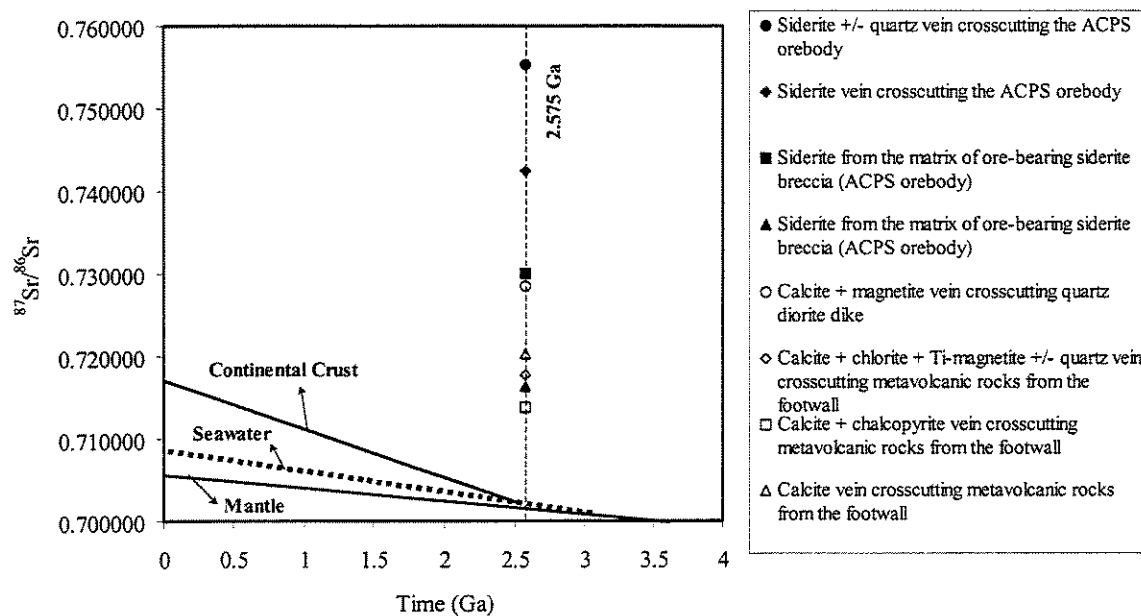
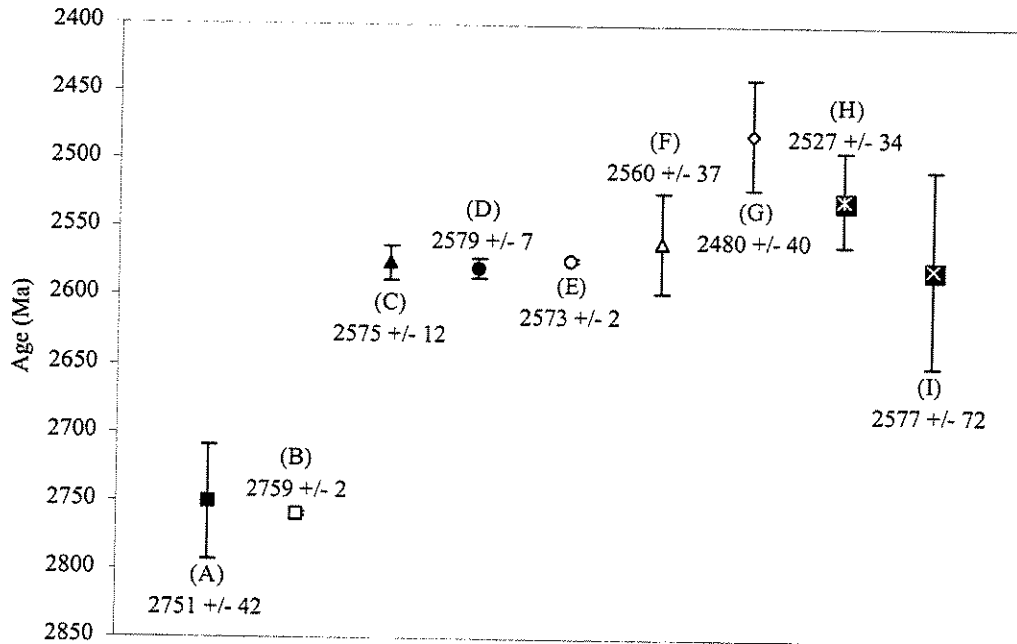


FIG. 11.  $^{87}\text{Sr}/^{86}\text{Sr}$  versus time diagram showing the isotopic evolution of continental seawater (Veizer and Compston 1976), continental crust and mantle (Faure and Powell, 1972) relatively to the carbonate minerals from the matrix of mineralized breccias and crosscutting veins of the Igarapé Bahia Fe-oxide Cu-Au-(U-REE) deposit.



- (A) Igarapé Bahia host metavolcanic rocks. SHRIMP II zircon 207Pb/206Pb age (this work)
- (B) Felsic volcanic rocks from the Grão Pará Group. Conventional zircon 207Pb/206Pb age (Machado et al. 1991)
- ▲ (C) Cu-Au-bearing magnetite breccias from the Igarapé Bahia deposit. SHRIMP II monazite 207Pb/206Pb age (this work)
- (D) Diabase dikes crosscutting the Igarapé Bahia deposit. SHRIMP II zircon 207Pb/206Pb age (this work)
- (E) Old Salobo Granite. Conventional zircon 207Pb/206Pb age (Machado et al. 1991)
- △ (F) Itacaiúnas alkaline granite. Conventional zircon 207Pb/206Pb age (Souza et al. 1996)
- ◊ (G) Itacaiúnas alkaline granite. Bulk-rock Rb-Sr age (Montalvão et al. 1984)
- ✖ (H) A-type Estrela Granitic Complex. Bulk-rock Rb-Sr age (Barros and Barbey 1998)
- ✖ (I) Igarapé Bahia host metavolcanic rocks. Bulk-rock Rb-Sr age (Ferreira Filho 1985)

FIG. 12. Summary of the SHRIMP II ages obtained in this work compared to conventional U-Pb zircon ages and Rb-Sr bulk-rock ages for the Estrela Granitic Complex, the Old Salobo Granite, the Itacaiúnas Granite and the host metavolcanic rocks of the Igarapé Bahia Deposit.

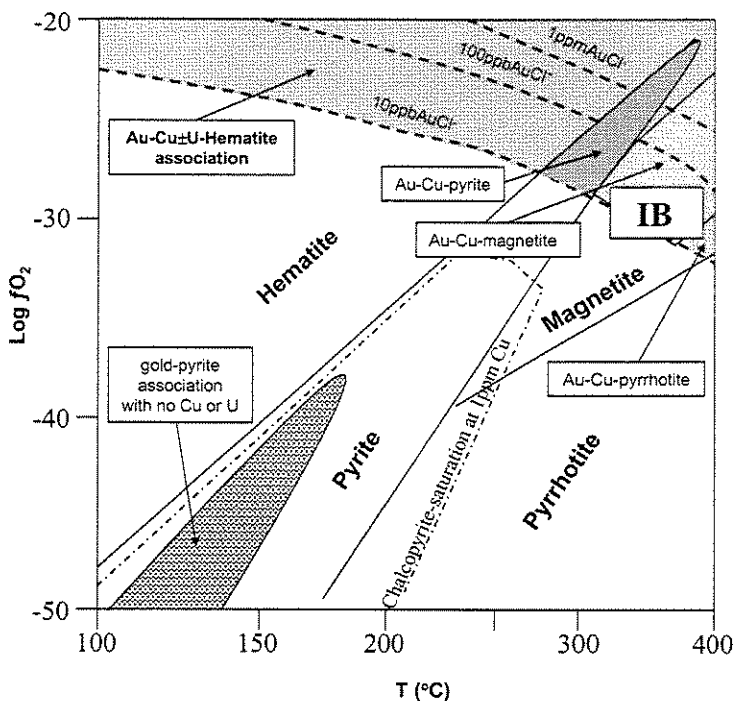


FIG. 13. Fields of gold transport and deposition in the Log  $f\text{O}_2$  versus temperature space after Davidson and Large (1994), showing the relative field for the Igarapé Bahia Fe-oxide Cu-Au-(U-REE) deposit (IB). Temperature estimates of the Igarapé Bahia hydrothermal system are based in chlorite thermometry (Tallarico et al., 2000) and fluid inclusion data (Ribeiro, 1989; Lindenmayer et al., 1998) and  $f\text{O}_2$  based on mineral equilibrium.

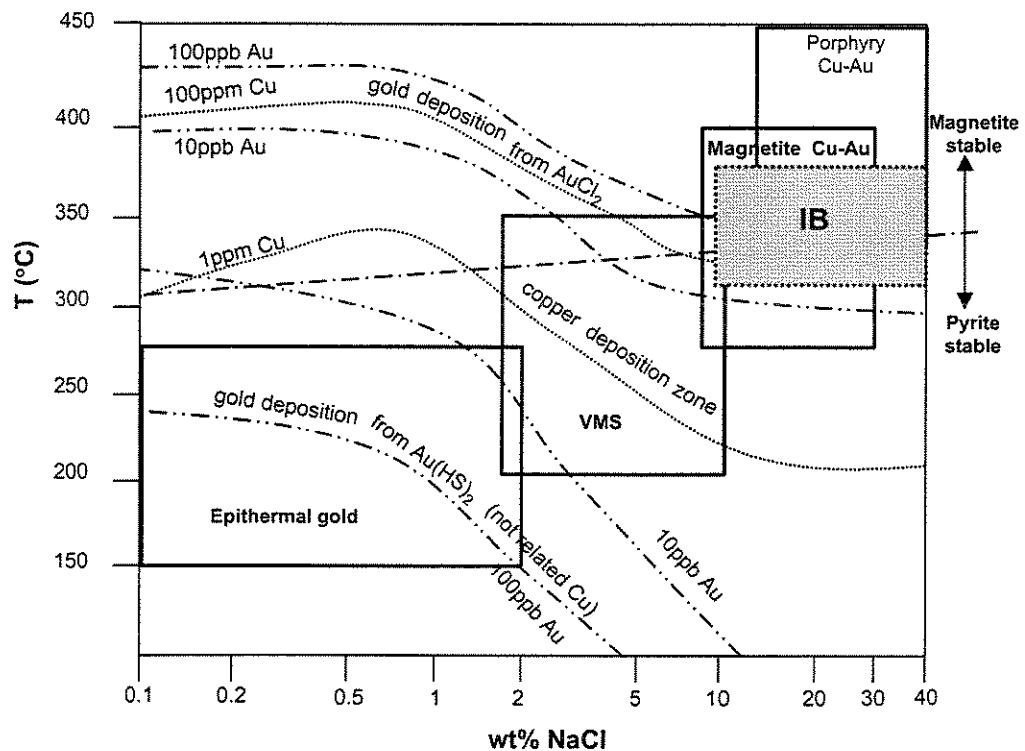


FIG. 14. Temperature-salinity diagram showing the relationship between fluid chemistry of different deposit-types after Davidson and Large (1994) relative to the Igarapé Bahia Fe-oxide Cu-Au-(U-REE) deposit (IB). Temperature and salinity data for the Igarapé Bahia hydrothermal system are based in chlorite thermometry (Tallarico et al., 2000) and fluid inclusion data (Ribeiro, 1989; Lindenmayer et al., 1998), respectively.

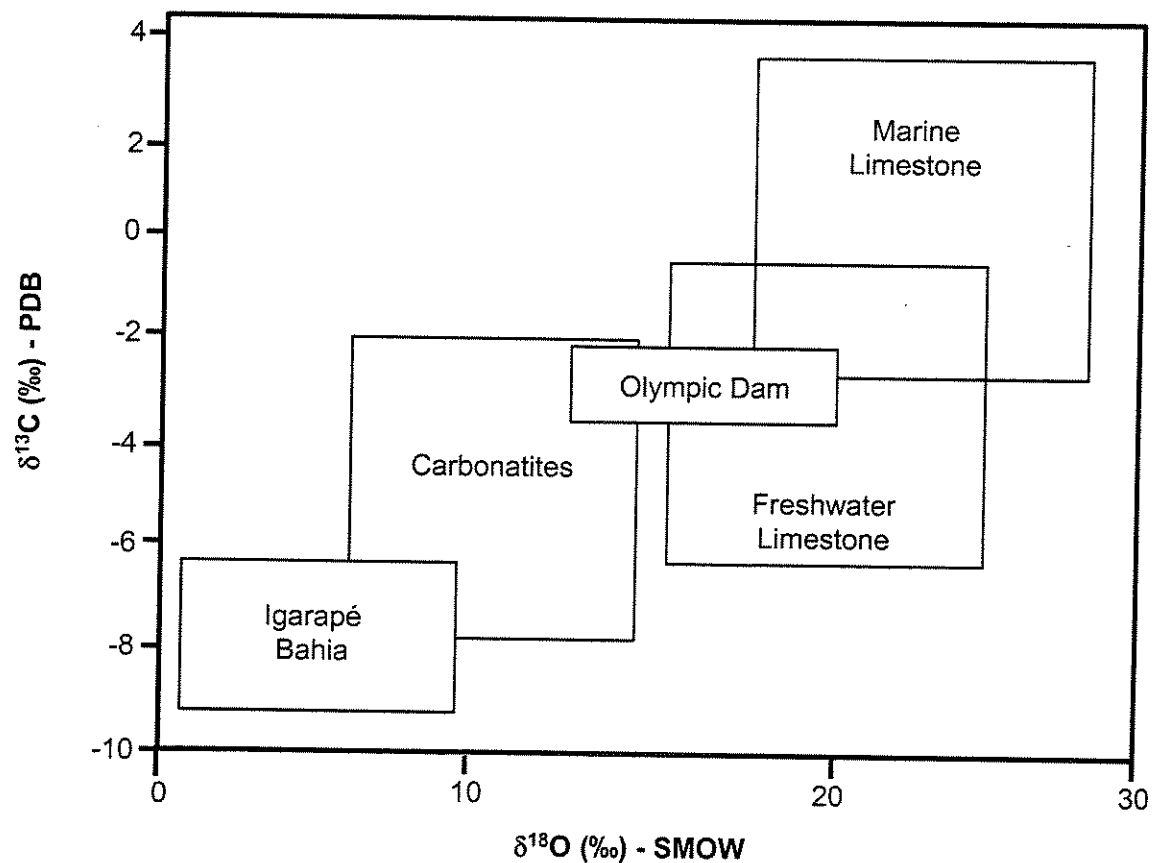


FIG. 15.  $\delta^{18}\text{O}$  versus  $\delta^{13}\text{C}$  diagram showing the fields from carbonates of the Igarapé Bahia F-oxide Cu-Au-(U-REE) deposit (Oliveira et al., 1998; Tazava, 1999) relative to carbonates from carbonatites, freshwater limestone, marine limestone and the Olympic Dam deposit, after Oreskes and Einaudi (1992).

## **ANEXO 5**

Geological and SHRIMP II U-Pb constraints on the age and origin of the Breves Cu-Au-(W-Bi-Sn) deposit, Carajás, Brazil



**Fernando Henrique Bucco Tallarico<sup>1,2</sup>**

**Neal Jesse McNaughton<sup>2</sup>**

**David Ian Groves<sup>2</sup>**

**Ian R. Fletcher<sup>2</sup>**

**Bernardino Ribeiro Figueiredo<sup>1</sup>**

**Jéssica Beatriz Carvalho<sup>3</sup>**

**José Luzimar Rego<sup>3</sup>**

**Alfredo Rossetto Nunes<sup>3</sup>**

1. Instituto de Geociências, Universidade Estadual de Campinas

Cx. Postal 6152, 13.083-970, Campinas, SP, Brazil

2. Centre for Global Metallogeny, Department of Geology & Geophysics, University of Western Australia

35 Stirling Highway, Crawley WA 6009, Australia

3. Companhia Vale do Rio Doce

Cx. Postal 51, Serra dos Carajás, 68.516-000, Parauapebas, PA, Brazil

**Geological and SHRIMP II U-Pb constraints on the age and origin of the**

**Breves Cu-Au-(W-Bi-Sn) deposit, Carajás, Brazil.**

**Campinas, June 12, 2003**



F. H. B. Tallarico<sup>1,2</sup> · N. J. McNaughton<sup>2</sup> · D. I. Groves<sup>2</sup> · I. R. Fletcher<sup>2</sup> · B. R. Figueiredo<sup>1</sup> · J. B. Carvalho<sup>3</sup> ·

J.L. Rego<sup>3</sup> · A. R. Nunes<sup>3</sup>

## Geological and SHRIMP II U-Pb constraints on the age and origin of the Breves Cu-Au-(W-Bi-Sn) deposit, Carajás, Brazil.

### Abstract

The Breves deposit in the Carajás Copper-Gold Belt, Brazil, a member of the Cu-Au-(W-Bi-Sn) group of deposits, contains about 50 Mt of 1.22% Cu, 0.75 g/t Au, 2.4 g/t Ag, 1200 g/t W, 70 g/t Sn, 175 g/t Mo and 75 g/t Bi. It is hosted by sandstones and siltstones of the Águas Claras Formation (minimum age of 2681 ± 5 Ma) in the roof zone of the apical part of a complex, highly-altered granite intrusion. The mineralisation is disseminated in a greisenized zone, resulting from alteration of probable monzogranites and syenogranites. The ore-bearing greisen contains abundant xenomorphic quartz in association with Fe-chlorite and muscovite. The gangue assemblage also includes fluorite, tourmaline, and minor amounts of monazite, xenotime, chlorapatite, thorite, zircon, calcite, siderite and bastäsrite. Copper mineralisation is dominated by chalcopyrite associated with pyrite, arsenopyrite, pyrrhotite and molybdenite. Gold particles, in equilibrium with native bismuth, are common as inclusions in chalcopyrite. The greisen contains sub-economic concentrations of tungsten and niobium that are related to the presence of ferberite, qitianlingite and Nb-rutile.

SHRIMP II zircon dating of the host granites gives  $^{207}\text{Pb}/^{206}\text{Pb}$  ages of 1878 ± 8 Ma and 1880 ± 9 Ma for two components, and a combined age of 1879 ± 6 Ma. SHRIMP II dating of monazite and xenotime grains in late- to post-mineralisation veins gives a combined  $^{207}\text{Pb}/^{206}\text{Pb}$  age of 1872 ± 7 Ma, indistinguishable from the ages of the granites. This provides a genetic connection between the Breves deposit and the ca. 1.88 Ga A-type granite magmatism that typifies the Carajás Belt as part of a much larger, intracratonic magmatic province that extends over much of the Amazonian Craton. The recognition of this association has exploration implications, not only for the geophysical signature of the granite roof zones, but also for likely geochemical dispersion around the deposits of this type.

Key words: copper, gold, SHRIMP II geochronology, phosphates, Carajás, Breves.

---

## **Introduction**

The Carajás Belt, located in the southeastern portion of the Amazon Craton, includes one of the best-preserved Archean volcano-sedimentary sequences of the world. The major known mineral deposits in the Carajás Belt are the giant supergene-enriched iron and manganese deposits, that are hosted by Archean (2.75 Ga) volcano-sedimentary rocks. Another important group of deposits is a variety of world-class (> 200 million tonnes) Fe-oxide Cu-Au-(U-REE) deposits (e.g. Salobo, Igarapé Bahia, Cristalino and Sossego), whose genesis has been widely debated. Previous models include syngenetic VHMS (Besshi-type) models (e.g. Ferreira Filho 1985; Almada 1998), epigenetic hydrothermal-magmatic models with ores related to Proterozoic (1.88 Ga) granites (Lindenmayer et al. 1998), and multistage models that claim an interplay of Archean and Proterozoic processes (Ribeiro 1989).

In addition to these, there is a particular group of Cu-Au-(W-Bi-Sn) deposits (e.g. Águas Claras, Gameleira and Breves) that differ not only in their metallic content, but also their lack of Fe-oxides, presence of relatively sulfur-rich ore paragenesis (pyrite ± pyrrhotite) and abundance of quartz. Those occur either in prominent veins systems or in extensive greisen-type alteration halos.

Thus, it appears that there are two distinct styles of Cu-Au mineralisation in the Carajás Belt. This paper provides a description of the Breves deposit, a representative of the Cu-Au-(W-Bi-Sn) group, and places constraints on the age of mineralisation via SHRIMP II U-Pb geochronology, so that a genetic connection to elements of its geological setting can be established. This is the first study in which the SHRIMP II technique has been applied to constrain the age of an ore deposit in the Carajás Belt, and provides new and original results that have regional metallogenetic implications.

---

## **Regional geology and metallogeny**

The Carajás Belt (Fig. 1) includes an exceptionally well-preserved Archean volcano-sedimentary succession. It lies in the eastern portion of the Amazonian Craton, being bordered to the east by the Neoproterozoic Araguaia Belt and to the west by overlying Paleoproterozoic sequences (Docegeo 1988; Araújo and Maia 1991; Tassinari and Macambira 1999). To the south, it is in contact with the Rio Maria Block (Docegeo 1988; Huhn et al. 1988), an older, typical granite-greenstone terrain, while, to the north, it is concealed by Paleozoic and Cenozoic sedimentary rocks of the Amazon Basin (Pinheiro and Holdsworth 1997).

Basement rocks consist of the gneiss and migmatite of the Xingu Complex and the orthogranulites of the Pium Complex. SHRIMP work conducted by Pidgeon et al. (2000) yield ages of  $3002 \pm 14$  Ma for the cores and  $2859 \pm 9$  Ma for the rims of zircons from granulite-facies edembergites of the Pium Complex. These are interpreted as the crystallization and metamorphism ages, respectively. These data agree with conventional U-Pb analysis, performed by Machado et al. (1991), on zircons extracted from gneiss and migmatites of the Xingu Complex, that yield an age of  $2859 \pm 2$  Ma for the migmatization of the basement rocks (Table 1).

The basement assemblage defines a broad, steeply-dipping, E-W-trending ductile shear zone, named the Itacaiúnas Shear Zone, that experienced several episodes of reactivation during the Archean and Paleoproterozoic (Pinheiro and Holdsworth 1997; Holdsworth and Pinheiro 2000).

The volcano-sedimentary rocks of the Carajás Belt, incorporated within the Itacaiúnas Supergroup, includes rocks of different metamorphic grades, ranging from intensely sheared amphibolite/granulite-facies rocks (Igarapé Salobo Group) at the northern edge of the Itacaiúnas Shear Zone, to virtually undeformed low greenschist-facies rocks (Grão Pará Group) in the innermost portion of the basin (Docegeo 1988). Accumulation of the volcanic rocks was determined by various authors at  $\sim 2.75$  Ga (Table 1). The Grão Pará Group is the dominant volcano-sedimentary sequence in the Carajás Belt, and includes low-grade metavolcanic rocks that host significant banded-iron formation. These contain the giant supergene-enriched iron deposits, such as Serra Norte, Serra Sul, Serra Leste and Serra de São Felix, that contain total resources of 17.3 billion tonnes @ 66% Fe (Tolbert et al. 1971). According to Gibbs et al. (1986), Olszewski et al. (1989) and Gibbs et al. (1990), the stratigraphy, geochemical and Sm-Nd isotopic composition of the volcanic rocks of the Grão Pará Group indicate that this volcano-sedimentary sequence was formed through rifting of older continental crust during the Archean.

Sandstones and siltstones, which formed in a shallow marine to fluvial environment (Águas Claras Formation - Nogueira et al. 1994, 2000), overlie the former units. A minimum age of  $2645 \pm 12$  Ma for the Águas Claras Formation was determined by Dias et al. (1996) from conventional U-Pb analysis of zircons from cross-cutting gabbro dikes. A SHRIMP II U-Pb age of  $2681 \pm 5$  Ma was determined by Trendall et al. (1998) from a sample of sandstone containing zircons apparently derived from syndepositional volcanic rocks. Based on this result, Trendall et al. (1998) inferred that the Águas Claras Formation could represent the uppermost unit of a continuous accumulation in the “Grão Pará Basin”, that lasted less than 100 million years.

The Carajás Belt was intruded by granitic magmas of distinct ages and compositions (Table 1). Archean intrusions include granites and diorites of the Plaquê Suite ( $2736 \pm 24$  Ma, Avelar et al. 1999), the Planalto granite ( $2747 \pm 2$  Ma, Huhn et al. 1999a) and the Cristalino diorite ( $2738 \pm 6$  Ma, Huhn et al. 1999b). Younger alkaline granites include the Old Salobo granite ( $2573 \pm 2$  Ma, Machado et al. 1991) and the Itacaiúnas granite ( $2560 \pm 37$  Ma, Souza et al. 1996). Paleoproterozoic intrusions include several anorogenic granitic plutons such as the Central Carajás granite ( $1880 \pm 2$  Ma, Machado et al. 1991) and the Cigano granite ( $1883 \pm 3$  Ma, Machado et al. 1991). The latter belong to the most-extensive A-type Proterozoic province in the world (e.g. Santos et al. 2001), that covers thousands of square kilometers of the Amazonian Craton, and is known to host several large tin deposits and smaller occurrences of F, Zr, REE, Y and W (Issler and Lima 1987; Dall'Agnol et al. 1993; Dall'Agnol et al. 1994).

A striking feature of the Carajás region is the clustering of a large number of world-class Cu-Au deposits that are collectively known as the Carajás Copper-Gold Belt (Fig. 1). The most abundant deposit-type in the belt is the Fe-oxide Cu-Au-(U-REE) group of deposits, that are hosted by a variety of rocks and have different orebody morphologies, although most are breccia bodies (Table 2). The most significant examples of this deposit-type are: Salobo with resources of 994 Mt @ 0.94 % Cu and 0.52 g/t Au (Farias and Saueressig 1982; Vieira et al 1988; Lindenmayer 1990; Figueiredo et al 1994; Réquia and Xavier 1995; Mellito and Tassinari 1998), Igarapé Bahia with resources of 219 Mt @ 1.4 % Cu and 0.86 g/t Au (Ferreira Filho 1985; Almada 1998; Tazava 1999; Tallarico 2000), Sossego with resources of 355 Mt @ 1.1 % Cu and 0.28 g/t Au (Cordeiro 1999; Lancaster et al. 2000), Cristalino with resources of 500 Mt @ 1.0 % Cu and 0.3 g/t Au (Huhn et al. 1999b) and Cento e Dezoito with resources of 170 Mt @ 1.0 % Cu and 0.3 g/t Au (Rigon et al. 2000). A second style of Cu-Au deposits are those characterized by a Cu-Au-(W-Bi-Sn) association (Table 2). This group includes a smaller number of deposits, all of medium to small size (Table 2), that are characterized by the association Cu-Au-(W-Bi-Sn). Representative examples are the Águas Claras Cu-Au-(W-Sn) deposit with total resources of 9.5 Mt of oxidized ore @ 2.43 g/t Au (Soares et al. 1994; Silva and Villas 1998), and the Breves Cu-Au-(W-Bi-Sn) deposit that is discussed in detail in this paper.

---

### **Descriptive geology of the Breves Cu-Au-(W-Bi-Sn) mineralisation**

The Breves Cu-Au-(W-Bi-Sn) deposit represents one of the most recent discoveries of Companhia Vale do Rio Doce (CVRD) and Rio Doce Geologia e Mineração S.A. (DOCEGEO) in the Carajás Copper-Gold Belt. The deposit

is located approximately 9 km northeast from the Igarapé Bahia gold mine, within the domain of the Carajás Fault-System (part of the Itacaúnas Shear Zone), one of the major crustal discontinuities in the Carajás area (Fig. 1).

According to Nunes et al. (2001), DOCEGEO located a lateritic crust at the Breves Plateau (Fig. 2) in the early 1990s, through the follow-up of anomalous copper contents in stream sediment and soil samples. Trenching and shallow drilling of the anomaly indicated the first resources of oxidized gold ore. In 1997, CVRD detailed the anomaly via reverse circulation drilling, resulting in definition of a reserve of 4 million tonnes of oxidized ore @ 0.75 g/t Au. An induced polarization survey was then undertaken to evaluate the extension of the mineralisation in depth and to test the existence of related primary ore. Further drilling of the induced polarization anomalies indicated resources of 50 million tonnes of primary ore @ 1.22% Cu, 0.75 g/t Au, 2.4 g/t Ag, 1200 g/t W, 70 g/t Sn, 175 g/t Mo and 75 g/t Bi.

The host rocks of the Breves deposit are sandstones and siltstones of the Águas Claras Formation (Nogueira et al. 1994; 2000). Unlike the Águas Claras deposit, where sandstones are the most abundant host rock, siltstone is dominant at the Breves deposit, suggesting that this sequence could represent the base of the Águas Claras Formation, as described by Nogueira et al. (2000).

The Breves deposit is located adjacent to the Carajás Fault, one of the major structures of the Itacaiúnas Shear Belt. According to Pinheiro and Holdsworth (1997) and Holdsworth and Pinheiro (2000), during the Paleoproterozoic, the Itacaiúnas Shear Zone was reactivated through sinistral movement, giving rise to extensional structures that controlled the ascent to shallow crustal levels of granite magmas through dilatant faults. It is probable that the Carajás Fault and subsidiary structures provided similar control on granite emplacement at the Breves deposit.

The Breves Cu-Au-(W-Bi-Sn) mineralisation is typically disseminated, occurring in an extensive greisen alteration halo, but is also associated with stockwork veins systems. The available drilling data, and the interpretation of vertical sections (Fig. 2), indicate that the greisen is an ore-shell that surrounds the apical portion of a granite intrusion. The geochemical signature of the greisen is distinctive. There is a strong enrichment in Cu, Au, W, Mn, Bi, Sn, La and As relative to the host sedimentary rocks and the underlying granite intrusion (Fig. 3). The contact between the greisen and the sedimentary rocks is transitional, with the hydrothermal alteration progressively decreasing in intensity, and finally terminating, outward from the ore zone. The contact between the greisen and the underlying granite is defined by narrow granite apophyses, with or without xenoliths. The typically angular

xenoliths are rimmed in places by microcline ± biotite as a consequence of reaction with the magma and thermal metamorphism (Fig. 4a). Some xenoliths exhibit internal sedimentary bedding, whereas others are intensely altered and exhibit a massive texture (Fig. 4a). Silicification is the most intense alteration in the zone of granite apophyses.

The intrusive rocks that underlie the greisen are intensely hydrothermally altered. Original compositions possibly included monzogranites and syenogranites, together with alkali-feldspar granites, typically with reduced amounts of plagioclase, although the intense potassic alteration of these rocks precludes unequivocal classification. Textural varieties include fine-grained xenomorphic, granophytic and granular hypidiomorphic rocks. The interstices of the quartz-feldspar fabric are filled mainly by late-stage poikilitic K-feldspar, muscovite and minor biotite, normally replaced by chlorite. The granites commonly include fine-grained anhedral quartz-muscovite domains, that are characteristically depleted in feldspars, as a result of endogenous greisen-type hydrothermal alteration. Accessory minerals include zircon, monazite, chalcopyrite, pyrite, arsenopyrite, ferberite, cassiterite, bismuthinite and native bismuth, fluorite and tourmaline.

Less commonly, an alkali-feldspar-rich rock occurs in the intrusive suite. Petrographically, the rock is characterized by altered equigranular alkali-feldspar (up to 70 wt%, 0.5 to 3 mm), and minor fine-grained xenomorphic quartz crystals. Fluorite is abundant in the interstices of the coarse-grained feldspar crystals. Textural evidence strongly suggests that the rock derives from the removal of quartz and alteration of feldspar during hydrothermal alteration of granite. Such an alteration-style, known as episyenitization, has been well documented in Europe in Hercynian and Variscan granites (e.g. Melcher et al. 1996, Recio et al. 1997).

The ore-bearing greisen typically has a xenomorphic texture, defined by abundant xenomorphic quartz crystals with chlorite and muscovite inclusions (Fig. 4b). Muscovite occurs most commonly in the interstices of the quartz fabric, as radial aggregates that are commonly replaced by Fe-chlorite. The gangue assemblage also includes fluorite and tourmaline, as well as trace amounts of rutile, monazite, xenotime, chlorapatite, thorite and zircon. Carbonate minerals (calcite, bastnäsite and siderite) occur in minor amounts in the greisen.

The copper mineralisation is characterized by xenomorphic and poikiloblastic crystals of chalcopyrite (up to 10 wt%) in the interstices of quartz-muscovite aggregates. Euhedral inclusions of arsenopyrite, with up to 12 wt % Co (Table 3), are apparently in equilibrium with the host chalcopyrite. Chalcopyrite also contains inclusions of pyrite and minor pyrrhotite, both replaced by the host (Fig. 4c). Rare molybdenite occurs as inclusions in pyrite and chalcopyrite.

Gold occurs as inclusions in chalcopyrite, commonly in equilibrium with native bismuth (Fig. 6). Gold from the Breves greisen typically contains a high silver content (up to 24 wt% Ag - see Table 3).

The significant concentrations of bismuth in the greisen relate mainly to bismuthinite and native bismuth that occur as inclusions in arsenopyrite and chalcopyrite. Additionally, there are traces of hedleyite as inclusions in apatite, pyrite and chalcopyrite.

Above-background concentrations of tungsten, that occur in association with the copper-gold mineralisation, are related to the occurrence of ferberite as inclusions in the sulfide minerals. Wave-length Dispersive Spectrometry data of ferberite indicate the presence of up to 25% of hubnerite molecule (Table 3). Scattered concentrations of tin in the greisen relate to cassiterite inclusions in the sulfide minerals. Sub-economic niobium concentrations in the greisen normally relate to rutile that contains up to 2 wt% of  $\text{Nb}_2\text{O}_5$  (Table 3). Scanning Electron Microscopy (SEM) investigation of the ore also indicates the presence of rare qitianlingite and pyrochlore group minerals.

Ore-bearing veins, that crosscut the greisen and the granite, represent a much less-abundant style of mineralisation. It is not possible to establish a sequence of vein formation due to equivocal crosscutting relations. The following types of veins are recognized: (a) comb structure quartz-veins that can be either vuggy or filled with chalcopyrite, ferberite and chlorite (Fig. 4d); (b) fluorite + chalcopyrite + arsenopyrite + chlorite + quartz veins; (c) chalcopyrite + tourmaline veins; and (d) zoned veins with beryl-rich rims and tourmaline + fluorite + arsenopyrite centers. There are trace amounts of bismuthinite, ferberite, wolframite, monazite, galena and spodumene in these veins. All the ore-minerals in the greisen are also weakly disseminated in the underlying granites and in veins that crosscut both the greisen and the granite.

When compared to the more typical Cu-Au deposits of the Carajás Belt (e.g. Igarapé Bahia, Salobo, Centro e Dezoito, Sossego), Breves is distinguished by features, such as: (a) quartz-rich hydrothermal halos and veins; (b) relatively reduced and sulfur-rich ore paragenesis (pyrite + chalcopyrite  $\pm$  pyrrhotite); (c) insignificant carbonate alteration; and (d) sub-economic concentrations of W, Bi and Sn.

---

#### **Sampling and analytical procedures for SHRIMP II U-Pb analysis**

Sample selection was focused on vertical section L800 (Fig. 2), which is considered representative of the deposit and includes drill holes with significant intersections of mineralized rock (e.g. FR61 and FR73). The samples

selected for SHRIMP II analyses in this work are indicated in Table 4. Bulk samples of representative intersections of the granite (UWA-B09A) and the episyenite (UWA-B30A) were collected, and zircons extracted, to determine the crystallization age(s) of the magma(s). Although the granite and the episyenite samples exhibit evidence of hydrothermal alteration, the textures of the zircons in both samples indicate a magmatic origin. Bulk samples of greisen (UWA-B09B and UWA-B30B) were collected and zircons separated in order to test their potential hydrothermal origin by comparison of their ages and U/Th ratios with the magmatic zircons from the granite. Samples of hydrothermal xenotime and monazite, from type-d veins (beryl-tourmaline-fluorite-arsenopyrite) that crosscut the greisen (UWA-B40A, UWA-B40B and UWA-B40C), were prepared to constrain the minimum age of ore deposition.

The separation of zircon samples was carried out at the Universidade Federal de Ouro Preto, Brazil, with final handpicking at the University of Western Australia. After identification of zircons in thin-section, the samples were crushed and a <60# fraction collected, cleaned, and the final selection of zircons hand-picked and mounted in epoxy resin together with chips of the 564 Ma CZ3 standard zircon (Pidgeon et al. 1994; Nelson 1997). After detailed photography and SEM imaging, the discs were cleaned and coated with high-purity gold.

Uranium-Th-Pb isotope analyses of sectioned single zircons were carried out on the SHRIMP II at Curtin University of Technology following the procedures documented by Compston et al. (1986), Williams and Claesson (1987) and Smith et al. (1998). Data were processed using the software package SQUID 1.00 (Ludwig 2001a).

Xenotime and monazite SHRIMP II analyses were performed *in situ* on discs and fragments of polished thin sections mounted in epoxy mounts. The xenotime standard (xtc, 2632 Ma) was mounted in a separate mount (Fletcher et al. 2000), whereas the monazite analyses used VK1 standards (488 Ma) within the same mount and also in a separate mount. Analytical and data reduction methods for xenotime are described by Fletcher et al. (2000) and those for monazite by Foster et al. (2000) and Rasmussen et al. (2001).

The uncertainties in the radiogenic Pb isotope ratios are governed principally by ion-counting precision in the isotopes of direct interest and also in  $^{204}\text{Pb}$ , which provides a measure of common Pb. As the  $^{204}\text{Pb}$  content indicated by the analyses of most of the sample zircons was similar to that obtained from the standard zircon analyses, it was assumed that all the Pb came from the gold coat (i.e. Broken Hill galena composition). The data used for age determinations all gave very low common-Pb corrections and are therefore insensitive to the choice of common-Pb composition. All analysis with higher levels of common Pb have other indications of isotopic

disturbance, and the common Pb cannot be assumed to be original, so the choice of composition is necessarily an estimate. The Pb data from each analysis were corrected for common Pb by stripping the common-Pb component from the measured  $^{206}\text{Pb}$ ,  $^{207}\text{Pb}$  and  $^{208}\text{Pb}$ , using the observed  $^{204}\text{Pb}$ , and Pb of Broken Hill composition.

Ages are calculated using U decay constants from Jaffey et al. (1971). Unless otherwise stated, analytical uncertainties given in the tables and shown in plots are  $1\sigma$ . The ages from pooled data are weighted means, with uncertainties given as 95% confidence limits. Plots were prepared using ISOPLOT 2.49 (Ludwig 2001b).

---

## SHRIMP II U-Pb results

### *Sample UWA-B09A: Granite*

A total of 38 spots were analysed on 30 zircon grains from sample UWA-B09A of the Breves Granite (Table 5). Apart from grain 13, which has a clearly inherited core with a  $^{207}\text{Pb}/^{206}\text{Pb}$  age  $\sim 2852$  Ma (spot 13-1) and a younger magmatic rim (spot 13-2, Fig. 5a), all analyzed grains have relatively uniform textures marked by well-defined magmatic zoning (e.g. Fig. 5c). Cathodoluminescence images (CL) were particularly useful to distinguish between low-U cores (bright CL zones) and relatively high-U rims (dark CL zones). A number of analysis on dark CL high-U zones yield strongly discordant data (e.g. spot 13-2, Fig. 5a), and apparently confirm the existence of a threshold U concentration for radiogenic Pb loss, as pointed out by Pidgeon et al. (2000). In the present case, the grain with highest U content and concordant U-Pb data has  $\sim 660$  ppm U (analysis 15-1). Half of the data are  $>5\%$  discordant, collectively displaying Pb loss over an extended time (possibly during the Brasiliano Event, Fig. 6), and are not used for age determination. The remaining 18 analysis define a single population with a weighted mean  $^{207}\text{Pb}/^{206}\text{Pb}$  age of  $1878 \pm 8$  Ma (MSWD = 1.1).

### *Sample UWA-B30A: Episyenite*

A total of 24 sites were analysed in 23 grains from sample UWA-B30A, an episyenite (Table 6). Again the CL images clearly distinguish between high and low-U zones in this population (Fig. 7). Apart from crystal 6, which has a partially resorbed inherited core with a  $^{207}\text{Pb}/^{206}\text{Pb}$  age  $\sim 2972$  Ma (spot 6-1), all remaining grains display typical magmatic zoning. Approximately 35% of the analyses, mostly from grains with higher U, are  $>5\%$  discordant. The remainder form a tight cluster in  $^{207}\text{Pb}/^{206}\text{Pb}$ , with a weighted mean age of  $1880 \pm 9$  Ma (MSWD = 1.4, n=15).

Omitting one (marginal)  $2\sigma$  outlier (spot 2-1) would increase this to  $1882 \pm 7$  Ma, with a MSWD of 1.2 (Fig. 8), but the exclusion of this one analysis is debatable and we use the more conservative value of  $1880 \pm 9$  Ma.

#### *Samples UWA-B09B and UWA-B30B: Greisen*

Sample UWA-B09B, a greisen potentially containing hydrothermal zircons, yielded a very limited number of zircons. To test the sample preparation techniques, a second bulk-sample of the greisen (UWA-B30B) was prepared. Again, the number of zircons was very limited. A total of 11 spots were analysed from three zircons from sample UWA-B09B and eight zircons from sample UWA-B30B (Table 7). No consistent pattern emerged from the data set. Given that the grains could be a detrital component of the host sedimentary rocks, this is not surprising. However, the data themselves are of very poor quality, with seven analyses of high-U zircons (above  $\sim 1000$  ppm) yielding highly discordant data. Among the low-U spots, two are unquestionably detrital, with  $^{207}\text{Pb}/^{206}\text{Pb}$  ages of  $\sim 2815$  (spot 5-1) and  $\sim 2730$  Ma (spot 6-1). These are consistent with previously reported ages for the Xingú Complex and the Grão Pará volcanic rocks, respectively (e.g. Machado et al. 1991). Spot 4-1 is the only analysis giving concordant data (95% of concordance) and a  $^{207}\text{Pb}/^{206}\text{Pb}$  age consistent with the age of the underlying granite (sample UWA-B09A), compatible with a hydrothermal origin for this zircon.

#### *Samples UWA-B40A, UWA-B40B and UWA-B40C: Late- to post-mineralisation veins*

When the zircons from the greisen did not yield a consistent age, monazite and xenotime grains from late- to post-mineralisation veins were analyzed to establish the minimum age of ore formation. The selected monazite and xenotime crystals are euhedral, and show equilibrium textures with the other phases of the vein, for example, quartz, arsenopyrite and chalcopyrite (Figs 9 and 10).

A total of 11 sites were analyzed on eight monazite grains from samples UWA-B40A, UWA-B40B and UWA-B40C (Table 8, Figs 9 and 11). Three discordant analyses are excluded from age considerations. The remaining eight analysis give a weighted mean  $^{207}\text{Pb}/^{206}\text{Pb}$  age of  $1871 \pm 14$  Ma (MSWD = 3.0). Omitting one  $3\sigma$  outlier (spot mC.1-3) changes this to  $1875 \pm 7$  Ma (MSWD = 1.10, n = 7).

Xenotime results include a total of 12 spots from ten grains from sample UWA-B40A (Table 6, Figs 10 and 11). Four discordant analyses (spots xA.10-3, xA.11-2, xA.12-1 and xA.8-1) are excluded from age considerations, although their  $^{207}\text{Pb}/^{206}\text{Pb}$  are generally consistent with the main data. The remaining eight analyses give a weighted

mean age of  $1867 \pm 12$  Ma (MSWD = 1.8). Omitting one  $2\sigma$  outlier (spot xA.5-1) changes this to  $1869 \pm 11$  Ma (MSWD 1.30, n = 7).

The  $^{207}\text{Pb}/^{206}\text{Pb}$  results from monazites and xenotime are statistically indistinguishable. The sharp contact between some monazite and xenotime grains (Fig. 10d), suggests that these phosphates crystallized simultaneously, and allows the results to be treated as a single data set. Combining all the monazite and xenotime analysis that are within 95% of concordance gives a  $^{207}\text{Pb}/^{206}\text{Pb}$  age of  $1869 \pm 8$  Ma, with a MSWD of 2.3 (n = 16). Omitting the outliers identified above results in a  $^{207}\text{Pb}/^{206}\text{Pb}$  age of  $1872 \pm 7$  Ma (MSWD = 1.2, n = 14; Fig. 11). This is the preferred  $^{207}\text{Pb}/^{206}\text{Pb}$  age for the late- to post-mineralisation veins.

---

## Discussion

### *Evolution of the Breves Cu-Au-(W-Bi-Sn) mineralisation*

The SHRIMP II results reported in this work are summarized in Table 9. The zircons extracted from the episyenite and granite, together with the *in situ* dating of monazite and xenotime, from veins that crosscut both the intrusive rocks and the ore-bearing greisen, provide good age constraints for the Breves Cu-Au-(W-Bi-Sn) mineralisation. The clustering of the  $^{207}\text{Pb}/^{206}\text{Pb}$  ages, within analytical errors, are consistent with a genetic model in which ore-forming processes that operated at Breves result from emplacement of a sequence of granite intrusions and associated hydrothermal alteration (Table 9).

As the  $^{207}\text{Pb}/^{206}\text{Pb}$  age of the episyenite ( $1880 \pm 9$  Ma) and the granite ( $1878 \pm 8$  Ma) are indistinguishable, and there is no field evidence to support different magmatic events, the data were pooled and the resulting  $^{207}\text{Pb}/^{206}\text{Pb}$  age of  $1879 \pm 6$  (MSWD = 1.2, n = 33) is taken to be the age of magma crystallization. The progressive cooling of the granite intrusion is interpreted to have produced a fluid/vapor-rich carapace during the latest stages of magma crystallization, resulting in the formation of a series of hydrothermal alteration zones in the roof zone of the stock. Intense hydrothermal alteration resulted in the removal of quartz and plagioclase, with concomitant K-feldspar enrichment. Field evidence suggests that episyenitization represents the early stages of hydrothermal alteration in the formation of the deposit, but it must be noted that there is no significant metal deposition related to this style of hydrothermal alteration. Subsequently, a series of hydrothermal reactions culminated in the deposition of economic concentration of Cu and Au, together with W, Bi and Sn. Both pre-ore and ore-associated alteration was governed mainly by hydrolysis reactions, in progressively acid conditions, causing the break-down of primary

feldspars according to the following reactions: (1) episyenitization:  $(\text{Na}, \text{Ca})\text{AlSi}_3\text{O}_8 + \text{K}^+ = \text{KAlSi}_3\text{O}_8 + \text{Ca}^+ + \text{Na}^+$ , and (2) greisen-type alteration:  $6 \text{KAlSi}_3\text{O}_8 + 4 \text{H}^+ = \text{K}_2\text{Al}_4(\text{Al}_2\text{Si}_6)\text{O}_{20}(\text{OH})_4 + 12 \text{SiO}_2 + 4 \text{K}^+ + 2 \text{O}_2$  (*cf.* Rose and Burt 1979, Bean and Titley 1981). K-feldspar formed during early episyenitization (1) was subsequently destroyed during greisen-type alteration (2). The latest stages of hydrothermal activity involved the development of a fracture controlled stockwork-type vein system that crosscuts both the ore-bearing greisen and the underlying altered granite. The *in situ* dating of monazite and xenotime, from these late- to post-mineralisation veins, indicates an age of  $1872 \pm 7 \text{ Ma}$ . The pooled age of  $1879 \pm 6 \text{ Ma}$  for the magmatic zircons, overlaps with that of the hydrothermal phosphates from the cross-cutting veins placing close constraints on the age of the main mineralization.

#### *Implications for regional metallogenesis*

The SHRIMP II U-Pb in zircon, monazite and xenotime data from the Breves granites and veins that cut the greisenised granites firmly places the age of Cu-Au-(W-Bi-Sn) mineralisation at ca. 1.88-1.87 Ga, the major period of emplacement of the A-type Paleoproterozoic granites in the Carajás Belt, and in the Amazonian Craton generally.

Elsewhere in the A-type granite province in the Amazonian Craton, major mineralisation is related to tin-specialized granites (e.g. Dall'Agnol et al. 1993). This cassiterite and/or fluorite mineralisation is associated with diagnostic post-magmatic alteration that includes: (a) fluorite-topaz replacement of plagioclase, (b) plagioclase-destructive alteration, producing the assemblage albite-muscovite-fluorite-topaz, (c) albitization or muscovite replacement of primary K-feldspar, (d) breakdown of biotite to muscovite, chlorite and ilmenite, and (e) the stability of siderophyllite (Dall'Agnol et al. 1993). In several ways, the Breves mineralisation is associated with similar alteration, resulting from the breakdown of magmatic feldspars, but the Breves system appears less F-rich, as fluorite is not as abundant and topaz is absent. It is possible that the different metal associations at Breves (Cu-Au-dominant) relative to the majority of Amazonian deposits related to A-type granites (Sn-F dominant) is due to the fact that the host granites at Breves intrude mafic volcanic and sedimentary rocks, which are more likely to contain elevated concentrations of Cu and Au, than the granitic and acid volcanic rocks which host the Sn-F deposits. Alternatively, the differences could be due to the different proportions of Cl and F in the granitic melts, as this can affect the ratios of metals transported via Cl-complexes (e.g. Webster and Hollaway, 1990). These alternatives need to be resolved by detailed geochemical studies of host rocks and fluid inclusion studies, which are beyond the scope of this study. It is noticeable, however, that other deposits which show least a spatial relationship to 1.88 Ga granites

in the Carajás Belt, for example, Águas Claras and Gameleira, are also Cu and Au bearing systems, with anomalous, but not economic, W and Sn concentrations (Soares et al. 1994; Silva and Villas 1998; Soares and Villas 1998).

The Paleoproterozoic Breves deposit shares some geochemical similarities with the intrusion-related gold deposits, particularly those that occur in the much younger Tintina Belt of Alaska-Yukon (Thompson et al. 1999; Lang et al. 2000), in that it is enriched in Au, Bi, W, As and Sn. However, the Cu enrichment is anomalous, perhaps due to different host rocks, a mafic volcanic sequence and overlying clastic sedimentary rocks at Breves compared to a dominantly shelf sequence, with abundant carbonate- and shale-rich sedimentary rocks in the Tintina Belt.

A major question to be resolved in the Carajás Belt is the relationship between the relatively small (< 50 Mt) Cu-Au-(W-Bi-Sn) deposits such as Breves and the world-class (>200 Mt) Fe-oxide Cu-Au-(U-REE) deposits, such as Cristalino, Igarapé Bahia-Alemão, Salobo and Sossego. One possibility is that they are both related to the ca. 1.88 Ga A-type granites, but a number of the features of the Fe-oxide Cu-Au-(U-REE) deposits suggest that this is unlikely because these features are extremely rare or non-existent in the Cu-Au-(W-Bi-Sn) deposits. These include: (a) the abundance of iron-oxides, (b) the quartz-deficient nature of the ore systems, (c) the extreme REE enrichment, (d) the S-deficient nature of ore sulfides, and (e) the extent of carbonate alteration, at least in the lower temperature deposits.

Irrespective of these uncertainties, the recognition that the Breves deposit is approximately the same age as the A-type granites that intrude the Carajás volcano-sedimentary succession has exploration implications. The better, less-eroded, deposits are likely to be sited in the roof zones above cupolas, plugs or swarms of apophyses of these 1.88 Ga A-type granites. These buried cupolas may be located via a combination of (a) gravity surveys to locate density contrasts, (b) induced polarization surveys to locate disseminated sulfides, and (3) fracture analysis from air photography or satellite images to locate ring and/or radial fractures related to the intrusions. In addition, the element association of Cu, Au, Bi, As, W and Sn is very distinctive, with some elements being dispersed into the weathering profile (e.g. Au, As, Cu, Bi) whereas Sn, and to a lesser extent W and Au, may be concentrated in stream samples. The combination of anomalous concentrations of one or more of the rare metals W, Bi, As, and Sn, coupled with significant Cu and Au anomalies, can provide fairly confident geochemical criteria for target selection. For example, according to Costa et al. (1999), the latosols, gossans and colluvium above the Águas Claras deposit had a diagnostic geochemical association of Au, As, B, Cu, Sn and W, that preserved the signature of the underlying primary ore.

---

### Acknowledgments

The authors wish to thank the Companhia Vale do Rio Doce (CVRD) for access to the area, support during field-work, and for access to their electron microprobe laboratory. Ms. Marion Marshall, from the Department of Geology and Geophysics at UWA, is thanked for technical assistance with SHRIMP II preparation. The authors are thankful to Professor Brendan J. Griffin and Ms. Sharon Platten, from the Centre for Microscopy and Microanalysis of UWA, for assistance during SEM work. We acknowledge Dr. Maurício Carneiro, from the Department of Geology at the Universidade Federal de Ouro Preto, for assistance during sample preparation. U-Pb analyses were performed at the Western Australian SHRIMP facilities operated by a university-government consortium with ARC support. We are indebted to the Fundação de Amparo à Pesquisa do Estado de São Paulo (FAPESP) for grants #98/14401-5 and #99/03058-0 which aided the research.

---

### References

- Almada MCO (1998) O Corpo Acampamento Sul do depósito Bahia, Carajás: características geológicas e fluidos hidrotermais. Masters thesis, Universidade Federal do Pará, 99 pp
- Araújo OJB, Maia RGN (1991) Serra dos Carajás, folha SB.22-Z-A, Estado do Pará. Brasília, Programa Levantamentos Geológicos Básicos do Brasil, DNPM, 136 pp
- Avelar VG, Lafon JM, Correia FC Jr, Macambira BEM (1999) O magmatismo arqueano da região de Tucumã, Província Mineral de Carajás, Amazônia Oriental, Brasil: novos dados geocronológicos. Rev Bras Geociênc 29:453-460
- Barros CEM, Barbey P (1998) A importância da granitogênese tardi-arqueana (2.5Ga) na evolução tectono-metamórfica da Província Mineral de Carajás – O Complexo Granítico Estrela e sua auréola de contato. Rev Bras Geociênc 28(4): 513-522
- Barros CEM, Dall'Agnoll R, Lafon JM, Teixeira NP, Ribeiro JW (1992). Geologia e geocronologia Rb-Sr do Gnaissé Estrela, Curionópolis, PA. Bol Museu Paraense Emílio Goeldi, Ciências da Terra, 4:83-104
- Barros CEM, Macambira MJB, Barbey P (2001) Idade de zircão do Complexo Granítico Estrela: relações entre magmatismo, deformação e metamorfismo na Província Mineral de Carajás. VII Simpósio de Geologia da Amazônia, Anais, pp 17-20

- Beane RE, Titley SR (1981) Porphyry copper deposits Part II. Hydrothermal alteration and mineralization. *Econ Geol*, 75<sup>th</sup> Anniversary volume: 235-269
- Compston W, Williams IS, Campbell IH, Gresham JJ (1986) Zircon xenocrysts from the Kambalda volcanics: age constraints and direct evidence for the older continental crust below the Kambalda-Norseman greenstones. *Earth Planet Sci Lett* 76: 299-311
- Cordeiro AAC (1999) Pesquisa mineral: panorama atual da CVRD na Amazônia. VI Simpósio de Geologia da Amazônia, Anais, pp 80-83
- Costa ML, Angélica RS, Costa NC (1999) The geochemical association Au-As-B-(Cu)-Sn-W in latosol, colluvium, laterite iron crust and gossan in Carajás, Brazil: importance for primary ore identification. *J Geochem Expl* 67: 33-49
- Dall'Agnol R, Teixeira NP, Magalhães MS (1993) Diagnostic features of the tin-specialized anorogenic granites of the Eastern Amazonian Region. *Anais da Academia Brasileira de Ciência* 65: 33-50
- Dall'Agnol R, Lafon JM, Macambira MJB (1994) Proterozoic anorogenic magmatism in the Central Amazonian Province, Amazonian Craton: geochronological, petrological and geochemical aspects. *Min Petrol* 50: 113-138
- Dias GS, Macambira MJB, Dall'Agnol R, Soares ADV, Barros CEM (1996) Datação de zircões de Sill de metagabro: comprovação da idade arqueana da Formação Águas Claras, Carajás, Pará. V Simpósio de Geologia da Amazônia, Anais, pp 376-379
- DOCEGEO - Rio Doce Geologia e Mineração S.A. (1988) Província Mineral de Carajás. Litoestratigrafia e principais depósitos minerais. In: SBG, Congresso Brasileiro de Geologia, 35, Belém, Anexo aos Anais, 165 pp
- Fletcher IR, Rasmussen B, McNaughton NJ (2000) High-precision SHRIMP U-Pb geochronology of authigenic xenotime. *Aust J Earth Sci* 47:845-859
- Farias NR, Saueressig R (1982) Jazida de cobre Salobo 3A. Simpósio de Geologia da Amazônia, I. 1982. Belém, Anais, pp 61-73
- Ferreira Filho CF (1985) Geologia e mineralizações sulfetadas do Prospecto Bahia, Província Mineral de Carajás. Brasília, Universidade de Brasília, Masters Thesis, 112 pp
- Figueiredo BR, Réquia KCM, Xavier RP (1994) Post-depositional changes in the Salobo ore deposit, Carajás Mineral Province, northern Brazil. *Comunicaciones* 45:23-32

- Foster G, Kinny P, Vance D, Prince C, Harris N (2000) The significance of monazite U-Th-Pb age data in metamorphic assemblages; a combined study of monazite and garnet chronometry. *Earth Planet Sci Lett* 181: 327-340
- Gonçalez AK, Dall'Agnol R, Vieira EAP, Macambira MJB, Della Senta N (1988) Geologia do maciço Cigano, Vale do Parauapebas (PA). In: Cong Bras Geol 35, Proceedings, SBG, vol 3, 1132-1146
- Holdsworth RE, Pinheiro RVL (2000) The anatomy of shallow-crustal transpressional structures: insights from the Archean Carajás fault zone, Amazon, Brazil. *J Struct Geol* 22:1105-1123
- Huhn SRB, Santos ABS, Amaral AF, Ledsham EJ, Gouvea JL, Martins LP, Montalvão RGM, Costa VG (1988) O terreno “granito greenstone” da região de Rio Maria - Sul do Pará. XXXV Cong Bras Geol, Anais, 3: pp 1438-1452
- Huhn SRB, Macambira MJB, Dall'Agnol R (1999a) Geologia e geocronologia Pb/Pb do granito alcalino Arqueano Planalto, Região da Serra do Rabo, Carajás - PA. In: SBG, Simpósio de Geologia da Amazônia, 6, Manaus, Resumos Expandidos, pp 463-466
- Huhn SRB, Souza CIJ, Albuquerque MC, Leal ED, Brustolin V (1999b) Descoberta do depósito Cu(Au) Cristalino: geologia e mineralização associada – Região da Serra do Rabo – Carajás – PA. VI Simpósio de Geologia da Amazônia, Anais, pp 140-143
- Issler RS, Lima MIC (1987) Amazonic Craton (Brazil) granitogenesis and its relation to geotectonic units. *Rev Bras Geociênc* 17(4): 426-441
- Jaffey AH, Flynn KF, Glendenin LE, Bentley WC, Essling AM (1971) Precision measurement of half lives and specific activities of  $^{235}\text{U}$  and  $^{238}\text{U}$ . *Physics Reviews C4*: 1889
- Lancaster Oliveira J, Fanton J, Almeida AJ, Leveille RA, Vieira S (2000) Discovery and geology of the Sossego copper-gold deposit, Carajás District, Pará State, Brazil. 31 International Geological Congress, Abstracts, Rio de Janeiro.
- Lang JR, Baker T, Hart CJR, Mortensen JK (2000) An exploration model for intrusion-related gold systems. *SEG Newsletter* 40: 1, 6-15
- Lindenmayer ZG (1990). Salobo Sequence, Carajás, Brazil: Geology, Geochemistry and Metamorphism. University of Western Ontario, Ph.D. Thesis, 407 pp

- Lindenmayer Z.G., Ronchi, L.H., Laux, J.H. (1998) Geologia e geoquímica da mineralização de Cu-Au primária da mina de Au do Igarapé Bahia, Serra dos Carajás. Rev Bras Geociênc 28(3): 257-268
- Ludwig KR (2001a) SQUID 1.00 – a User's manual. Barkeley Geochronology Centre, Spec Publ 2
- Ludwig KR (2001b) User manual for Isoplot/Ex rev. 2.49 – a geochronological toolkit for Microsoft Excel. Barkeley Geochronology Centre, Spec Publ 1a
- Macambira MJB, Lancelot J (1996) Time contraints of the Archean Rio Maria crust, Southeastern Amazonian Craton, Brazil. Int Geol Rev 38:1134-1142
- Machado N, Lindenmayer ZG, Krogh TE, Lindenmayer D (1991) U-Pb geochronology of Archean magmatism and basement reactivation in the Carajás area, Amazon Shield, Brazil. Precamb Res 49:329-354
- Melcher F, Prochaska W, Raith JG, Saini-Eidukat B (1996) The metamorphosed molybdenum vein-type deposit of the Alpeinerscharte, Tyrol (Austria) and its relation to Variscan granitoids. Mineral Deposita 31: 277-289
- Mellito KM, Tassinari CCG (1998) Aplicação do método Rb-Sr e Pb-Pb à evolução da mineralização cuprifera do depósito de Salobo 3α, Província Mineral de Carajás, Pará. In: Cong Bras Geol 40, Proceedings, Belo Horizonte, SBG, p 119
- Nelson DR (1997). Compilation of SHRIMP U-Pb zircon geochronology data, 1996. Geological Survey of Western Australia, Record 1997/2.
- Nogueira ACR, Truckenbrod W, Costa JBS, Pinheiro RVL (1994) Análise faciológica e estrutural da Formação Águas Claras, Pré-Cambriano da Serra dos Carajás. In: 4 Simpósio de Geologia da Amazônia, Belém, Resumos Expandidos, SBG, pp 363-364
- Nogueira ACR, Truckenbrod W, Pinheiro RVL (2000) Storm and tide-dominated siliciclastic deposits of the Archean Águas Claras Formation, Serra dos Carajás, Brazil. In: 31 International Geological Congress, Rio de Janeiro, Abstracts
- Nunes AR, Rego JL, Meireles HP, Carvalho JB, Lima da Silva PE, Siqueira JB, Ferreira FJF (2001) A descoberta do depósito Breves na Província Mineral de Carajás. Simpósio de Geologia da Amazônia, Abstracts
- Pidgeon RT, Furfaro D, Kennedy AK, Nemchin AA (1994) Calibration of zircon standards for the Curtin SHRIMP II. Abstracts of the 8<sup>th</sup> International Conference on Geochronology, Cosmochemistry and Isotope Geology, Berkeley, USA. U.S. Geological Survey, Circular 1107, pp 251

UNICAMP  
BIBLIOTECA CENTRAL  
SEÇÃO CIRCULANTE

- Pidgeon RT, Macambira MJB, Lafon JM (2000) Th-U-Pb isotopic systems and internal structures of complex zircons from enderbite from the Pium Complex, Carajás Province, Brazil: evidence for ages of granulite facies metamorphism and protolith of the enderbite. *Chem Geol* 166: 157-171
- Pimentel MM, Machado N (1994) Geocronologia U-Pb dos terrenos granito-greenstone de Rio Maria, Pará. In: *Cong Bras Geol* 38, Proceedings, SBG, Camburiu, vol 2, pp 390-391
- Pinheiro RVL, Holdsworth RE (1997) Reactivation of Archean strike-slip fault systems, Amazon region, Brazil. *J Geol Soc* 154: 99-103
- Rasmussen B, Fletcher IR, McNaughton NJ (2001) Dating low-grade metamorphic events by SHRIMP U-Pb analysis of monazite in shales. *Geology* 29(10): 963-966
- Recio C, Fallick AE, Ugidos JM, Stephens WE (1997) Characterization of multiple fluid-granite interaction processes in the episyenites of Avila-Béjar, Central Iberian Massif, Spain. *Chem Geol* 143:127-144
- Réquia KCM, Xavier RP (1995) Fases fluidas na evolução metamórfica do depósito polimetálico de Salobo, Província Mineral de Carajás, Pará. *Rev Escola de Minas* 49(2):117-122
- Ribeiro AMR (1989) Estudo geoquímico do sistema hidrotermal relacionado a mineralização cuprífera da área Bahia, Serra dos Carajás. Unpublished Masters Thesis, Universidade Federal do Pará, 134 pp
- Rigon JC, Munaro P, Santos LA, Nascimento JAS, Barreira CF (2000) The Alvo 118 copper-gold deposit: geology and mineralization, Serra dos Carajás, Pará. 31 International Geological Congress, Abstracts.
- Rodrigues ES, Lafon JM, Scheller T (1992) Geocronologia Pb-Pb da Província Mineral de Carajás: primeiros resultados. *Cong Bras Geol* 37, Bull Extended Abstr, SBG, São Paulo, vol 2, pp 183-184
- Rose AW, Burt DM (1979) Hydrothermal alteration. In: Barnes, H.L. (ed), *Geochemistry of Hydrothermal Ore Deposits*, Second Edition, pp 173-235
- Santos JOS, Groves DI, Hartmann LA, Moura MA, McNaughton NJ (2001) Gold deposits of the Tapajós and Alta Floresta Domains, Tapajós-Parima orogenic belt, Amazon Craton, Brazil. *Mineralium Deposita* 36(3/4): 278-299
- Silva CMG, Villas RN (1998) The Águas Claras Cu-sulfide ± Au Deposit, Carajás region, Pará, Brazil: geological setting, wall-rock alteration and mineralizing fluids. *Rev Bras Geociênc* 28(3): 315-326
- Soares AV, Santos AB, Vieira EA, Bella VM, Martins LPB (1994) Área Águas Claras: contexto geológico e mineralizações. In: 4 Simpósio de Geologia da Amazônia, Belém, Resumos Expandidos, SBG, pp 379-382

- Smith JB, Barley ME, Groves DI, Krapez B, McNaughton NJ, Bickle MJ, Chapman HJ (1998) The Scholl Shear zone, West Pilbara: evidence for a domain boundary structure from integrated tectonostratigraphic analyses, SHRIMP U-Pb dating and isotopic and geochemical data of granitoids. *Precamb Res* 88:143-171
- Souza SRB, Macambira MJB, Scheller T (1996) Novos dados geocronológicos para os granitos deformados do Rio Itacaúnas (Serra dos Carajás, PA); implicações estratigráficas: V Simpósio de Geologia da Amazônia, Belém, 1996, SBG, pp 380-382
- Tallarico FHB, Oliveira CG, Figueiredo BR (2000) The Igarapé Bahia Cu-Au mineralization, Carajás Province. *Rev Bras Geoc* 30:230-233.
- Tassinari CCG, Macambira MJB (1999) Geochronological provinces of the Amazonian Craton. *Episodes* 22(3): 174-182
- Tazava E (1999) Mineralização de Au-Cu-(±ETR-U) associada às brechas hidrotermais do depósito de Igarapé Bahia, Província Mineral de Carajás, PA. Unpublished Masters Thesis. Universidade Federal de Ouro Preto, 81 pp
- Thompson JFH, Sillitoe RH, Baker T (1999) Intrusion-related gold deposits associated with tungsten-tin provinces. *Mineralium Deposita* 34: 323-334
- Trendall AF, Basei MAS, Laeter JR, Nelson DR (1998) SHRIMP zircon U-Pb constraints on the age of the Carajás formation, Grão Pará Group, Amazon Craton. *J S Am Earth Sci* 11(3): 265-277
- Tolbert GE, Tremaine JW, Melcher GC, Gomes CB (1971) The recently discovered Serra dos Carajás iron deposit, northern Brazil. *Econ Geol* 66: 985-994
- Vieira EAP, Saueressig R, Siqueira JB, Silva ERP, Rego JL, Castro FDC (1988) Caracterização geológica da jazida polimetálica do Salobo 3A – reavaliação. 35 Congresso Brasileiro de Geologia, Anexo aos Anais, 165 pp
- Villas RN, Santos MD (2001) Gold deposits of the Carajás mineral province: deposit types and metallogenesis. *Mineralium Deposita* 36:300-331
- Webster JD, Holloway JR (1990) Partitioning of F and Cl between magmatic hydrothermal fluids and highly evolved granitic magmas. In: Ore-bearing granite systems; petrogenesis and mineralizing processes. Stein, H.J. and Hannah, J.L. (eds). *Geol Soc Am, Spec Pap* 246, pp 21-34

Williams IS, Claesson S (1987) Isotopic evidence for the Precambrian provenance and Caledonian metamorphism of high grade paragneisses from the Steve Nappes, Scandinavian Caledonides, II. Ion microprobe zircon U-Th-Pb. *Cont Min Petrol* 97: 205-217

Wirth KR, Gibbs AK, Olszewski WJ Jr (1986). U-Pb ages of zircons from the Grão Pará and Serra dos Carajás granite, Pará, Brazil. *Rev Bras Geociênc* 16:195-200

**Table 1** Stratigraphic column and summary of geochronological data from the Carajás Copper-Gold Belt (modified from Docegeo 1988 and Villas and Santos 2001)

Eras	Complexes or supergroups	Groups or formations	Intrusive rocks	Age (Ma)	Methods, Material (Reference)
Proterozoic			Central Carajás granite	1,820 ± 49	U-Pb, zircon (1)
			Cigano granite	1,880 ± 2	U-Pb, zircon (2)
			1,883 ± 3	U-Pb, zircon (2)	
			1,731 ± 28	Rb-Sr, whole rock (3)	
			Pojuca granite	1,874 ± 2	U-Pb, zircon (2)
Archean		Santa Inês gabbro (?)	Santa Inês gabbro (?)	-	-
			Old Salobo granite	2,573 ± 2	U-Pb, zircon (2)
			Itacaiúnas granite	2,560 ± 37	Pb-Pb, zircon (4)
			Águas Claras gabbroic sill	2,645 ± 12	Pb-Pb, zircon (9)
			Aguas Claras Formation	2,681 ± 5	U-Pb SHRIMP, detrital zircon (10)
		Itacaiúnas Supergroup	Estrela granite	2,527 ± 34	Rb-Sr, whole rock (5)
			2,763 ± 7	Pb-Pb, zircon (17)	
			Plaquê granitoid suite	2,736 ± 24	Pb-Pb, zircon (7)
			Planalto granite	2,747 ± 2	Pb-Pb, zircon (8)
			Cristalino diorite	2,738 ± 6	Pb-Pb, zircon (8)
Itacaiúnas Supergroup		Buritirama Group	Buritirama Group	-	-
			Igarapé Pojuca Group	2,732 ± 3	U-Pb, zircon (2)
			Igarapé Bahia Group	2,577 ± 72	Rb-Sr, whole rock (11)
			2,747 ± 2	Pb-Pb, zircon (6)	
			Grão Pará Group	2,759 ± 2	U-Pb, zircon (2)
		Igarapé Salobo Group	2,758 ± 39	U-Pb, zircon (1)	
			2,760 ± 11	U-Pb SHRIMP, zircon (10)	
			2,761 ± 3	U-Pb, zircon (2)	
			2,776 ± 240	Pb-Pb, magnetite (12)	
			Luanga mafic-ultramafic intrusion	2,763 ± 6	U-Pb, zircon (2)
Xingu Complex		Rio Novo Group (?)	Rio Novo Group (?)	-	-
			Xingu Complex	2,859 ± 2	U-Pb, zircon (2)
			2,974 ± 15	Pb-Pb, zircon (7)	
			2,971 ± 30	U-Pb, zircon (13)	
			2,798	Pb-Pb, titanite (14)	
Pium Complex			Pium Complex	3,050 ± 57	Pb-Pb, whole rock (15)
			2,859 ± 9	U-Pb SHRIMP, zircon rim (16)	
			3,002 ± 14	U-Pb SHRIMP, zircon core (16)	

1 Wirth et al. (1986); 2 Machado et al. (1991); 3 Gonçalez et al (1988); 4 Souza et al. (1996); 5 Barros et al. (1992); 6 personal communications cited in Villas and Santos (2001); 7 Avelar et al. (1999); 8 Huhn et al. (1999b); 9 Dias et al. (1996); 10 Trendall et al. (1998); 11 Ferreira Filho (1985); 12 Mellito and Tassinari (1998); 13 Macambira and Lancelot (1996); 14 Pimentel and Machado (1994); 15 Rodrigues et al. (1992); 16 Pidgeon et al. (2000); 17 Barros et al. (2001)

**Table 2** Summary of the grade-tonnage data, hydrothermal alteration and gangue and ore mineralogy of selected copper-gold deposits of the Carajás Belt

Deposit	Salobo	Igarapé Bahia	Águas Claras	Breves
Type	Fe-oxide Cu-Au-(U-ETR)	Fe-oxide Cu-Au-(U-ETR)	Cu-Au-(W-Bi-Sn)	Cu-Au-(W-Bi-Sn)
Tonnage	994 Mt	219 Mt	9.5 Mt	50 Mt
Grades	0.94% Cu, 0.52 g/t Au	1.4% Cu, 0.86 g/t Au	2.43 g/t Au	1.22% Cu, 0.75 g/t Au, 2.4 g/t Ag, 1200 g/t W, 70 g/t Sn, 175 g/t Mo, 75 g/t Bi
Orebody morphology and texture	Fault-controlled, steeply-dipping tabular and massive body	Fault-controlled, steeply-dipping, circular-shaped cluster of breccias	Fault-controlled, steeply-dipping, tabular breccia body	Ore-shell in the roof zone of a highly altered granite intrusion
Host rocks	High-grade metavolcano-sedimentary rocks (Igarapé Salobo Group)	Low-grade metavolcano-sedimentary rocks (Igarapé Bahia Group)	Sandstone and siltstone (Águas Claras Formation)	Sandstone and siltstone (Águas Claras Formation)
Hydrothermal alteration	Chloritization and K-Fe-metassomatism	Chloritization, carbonate alteration, K-Fe-metassomatism	Abundant silicification and quartz veins, chloritization, sericitization, tourmalinization, kaolinization	Greisen (quartz + muscovite ± chlorite), abundant quartz veins
Cu-Fe-sulfides (other sulfides)	Chalcopyrite + bornite ± chalcocite	Chalcopyrite ± bornite	Chalcopyrite + pyrite ± pyrrhotite (galena, sphalerite, tennantite)	Chalcopyrite + pyrite ± pyrrhotite
Au-Ag	Native gold	Native gold with ~12% Ag, hessite, muthmannite	Native gold (~25% Ag)	Native gold (~24% Ag)
W-Bi-Sn	-	-	Wolframite, ferberite, cassiterite, bismuthinite, stannite	Ferberite, bismuthinite, native bismuth, cassiterite
Fe-oxides and silicates	Grunerite, fayalite, magnetite	Grunerite, magnetite	Rare magnetite and hematite	-
U-Th	Uraninite	Uraninite, uranofane, thorite, thorianite	-	-
F-Cl	Fluorite	Fluorite, escapolite, ferripirosmalite	-	Rare fluorite
ETR-P	Allanite, apatite	Allanite, parisite, bastnasite, monazite, apatite	Apatite	Monazite, xenotime
Mo	Molybdenite	Molybdenite	-	-
As-Co	Co-pentlandite, cobaltite, saflorite	Cobaltite	Arsenopyrite	Arsenopyrite (with 12% Co)
Gangue	Biotite, almandine, chlorite, greenalite	Siderite, biotite, chlorite, stilpnomelane, tourmaline	Dominant quartz, chlorite, tourmaline, sericite, kaolin	Dominant quartz, chlorite, tourmaline, sericite
References	Lindenmayer (1990); Figueiredo et al. (1994); Réquia and Xavier (1995)	Ferreira Filho (1985); Almada (1998); Tazava (1999); Tallarico (2000)	Soares et al. (1994); Silva and Villas (1998)	This work

**Table 3** Representative wavelength dispersive spectrometry microanalysis of gold, Nb-rutile, arsenopyrite and ferberite from the Breves deposit

	1	2	3	4	5	FeO <sub>t</sub> *	6	7	8	9
Fe	1.25	1.51	1.38	22.71	27.24	FeO <sub>t</sub> *	2.77	2.54	18.44	16.86
Cu	1.01	1.21	2.15	0.01	0.54	MnO	-	-	4.46	5.73
Ni	-	-	-	0.11	0.05	TiO <sub>2</sub>	94.02	94.59	-	-
Co	-	-	-	12.08	6.36	Nb <sub>2</sub> O <sub>5</sub>	2.26	2.04	-	-
As	-	-	-	46.14	48.06	Ta <sub>2</sub> O <sub>5</sub>	0.18	0.21	0.00	0.00
S	0.73	0.76	0.65	18.95	18.14	CaO	-	-	0.05	0.05
Te	0.03	0.10	0.01	-	-	WO <sub>3</sub>	-	-	76.83	76.69
Ag	24.62	22.63	22.39	-	-	SnO <sub>2</sub>	-	-	0.04	0.00
Au	73.38	73.73	71.33	-	-					
Total	101.03	99.94	97.92	99.98	100.39	Total	99.23	99.38	99.83	99.34

1 to 3: gold (sample FR61/182,00m); 4 and 5: arsenopyrite (sample FR61/260.00m); 6 and 7: Nb-rutile (sample FR61/260.00m); 8 and 9: ferberite (samples FR61/191.90m and FR61/272,68m, respectively). Data were acquired at the CVRD research laboratory using a JEOL JCXA-733 microprobe at 25 kV and 50 nA using natural standards. The PROZA correction was applied for matrix effect. \* Total Fe expressed as FeO.

**Table 4** Samples from the Breves Cu-Au-(W-Bi-Sn) mineralisation selected for SHRIMP II analysis

SHRIMP Mount (#)*	Sample Type (Code)	Field Reference	Rock Type	Mineral
				Analysed
UWA-B09A (1)	Bulk sample (OPU-1274)	FR61/323.00-325.00m	Granite	Zircon
UWA-B09B (2)	Bulk sample (OPU-1275)	FR73/312.00-314.00m	Greisen	Zircon
UWA-B30A (3)	Bulk sample (OPU-1277)	FR73/351.00-353.00m	Episyenite	Zircon
UWA-B30B (4)	Bulk sample (OPU-1278)	FR61/181.00-183.00m	Greisen	Zircon
UWA-B40A (5)	Thin section	FR73/174.00m (#2)	Vein crosscutting the greisen	Monazite and xenotime
UWA-B40B (5)	Thin section	FR73/174.00m (#1)	Vein crosscutting the greisen	Monazite
UWA-B40C (6)	Thin section	FR61/201.35m (#1)	Vein crosscutting the greisen	Monazite

\* Numbers between brackets refer to the location of the sample in the vertical section L800 (Fig. 2).

**Table 5.**  $^{204}\text{Pb}$ -corrected SHRIMP II isotopic data for zircons from the Breves Granite, sample UWA-B09A.

grain-spot	U (ppm)	Th (ppm)	4f206 (%)	$^{207}\text{Pb}/^{206}\text{Pb}$	$^{206}\text{Pb}/^{238}\text{U}$	$^{207}\text{Pb}/^{235}\text{U}$	$^{208}\text{Pb}/^{232}\text{Th}$	conc. (%)	$^{207}\text{Pb}/^{206}\text{Pb}$	Age (Ma)
1-1	204	85	0.100	0.1130 ± 11	0.3186 ± 81	4.964 ± 136	0.0931 ± 32	96	1848 ± 18	
2-1	124	43	-0.258	0.1178 ± 17	0.3405 ± 73	5.531 ± 142	0.1031 ± 39	98	1923 ± 25	
4-1	125	56	0.000	0.1139 ± 14	0.3434 ± 75	5.392 ± 135	0.0968 ± 27	102	1862 ± 22	
5-1	99	31	0.000	0.1157 ± 15	0.3372 ± 86	5.378 ± 154	0.0992 ± 34	99	1890 ± 23	
7-1	106	35	0.249	0.1130 ± 17	0.3226 ± 73	5.028 ± 135	0.0853 ± 33	97	1849 ± 27	
9-1	497	255	0.035	0.1161 ± 7	0.3407 ± 65	5.457 ± 109	0.0954 ± 20	100	1898 ± 11	
10-1	589	313	0.000	0.1158 ± 6	0.3383 ± 64	5.403 ± 106	0.0959 ± 19	99	1893 ± 9	
11-1	230	130	0.000	0.1145 ± 10	0.3351 ± 67	5.291 ± 115	0.0860 ± 20	100	1872 ± 15	
12-1	200	69	0.026	0.1133 ± 13	0.3374 ± 69	5.272 ± 124	0.0965 ± 26	101	1853 ± 21	
15-1	663	170	0.039	0.1146 ± 7	0.3256 ± 64	5.143 ± 106	0.0920 ± 26	97	1873 ± 11	
17-1	126	40	0.230	0.1146 ± 14	0.3308 ± 71	5.225 ± 130	0.0930 ± 31	98	1873 ± 23	
17-2	108	33	-0.027	0.1153 ± 20	0.3428 ± 97	5.448 ± 181	0.0973 ± 35	101	1884 ± 31	
18-1	116	48	0.000	0.1137 ± 13	0.3365 ± 72	5.275 ± 129	0.0967 ± 27	101	1859 ± 21	
20-1	482	216	0.077	0.1147 ± 8	0.3318 ± 86	5.245 ± 141	0.0972 ± 45	99	1875 ± 12	
20-2	557	254	0.017	0.1153 ± 6	0.3384 ± 63	5.379 ± 105	0.0961 ± 20	100	1884 ± 10	
23-1	145	62	0.224	0.1135 ± 13	0.3280 ± 68	5.131 ± 123	0.0885 ± 26	99	1856 ± 21	
24-2	139	59	-0.149	0.1131 ± 18	0.3260 ± 84	5.085 ± 154	0.0905 ± 32	98	1850 ± 29	
29-1	451	206	0.335	0.1144 ± 11	0.3464 ± 66	5.464 ± 117	0.1104 ± 31	103	1870 ± 18	
<b>Discordant</b>										
3-1	3550	6698	0.706	0.0992 ± 27	0.1984 ± 80	2.712 ± 132	0.0155 ± 15	73	1608 ± 51	
6-1	545	361	0.346	0.1142 ± 9	0.3089 ± 58	4.864 ± 99	0.0802 ± 18	93	1867 ± 14	
8-1	136	33	0.000	0.1161 ± 22	0.2992 ± 77	4.789 ± 152	0.0898 ± 40	89	1896 ± 34	
13-1	302	308	0.134	0.2032 ± 16	0.4611 ± 125	12.918 ± 365	0.0901 ± 26	86	2852 ± 13	
13-2	3548	1532	1.985	0.0802 ± 19	0.1115 ± 22	1.234 ± 37	0.0424 ± 18	57	1203 ± 46	
14-1	1071	366	0.220	0.0918 ± 7	0.1565 ± 30	1.981 ± 41	0.0387 ± 10	64	1463 ± 15	
16-1	592	194	0.903	0.1116 ± 15	0.1527 ± 31	2.351 ± 58	0.0725 ± 23	50	1826 ± 25	
19-1	756	526	0.489	0.1152 ± 13	0.1686 ± 97	2.678 ± 156	0.0395 ± 24	53	1883 ± 20	
20-3	785	400	0.490	0.1064 ± 12	0.2063 ± 38	3.026 ± 66	0.0472 ± 12	70	1738 ± 21	
21-1	682	326	0.015	0.1119 ± 6	0.2968 ± 57	4.580 ± 92	0.0856 ± 18	92	1831 ± 10	
21-2	954	217	0.161	0.1059 ± 6	0.2463 ± 45	3.597 ± 70	0.0777 ± 19	82	1730 ± 11	
22-1	774	555	0.145	0.1099 ± 12	0.2407 ± 51	3.646 ± 86	0.0536 ± 13	77	1797 ± 19	
24-1	340	228	0.113	0.1154 ± 12	0.2165 ± 58	3.446 ± 98	0.0501 ± 15	67	1887 ± 18	
25-1	856	349	0.040	0.0820 ± 6	0.1367 ± 25	1.546 ± 31	0.0427 ± 9	66	1246 ± 15	
26-1	1772	446	0.067	0.0994 ± 11	0.1855 ± 46	2.542 ± 70	0.0539 ± 35	68	1613 ± 21	
25-1	202	131	0.242	0.1135 ± 11	0.2965 ± 60	4.639 ± 104	0.0534 ± 15	90	1856 ± 18	
26-1	1012	1192	0.610	0.0999 ± 14	0.1274 ± 33	1.755 ± 52	0.0223 ± 8	48	1622 ± 27	

27-1	320	308	0.320	0.1177 ± 15	0.2018 ± 39	3.274 ± 75	0.0308 ± 9	62	1921 ± 22
28-1	588	377	0.167	0.1056 ± 26	0.2210 ± 81	3.218 ± 143	0.0602 ± 30	75	1725 ± 46
30-1	195	143	-0.012	0.1148 ± 12	0.2826 ± 57	4.473 ± 102	0.0394 ± 11	85	1877 ± 19

$4f_{206} (\%) = 100 \times \frac{^{206}\text{Pb}_{\text{common}}}{^{206}\text{Pb}_{\text{Total}}}$ , i.e., % of  $^{206}\text{Pb}$  attributed as common Pb.  
 conc. = concordance, as  $100 \times t(206/238)/t(207/206)$ . Uncertainties refer to the last digits listed.

**Table 6**  $^{204}\text{Pb}$ -corrected SHRIMP II isotopic data for zircons from the Breves Episyenite, sample UWA-B30A.

grain-spot	U (ppm)	Th (ppm)	4f206 (%)	$^{207}\text{Pb}/^{206}\text{Pb}$	$^{206}\text{Pb}/^{238}\text{U}$	$^{207}\text{Pb}/^{235}\text{U}$	$^{208}\text{Pb}/^{232}\text{Th}$	conc. (%)	$^{207}\text{Pb}/^{206}\text{Pb}$ Age (Ma)
1-1	152	59	0.072	0.1146 ± 9	0.3384 ± 58	5.349 ± 101	0.0976 ± 22	100	1874 ± 15
4-1	145	55	-0.027	0.1141 ± 8	0.3346 ± 57	5.262 ± 97	0.0969 ± 20	100	1865 ± 13
7-1	144	63	-0.016	0.1139 ± 12	0.3274 ± 56	5.141 ± 103	0.0935 ± 19	98	1862 ± 19
9-1	140	59	0.090	0.1154 ± 9	0.3380 ± 70	5.378 ± 120	0.0934 ± 23	100	1886 ± 14
8-1	135	46	-0.068	0.1158 ± 10	0.3312 ± 58	5.286 ± 103	0.0949 ± 23	97	1892 ± 16
10-1	432	239	0.017	0.1148 ± 5	0.3397 ± 53	5.378 ± 88	0.0956 ± 16	100	1877 ± 8
12-1	313	101	-0.030	0.1150 ± 6	0.3338 ± 53	5.292 ± 89	0.0967 ± 19	99	1879 ± 9
13-1	196	89	-0.058	0.1156 ± 7	0.3294 ± 86	5.250 ± 141	0.0968 ± 31	97	1889 ± 11
16-1	150	53	-0.106	0.1155 ± 9	0.3348 ± 57	5.332 ± 101	0.0996 ± 23	99	1888 ± 15
17-1	141	61	0.068	0.1152 ± 9	0.3384 ± 58	5.375 ± 101	0.0975 ± 20	100	1883 ± 14
19-1	144	58	0.082	0.1136 ± 9	0.3240 ± 55	5.074 ± 97	0.0889 ± 20	97	1857 ± 15
20-1	159	81	0.041	0.1158 ± 9	0.3312 ± 56	5.289 ± 99	0.0940 ± 20	97	1893 ± 15
22-1	58	29	-0.134	0.1189 ± 20	0.3313 ± 69	5.429 ± 145	0.0959 ± 29	95	1939 ± 30
23-1	137	52	-0.062	0.1167 ± 9	0.3279 ± 57	5.277 ± 100	0.0947 ± 20	96	1907 ± 14
Young outlier									
2-1	113	35	0.057	0.1129 ± 10	0.3283 ± 58	5.111 ± 101	0.0932 ± 22	99	1847 ± 15
Discordant									
3-1	216	181	0.130	0.1148 ± 8	0.2732 ± 45	4.324 ± 78	0.0468 ± 10	83	1876 ± 13
5-1	191	153	0.513	0.1181 ± 15	0.3122 ± 52	5.085 ± 107	0.0610 ± 22	91	1928 ± 23
6-1	205	123	0.017	0.2188 ± 9	0.4617 ± 88	13.929 ± 272	0.0982 ± 22	82	2972 ± 7
10-2	400	539	0.006	0.1161 ± 6	0.2661 ± 42	4.261 ± 70	0.0293 ± 5	80	1897 ± 9
11-1	294	261	0.029	0.1136 ± 8	0.2128 ± 37	3.334 ± 63	0.0299 ± 6	67	1858 ± 12
14-1	538	536	0.834	0.1140 ± 24	0.2695 ± 44	4.236 ± 112	0.0374 ± 19	83	1864 ± 38
15-1	1118	926	0.198	0.1018 ± 5	0.1551 ± 36	2.177 ± 52	0.0227 ± 6	56	1657 ± 9
18-1	684	361	0.040	0.1134 ± 4	0.3065 ± 47	4.794 ± 76	0.0851 ± 14	93	1855 ± 7
21-1	2307	1301	0.775	0.0842 ± 11	0.0744 ± 11	0.864 ± 17	0.0208 ± 5	36	1297 ± 25

4f206 (%) =  $100 \times \frac{\text{Pb}_{\text{common}}}{\text{Pb}_{\text{Total}}} / \frac{\text{Pb}_{\text{Total}}}{\text{Pb}_{\text{Total}}}$ , i.e., % of  $^{206}\text{Pb}$  attributed as common Pb.

conc. = concordance, as  $100 \times t(206/238)/t(207/206)$ . Uncertainties refer to the last digits listed.

**Table 7**  $^{204}\text{Pb}$ -corrected SHRIMP II isotopic data for zircons from the Breves Greisen, samples UWA-B30B and UWA-B09B.

grain-spot	U (ppm)	Th (ppm)	4f206 (%)	$^{207}\text{Pb}/^{206}\text{Pb}$	$^{206}\text{Pb}/^{238}\text{U}$	$^{207}\text{Pb}/^{235}\text{U}$	$^{208}\text{Pb}/^{232}\text{Th}$	conc. (%)	$^{207}\text{Pb}/^{206}\text{Pb}$	Age (Ma)
<b>B30B</b>										
1-1	7303	3298	0.244	0.0620 $\pm$ 24	0.0743 $\pm$ 57	0.635 $\pm$ 54	0.0228 $\pm$ 24	69	674 $\pm$ 83	
2-1	5633	2117	0.439	0.0682 $\pm$ 12	0.0749 $\pm$ 42	0.704 $\pm$ 42	0.0272 $\pm$ 19	53	874 $\pm$ 35	
3-1	9934	2345	0.058	0.0500 $\pm$ 30	0.0275 $\pm$ 16	0.190 $\pm$ 16	0.0056 $\pm$ 19	90	196 $\pm$ 141	
4-1	322	143	0.150	0.1140 $\pm$ 7	0.3174 $\pm$ 51	4.988 $\pm$ 85	0.1089 $\pm$ 20	95	1864 $\pm$ 11	
5-1	325	636	0.052	0.1986 $\pm$ 19	0.4017 $\pm$ 64	11.002 $\pm$ 202	0.0507 $\pm$ 11	77	2815 $\pm$ 15	
6-1	596	258	0.352	0.1882 $\pm$ 7	0.3171 $\pm$ 53	8.229 $\pm$ 141	0.0996 $\pm$ 20	65	2727 $\pm$ 6	
7-1	1439	2612	0.844	0.1035 $\pm$ 14	0.0532 $\pm$ 9	0.759 $\pm$ 16	0.0093 $\pm$ 2	20	1688 $\pm$ 24	
8-1	4951	1170	0.296	0.0703 $\pm$ 19	0.0505 $\pm$ 43	0.490 $\pm$ 44	0.0235 $\pm$ 21	34	938 $\pm$ 55	
<b>B09B</b>										
1-1	1000	460	0.067	0.1173 $\pm$ 4	0.4228 $\pm$ 83	6.837 $\pm$ 136	0.1186 $\pm$ 24	119	1915 $\pm$ 7	
2-1	11404	4233	0.036	0.1080 $\pm$ 3	0.3024 $\pm$ 58	4.504 $\pm$ 87	0.0923 $\pm$ 18	96	1767 $\pm$ 5	
3-1	371	99	0.065	0.0994 $\pm$ 11	0.1933 $\pm$ 37	2.650 $\pm$ 58	0.0577 $\pm$ 19	71	1614 $\pm$ 20	

4f206 (%) =  $100 \times \frac{^{206}\text{Pb}_{\text{common}}}{^{206}\text{Pb}_{\text{Total}}}$ , i.e., % of  $^{206}\text{Pb}$  attributed as common Pb.

conc. = concordance, as  $100 \times t(206/238)/t(207/206)$ . Uncertainties refer to the last digits listed.

**Table 8**  $^{204}\text{Pb}$ -corrected SHRIMP II isotopic data for monazite (samples UWA-B40A, UWA-B40B and UWA-B40C) and xenotime (sample UWA-B40A) from late- to post-mineralisation veins that crosscut the Breves Geisen.

grain-spot	U (ppm)	Th (ppm)	Th/U	4f206 (%)	$^{207}\text{Pb}/^{206}\text{Pb}$	$^{208}\text{Pb}/^{206}\text{Pb}$	$^{207}\text{Pb}/^{235}\text{U}$	$^{206}\text{Pb}/^{238}\text{U}$	$^{208}\text{Pb}/^{232}\text{Th}$	conc. (%)	$^{207}\text{Pb}/^{206}\text{Pb}$ Age (Ma)
<b>Monazite</b>											
mA.1-1	722	7714	10.68	0.062	$0.1142 \pm 9$	$2.6801 \pm 17$	$0.3571 \pm 55$	$5.621 \pm 100$	$0.1005 \pm 18$	105	$1867 \pm 14$
mA.1-2	255	4111	16.09	0.132	$0.1152 \pm 15$	$4.2258 \pm 35$	$0.3413 \pm 72$	$5.420 \pm 140$	$0.0998 \pm 21$	101	$1883 \pm 23$
mA.2-1	4691	2350	0.50	0.031	$0.1151 \pm 3$	$0.1264 \pm 1$	$0.3556 \pm 40$	$5.642 \pm 66$	$0.1010 \pm 26$	104	$1881 \pm 5$
mA.2-2	813	2875	3.54	0.394	$0.1139 \pm 11$	$0.8590 \pm 8$	$0.3371 \pm 49$	$5.295 \pm 98$	$0.0966 \pm 24$	101	$1862 \pm 18$
mA.4-1	2775	2616	0.94	0.019	$0.1140 \pm 4$	$0.2360 \pm 2$	$0.3443 \pm 40$	$5.412 \pm 68$	$0.0994 \pm 25$	102	$1864 \pm 7$
mC.1-1	256	411	1.61	0.000	$0.1141 \pm 14$	$0.4247 \pm 9$	$0.3454 \pm 77$	$5.435 \pm 144$	$0.1033 \pm 75$	102	$1866 \pm 21$
mC.1-4	778	180	0.23	0.015	$0.1156 \pm 8$	$0.0642 \pm 2$	$0.3390 \pm 50$	$5.406 \pm 92$	$0.1026 \pm 88$	100	$1890 \pm 12$
Young outlier											
mC.1-3	797	205	0.26	0.000	$0.1120 \pm 7$	$0.0528 \pm 2$	$0.3262 \pm 52$	$5.039 \pm 90$	$0.0878 \pm 74$	99	$1832 \pm 11$
>5% discordant											
mB.1-1	156	7679	49.32	0.866	$0.1040 \pm 33$	$11.7651 \pm 109$	$0.3702 \pm 102$	$5.309 \pm 231$	$0.0974 \pm 18$	120	$1697 \pm 58$
mC.1-2	152	2444	16.12	0.190	$0.1171 \pm 21$	$4.6981 \pm 51$	$0.3148 \pm 80$	$5.082 \pm 165$	$0.1018 \pm 27$	92	$1912 \pm 32$
mC.2-1	28	3147	113.19	0.000	$0.1182 \pm 38$	$31.0779 \pm 558$	$0.3194 \pm 181$	$5.207 \pm 355$	$0.1009 \pm 24$	93	$1930 \pm 58$
<b>Xenotime</b>											
xA10-1	2188	8626	3.94	0.039	$0.1136 \pm 6$	$1.1393 \pm 49$	$0.3480 \pm 51$	$5.453 \pm 89$	$0.1006 \pm 17$	104	$1858 \pm 10$
xA.10-2	2035	7968	3.91	0.046	$0.1138 \pm 7$	$1.1200 \pm 56$	$0.3492 \pm 53$	$5.478 \pm 94$	$0.0999 \pm 18$	104	$1860 \pm 11$
xA.10-1A	2004	7586	3.78	0.062	$0.1147 \pm 7$	$1.1255 \pm 56$	$0.3476 \pm 52$	$5.496 \pm 93$	$0.1033 \pm 18$	103	$1875 \pm 11$
xA.11-1	1295	5893	4.55	0.087	$0.1132 \pm 8$	$1.3360 \pm 69$	$0.3332 \pm 55$	$5.198 \pm 99$	$0.0978 \pm 20$	100	$1851 \pm 13$
xA.11-3	5842	6867	1.18	0.024	$0.1150 \pm 4$	$0.3429 \pm 17$	$0.3461 \pm 44$	$5.489 \pm 76$	$0.1010 \pm 15$	102	$1880 \pm 7$
xA.3-1	1255	853	0.68	0.106	$0.1148 \pm 9$	$0.1970 \pm 24$	$0.3514 \pm 59$	$5.564 \pm 108$	$0.1018 \pm 24$	103	$1877 \pm 13$
xA.5-2	1299	911	0.70	0.222	$0.1134 \pm 11$	$0.2055 \pm 31$	$0.3372 \pm 57$	$5.270 \pm 107$	$0.0987 \pm 25$	101	$1854 \pm 17$
Young outlier											
xA.5-1	1052	1741	1.65	0.233	$0.1118 \pm 11$	$0.4893 \pm 43$	$0.3418 \pm 59$	$5.269 \pm 111$	$0.1010 \pm 23$	104	$1829 \pm 18$
>5% discordant											
xA.10-3	1295	3806	2.94	1.145	$0.1120 \pm 20$	$0.7855 \pm 72$	$0.2625 \pm 48$	$4.054 \pm 111$	$0.0702 \pm 17$	82	$1832 \pm 32$
xA.11-2	6299	12750	2.02	0.991	$0.1123 \pm 12$	$0.9090 \pm 54$	$0.0926 \pm 17$	$1.433 \pm 32$	$0.0416 \pm 10$	31	$1836 \pm 20$
xA.12-1	10484	29437	2.81	7.861	$0.1203 \pm 36$	$1.0279 \pm 126$	$0.0492 \pm 7$	$0.816 \pm 31$	$0.0180 \pm 4$	16	$1961 \pm 54$
xA.8-1	1153	3166	2.75	0.204	$0.1137 \pm 13$	$0.8624 \pm 71$	$0.2656 \pm 47$	$4.163 \pm 94$	$0.0834 \pm 19$	82	$1859 \pm 21$

4f206 (%) =  $100 \times \frac{{}^{206}\text{Pb}_{\text{common}}}{{}^{206}\text{Pb}_{\text{Total}}}$ , i.e., % of  ${}^{206}\text{Pb}$  attributed as common Pb.

conc. = concordance, as  $100 \times t(206/238)/t(207/206)$ . Uncertainties refer to the last digits listed.

**Table 9** Summary table of SHRIMP II ages for the Breves Cu-Au-(W-Bi-Sn) deposit

Sample (mineral)	Rock-Type	Age (Ma)	Error (Ma)	Event dated
UWA-B40A/B/C (xenotime and monazite)	Vein crosscutting greisen	1872	± 7	Late-stage hydrothermal activity / minimum age of ore formation
UWA-B09A (zircon)	Granite	1878	± 8	Magmatic crystallization
UWA-B30A (zircon)	Episyenite	1880	± 9	Magmatic crystallization

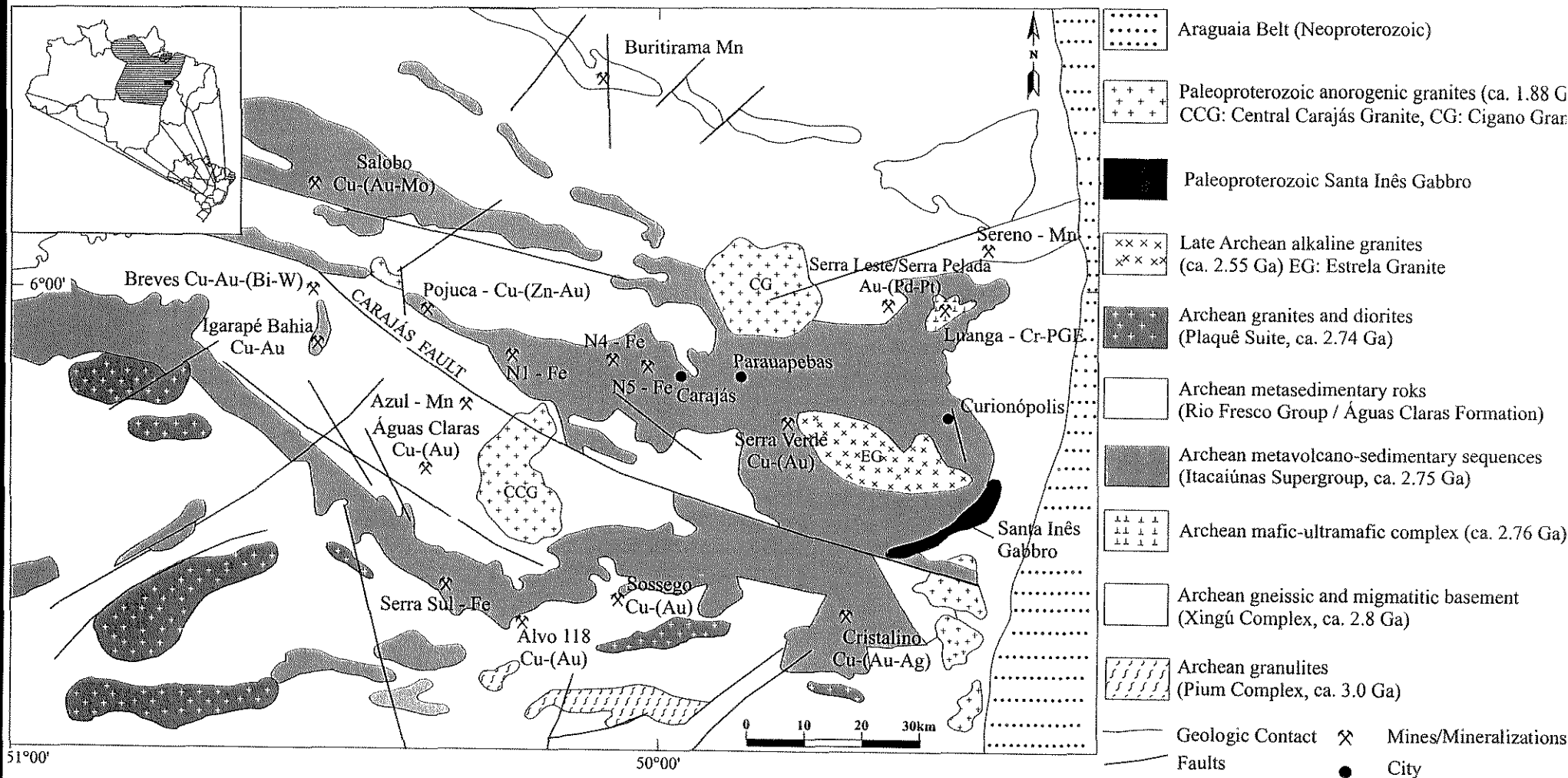


**Fig. 1** Geological map of the Carajás Copper-Gold Belt, showing the major iron, manganese, Fe-oxide Cu-Au-(U-REE) deposits and the Breves Cu-Au-(W-Bi) deposit (simplified from Docegeo 1988, Araújo and Maia 1991, Barros and Barbey 1998).

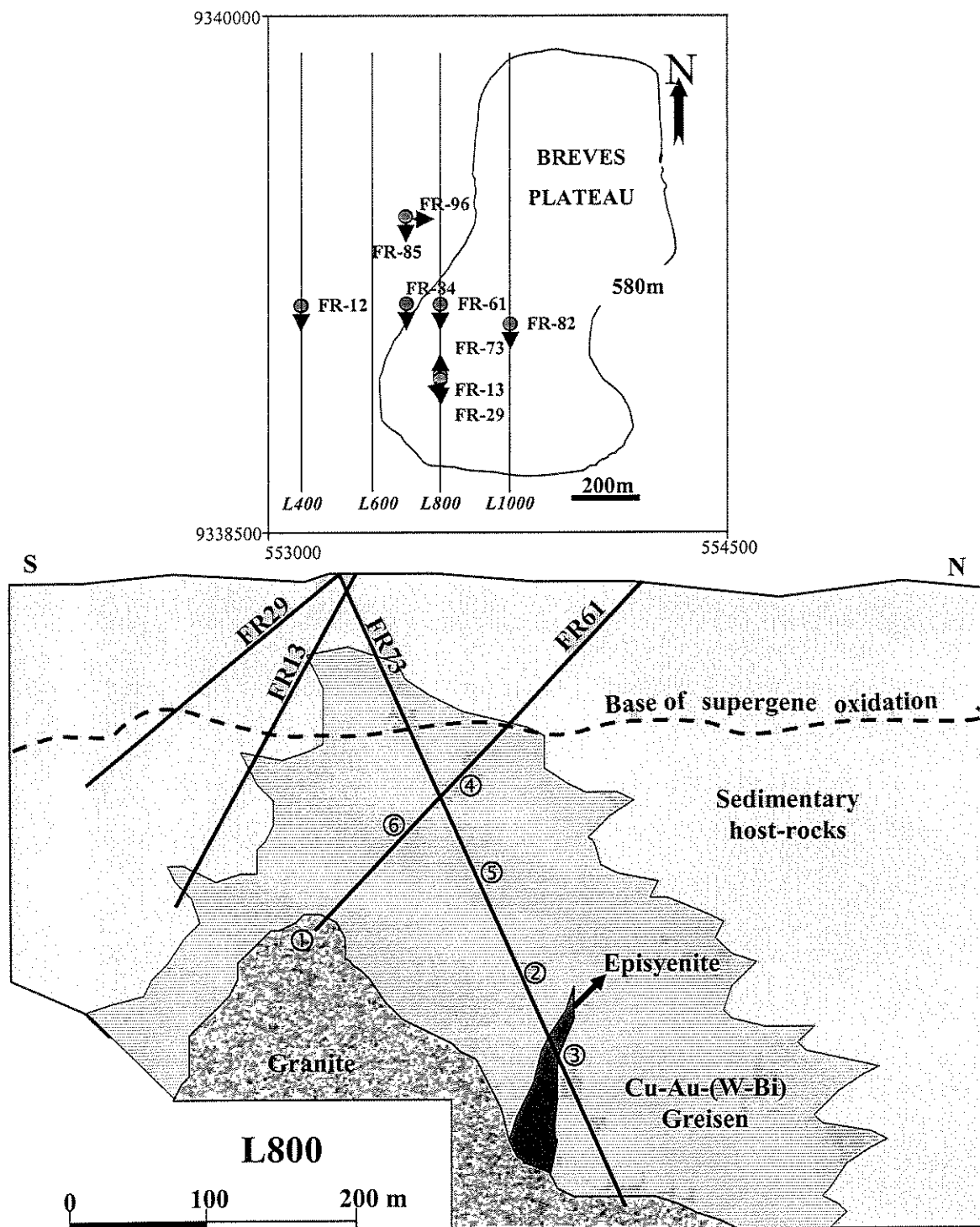
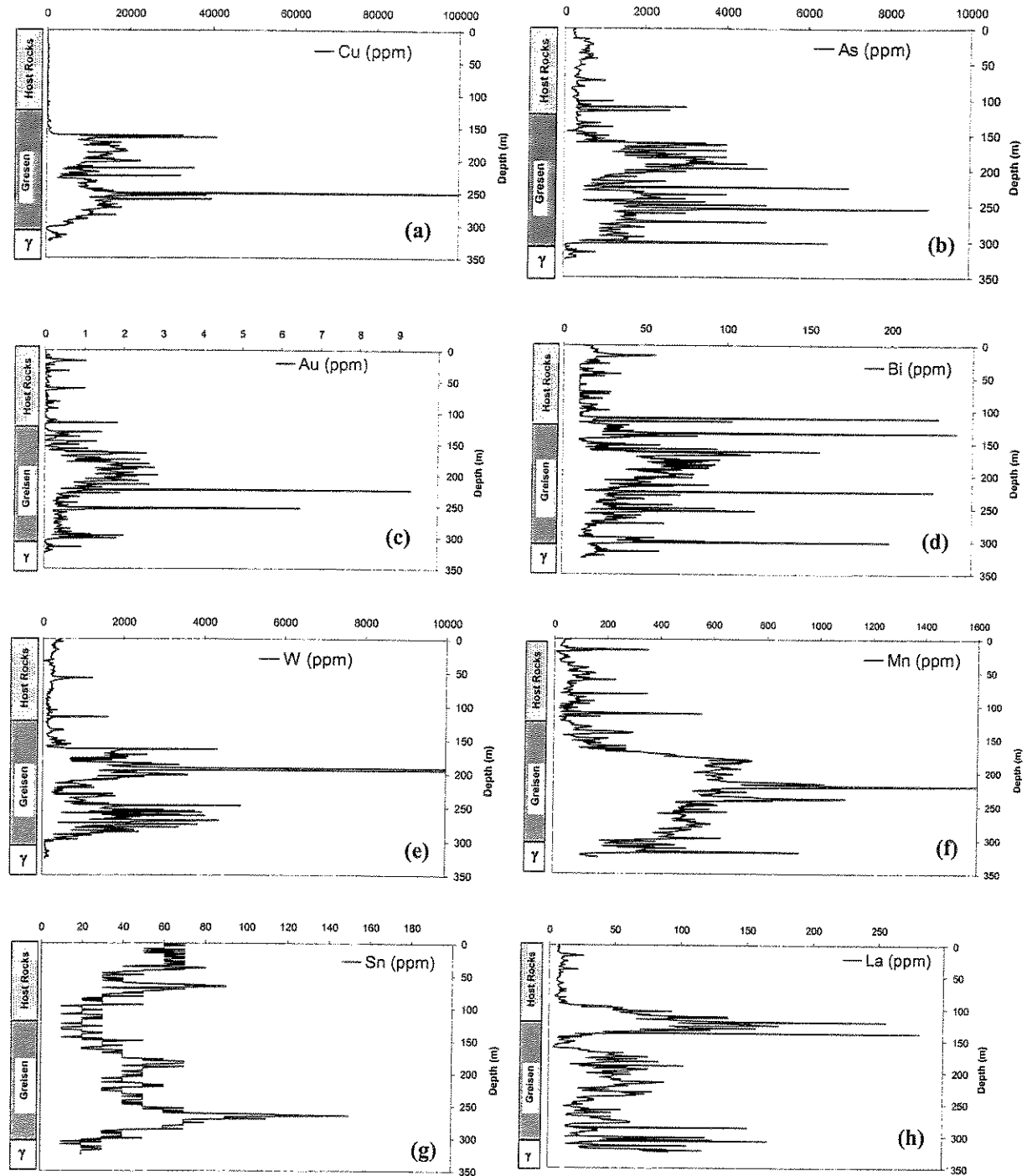
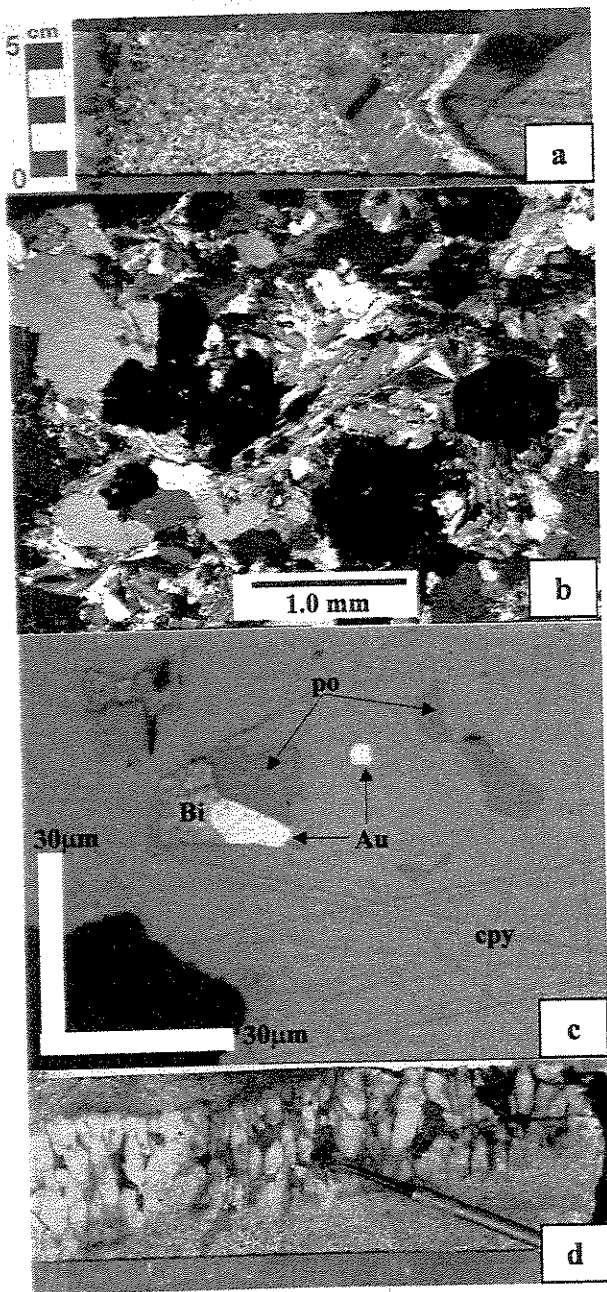


Fig. 2 Vertical section L800 of the Breves Cu-Au-(Bi-W) Deposit – Carajás Copper-Gold Belt. Numbers represent the locations of the samples selected for SHRIMP analyses: (1) UWA-B09A, (2) UWA-B09B, (3) UWA-B30A, (4) UWA-B30B, (5) UWA-B40A and UWA-B40B, and (6) UWA-B40C. Inset shows a plan view of the Breves Plateau (outlined by the 580 meter contour line) with the drill hole positions shown.



**Fig. 3** Geochemical log of drill hole FR61, vertical section L800 of the Breves Cu-Au-(Bi-W) deposit, showing the distribution of Cu (a), As (b), Au (c), Bi (d), W (e), Mn (f), Sn (g) and La (h) in the mineralized zone relatively to the host sedimentary rocks and underlying granite intrusion.  $\gamma$  - Breves Granite



**Fig. 4** (a) Bore hole sample of the apophysis zone, showing xenoliths of sedimentary rock with preserved internal bedding (right). Note reaction rim of microcline and the development of biotite-rich zones at the periphery of the sedimentary xenoliths (left). (b) Alotriomorphic texture of the greisen, with radial aggregates of muscovite associated with xenomorphic quartz and chalcopyrite (opaque minerals). Transmitted light, NX, sample: FR73-313.00m. (c) Detail of gold (Au) in equilibrium with pyrrhotite (po) and native bismuth (Bi), as inclusions in chalcopyrite (cpy). Reflected light, N//, sample: FR61/182.00m. (d) Bore hole sample showing comb structure quartz-vein, that crosscuts the greisen, filled with chalcopyrite, ferberite (indicated by the scribe) and chlorite.

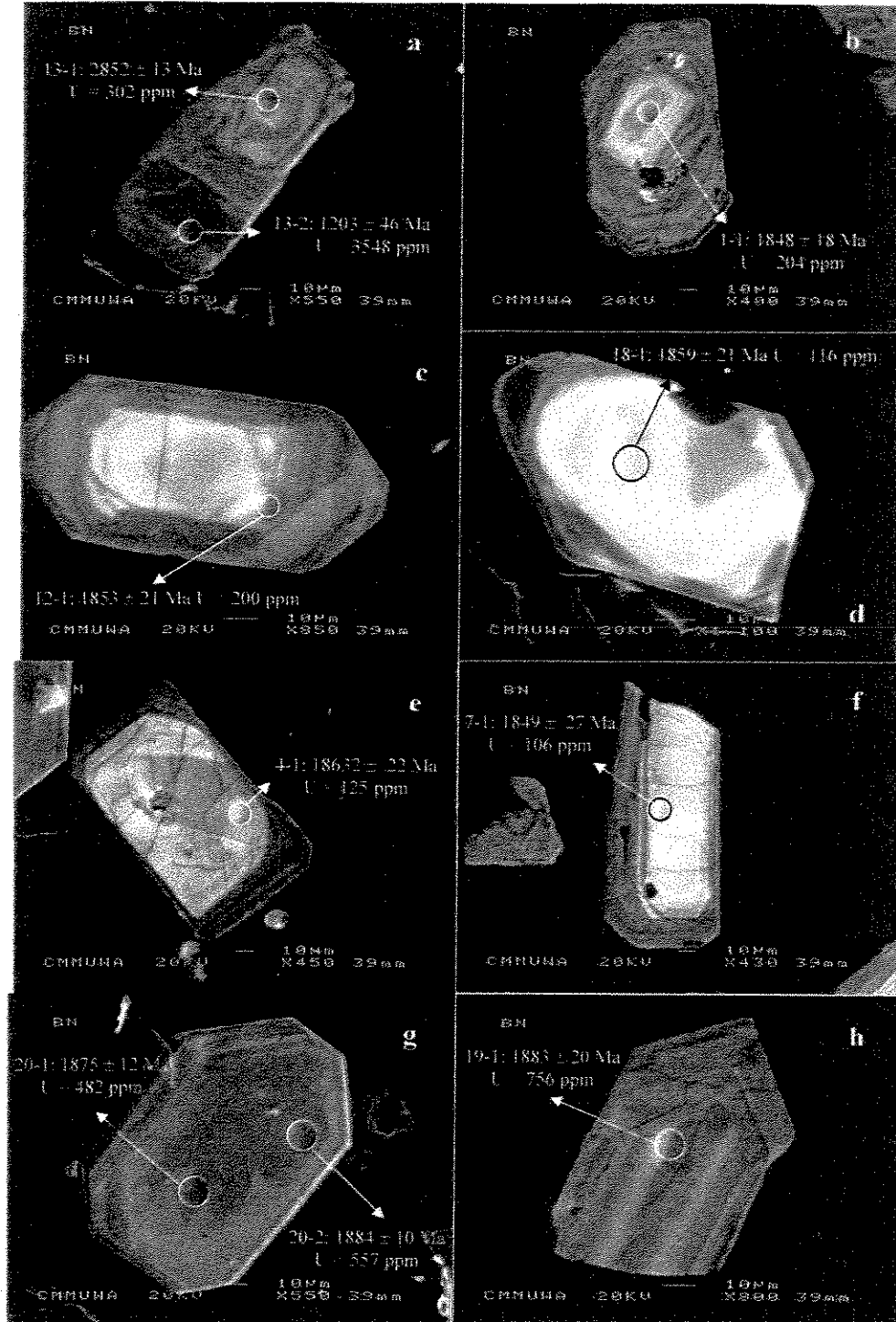


**Fig. 5** Cathodoluminescence images of cross-sections of representative zircons from the Breves granite, sample UWA-B09A, showing typical magmatic zoning. SHRIMP analytical areas are indicated by circles and are approximately 12  $\mu\text{m}$  in diameter. A description of the zircons is included in the text. Refer to Table 3 for full analytical results; analysis numbers: (A) 13-1 and 13-2, (B) 1-1, (C) 12-1, (D) 18-1, (E) 4-1, (F) 7-1, (G) 20-1 and 20-2, and (H) 19-1. Cathodoluminescence images were acquired at the CMM-UWA, using a JEOL 6400, at 20 kV, 10 nA and a working distance of 39 mm.

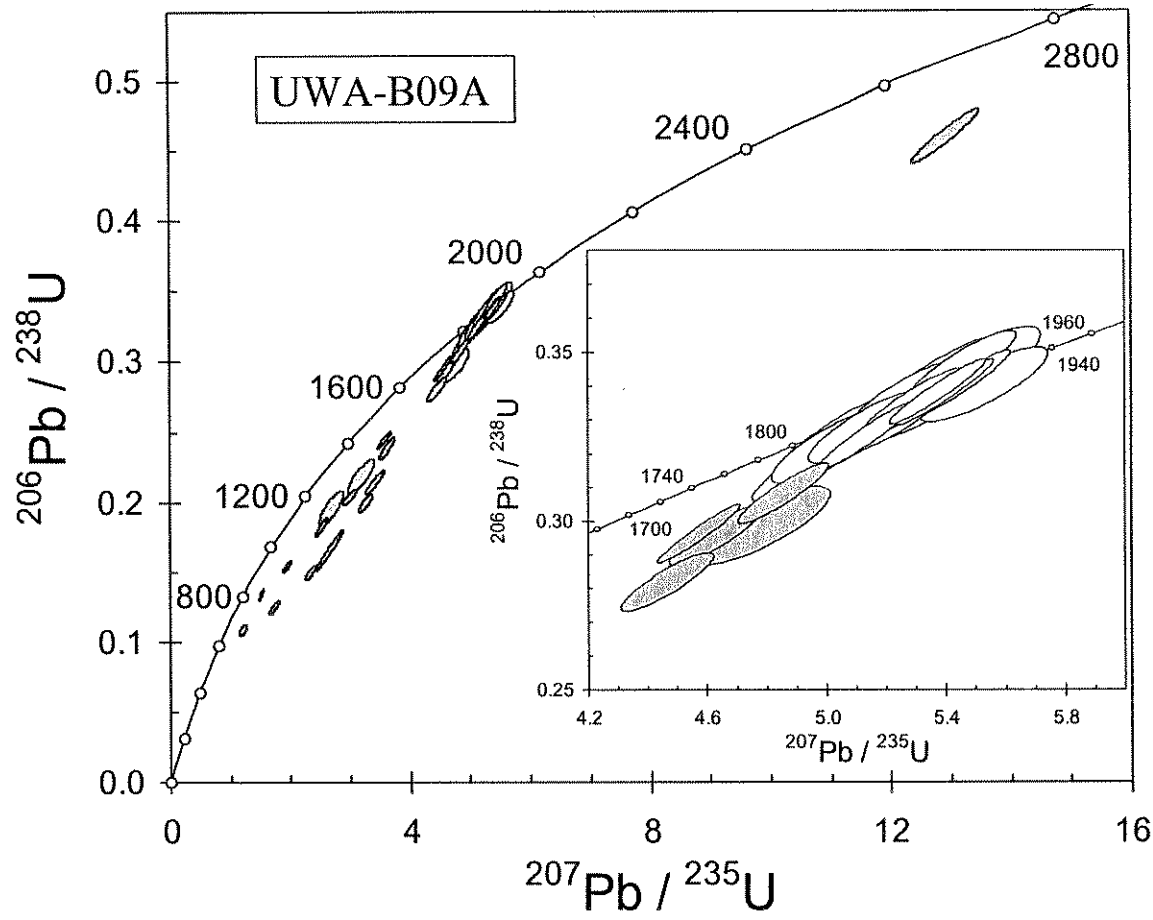


**Fig. 6** Concordia plot showing all SHRIMP II data points for zircons from the Breves Granite, sample UWA-B09A. Weighted mean age of concordant data, shown on the inset, is  $1878 \pm 8$  Ma (MSWD = 1.1, n = 18). White and gray symbols indicate concordant and discordant data points, respectively.

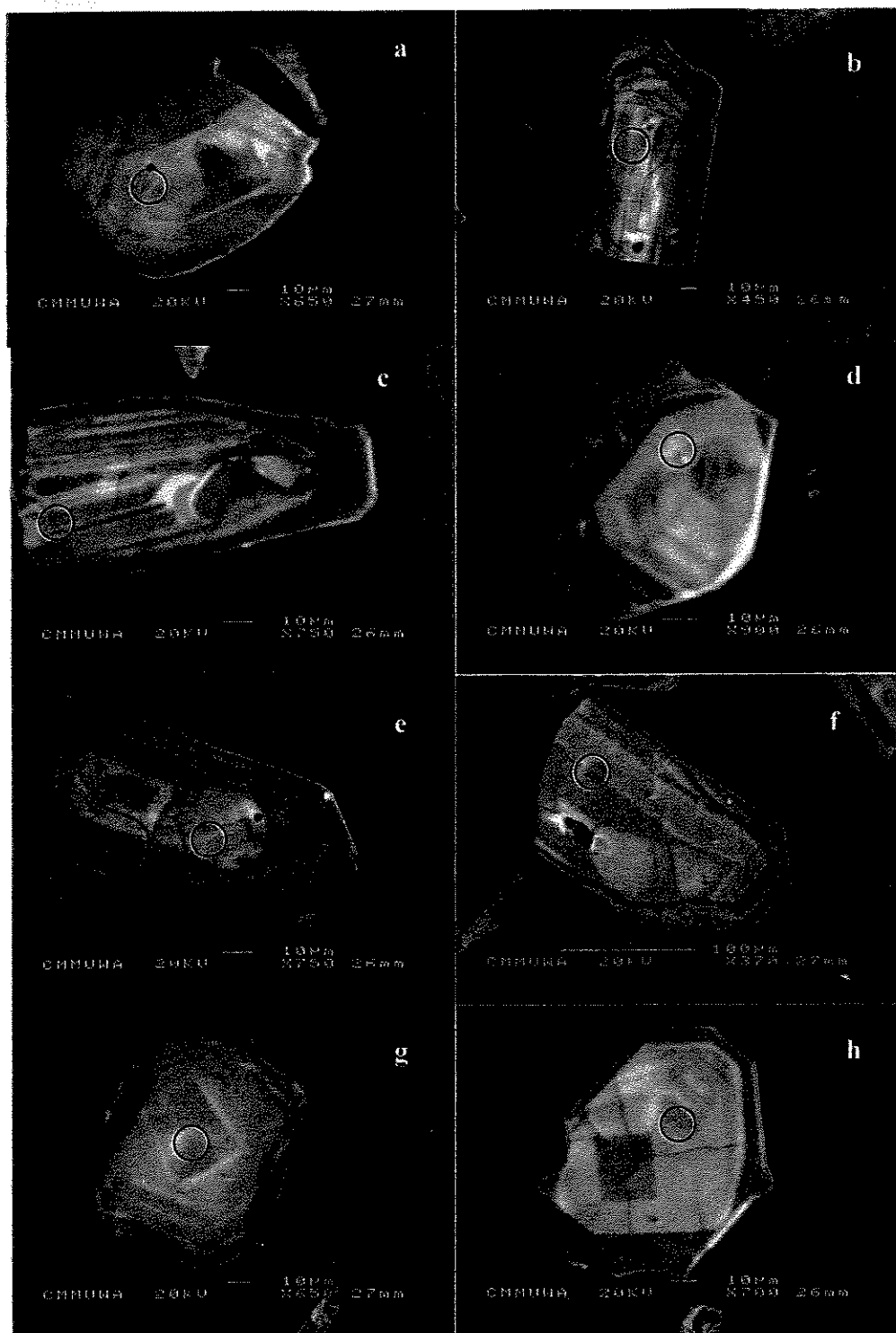


**Fig. 7** Cathodoluminescence images of cross-sections of representative zircons from the Breves episyenite, sample UWA-B30A. SHRIMP analytical areas are indicated by circles and are approximately 12 µm in diameter. A description of the zircons is included in the text. Refer to Table 4 for full analytical results; analysis numbers: (A) 3-1, (B) 5-1, (C) 6-1, (D) 7-1, (E) 11-1, (F) 18-1, (G) 20-1, (H) 23-1. Cathodoluminescence images were acquired at the CMM-UWA, using a JEOL 6400, at 20 kV, 10 nA and a working distance of 39 mm.

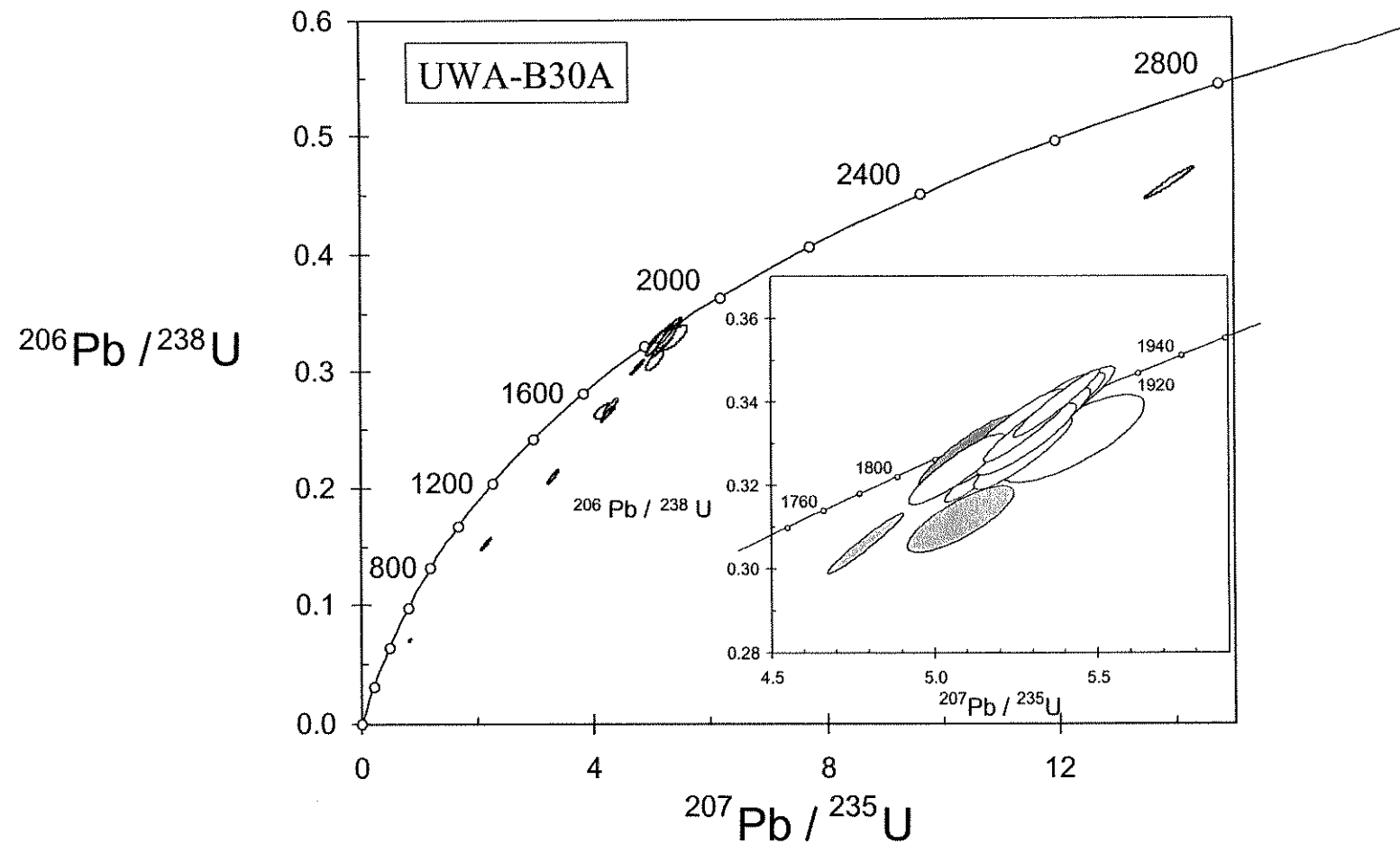


**Fig. 8** Concordia plot showing all SHRIMP II data points for zircons from the Breves episyenite, sample UWA-B30A. Weighted mean age of concordant data, shown on the inset, is  $1881.8 \pm 6.8$  Ma (MSWD = 1.2, n = 14). White and gray symbols indicate concordant and discordant data points, respectively. Black symbols is a possible young outlier ( $\sim 2\sigma$ )

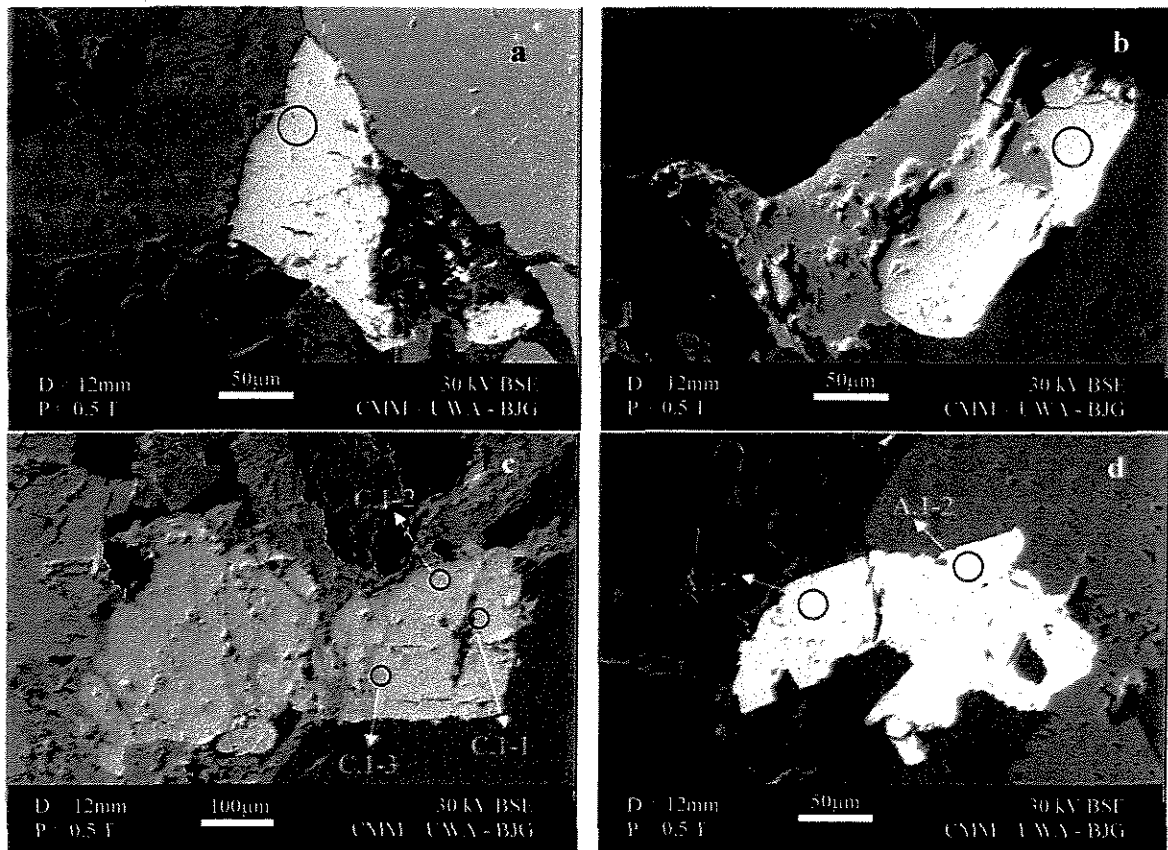


**Fig. 9** Back-scattered electron images of monazites from late- to post-mineralisation veins, sample UWA-B40A, that crosscut the ore-bearing greisen. SHRIMP analytical areas are indicated by circles and are approximately 7µm in diameter. Refer to Table 6 for complete analytical results; analysis numbers: (A) B.1-1, (B) C.2-1, (C) C.1-1, C.1-2 and C.1-3, and (D) A.1-1 and A.1-2. Back-scattered electron images were acquired at the CMM-UWA, using an environmental SEM, Eletroscan, at 30 kV, 2 nA and a working distance of 12 mm.

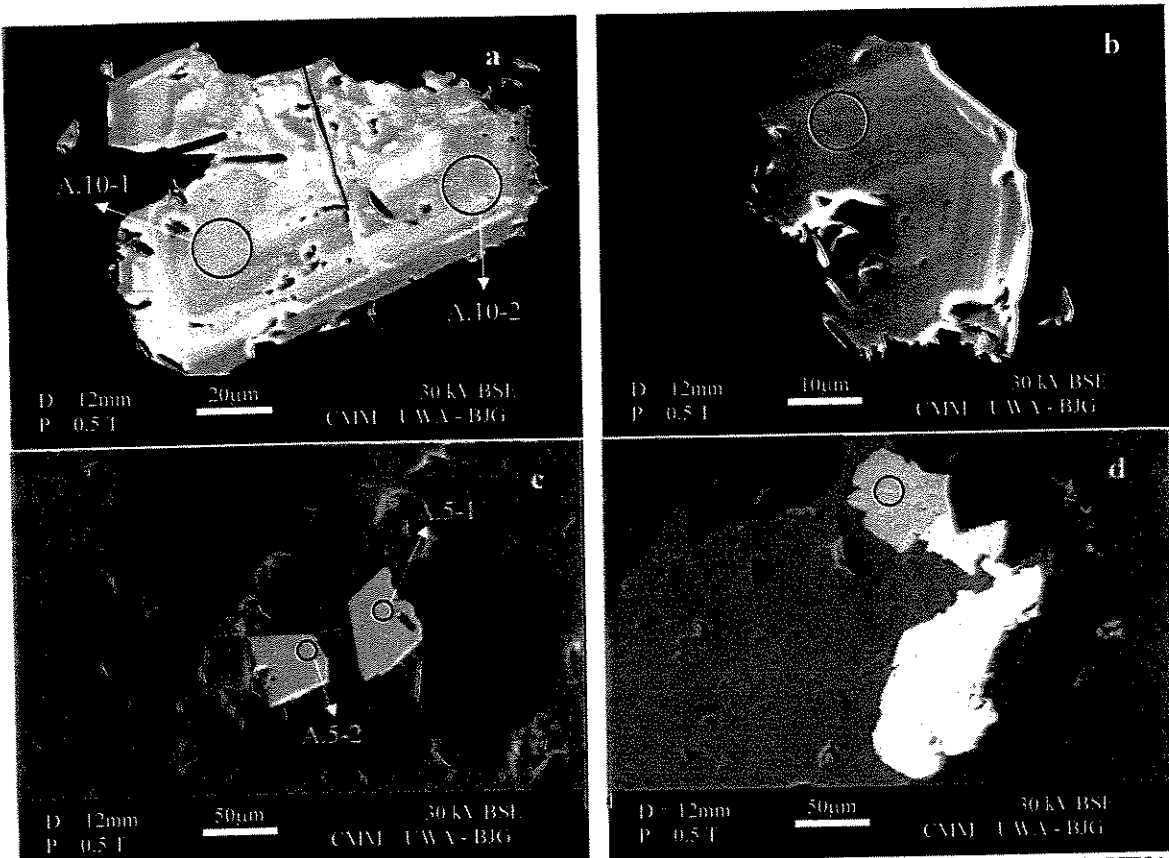


**Fig. 10** Back-scattered electron images of xenotimes from late- to post-mineralisation veins, sample UWA-B40A, that crosscut the ore-bearing greisen. SHRIMP analytical areas are indicated by circles and are approximately 7  $\mu\text{m}$  in diameter. Refer to Table 7 for complete analytical results; analysis numbers: (A) A.10.1 and A.10.2, (B) A.3-1, (C) A.5-1 and A.5-2, and (D) A.8-1. Back-scattered electron images were acquired at the CMM-UWA, using an environmental SEM, Eletroskan, at 30 kV, 2 nA and a working distance of 12 mm.

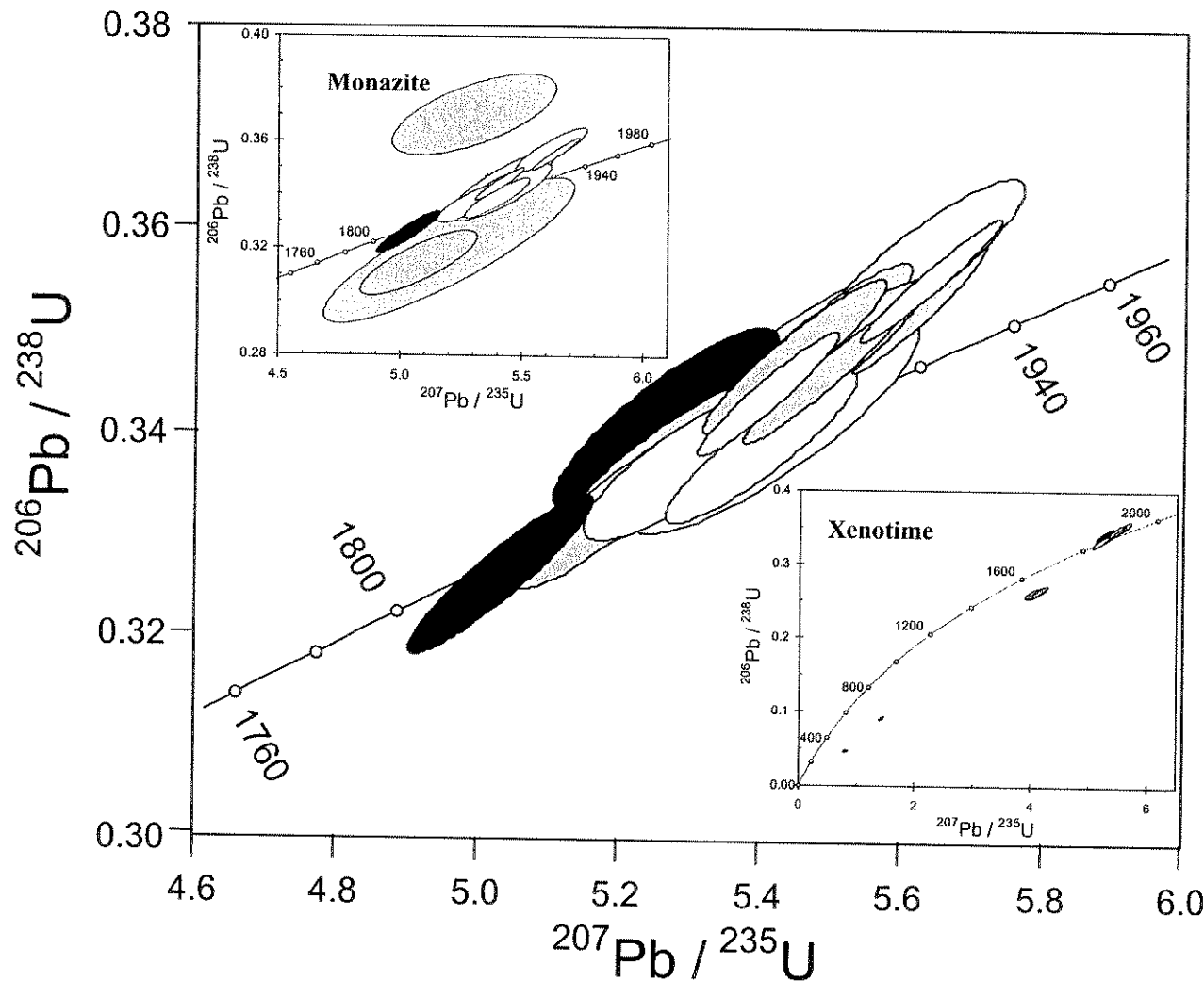
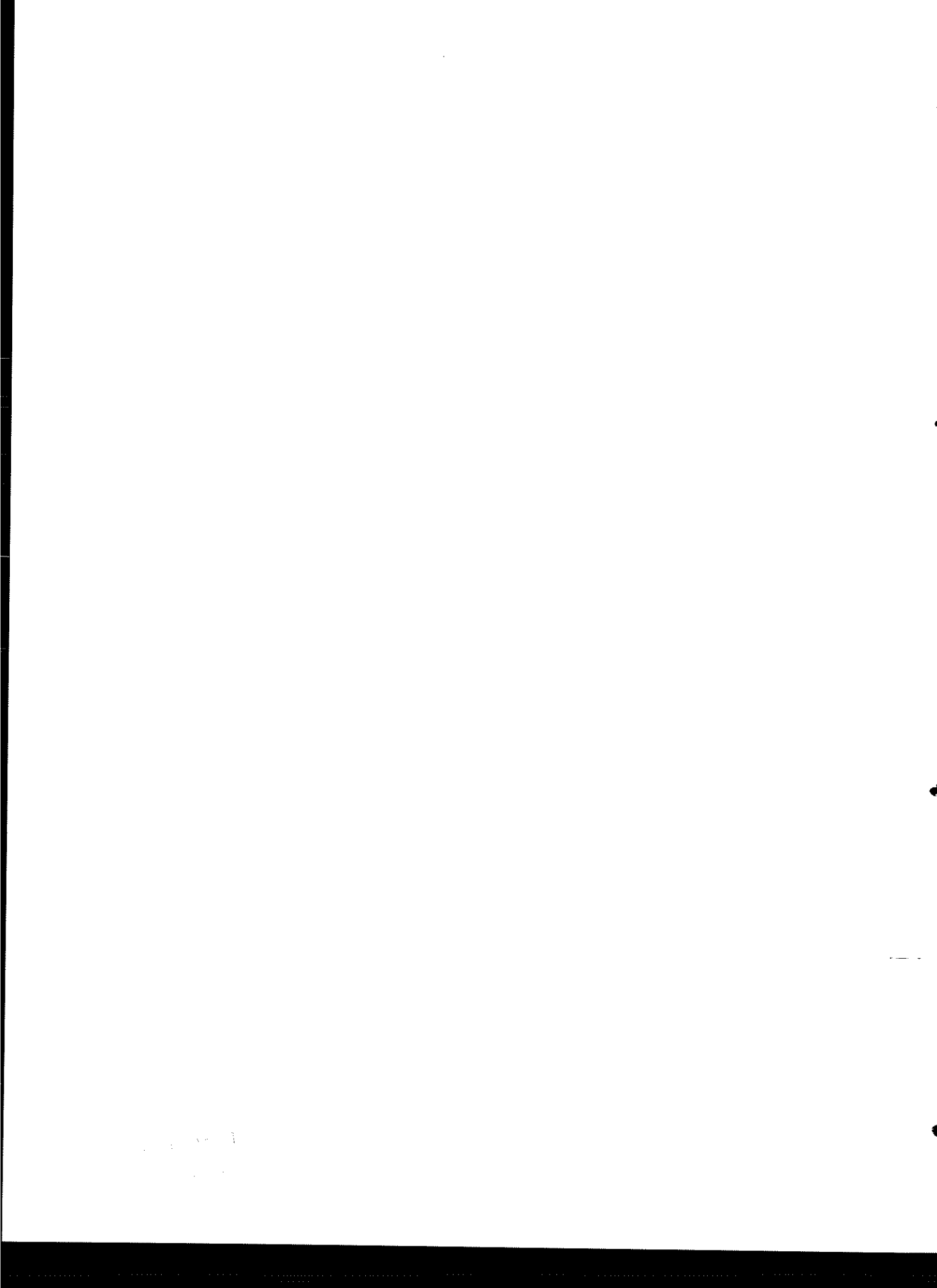


**Fig. 11** Concordia plot showing the main cluster of concordant SHRIMP II data points for monazites and xenotime from late- to post-mineralisation veins, samples UWA-B40A, UWA-B40B and UWA-B40C. Weighted mean age of concordant data is  $1872 \pm 7$  Ma (MSWD = 1.2, n = 14). Complete data sets of monazite and xenotime are shown as insets. In the main figure white and gray symbols indicate monazite and xenotime data points, respectively. Black symbols are young outliers, not used in the weighted mean age.

## **ANEXO 6**

Geologia e geocronologia SHRIMP II do depósito de Cu-Au Cento e Dezoito, Carajás,  
Brasil

UNICAMP  
BIBLIOTECA CENTRAL  
SEÇÃO CIRCULANTE



## **GEOLOGIA E GEOCRONOLOGIA SHRIMP II DO DEPÓSITO DE CU-AU CENTO E DEZOITO, CARAJÁS, BRASIL.**

### **1. Introdução**

O depósito de Cu-(Au) Cento e Dezoito representa mais uma das recentes descobertas da Companhia Vale do Rio Doce no Cinturão Cupro-Aurífero de Carajás. Localiza-se no Município de Canaã dos Carajás, entre os rios Pium e Parauapebas, a aproximadamente 70 km à SW da cidade de Parauapebas (Figura 1). Rigon et al. (2000) assinalam que o depósito alinha-se com as mineralizações de Sossego e Cristalino, definindo um trend EW na porção sul da Província Mineral de Carajás.

Regionalmente este domínio da província inclui exposições das rochas do embasamento que incluem ortogranulitos do Complexo Pium (~3,0 Ga - Rodrigues et al. 1992) e rochas gnaissicas e migmatíticas do Complexo Xingú (~2,9 Ga - Machado et al. 1991). Ocorrem também domínios restritos de rochas meta-vulcânicas foliadas, supostamente do Supergrupo Andorinhas (Docegeo 1988), e rochas supracrustais não tectonizadas do Grupo Grão Pará (Docegeo 1988) situadas a norte do depósito Cento e Dezoito. Este conjunto de rochas é intrudido por rochas graníticas da Suíte Plaquê (ca. 2,74 Ga - Huhn et al. 1999).

### **2. Geologia**

O depósito de Cu-Au Cento e Dezoito inclui corpos de espessura variada que definem dois “trends” distintos. O “Trend 2” e o “Trend Principal”, o mais significativo, são balizados respectivamente por estruturas dúcteis transcorrentes de orientação geral EW e por estruturas transtensionais mais jovens de orientação geral N60W (Figuras 2). Os corpos de minério sulfetado são em geral tabulares e sub-verticais (Figura 3), e segundo Rigon et al. (2000) totalizam recursos estimados da ordem de 70 Mt @ 1,0 % Cu e 0,3 g/t Au.

Predominam como rochas encaixantes no depósito Cento e Dezoito, tanto na capa quanto na lapa, rochas ítrusivas de composição tonalítica a granodiorítica. Estas rochas apresentam textura granular hipidiomórfia ou granofírica caracterizada pelo

desenvolvimento de coroas de quartzo intercrescido com K-feldspato ± albita ao redor de ripas de plagioclásio primário. Ilmenita é o principal mineral acessório, e ocorre confinada aos interstícios da trama quartzo-feldspática.

Estas intrusões têm como rochas encaixantes quartzo-clorita xistos. Estes tectonitos, contêm localmente *pods*, isentos de deformação, onde se observam micrólitos de plagioclásio com textura seriada, sugerindo vulcanitos básicos como protolito. Os xistos possuem foliação penetrativa, balizada pela orientação preferencial da clorita. Intercalam-se domínios de quartzo recristalizado e estirado, que ocasionalmente são boudinados e rompidos, quando há o desenvolvimento de sombras e franjas de pressão.

Este conjunto de rochas é cortados por duas gerações de diques. Os mais antigos são de composição ácida, variando de dacítica a riolítica. Estas rochas caracteristicamente possuem textura porfirítica ou glomeroporfirítica com fenocristais euédricos de quartzo biterminados e plagioclásio cimentados por matriz microcristalina. Ocassionalmente ocorrem xenólitos de clorita xisto que são soldados por matriz porfirítica contendo fenocristais euédricos e biterminados de quartzo. Já os diques mais jovens, são de diabásio com textura subofítica, que são identificados em campo pelo elevado teor de magnetita (até 10 wt%) e pela ausência de alterações hidrotermal.

### 3. Alteração hidrotermal

As rochas tonalítica a granodiorítica foram submetidas a alteração hidrotermal de intensidade variada, caracterizada principalmente pela cloritização, potassificação e carbonatação. Frequentemente, ocorrem relictos da mineralogia e textura primária que permitem o reconhecimento da rocha original. O plagioclásio primário é convertido em clorita, que pode ou não estar associado a traços de epidoto e clinozoisita. Tremolita tem ocorrência restrita e freqüentemente é consumida em reações progressivas de hidrólise que originam biotita e posteriormente clorita. Halos de potassificação ocorrem adjacentes aos corpos de minério, incluindo principalmente microclina e subordinadamente biotita. É constante a presença de Fe-óxidos (hematita ± magnetita) como inclusões no K-feldspato, conferindo ao tonalito hidrotermalizado uma coloração vermelha muito intensa. A carbonatação inclui principalmente veios entrecortados de calcita + quartzo ± titanita ±

apatita, que tornam-se progressivamente mais intensos em direção às zonas mineralizadas. Em menor proporção, calcita ocorre ainda de forma disseminada como produto da quebra do plagioclásio primário. Calcita em geral exibe elevados teores de Mn e Fe ( $MnO \sim 1\%$ ,  $FeO_t \sim 2\%$ ). Integram ainda o quadro de alterações hidrotermais a pronunciada silicificação, expressa principalmente em veios, e a oxidação da ilmenita para rutilo + hematita/magnetita  $\pm$  titanita.

Dentro dos domínios de tonalitos e granodioritos cloritizados, ocorrem porções de rocha fortemente foliada, interpretados como enclaves dos xistos encaixantes. A trama dúctil dos quartzo-clorita xistos é recortada por veios de quartzo + clorita + calcita oblíquos à  $S_n$ . Esta evidência textural, indica que o hidrotermalismo relaciona-se a estruturas de caráter rúptil mais jovens que a trama milonítica que predomina regionalmente.

Os diques de composição ácida foram também submetidos a uma série de alterações hidrotermais. Ocorrem zonas métricas de calcopirita maciça, a localmente brechada, associadas a intensa potassificação que são recortadas por veios tardios contendo abundante quartzo + calcita.

Localmente tem-se a associação de alteração sódica na periferia dos corpos mineralizados. Ocorrem albititos contendo proporções variadas de clorita, turmalina e apatita com até 3 % de flúor. A rocha é cortada por veios de clorita e quartzo, que contém ainda pontuações de fluorita, calcita, yttrialita e apatita.

A abundante venulação de quartzo e a cloritzação generalizada são os estilos de alteração mais frequentes no depósito afetando grandes volumes de rocha. Análises químicas de clorita via microssonda, permitiram uma estimativa da temperatura do sistema hidrotermal (Tabela 1). Note que as temperaturas veriam num intervalo de 271 a 344°C, estando as temperaturas mais baixas associada às rochas mais intensamente hidrotermalizadas.

**Tabela 1** - Estimativas de temperatura utilizando o termômetro da clorita de Cathelineau (1988)

<b>Tipo de Rocha (número de análises químicas*)</b>	<b>T°C</b>
Granodiorito pouco hidrotermalizado (8)	347
Granodiorito intensamente hidrotermalizado (13)	271
Tonalito hidrotermalizado (4)	246
Alcalifeldspato riolito hidrotermalizado (6)	344
Dacito hidrotermalizado (13)	326
Dique riolítico brechado e hidrotermalizado (4)	318
Albitito (8)	278
K-Fe-Metassomatito (12)	318

\* *Análises químicas por WDS em microssonda Jeol 733.*

#### 4. Mineralização sulfetada

Os corpos mineralizados consistem de zonas com alta densidade de veios entrecortados, em padrão *stockwork*, que estão tipicamente circunscritos a domínios de intensa cloritização e alteração potássica. Os veios incluem abundante quartzo e calcopirita associados a proporções variadas de calcita ± clorita. Em menor proporção podem ocorrer domínios métricos de sulfeto maciço a localmente disseminado, contendo abundante Cu-sulfetos (calcopirita-bornita) em associação com Fe-óxidos (hematita-magnetita). Portanto, no depósito Cento e Dezoito a mineralização primária de cobre exibe dois modos de ocorrência: (a) venular, que é amplamente predominante, e (b) maciça, que tem ocorrência mais restrita (Figura 4).

A mineralização de cobre relaciona-se principalmente à calcopirita e subordinadamente bornita que ocorrem intercrescidas denotando equilíbrio textural. Hematita ocorre freqüentemente associa-se às bordas da calcopirita em zonas de minério maciço, podendo conter relictos de magnetita sugerindo progressiva oxidação do sistema hidrotermal (Prancha 1).

Ouro não foi observado na paragênese metálica. Prata nativa e hessita ocorrem como inclusões na calcopirita. Associam-se ainda ao minério traços de altaíta, fluorita, cassiterita, thorita e minerais de ETR (apatita, allanita, monatita e xenotima). Yttrialita é um mineral traço mais comum, ocorrendo principalmente em associação com hematita (Prancha 1).

O manto intempérico, de espessura aproximada de 100 m, dá origem a uma mineralização de cobre secundária. Os recursos estimados são de 100 milhões de toneladas de minério oxidado, com teores similares aos do minério sulfetado (Rigon et al. 2000).

## 5. Geocronologia U-Pb SRHIMP II

No depósito Cento e Dezoito foram datadas as seguintes rochas: (a) tonalito que representa a hospedeira imediata da mineralização, (b) diques de composição dacítica e riolítica que cortam o tonalito, (c) xenotima extraída de amostra composta de minério maciço, e (d) xenotima extraída de veios de quartzo + calcopirita que cortam o minério maciço. Um resumo dos resultados geocronológicos encontra-se disponível na Tabela 2, estando os dados completos nas Tabelas de 3 a 7.

Os resultados de SHRIMP revelarem que o tonalito encaixante é uma intrusão Arqueana ( $2743 \pm 3$  Ma – Tabela 3 e Figura 5) correlata aos granitos e dioritos da Suíte Plaquê, que foram datados em  $\sim 2.74$  Ga por vários autores (e.g. Huhn et al. 1999). Resultados inéditos foram obtidos nos diques de composição dacítica e riolítica que forneceram idades  $^{207}\text{Pb}/^{206}\text{Pb}$  de  $2645 \pm 9$  Ma (Tabela 4 e Figura 6) e  $2654 \pm 9$  Ma (Tabela 5 e Figura 7) respectivamente. Este evento magmático de  $\sim 2.65$  Ga é pouco na região de Carajás, tendo sido publicada apenas uma idade de  $2645 \pm 12$  Ma em zircões extraídos de um dique de gabbro que corta a Formação Águas Claras (Dias et al. 1996).

Na tentativa de se circunscrever a idade da mineralização foram preparadas duas amostras para geocronologia. A primeira consiste de uma amostra composta de minério maciço, rica em calcopirita em equilíbrio com hematita, que foi britada e a partir da qual foram concentrados cristais de xenotima. A segunda consiste de cristais de xenotima, de veios quartzo + calcopirita que cortam o minério maciço, que foram extraídos a partir de lâmina delgada. Ambas as amostras forneceram idade Proterozóica de  $1869 \pm 7$  Ma para o minério maciço (Tabela 6 e Figura 8) e  $1868 \pm 7$  para os veios mineralizados (Tabela 7 e Figura 9). Os resultados indicam a atuação de um evento hidrotermal correlato ao observado no depósito de Breves. Porém, dado ao fato da amostra de minério maciço ter sido preparada pelo método convencional de concentração, os cristais datados podem derivar de veios portadores de xenotima que cortam o minério. Assim, assume-se que no

deposito de Cento e Dezoito foi determinada apenas a idade do último episódio formador de minério, que é representado pelos veios de quartzo + calcopirita  $\pm$  xenotima. O minério maciço que é cortado por estes veios e se caracteriza pela associação Fe-óxido + calcopirita não foi diretamente datado.

**Tabela 2.** Resumo das idades  $^{207}\text{Pb}/^{206}\text{Pb}$ , pelo método SHRIMP, do depósito de Cu-(Au) Cento e Dezoito.

Amostra (mineral datado)	Rocha	Idade (Ma)	Erro (Ma)	Evento Datado
UWA-B35 (xenotima)	Veios de quartzo + calcopirita	1868	$\pm 7$	Alteração hidrotermal
UWA-B36D (xenotima)	Minério de Cu-Au maciço	1869	$\pm 7$	Alteração hidrotermal
UWA-B21A (zircão magnético)	Dique de riolito	2654	$\pm 9$	Idade de cristalização
UWA-B21B (zircão magnético)	Dique de dacito	2645	$\pm 9$	Idade de cristalização
UWA-B30C (zircão magnético)	Tonalito	2743	$\pm 3$	Idade de cristalização

## 6. Discussão

Os dados levantados até o presente indicam que depósito Cento e Dezoito é uma mineralização de Cu-(Au) predominantemente do tipo *stockwork*, contendo localmente zonas maciças, alojada ao longo de estruturas regionais reativadas. A observação é corroborada pela ocorrência de veios portadores de Cu-sulfetos, transgressivos a foliação milonítica de xistos encaixantes. O caráter epigenético da mineralização também é demonstrado pela natureza das rochas encaixantes que incluem principalmente granodioritos e tonalitos.

As características de campo indicam que no depósito Cento e Dezoito existam dois tipos distintos de mineralização de cobre, são eles:

- (a) Minério maciço contendo calcopirita  $\pm$  bornita  $\pm$  Fe-óxidos (hematita  $\pm$  magnetita) que se associam preferencialmente a zonas de intensa alteração potássica (K-feldspato  $\pm$  biotita). A generalizada cloritização observada no depósito aparentemente está também relacionada a esta etapa de alteração hidrotermal, pois ocorrem nas zonas cloritizadas disseminações de calcopirita  $\pm$  bornita  $\pm$  hematita.
- (b) Minério venular contendo calcopirita associada a abundante quartzo e calcita  $\pm$  xenotima. Este estilo de mineralização predomina no depósito desenvolvendo zonas de *stockwork* estruturalmente controladas. Note que a esta etapa não se associam fases relativamente oxidadas como bornita e Fe-óxidos.

As relações texturais sugerem que o minério maciço representa um estágio de alteração hidrotermal precoce que é superposto por veios tardios, localmente desenvolvendo domínios brechados (Figura 4). As diferenças mineralógicas e texturais observadas entre os dois estilos de hidrotermalismo, refletem características distintas dos fluidos envolvidos. A alteração precoce se caracteriza por ser relativamente mais oxidada e empobrecida em enxofre, conforme denota o equilíbrio calcopirita-bornita-hematita/magnetita. Já a alteração tardia, concentrada ao longo de veios, caracteriza-se pela abundância de quartzo associado à calcita e calcopirita.

Dada a evidência de dois eventos metalogenéticos distintos no Cinturão Cupro-Aurífero de Carajás, um no Neoarqueano ( $\sim 2,57$  Ga) e outro no Paleoproterozóico ( $\sim 1,88$  Ga), há a possibilidade de existirem na região depósitos híbridos resultantes da superposição destes eventos. O depósito Cento e Dezoito é um potencial exemplo, pois inclui atributos análogos aos do depósito neoarqueano de Igarapé Bahia, como a ocorrência de minério maciço, relativamente oxidado e pobre em enxofre, porém também portando vênulas com a associação quartzo + calcopirita  $\pm$  xenotima, similar a do depósito paleoproterozóico de Breves. Além da idade  $^{207}\text{Pb}/^{206}\text{Pb}$  SHRIMP de  $1868 \pm 7$  da xenotima, extraída de veios de quartzo, a ocorrência de fragmentos de calcopirita  $\pm$  bornita  $\pm$  Fe-óxidos soldados por matrix rica em quartzo é coerente com a sugestão de um modelo multi-estágio para o depósito Cento e Dezoito.

## 7. Referências

- Araújo, O.J.B; Maia, R.G.N. 1991. *Serra dos Carajás, folha SB.22-Z-A, Estado do Pará.* Brasília, DNPM, 136p. (Programa Levantamentos Geológicos Básicos do Brasil)
- Barros, C.E.M. e Barbey, P. 1998. A importância da granitogênese tardí-arqueana (2.5 Ga) na evolução tectono-metamórfica da Província Mineral de Carajás - Complexo Granítico Estrela e sua auréola de contato. *Revista Brasileira de Geociências*, 28:513-522
- Cathelineau M. 1988. Cation site occupancy in chlorites and illites as a function of temperature. *Clay Minerals*, 23:471-485.
- Dias, G.S.; Macambira, M.J.B.; Dall'Agnol, R.; Soares, A.D.V.; Barros, C.E.M. 1996. Datação de zircões de *sill* de metagabro: comprovação da idade arqueana da Formação Águas Claras, Carajás, Pará. V Simpósio de Geologia da Amazônia, 376-379 p.
- DOCEGEO (Rio Doce Geologia e Mineração S.A.). 1988. Província Mineral de Carajás. Litoestratigrafia e principais depósitos minerais. In: SBG, Congresso Brasileiro de Geologia, 35, Belém, *Anexo aos Anais*, 165p.
- Huhn, S.R.B.; Macambira, M.J.B.; Dall'Agnol, R. 1999. Geologia e geocronologia Pb/Pb do granito alcalino Arqueano Planalto, Região da Serra do Rabo, Carajás - PA. VI Simpósio de Geologia da Amazônia, 463-466 p.
- Machado, N.; Lindenmayer, Z; Krogh, T.E.; Lindenmayer, D. 1991. U-Pb geochronology of Archean magmatism and basement reactivation in the Carajás area, Amazon Shield, Brazil. *Precambrian Research*, 49:329-354
- Rigon, J.C.; Munaro, P.; Santos, L.A.; Nascimento, J.A.S.; Barreira, C.F. 2000. The Alvo 118 Copper-Gold Deposit: geology and mineralization, Serra dos Carajás, Pará. 31 Int. Geol. Cong. Rio de Janeiro. Abstracts.
- Rodrigues, E.S.; Lafon, J.M.; Scheller, T. 1992. Geocronologia Pb-Pb da Província Mineral de Carajás: primeiros resultados. In: SBG, Congresso Brasileiro de Geologia, 37, São Paulo, *Resumos Expandidos*, 2: 183-184

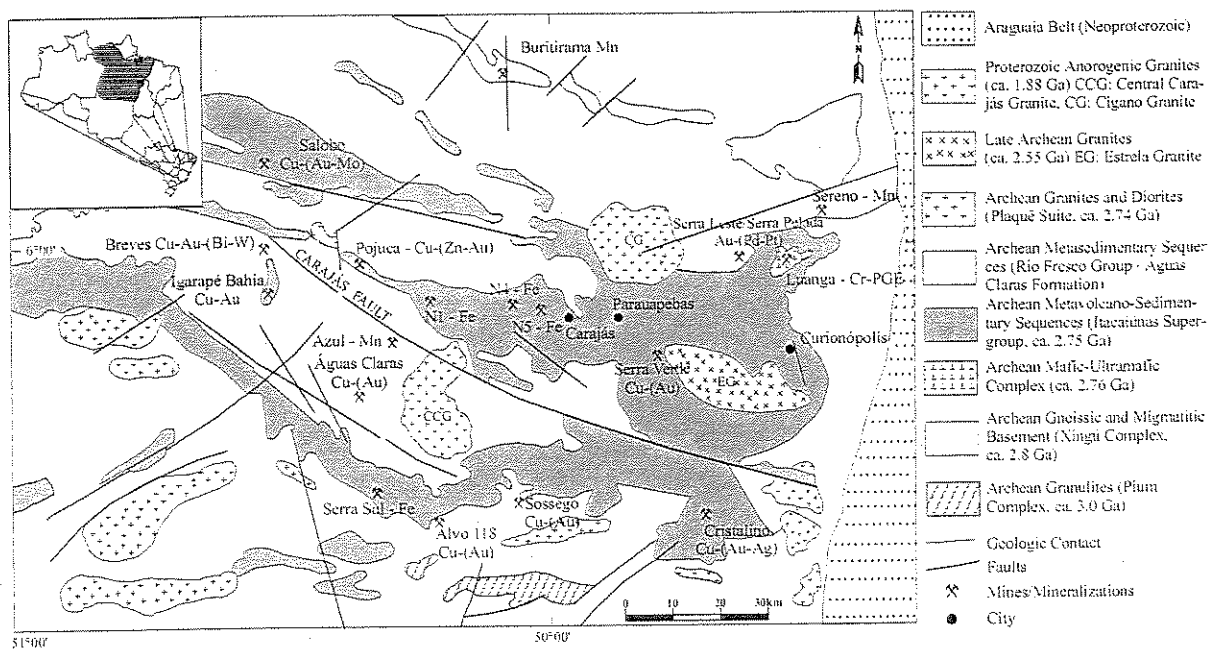


Figura 1 - Mapa geológico simplificado do Cinturão Cupro-Aurífero de Carajás (baseado em Docegeo 1988, Araújo e Maia 1991, Barros e Barbey 1998)

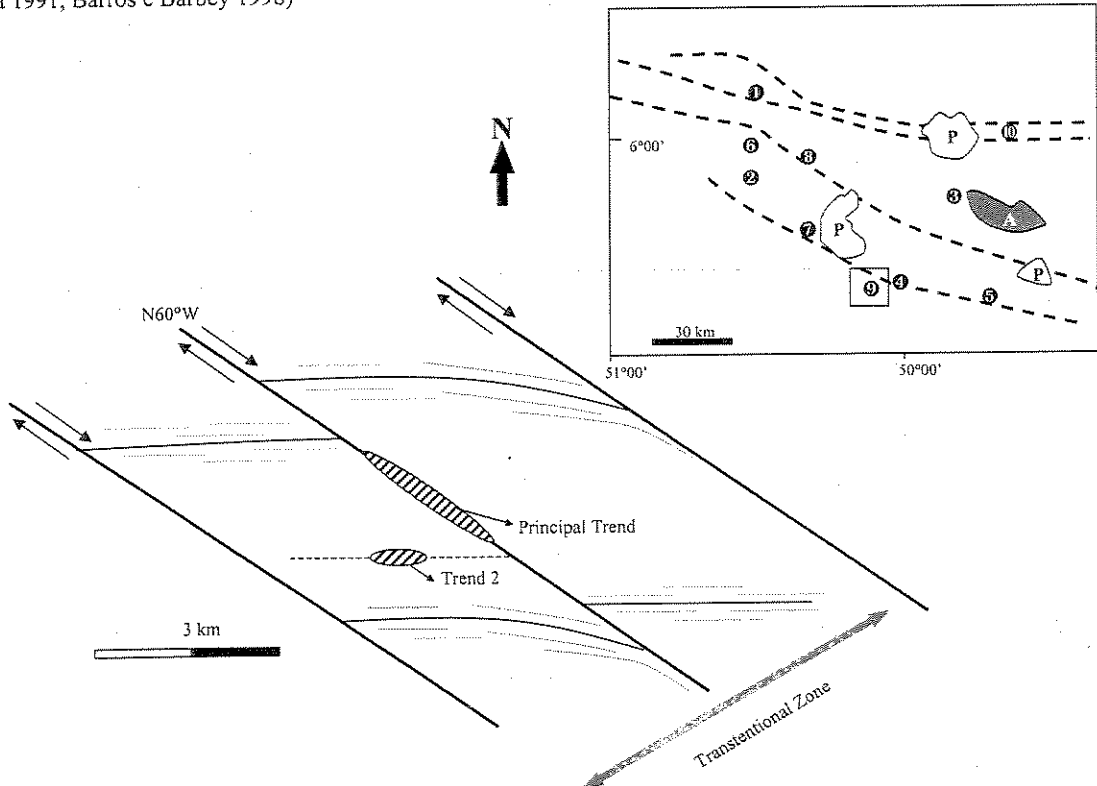


Figura 2 – Modelo estrutural esquemático para o depósito Cento e Dezoito, mostrando corpos de minério controlados pelo Trend Principal e o Trend 2. No canto superior direito tem-se uma representação da estruturação regional que condiciona a ocorrência de depósitos no Cinturão Cupro-Aurífero de Carajás. O posicionamento de granitóides Neoarqueanos (A) é aparentemente controlada por estruturas dúcteis E-W, enquanto os granitos Paleoprotezóicos (P) parecem ser controlados pela interseção destas com estruturas transtencionais NW-SE. Depósitos (1) Salobo, (2) Igarapé Bahia, (3) Serra Verde, (4) Sossego, (5) Cristalino, (6) Breves, (7) Águas Claras, (8) Pojuca-Gameleira, (9) Cento e Dezoito e (10) Serra Pelada.

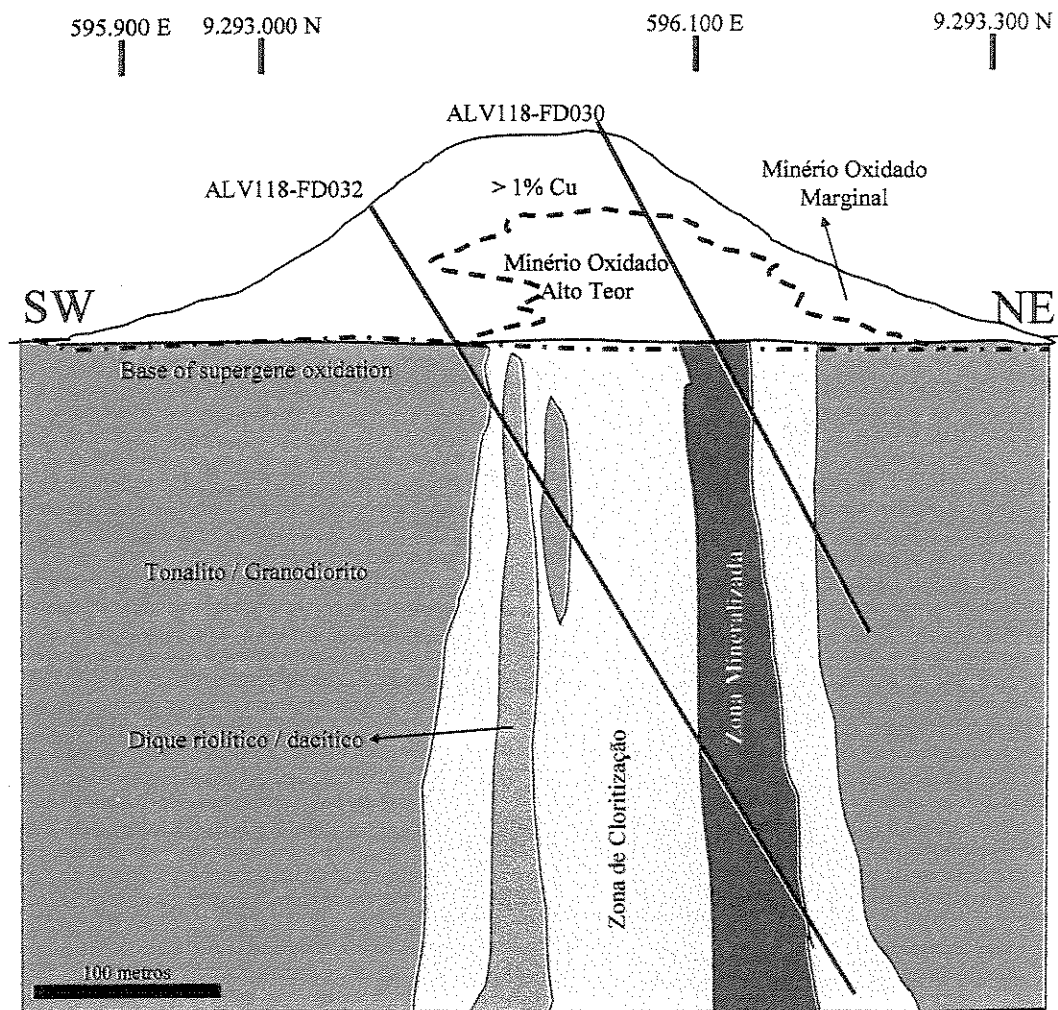


Figura 3 - Seção geológica vertical 1500NW ao longo do Trend Principal do depósito de Cu-(Au) Cento e Dezoito.

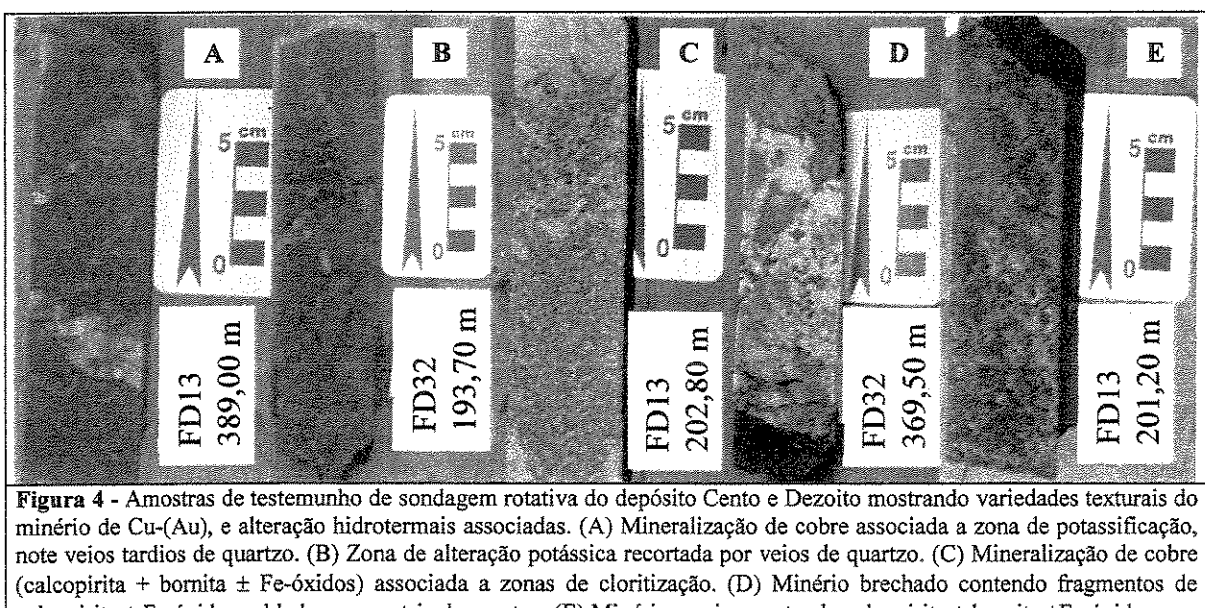
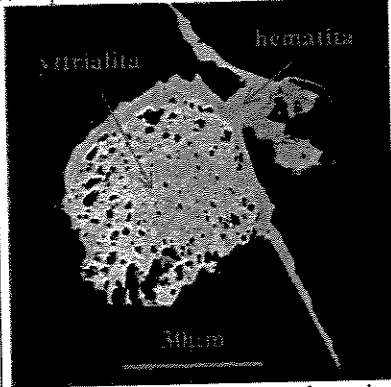


Figura 4 - Amostras de testemunho de sondagem rotativa do depósito Cento e Dezoito mostrando variedades texturais do minério de Cu-(Au), e alteração hidrotermal associadas. (A) Mineralização de cobre associada a zona de potassificação, note veios tardios de quartzo. (B) Zona de alteração potássica recortada por veios de quartzo. (C) Mineralização de cobre (chalcopyrita + bornita ± Fe-óxidos) associada a zonas de cloritação. (D) Minério brechado contendo fragmentos de calcopirita ± Fe-óxidos soldados por matriz de quartzo. (E) Minério maciço contendo calcopirita ± bornita ± Fe-óxidos.

**Prancha 1 – Imagens de elétrons retro-espalhados do minério primário do depósito Cento e Dezoito.**



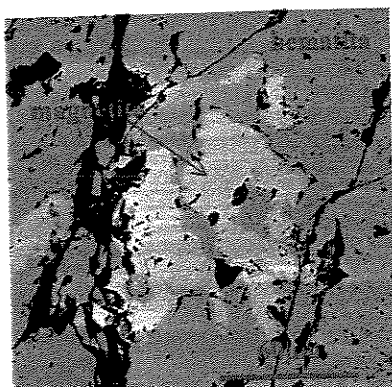
Cristais de hematita associados a calcocirita. Amostra: FD32/369,50m.



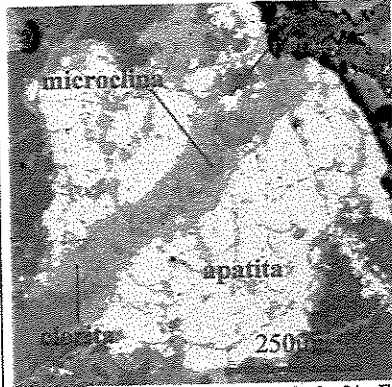
Associação de yttrialia e hematita. Amostra: FD32/369,50m.



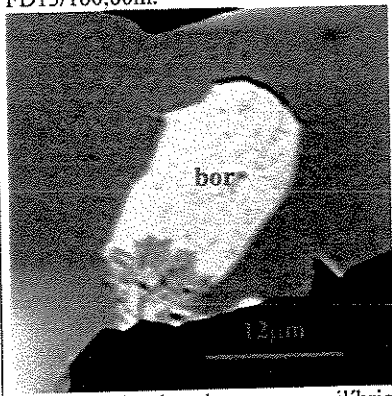
Cristal de turmalina com zonações no conteúdo de FeO. Amostra: FD13/160,80m.



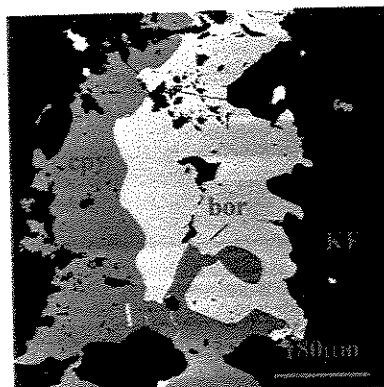
Relictos de magnetita em meio a hematita. Amostra: FD32/369,50m.



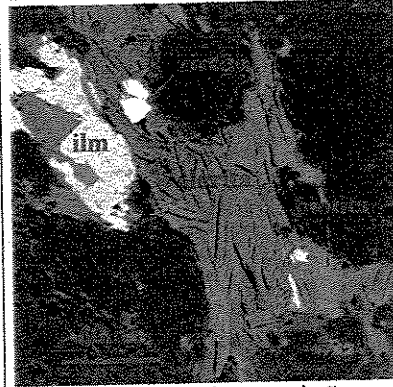
Cristal de apatita com até 3 % F, cortado por veio de clorita ± rutilo ± microclina. Amostra: FD13/160,80m.



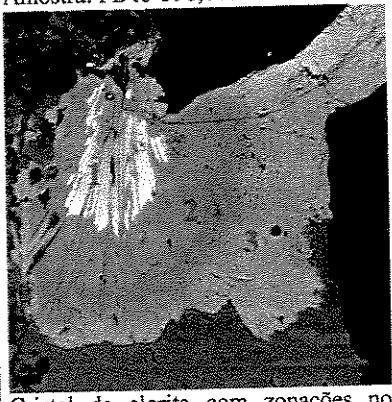
Inclusão de bornita em equilíbrio textural com a calcocirita hospedeira. Amostra: FD13-398,00m.



Intercrescimento de bornita e calcocirita em matriz rica em microclina. Amostra: FD13-398,00m.



Cristais de ilmenita e zircão em associação biotita cloritizada. Amostra: FD32/111,00m.



Cristal de clorita com zonações no conteúdo de FeO<sub>t</sub> (%): 1 = 38,29; 2 = 26,10 e 3 = 29,91 (WDS). Amostra: FD32/148,80m.

**Tabela 3.** Dados isotópicos SHRIMP II corrigidos para  $^{204}\text{Pb}$  para zircões (amostra UWA-B30C) extraídos de tonalito (FD32/101,90-113,60 metros) do depósito Cento e Dezoito.

Grão-área	U (ppm)	Th (ppm)	$f_{206}$ (%) <sup>1</sup>	$^{207}\text{Pb}/^{206}\text{Pb}$	% error	$^{208}\text{Pb}/^{206}\text{Pb}$	% error	$^{206}\text{Pb}/^{238}\text{U}$	% error	$^{207}\text{Pb}/^{235}\text{U}$	% error	$^{208}\text{Pb}/^{232}\text{Th}$	% error	$^{207}\text{Pb}/^{206}\text{Pb}$ Age (Ma)	$^{207}\text{Pb}/^{206}\text{Pb}$ Age $1\sigma$ error
1-1	520	233	0.003	0.19078	0.25432	0.12592	0.45844	0.52573	1.55399	13.82672	1.57484	0.14252	1.62302	2749	4
2-1	459	445	0.018	0.19022	0.28007	0.27150	0.48574	0.53231	1.56250	13.94658	1.58813	0.14424	1.63864	2743	5
3-1	243	159	0.020	0.19048	0.38875	0.18705	0.59163	0.52761	1.61563	13.84073	1.66313	0.14549	1.72994	2745	6
4-1	471	390	0.022	0.19019	0.30621	0.23458	0.43979	0.50095	1.57021	13.12041	1.60132	0.13691	1.63753	2742	5
5-1	119	91	0.029	0.23057	0.52311	0.21413	2.49818	0.59779	2.01701	18.97766	2.08886	0.16180	3.23976	3054	9
6-1	2077	1856	0.214	0.14332	0.37647	0.29897	0.31721	0.17486	1.61540	3.40240	1.67239	0.05568	1.66942	2245	7
7-1	518	454	0.004	0.19088	0.27279	0.24344	0.37136	0.53647	1.78065	14.11558	1.80151	0.14418	1.81928	2749	4
8-1	723	460	0.086	0.18617	0.27160	0.18444	0.67042	0.47622	1.55125	12.16354	1.57751	0.13209	1.70793	2702	5
9-1	490	365	0.027	0.18943	0.33141	0.20760	0.46978	0.52746	1.66188	13.75566	1.69498	0.14196	1.72873	2735	5
10-1	624	458	0.008	0.19035	0.23904	0.20500	0.34913	0.52043	1.54821	13.65289	1.56667	0.14056	1.58771	2745	4
11-1	497	431	0.037	0.18975	0.26848	0.24233	0.36517	0.52566	1.55964	13.72369	1.58348	0.14152	1.60553	2737	5
12-1	483	404	-0.003	0.18998	0.27679	0.23375	0.38361	0.51464	1.56277	13.48253	1.58708	0.13934	1.60916	2742	5
11-2	508	445	0.029	0.18958	0.26805	0.24185	0.36577	0.52869	1.56220	13.79674	1.58600	0.14081	1.60845	2736	4
13-1	455	386	0.050	0.19044	0.28352	0.23679	0.39078	0.51922	1.56612	13.59422	1.59329	0.13962	1.62172	2742	5
14-1	2382	2410	0.016	0.18311	0.14499	0.28831	0.18266	0.39626	1.58054	9.99529	1.58743	0.10912	1.59179	2680	2
15-1	519	452	-0.002	0.18938	0.32083	0.24677	0.39395	0.49409	1.56338	12.90248	1.59597	0.13554	1.61232	2737	5
16-1	607	527	0.005	0.19077	0.33743	0.24778	0.45790	0.51371	1.58163	13.50891	1.61774	0.14177	1.64871	2748	6
17-1	513	442	0.142	0.18935	0.34199	0.24237	0.46639	0.53877	1.59256	13.95223	1.63515	0.14452	1.68625	2725	6
18-1	437	405	-0.021	0.19117	0.31884	0.26359	0.39537	0.52267	1.56964	13.79353	1.60222	0.14429	1.62100	2754	5
19-1	453	434	-0.006	0.18915	0.32383	0.27127	0.42206	0.51030	1.58393	13.31319	1.61676	0.13976	1.63948	2735	5

1 -  $f_{206}$  (%) =  $100 \times \frac{\text{Pb}_{\text{comum}}}{\text{Pb}_{\text{Total}}} / \frac{\text{Pb}_{\text{comum}}}{\text{Pb}_{\text{Total}}}$ , % de  $^{206}\text{Pb}$  atribuído ao Pb comum. Itálico dados rejeitados

**Tabela 4.** Dados isotópicos SHRIMP II corrigidos para  $^{204}\text{Pb}$  para zircões (amostra UWA-B21B) extraídos de diques de composição dacítica (FD32/147,00-150,00 metros) do depósito Cento e Dezoito.

Grão-área	U (ppm)	Th (ppm)	$f_{206}$ (%) <sup>1</sup>	$^{207}\text{Pb}/^{206}\text{Pb}$	% erro	$^{208}\text{Pb}/^{206}\text{Pb}$	% erro	$^{206}\text{Pb}/^{238}\text{U}$	% erro	$^{207}\text{Pb}/^{235}\text{U}$	% erro	$^{208}\text{Pb}/^{232}\text{Th}$	% erro	Idade (Ma)	$^{207}\text{Pb}/^{206}\text{Pb}$	1σ error
1-1	118	191	0.200	0.18094	1.14205	0.44899	1.21955	0.50351	1.82112	12.41281	2.20334	0.13307	2.24551	2645	21	
1-2	78	86	-0.011	0.18151	1.40951	0.29754	2.28017	0.49332	2.16967	12.35403	2.58682	0.12885	3.14749	2668	23	
2-1	456	938	0.059	0.18127	0.58792	0.56664	0.58579	0.51402	0.99695	12.80229	1.17031	0.13656	1.16512	2660	10	
3-1	224	457	0.464	0.18308	0.84356	0.57350	0.83405	0.49087	1.94574	12.05433	2.32070	0.13082	2.25893	2643	21	
3-2	221	397	0.293	0.17886	0.84148	0.48775	0.94340	0.49758	2.07589	12.05545	2.30643	0.12865	2.33879	2618	17	
4-1	282	540	0.171	0.18207	0.75605	0.53766	0.76316	0.50153	1.19987	12.46318	1.48287	0.13529	1.47237	2658	14	
4-2	251	539	0.173	0.18003	0.78964	0.59159	0.77105	0.50246	2.25324	12.34358	2.40455	0.13273	2.39125	2639	14	
5-1	368	976	0.099	0.18456	0.63618	0.74198	0.58937	0.51415	1.07543	13.00829	1.27418	0.13873	1.23683	2686	11	
6-1	65	66	0.364	0.18636	1.53795	0.29278	1.92527	0.51839	3.27469	13.04079	3.75699	0.13983	4.14773	2681	30	
7-1	190	315	0.232	0.18239	0.91685	0.46711	0.96655	0.49072	1.45439	12.17244	1.76126	0.13203	1.78547	2656	16	
8-1	349	847	0.202	0.18036	0.68183	0.67182	0.64415	0.47485	1.09636	11.66637	1.33110	0.12627	1.29091	2639	12	
9-1	241	538	0.230	0.17829	0.78995	0.59567	0.76745	0.52106	1.32866	12.63297	1.57266	0.13338	1.54895	2618	14	

1 -  $f_{206} (\%) = 100 \times \frac{{}^{206}\text{Pb}_{\text{comum}}}{{}^{206}\text{Pb}_{\text{Total}}}$ , % de  $^{206}\text{Pb}$  atribuído ao Pb comum. Itálico dados rejeitados

**Tabela 5.** Dados isotópicos SHRIMP II corrigidos para  $^{204}\text{Pb}$  para zircões (amostra UWA-B21A) extraídos de diques de composição riolítica (FD17/201,59-206,26 metros) do depósito Cento e Dezoito.

Grão-área	U (ppm)	Th (ppm)	$f_{206}$ (%) <sup>1</sup>	Idade $\frac{^{207}\text{Pb}}{^{206}\text{Pb}}$											
				$^{207}\text{Pb}/^{206}\text{Pb}$	% erro	$^{208}\text{Pb}/^{206}\text{Pb}$	% erro	$^{206}\text{Pb}/^{238}\text{U}$	% erro	$^{207}\text{Pb}/^{235}\text{U}$	% erro	$^{208}\text{Pb}/^{232}\text{Th}$	% erro	(Ma)	1 $\sigma$ error
1-1	71	91	0.000	0.18227	1.55100	0.36428	1.78363	0.49051	2.37704	12.32705	2.83829	0.13467	2.97181	2674	26
1-2	181	332	0.294	0.18195	0.93580	0.51856	1.69744	0.49871	1.52048	12.29493	1.87270	0.13444	2.33485	2647	18
2-1	37	28	0.471	0.16764	2.23226	0.21659	3.05006	0.44484	6.12149	9.97797	6.61418	0.11587	7.15543	2492	42
3-1	677	315	3.039	0.21274	0.54538	0.19631	0.90003	0.37096	0.88641	9.20701	1.79490	0.09410	6.70587	2704	25
4-1	35107	11165	0.457	0.05741	0.39607	0.15225	0.42431	0.05718	0.51085	0.42160	1.01138	0.02483	1.14212	360	20
5-1	211	320	0.381	0.18386	0.88744	0.42325	0.97217	0.48433	1.39958	12.00529	1.81961	0.12781	1.90626	2657	19
6-1	98	205	0.323	0.17958	1.27278	0.57417	1.24997	0.50330	3.53659	12.22234	3.83428	0.13215	3.79838	2622	25
7-1	2599	8553	11.476	0.18833	3.31167	0.99177	0.94401	0.10683	1.23651	1.17422	13.32365	0.02320	4.23964	1427	252
8-1	144	345	0.188	0.19189	1.05023	0.66747	1.00351	0.49566	1.68915	12.97462	2.13292	0.13325	2.04967	2744	21
9-1	198	776	0.302	0.18089	0.90966	1.09416	0.97366	0.51050	1.56280	12.50520	1.99037	0.13723	1.87564	2636	20
10-1	304	979	0.089	0.18419	0.71166	0.83961	0.63500	0.52539	1.69883	13.27374	1.86438	0.13207	1.82109	2684	13
11-1	88	246	0.923	0.18637	1.34397	0.77043	1.30836	0.52059	2.16245	12.66845	2.79620	0.13488	2.62038	2636	29
12-1	536	1362	0.927	0.17294	0.67350	0.67127	0.62657	0.36302	1.17195	8.16611	1.69822	0.08978	1.50060	2504	20
13-1	883	2991	0.237	0.18185	0.43553	0.91960	0.38776	0.50701	0.82520	12.53477	0.96595	0.13234	0.92105	2650	8
14-1	433	942	0.231	0.18039	0.60372	0.59346	0.59230	0.50982	1.03328	12.50667	1.25032	0.13324	1.22499	2637	12
6-2	134	273	0.337	0.18310	1.08409	0.57183	1.07487	0.51436	1.68550	12.72934	2.13819	0.13780	2.09088	2654	22
15-1	1029	437	0.188	0.16334	0.54991	0.06623	1.24339	0.27973	0.77761	6.22372	0.99893	0.03934	2.51313	2473	11
16-1	6267	2515	0.745	0.06723	0.79079	0.12508	0.97029	0.04387	0.61975	0.36695	1.96546	0.01156	2.87640	643	40
17-1	778	541	0.314	0.16328	0.64128	0.10162	1.19347	0.26796	1.01335	5.91050	1.30696	0.03513	2.78835	2461	14

1 -  $f_{206}$  (%) =  $100 \times \frac{\text{Pb}_{\text{comum}}}{\text{Pb}_{\text{Total}}} / \frac{^{206}\text{Pb}_{\text{Total}}}{^{206}\text{Pb}_{\text{comum}}}$ , % de  $^{206}\text{Pb}$  atribuído ao Pb comum. Itálico dados rejeitados

**Tabela 6.** Dados isotópicos SHRIMP II corrigidos para  $^{204}\text{Pb}$  para xenotitas (amostra UWA-B36D) extraídas de minério maciço (FD77/116,00 metros) do depósito Cento e Dezoito.

grain-spot	U (ppm)	Th (ppm)	Th/U	4f206 (%)	$^{207}\text{Pb}^*/^{206}\text{Pb}$	$^{208}\text{Pb}^*/^{206}\text{Pb}^*$	$^{207}\text{Pb}^*/^{235}\text{U}$	$^{206}\text{Pb}^*/^{238}\text{U}$	$^{208}\text{Pb}^*/^{232}\text{Th}$	conc. (%)	$^{207}\text{Pb}^*/^{206}\text{Pb}$ Age (Ma)
2-1	604	60	0.10	0.076	$0.1137 \pm 9$	$0.0281 \pm 12$	$0.3242 \pm 78$	$5.080 \pm 133$	$0.0917 \pm 46$	97	$1859 \pm 14$
4-1	778	1327	1.71	0.042	$0.1133 \pm 8$	$0.4930 \pm 37$	$0.3180 \pm 72$	$4.967 \pm 121$	$0.0920 \pm 23$	96	$1853 \pm 13$
5-1	715	157	0.22	0.164	$0.1138 \pm 9$	$0.0548 \pm 16$	$0.3292 \pm 75$	$5.166 \pm 130$	$0.0821 \pm 31$	99	$1861 \pm 14$
6-1	1518	4921	3.24	0.025	$0.1142 \pm 6$	$0.9453 \pm 43$	$0.3115 \pm 66$	$4.907 \pm 112$	$0.0909 \pm 21$	94	$1868 \pm 9$
7-1	3250	987	0.30	0.035	$0.1150 \pm 4$	$0.0876 \pm 7$	$0.3296 \pm 69$	$5.226 \pm 112$	$0.0950 \pm 22$	98	$1880 \pm 6$
8-1	644	2675	4.15	0.015	$0.1151 \pm 9$	$1.2303 \pm 71$	$0.3204 \pm 76$	$5.085 \pm 131$	$0.0950 \pm 25$	95	$1881 \pm 13$
9-1	4304	8871	2.06	0.012	$0.1142 \pm 3$	$0.6059 \pm 17$	$0.3280 \pm 67$	$5.167 \pm 109$	$0.0964 \pm 20$	98	$1868 \pm 5$
10-1	1469	742	0.51	0.013	$0.1146 \pm 5$	$0.1370 \pm 13$	$0.3335 \pm 70$	$5.268 \pm 119$	$0.0905 \pm 22$	99	$1873 \pm 8$
12-1	847	2222	2.62	0.149	$0.1131 \pm 8$	$0.7564 \pm 44$	$0.3155 \pm 71$	$4.918 \pm 120$	$0.0910 \pm 23$	96	$1849 \pm 13$
15-1	1111	1538	1.38	0.006	$0.1148 \pm 6$	$0.4043 \pm 25$	$0.3238 \pm 69$	$5.125 \pm 118$	$0.0946 \pm 22$	96	$1877 \pm 10$
18-1	1052	910	0.87	0.037	$0.1144 \pm 7$	$0.1579 \pm 23$	$0.3203 \pm 70$	$5.053 \pm 117$	$0.0585 \pm 16$	96	$1870 \pm 11$
19-1	1045	1167	1.12	0.129	$0.1129 \pm 8$	$0.3189 \pm 26$	$0.3308 \pm 73$	$5.150 \pm 123$	$0.0945 \pm 23$	100	$1847 \pm 12$
Young outlier											
13-1	1501	1312	0.87	0.069	$0.1122 \pm 5$	$0.2610 \pm 18$	$0.3039 \pm 63$	$4.699 \pm 105$	$0.0908 \pm 21$	93	$1835 \pm 9$
High common Pb											
3-1	1110	3131	2.82	19.398	$0.1152 \pm 418$	$0.1762 \pm 963$	$0.0218 \pm 11$	$0.348 \pm 122$	$0.0014 \pm 7$	7	$1883 \pm 699$
11-1	4958	7303	1.47	11.198	$0.1206 \pm 46$	$0.3002 \pm 106$	$0.3463 \pm 86$	$5.757 \pm 275$	$0.0706 \pm 31$	98	$1965 \pm 68$
14-1	794	14	0.02	20.956	$0.1358 \pm 254$	$0.1744 \pm 588$	$0.0318 \pm 12$	$0.595 \pm 109$	$0.3112 \pm 989$	9	$2174 \pm 331$
16-1	2189	1536	0.70	2.917	$0.1155 \pm 20$	$0.2198 \pm 47$	$0.2193 \pm 46$	$3.491 \pm 101$	$0.0687 \pm 21$	68	$1887 \pm 31$

Uncertainties refer to the last digits listed.

**Tabela 7.** Dados isotópicos SHRIMP II corrigidos para  $^{204}\text{Pb}$  para xenotitas (amostra UWA-B35) extraídas de veio de quartzo + calcita (FD36/112.5-112.6m metros) do depósito Cento e Dezoito.

grain-spot	U (ppm)	Th (ppm)	Th/U	4f206 (%)	$^{207}\text{Pb}^*/^{206}\text{Pb}$	$^{208}\text{Pb}^*/^{206}\text{Pb}^*$	$^{207}\text{Pb}^*/^{235}\text{U}$	$^{206}\text{Pb}^*/^{238}\text{U}$	$^{208}\text{Pb}^*/^{232}\text{Th}$	conc. (%)	$^{207}\text{Pb}^*/^{206}\text{Pb}$ Age (Ma)
B35.5-2	3413	9563	2.80	0.019	$0.1145 \pm 4$	$0.8072 \pm 24$	$0.3312 \pm 68$	$5.229 \pm 112$	$0.0954 \pm 20$	99	$1872 \pm 6$
B35.5-3	3607	348	0.10	0.029	$0.1145 \pm 4$	$0.0270 \pm 5$	$0.3257 \pm 66$	$5.141 \pm 111$	$0.0911 \pm 25$	97	$1872 \pm 7$
B35.6-1	922	35	0.04	0.076	$0.1150 \pm 8$	$0.0096 \pm 11$	$0.3191 \pm 71$	$5.061 \pm 124$	$0.0796 \pm 86$	95	$1880 \pm 13$
B35.6-2	2647	260	0.10	0.024	$0.1148 \pm 4$	$0.0277 \pm 5$	$0.3281 \pm 68$	$5.196 \pm 112$	$0.0925 \pm 25$	97	$1877 \pm 7$
B35.6-3	1593	117	0.07	0.043	$0.1144 \pm 6$	$0.0198 \pm 8$	$0.3265 \pm 69$	$5.152 \pm 117$	$0.0879 \pm 38$	97	$1871 \pm 9$
B35.6-4	3300	269	0.08	0.052	$0.1137 \pm 5$	$0.0243 \pm 5$	$0.3228 \pm 69$	$5.060 \pm 115$	$0.0961 \pm 30$	97	$1859 \pm 9$
B35.6-5	2888	205	0.07	0.029	$0.1144 \pm 5$	$0.0196 \pm 4$	$0.3295 \pm 69$	$5.199 \pm 113$	$0.0909 \pm 28$	98	$1871 \pm 7$
B35.6-6	754	25	0.03	0.167	$0.1137 \pm 9$	$0.0060 \pm 12$	$0.3238 \pm 75$	$5.078 \pm 128$	$0.0589 \pm 114$	97	$1860 \pm 14$
B35.6-7	2145	418	0.19	0.054	$0.1140 \pm 5$	$0.0532 \pm 7$	$0.3340 \pm 70$	$5.251 \pm 114$	$0.0913 \pm 23$	100	$1864 \pm 7$
B35.6-8	1025	491	0.48	0.130	$0.1129 \pm 7$	$0.1469 \pm 18$	$0.3336 \pm 74$	$5.191 \pm 125$	$0.1024 \pm 28$	101	$1846 \pm 12$
B35.6-9	2108	385	0.18	0.154	$0.1128 \pm 7$	$0.0484 \pm 11$	$0.3395 \pm 73$	$5.279 \pm 124$	$0.0900 \pm 29$	102	$1845 \pm 10$
B35.6-10	2758	277	0.10	0.037	$0.1143 \pm 6$	$0.0314 \pm 7$	$0.3283 \pm 71$	$5.172 \pm 118$	$0.1027 \pm 34$	98	$1868 \pm 9$
Young outliers											
B35.5-7	1526	5804	3.80	0.179	$0.1110 \pm 7$	$1.1103 \pm 46$	$0.3080 \pm 65$	$4.715 \pm 109$	$0.0899 \pm 21$	95	$1816 \pm 11$
B35.5-8	1284	2412	1.88	0.169	$0.1121 \pm 8$	$0.5532 \pm 35$	$0.3424 \pm 76$	$5.291 \pm 128$	$0.1008 \pm 25$	103	$1834 \pm 13$
Discordant											
B35.5-1	1499	5367	3.58	0.326	$0.1138 \pm 10$	$0.9781 \pm 56$	$0.4389 \pm 116$	$6.886 \pm 199$	$0.1199 \pm 36$	126	$1861 \pm 16$
B35.5-4	1994	6460	3.24	0.070	$0.1107 \pm 5$	$0.9708 \pm 36$	$0.2794 \pm 57$	$4.265 \pm 94$	$0.0837 \pm 18$	88	$1811 \pm 8$
B35.5-5	1211	1184	0.98	0.070	$0.1112 \pm 10$	$0.3185 \pm 33$	$0.2634 \pm 67$	$4.037 \pm 114$	$0.0858 \pm 27$	83	$1819 \pm 16$
B35.5-6	1249	2377	1.90	0.214	$0.1115 \pm 8$	$0.5635 \pm 35$	$0.2996 \pm 66$	$4.607 \pm 110$	$0.0887 \pm 22$	93	$1825 \pm 13$

Uncertainties refer to the last digits listed.

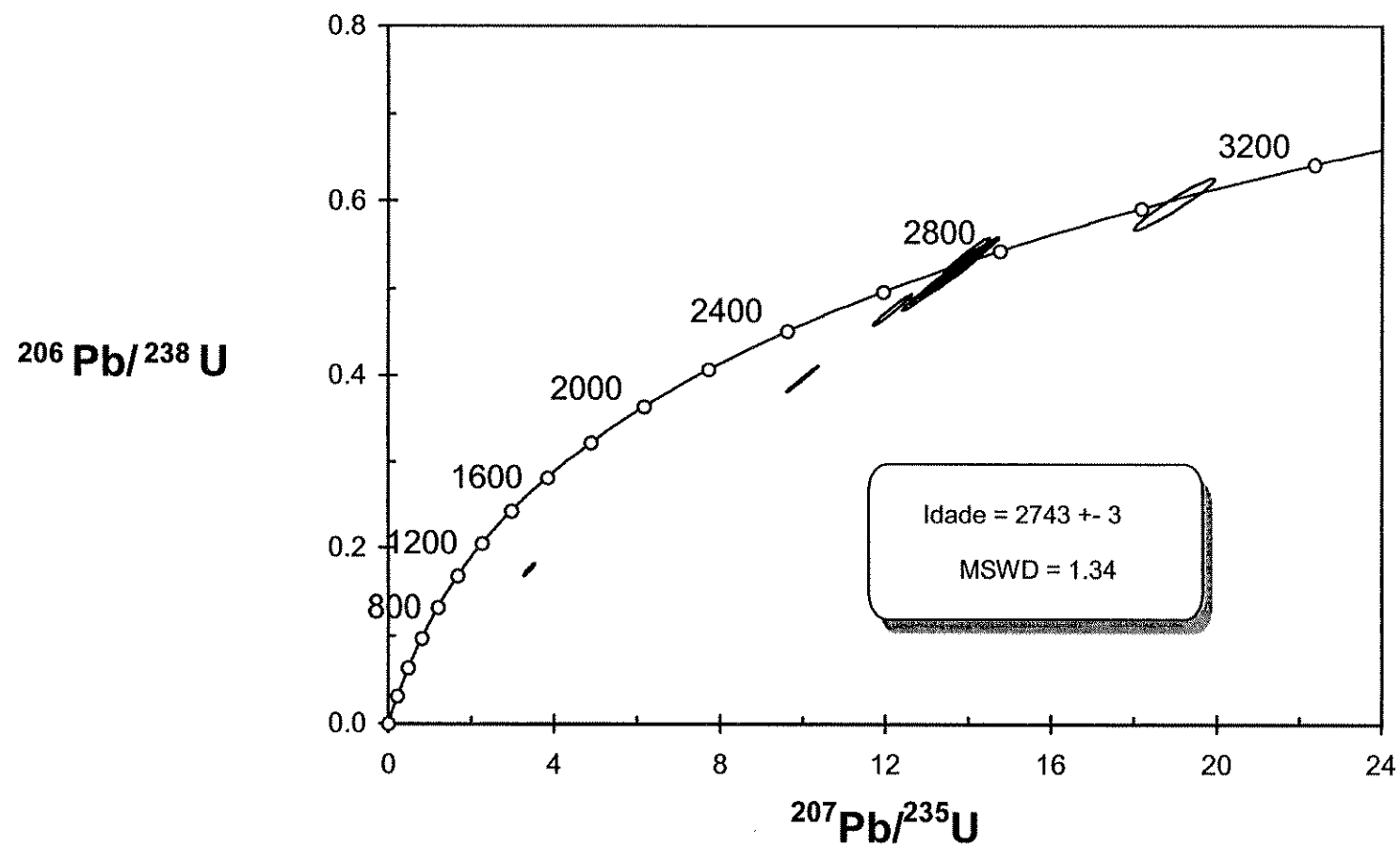


**Figura 5.** Diagrama concórdia mostrando os resultados de SHRIMP II obtidos em zircões (UWA-B30C) extraídos de tonalito (FD32/101,90-113,60 m) do depósito Cento e Dezoito.

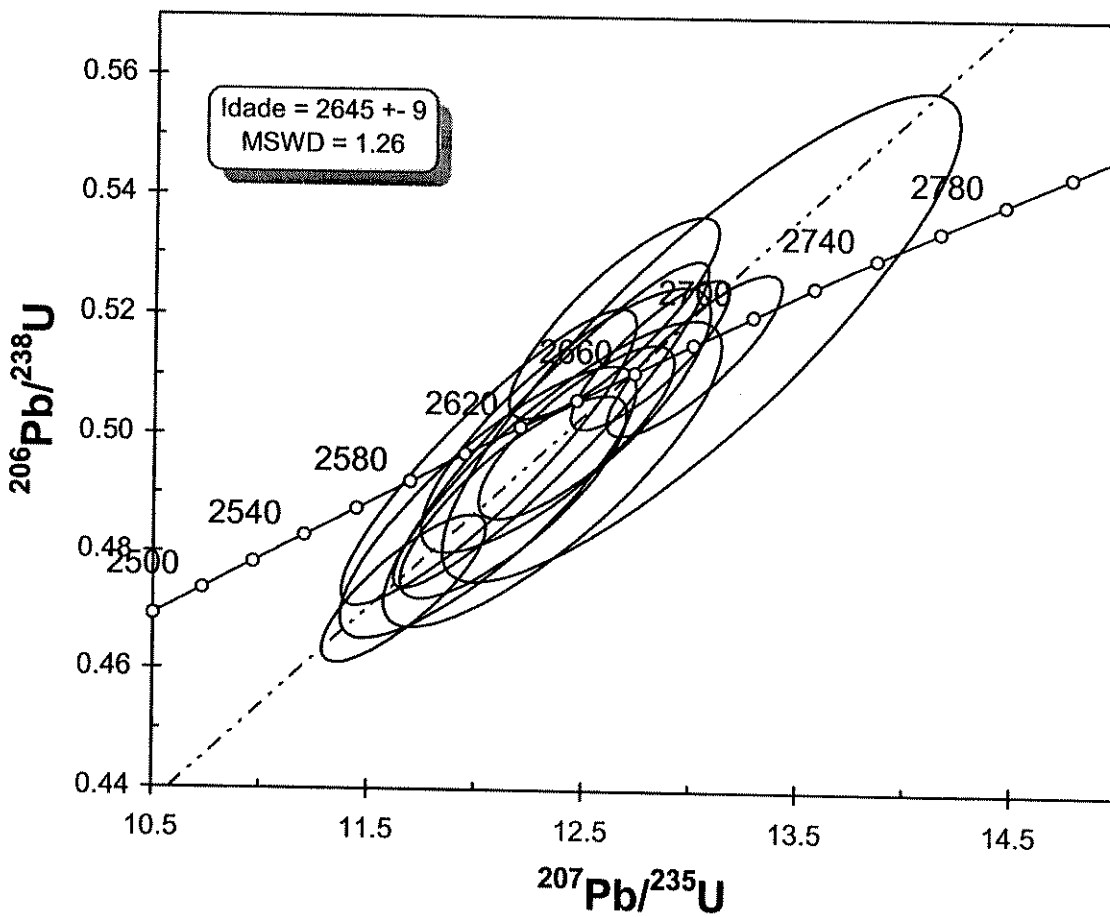


**Figura 6.** Diagrama concórdia mostrando os resultados de SHRIMP II obtidos em zircões (UWA-B21B) extraídos de dique de composição dacítica (FD32/147.00-150.00m) do depósito Cento e Dezoito.

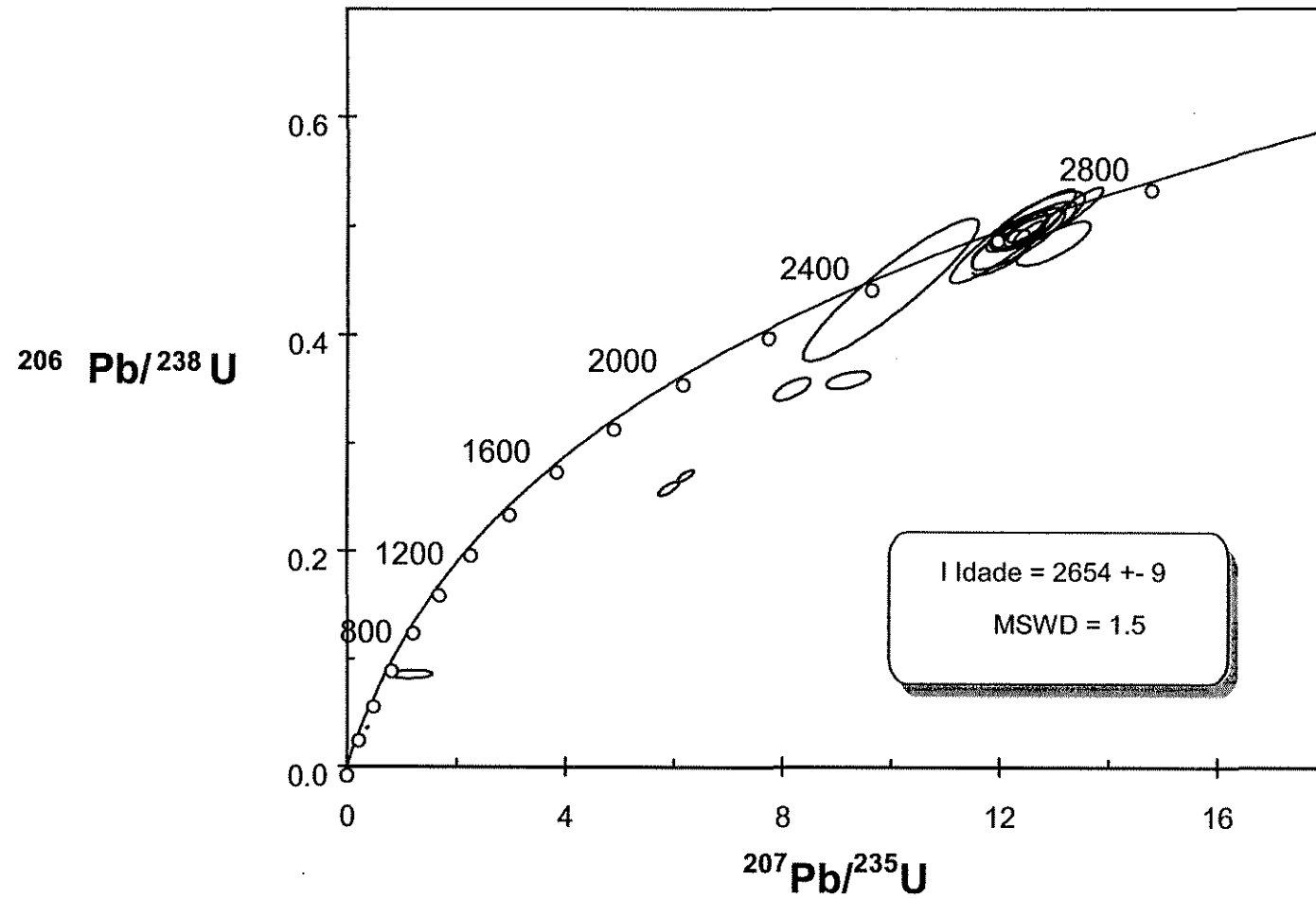


**Figura 7.** Diagrama concórdia mostrando os resultados de SHRIMP II obtidos em zircões (UWA-B21A) extraídos de dique de composição riolítica (FD17/201,59-206,26 m) do depósito Cento e Dezoto.

SHRIMP mount: UWA-B36D; Mineral: Xenotime Sample Code: OPU-1641;  
Field Reference: FD77116m; Rock Type: Bulk Cu-(Au) Ore;  
Deposit: 118 Cu-(Au) mineralization, Carajás Copper-Gold Belt, Brazil

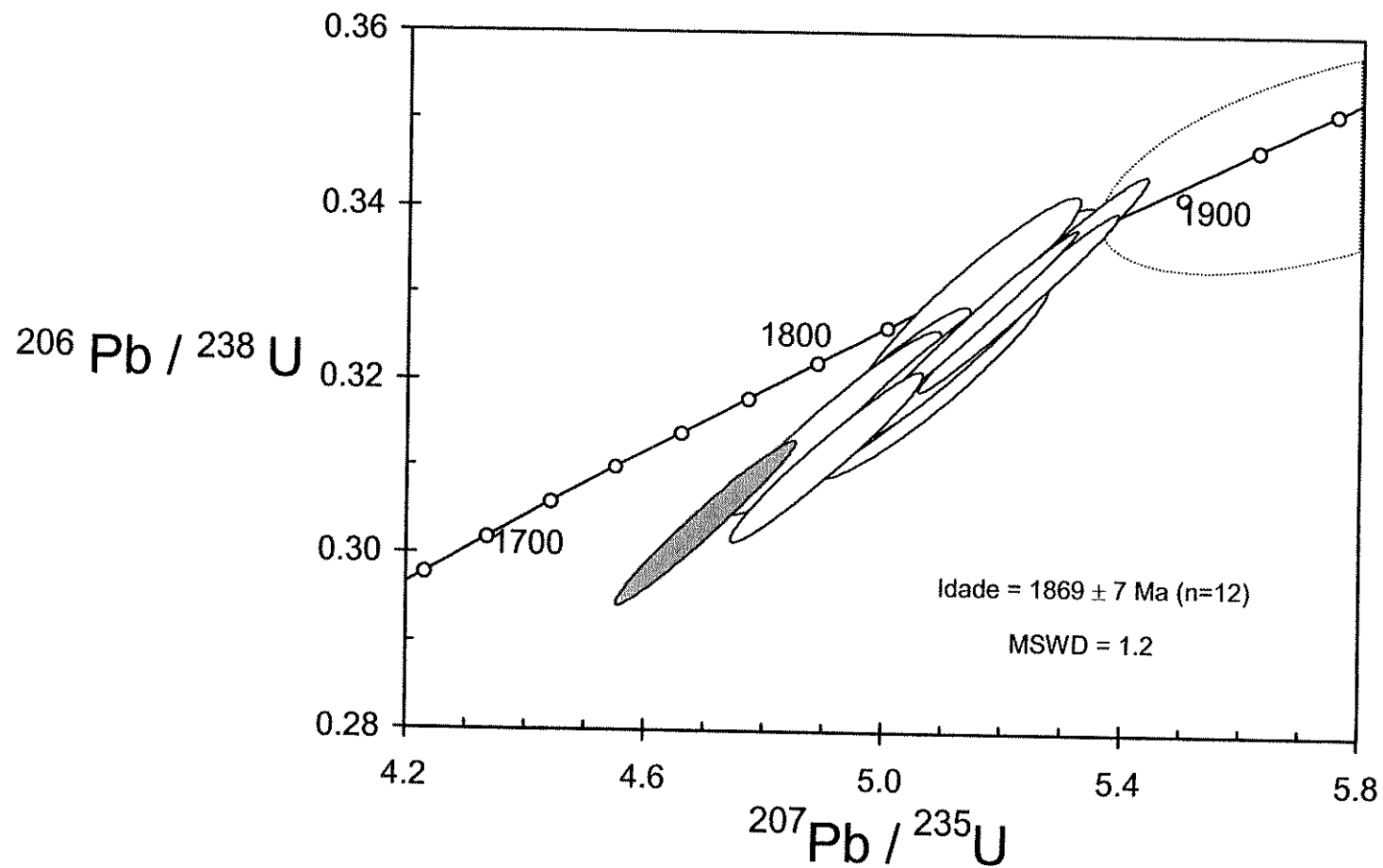


Figura 8. Diagrama concórdia mostrando os resultados de SHRIMP II obtidos em xenotimas (UWA-B36D) extraídas de minério maciço (FD77/116,00 m) do depósito Cento e Dezoito.

SHRIMP mount: UWA-B35; Mineral: Xenotime Sample Code: PT-011;  
Field Reference: FD36/112.5-112.6m; Rock Type: Quartz-calcite vein;  
Deposit: 118 Cu-(Au) mineralization, Carajás Copper-Gold Belt, Brazil

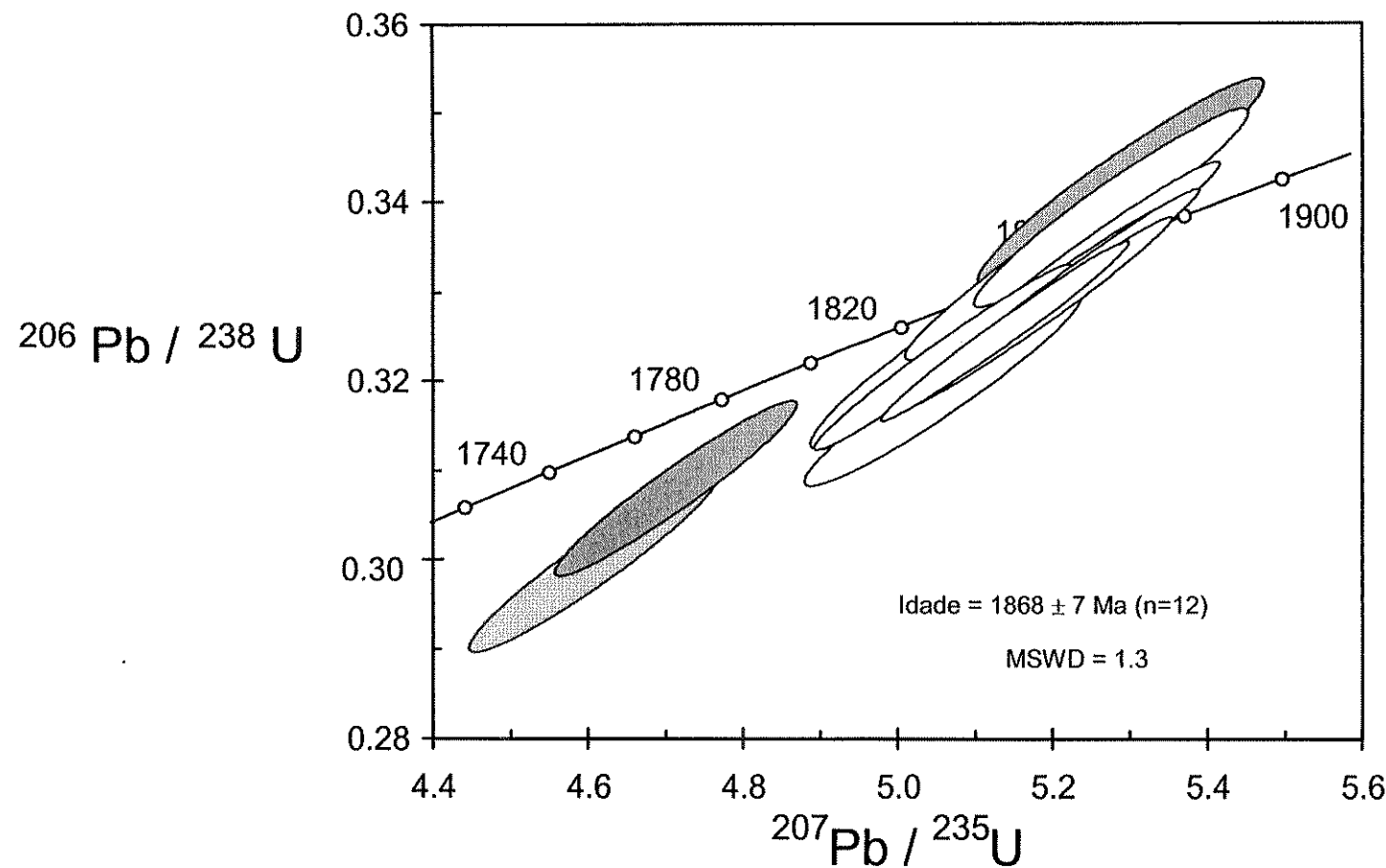


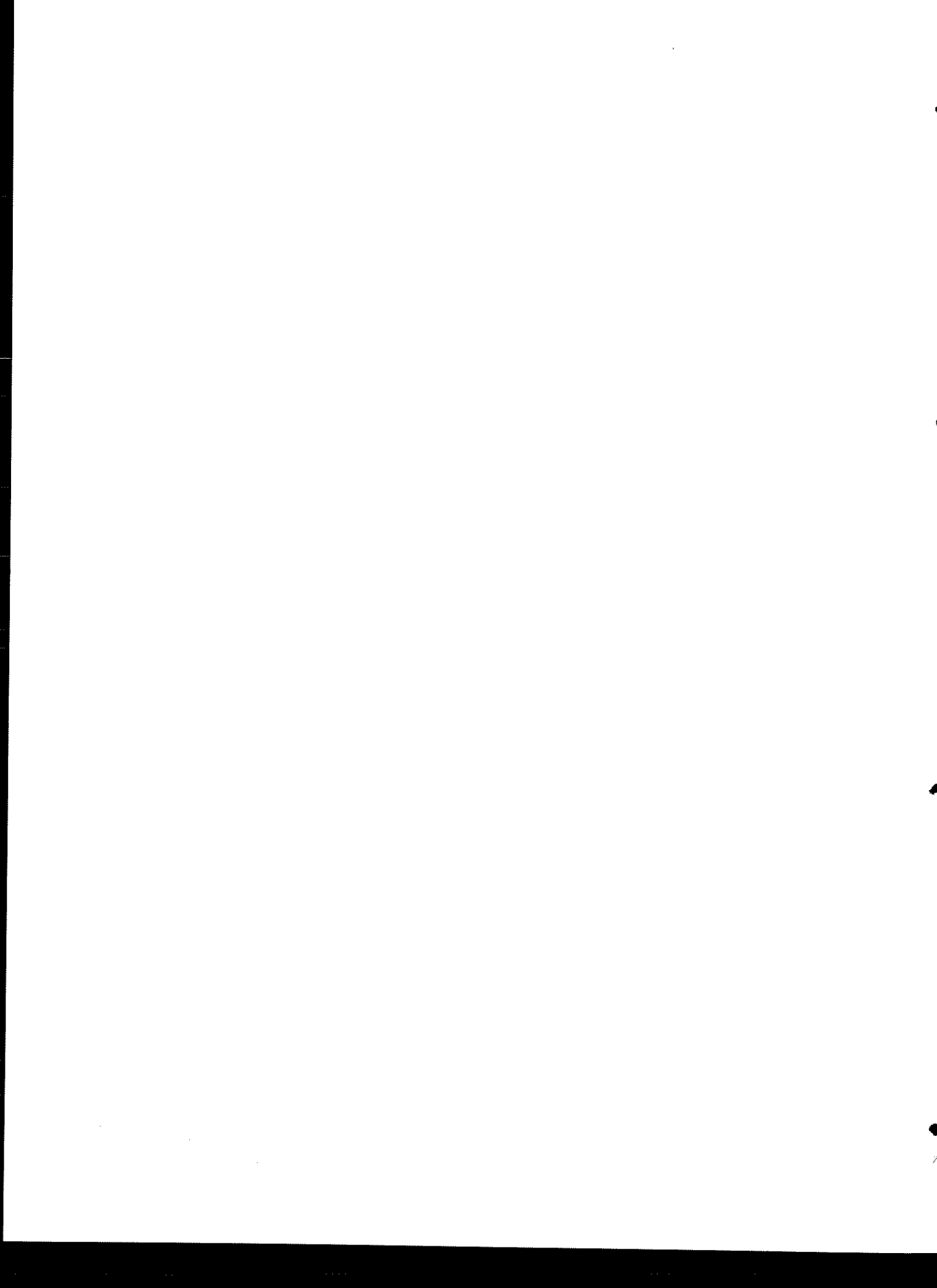
Figura 9. Diagrama concórdia mostrando os resultados de SHRIMP II obtidos em xenotimas (UWA-B35) extraídas de veio de quartzo + calcita (FD36/112,50-112,60 m) do depósito Cento e Dezoito.



## **ANEXO 7**

Report to the Society of Economic Geologists Foundation, Inc.  
Hugh E. McKinstry Grant for year 2000  
Pb-Pb Isotopic Results

**UNICAMP**  
**BIBLIOTECA CENTRAL**  
**SEÇÃO CIRCULANTE**



# Report to the Society of Economic Geologists Foundation, Inc.

## Hugh E. McKinstry Grant for year 2000

### Pb-Pb Isotopic Results

*Project:* Genesis of the Igarapé Bahia copper-gold mineralization, Carajás Province, Brazil.

*Ph.D. student:* Fernando Henrique Bucco Talarico (Instituto de Geociências - UNICAMP).

*Supervisor:* Dr. Bernardino Ribeiro Figueiredo (Instituto de Geociências - UNICAMP).

#### 1. Introduction

The project "Genesis of the Igarapé Bahia copper-gold mineralization, Carajás Province, Brazil" is being developed at the State University of Campinas – UNICAMP, Brazil.

The Igarapé Bahia deposit is today the largest Brazilian gold mine, with an annual production of ca. 12 tons. Although the obvious economic significance, the absence of systematic data has precluded the construction of consistent genetic and prospective models.

This project includes detailed fieldwork, followed by a series of petrographical, mineralogical and geochemical investigations. This information will support the conduction of radioactive isotope analysis, that represents the core of the project. By determining the age of the mineralization, as well as the source of fluids and metals, we expect to elaborate a genetic model that can possibly improve further exploration programs in the Carajás Copper-Gold Belt.

#### 2. Field work, petrography, SEM, EMPA and geochemistry

The results of fieldwork, petrography, SEM, EMPA and bulk geochemistry were summarized in descriptive model of the Igarapé Bahia Cu-Au mineralization that was published as an abstract at the 31 International Geological Congress (Rio de Janeiro, 2000), and latter as a complete article in the Revista Brasileira de Geociências (Brazilian Geoscience Journal).

#### 3. Radioactive Isotopes

The isotopic investigation of the Igarapé Bahia mineralization is focussed on Pb-Pb, Sr-Sr and U-Pb SHRIMP methods. The Pb-Pb and Sr-Sr analyses are being conducted at the University of São Paulo (USP), Brazil, under the supervision of Dr. Babinski and Dr. Tassinari. The U-Pb SHRIMP analyses will be carried out at the University of Western Australia (UWA) and will be supervised by Dr. Neal McNaughton. The funds from SEGf grant were totally applied to cover part of the Pb-Pb analyses that were held at USP.

#### 4. Pb-Pb results

Sample preparation involved routine techniques of heavy liquids and magnetic separations followed by hand picking. For the Pb-Pb analyses we adopted the step leaching method, that has been successfully employed on pyrite, chalcopyrite, pyrrhotite, molybdenite, magnetite and also on some silicate minerals (e.g. Carignan & Gariépy 1993; Carignan et al. 1993). This method was also adopted successfully on sulfide minerals, magnetite and tourmaline from the Carajás Copper-Gold Belt (e.g. Mellito 1998; Mougeot 1996).

The method consists of sequence of leaching where the concentration of the acid, or combination of acids, is progressively increased. Lead is purified via ionic exchange column and analyzed in a mass spectrometer. The isotopic diagrams were produced using ISOPLOT from Ludwig (1993), with an error of  $2\sigma$  and a confidence of 95%. Three samples of Igarapé Bahia, including siderite, magnetite and chalcopyrite were analyzed. The results are available in Table 1.

The isotopic analyses of chalcopyrite yielded the following ratios:  $^{207}\text{Pb}/^{204}\text{Pb}$ : 26.402 to 27.298,  $^{206}\text{Pb}/^{204}\text{Pb}$ : 63.823 to 69.832 and  $^{208}\text{Pb}/^{204}\text{Pb}$ : 61.865 to 65.760. From the alignment of data on the  $^{206}\text{Pb}/^{204}\text{Pb}$  vs.  $^{207}\text{Pb}/^{204}\text{Pb}$  diagram an age of  $2303 \pm 120$  Ma was calculated (Figure 1). It is important to point out that the analytical data from chalcopyrite showed a very limited spread, which is extremely undesired. The  $^{206}\text{Pb}/^{204}\text{Pb}$  vs.  $^{208}\text{Pb}/^{204}\text{Pb}$  diagram (Figure 2) revealed a poor alignment of the data, possibly denoting that chalcopyrite was not in equilibrium with the U-Th-bearing fluid phase from which it crystallized. Inclusions of monazite and uraninite in chalcopyrite (Figure 3) could be responsible for the spread of the  $^{206}\text{Pb}/^{204}\text{Pb}$  vs.  $^{208}\text{Pb}/^{204}\text{Pb}$  data.

The isotopic analyses of siderite yielded the following ratios:  $^{207}\text{Pb}/^{204}\text{Pb}$ : 22.547 to 41.838,  $^{206}\text{Pb}/^{204}\text{Pb}$ : 34.738 to 101.247 and  $^{208}\text{Pb}/^{204}\text{Pb}$ : 34.542 to 37.388. These results when plotted on the  $^{206}\text{Pb}/^{204}\text{Pb}$  vs.  $^{207}\text{Pb}/^{204}\text{Pb}$  diagram yielded an age of  $3414 \pm 800$  Ma (Figure 4). Although the spreading of

data is satisfactory, the analytical errors are extremely high (Table 4), leading to an unacceptable error of  $\pm$  800 Ma. The relative alignment of the data on the  $^{206}\text{Pb}/^{204}\text{Pb}$  vs.  $^{208}\text{Pb}/^{204}\text{Pb}$  diagram (Figure 5) suggests equilibrium of siderite with the U-Th-bearing fluid phase.

The isotopic analyses of magnetite yielded the following ratios:  $^{207}\text{Pb}/^{204}\text{Pb}$ : 15.624 to 44.846,  $^{206}\text{Pb}/^{204}\text{Pb}$ : 16.814 to 162.666 and  $^{208}\text{Pb}/^{204}\text{Pb}$ : 36.514 to 179.349. The  $^{206}\text{Pb}/^{204}\text{Pb}$  vs.  $^{207}\text{Pb}/^{204}\text{Pb}$  diagram allowed the calculation of an age of  $2865 \pm 220$  Ma (Figure 6). Although the data presented a good spreading, the error of sample L3 and the low emission of L1 resulted in a high error in the age. The alignment of the data on the  $^{206}\text{Pb}/^{204}\text{Pb}$  vs.  $^{208}\text{Pb}/^{204}\text{Pb}$  diagram suggests equilibrium of magnetite with the U-Th-bearing fluid phase (Figure 7).

### 5. Discussion

In addition to the mentioned restrictions related to the Pb-Pb results, the ages obtained from siderite and magnetite are older than the Grão Pará volcano-sedimentary sequence that was dated by various authors in ca. 2.75 Ga (e.g. Gibbs et al. 1986; Olszewski et al. 1989; Machado et al. 1991). The calculated ages of siderite and magnetite are incoherent with the geological framework, once the volcano-sedimentary rocks that host the Igarapé Bahia mineralization are probably related to the Grão Pará sequence. In the Carajás region, older ages were only reported on the basement rocks, that includes the Xingú Complex (ca. 2.8 Ga - Machado et al. 1991) and the Pium Complex (ca. 3.0 Ga - Rodrigues et al. 1992) and also on the metavolcanic rocks of the Lagoa Seca Group (ca. 2.9 Ga - Pimentel e Machado 1994). The latter occurs only at the southern portion of the Carajás Province and are not related to the Grão Pará sequence that occurs at the northern portion. Likewise, the age obtained from chalcopyrite also seems inconsistent with the regional setting, once no geological event of equivalent age yet known in the province.

All the Pb-Pb ratios of hydrothermal minerals from the Igarapé Bahia deposit are extremely radiogenic and strongly suggest crustal derivation.

### 6. References

- Carignan, J.; Garaiépy, C. 1993. Pb isotope geochemistry of the Slidor and Launay gold deposits: Implications for the source of the Archean Au in the Abitibi Subprovince. *Economic Geology*, 88: 1722-1730.
- Carignan, J.; Machado, N.; Garaiépy, C. 1993. Pb isotope composition of Ni-Cu-Pb ore deposits in an Archean greenstone belt: evidence for Proterozoic remobilization in the Pontiac Subprovince of Canada. *Economic Geology*, 88: 709-715.
- Gibbs, A.K.; Wirth, K.R.; Hirata, W.K.; Olszewski, W.J. 1986. Age and composition os the Grão Pará Group volcanics, Serra dos Carajás. *Revista Brasileira de Geociências*, 16(2): 201-211.
- Huhn, S.R.B.; Macambira, M.J.B.; Dall'Agnol, R. 1999. Geologia e geocronologia Pb/Pb do granito alcalino Arqueano Planalto, Região da Serra do Rabo, Carajás - PA. In: SBG, Simpósio de Geologia da Amazônia, 6, Manaus, *Resumos Expandidos*, 463-466
- Ludwig, K.R. 1993. Isoplot: a plotting and regression program for radiogenic-isotope data, version 2.70. Open-file report 91-445. United States Geological Survey. 42p.
- Machado, N.; Lindenmayer, Z; Krogh, T.E.; Lindenmayer, D. 1991. U-Pb geochronology of Archean magmatism and basement reactivation in the Carajás area, Amazon Shield, Brazil. *Precambrian Research*, 49:329-354
- Mellito, K.M. 1998. Aplicações dos sistemas Rb-Sr, Pb-Pb e Sm-Nd no depósito polimetálico do Salobo 3A, Província Mineral de Carajás, Pará. Inst. Geociências, USP, São Paulo, Master Thesis, 113p.
- Mougeot, R. 1996. Etude de la limite Archeen-Proterozoique et des mineralizations Au,  $\pm$  U associees: Exemples des regions de Jacobina (Etat de Bahia, Bresil) et de Carajás (Etat de Para, Bresil). Université Montpellier II, Ph. D. Thesis, 309p.
- Olszewski, W.J.; Wirth, K.R.; Gibbs, A.K.; Gaudette, H.E. 1989. The age, origin and tectonics of the Grão Pará Group and associated rocks, Serra dos Carajás, Brazil: Archean continental vulcanism and rifting. *Precambrian Research*, 42:229-254.
- Pimentel , M.M. e Machado, N. 1994. Geocronologia U-Pb dos terrenos granito-greenstone do Rio Maria, Pará. 38 Cong. Bras. Geol. Camburiú. *Anais...*390-391.
- Rodrigues, E.S.; Lafon, J.M.; Scheller, T. 1992. Geocronologia Pb-Pb da Província Mineral de Carajás: primeiros resultados. In: SBG, Congresso Brasileiro de Geologia, 37, São Paulo, *Resumos Expandidos*, 2: 183-184

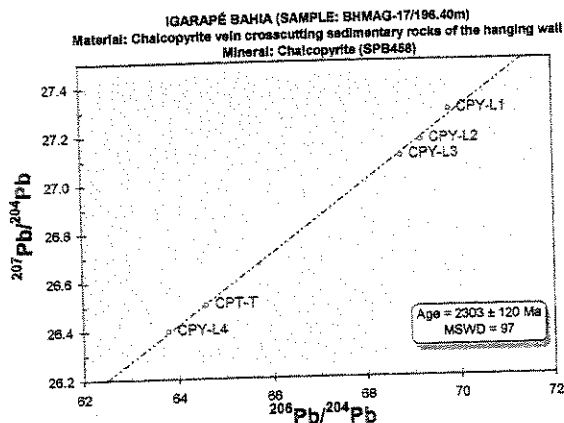


Figure 1 –  $^{207}\text{Pb}/^{204}\text{Pb}$  vs.  $^{206}\text{Pb}/^{204}\text{Pb}$  isochronic diagram with the calculated age obtained from chalcopyrite.

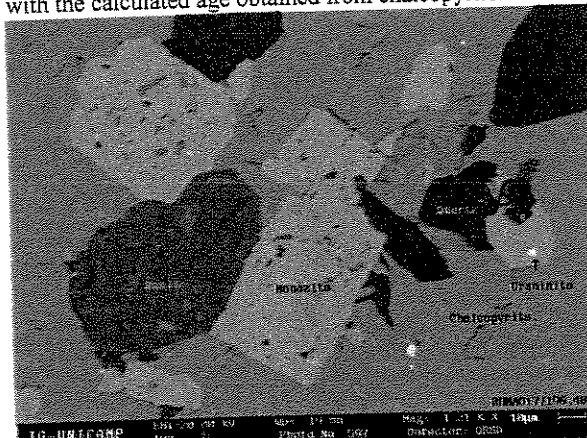


Figure 3 - BSE image of chalcopyrite vein crosscutting sedimentary rocks of the hanging wall. Note the abundance of monazite and uraninite inclusions.

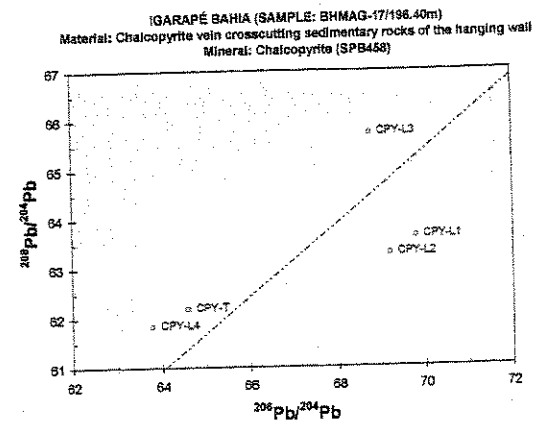


Figure 2 –  $^{208}\text{Pb}/^{204}\text{Pb}$  vs.  $^{206}\text{Pb}/^{204}\text{Pb}$  isotopic diagram for chalcopyrite. Note that data are poorly aligned.

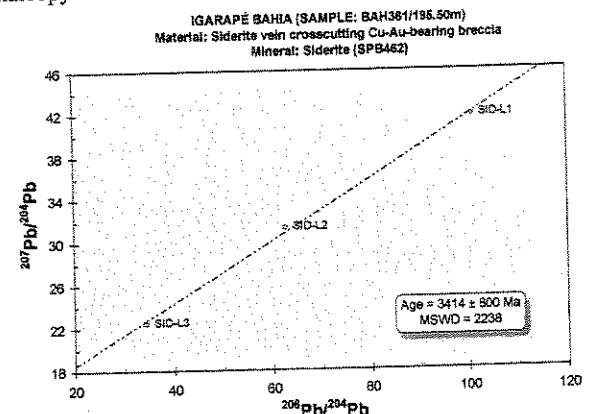


Figure 4 –  $^{207}\text{Pb}/^{204}\text{Pb}$  vs.  $^{206}\text{Pb}/^{204}\text{Pb}$  isochronic diagram with the calculated age obtained from siderite.

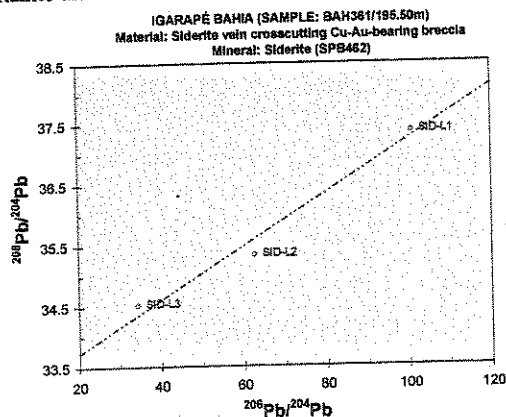


Figure 5 –  $^{208}\text{Pb}/^{204}\text{Pb}$  vs.  $^{206}\text{Pb}/^{204}\text{Pb}$  isotopic diagram for siderite showing a relatively good alignment of data.

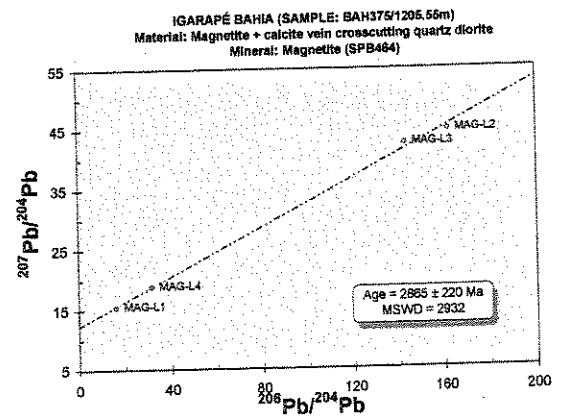


Figure 6 –  $^{207}\text{Pb}/^{204}\text{Pb}$  vs.  $^{206}\text{Pb}/^{204}\text{Pb}$  isochronic diagram with the calculated age obtained from magnetite.

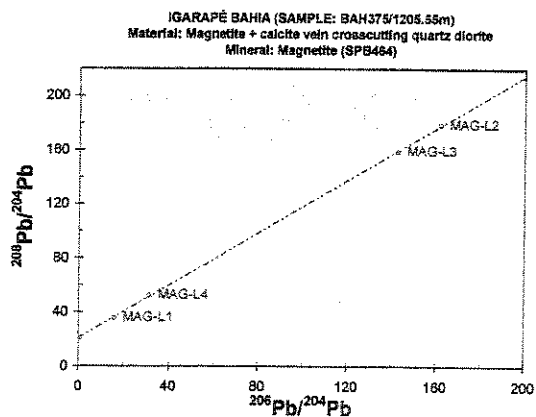


Figure 7 -  $^{208}\text{Pb}/^{204}\text{Pb}$  vs.  $^{206}\text{Pb}/^{204}\text{Pb}$  isotopic diagram for magnetite showing relatively good alignment of data.

**Table 4 - Results from Pb-Pb analyses (held at USP) on siderite, chalcopyrite and magnetite from Igarapé Bahia**

Sample	Sample Description	Mineral	Leaching	Lab. Code <sup>1</sup>	$^{206}\text{Pb}/^{204}\text{Pb}$ (error)	$^{207}\text{Pb}/^{204}\text{Pb}$ (error)	$^{208}\text{Pb}/^{204}\text{Pb}$ (error)
BAH361/195.50m	Siderite vein crosscutting the Cu-Au ore.	Siderite	0.5 ml HBr 0.7N	SPB465-L1	$101.247 \pm 0.268$	$41.838 \pm 0.259$	$37.388 \pm 0.267$
			3.0 ml HBr 0.7N	SPB465-L2	$63.035 \pm 0.116$	$31.436 \pm 0.115$	$35.359 \pm 0.116$
			1.0 ml HBr 0.7 N	SPB465-L3	$34.738 \pm 0.062$	$22.547 \pm 0.062$	$34.542 \pm 0.064$
BH MAG-17/196.40m	Chalcopyrite vein crosscutting sedimentary rocks of the hanging wall.	Chalcopyrite	Aqua Regia 50%	SPB458-T	$64.620 \pm 0.121$	$26.509 \pm 0.125$	$62.214 \pm 0.119$
			HBr + HCl	SPB458-L1	$69.832 \pm 0.014$	$27.298 \pm 0.015$	$63.656 \pm 0.015$
			HBr 1N	SPB458-L2	$69.239 \pm 0.071$	$27.174 \pm 0.026$	$63.316 \pm 0.026$
			HCl 6 N	SPB458-L3	$68.795 \pm 0.040$	$27.111 \pm 0.041$	$65.760 \pm 0.041$
			4 ml Aqua Regia	SPB458-L4	$63.823 \pm 0.061$	$26.402 \pm 0.055$	$61.865 \pm 0.060$
BAH375/1205.55m	Magnetite + calcite vein crosscutting a quartz diorite intrusion.	Magnetite	HBr + HCl	SPB464R-L1	$16.814 \pm 0.006$	$15.624 \pm 0.006$	$36.514 \pm 0.007$
			HCl 1N	SPB464-L2	$162.666 \pm 0.290$	$44.846 \pm 0.305$	$179.349 \pm 0.304$
			HCl 3N	SPB464-L3	$143.639 \pm 1.506$	$42.630 \pm 1.499$	$159.822 \pm 1.506$
			HCl 6N	SPB464R-L4	$32.299 \pm 0.013$	$18.990 \pm 0.012$	$53.055 \pm 0.013$

1 – The extensions to the laboratory codes T, L1, L2, L3 e L4 indicates respectively: bulk sample, 1<sup>st</sup> solute, 2<sup>nd</sup> solute... successively.



## **ANEXO 8**

The Serra Leste sediment-hosted Au-(Pd-Pt) mineralization, Carajás Province



# THE SERRA LESTE SEDIMENT-HOSTED AU-(PD-PT) MINERALIZATION, CARAJÁS PROVINCE

FERNANDO HENRIQUE BUCCO TALLARICO<sup>1</sup>, CLÁUDIO RODRIGUES COIMBRA<sup>2</sup>  
AND CARLOS HENRIQUE CRAVO COSTA<sup>2</sup>

**ABSTRACT** The Serra Leste Au-(Pt-Pd) mineralization is hosted by a folded low-grade metasedimentary sequence known as Rio Fresco Formation. The orebodies are located at the hinge zone of a recumbent syncline at the contact between carbonaceous metasiltstone and dolomitic marble. Ore mineralogy includes quartz, kaolinite, goethite, Mn-oxides, muscovite, amorphous carbon together with gold, Pd-Pt-(Hg) minerals and minor Cu-Co-Ni-sulfides. The orebodies are oxidized, and hypogene mineralization is not known beyond the base of supergene alteration. The widespread occurrence of the actinolite-calcite pair and the local association with diopside, indicate a minimum of 550°C for peak metamorphic temperature of the dolomitic marble. This temperature is inconsistent with the low-grade metamorphic assemblage of metasiltstones, thence with regional metamorphism, and is better accommodated in a thermal-aureole hypothesis. Cooling of the aureole triggered the breakdown of actinolite to calcite + quartz, at temperatures of about 400-450°C. Later hydrothermal activity, between 230°C and 360°C, developed chlorite alteration and sulfide precipitation in both dolomitic marble and diorite intrusion(s) that crosscut the metasedimentary sequence. The carbonaceous metasiltstone possibly acted as a chemical barrier, triggering focused deposition of precious metals through a rapid decrease of the oxidation conditions of the hydrothermal fluid. This process was possibly coupled with carbonate dissolution of dolomitic marble that triggered open-space-filling processes, developed an external jasperoid envelope around the orebodies and caused a pH increase.

**Keywords:** Carajás Province, Serra Leste, Serra Pelada, gold, palladium, platinum

**INTRODUCTION** The Itacaiunas Supergroup is an Archean volcano-sedimentary sequence, located in the northern portion of the Carajás Province, on the eastern border of the Archean Amazon Craton (Docegeo 1988, Tassinari and Macambira 1999). The economic significance of this basin derives from the occurrence of a wide variety of ore deposits including iron, manganese as well as a large number of Cu-(Au) mineralizations stratigraphically and tectonically related, that are collectively known as the Carajás Copper-Gold Belt (e.g. Salobo, Pojca, Igarapé Bahia - Docegeo 1988). The Serra Leste Deposit, previously known as Serra Pelada Deposit (Meireles and Silva 1988), is distinct from the above mineralizations and constitutes a unique occurrence of sediment-hosted Au-(Pd-Pt) mineralization within the Carajás Province.

The aim of this paper is to present the diagnostic geological attributes, *i.e.* the descriptive model (Barton 1993) of the Serra Leste Deposit, based on the results of field work, including mapping and drill logging. Petrographic, geochemical and mineralogical investigations via XRD, SEM and EMPA, were also performed.

Mineralogical data are presented in wt%, since they are derived from the integration of XRD and modal analysis. Finally, a conceptual (or genetic) model is suggested and discussed.

**GEOLOGIC AND TECTONIC SETTING** The Serra Leste mineralization is located at the eastern portion of the Carajás Province, 30 km northeast of the town of Curionópolis, Pará State (Fig. 1). The basement assemblage consists of Archean gneissic and migmatitic rocks of the Xingú Complex (*ca.* 2.8 Ga - Machado *et al.* 1991) that does not crop out in the immediate vicinity of the Deposit. The supracrustal sequence comprises a set of Archean metavolcano-sedimentary rocks, encompassing mafic-ultramafic schists and minor felsic rocks, iron formations and chert, named the Rio Novo Sequence (Hirata 1982).

The Rio Novo Sequence is intruded by the differentiated mafic-ultramafic Luanga Complex (2763 ± 6 Ma - Machado *et al.* 1991), which hosts chromite and PGE mineralizations (Suita and Nilson 1988, Diella *et al.* 1995). These rocks are unconformably overlain by

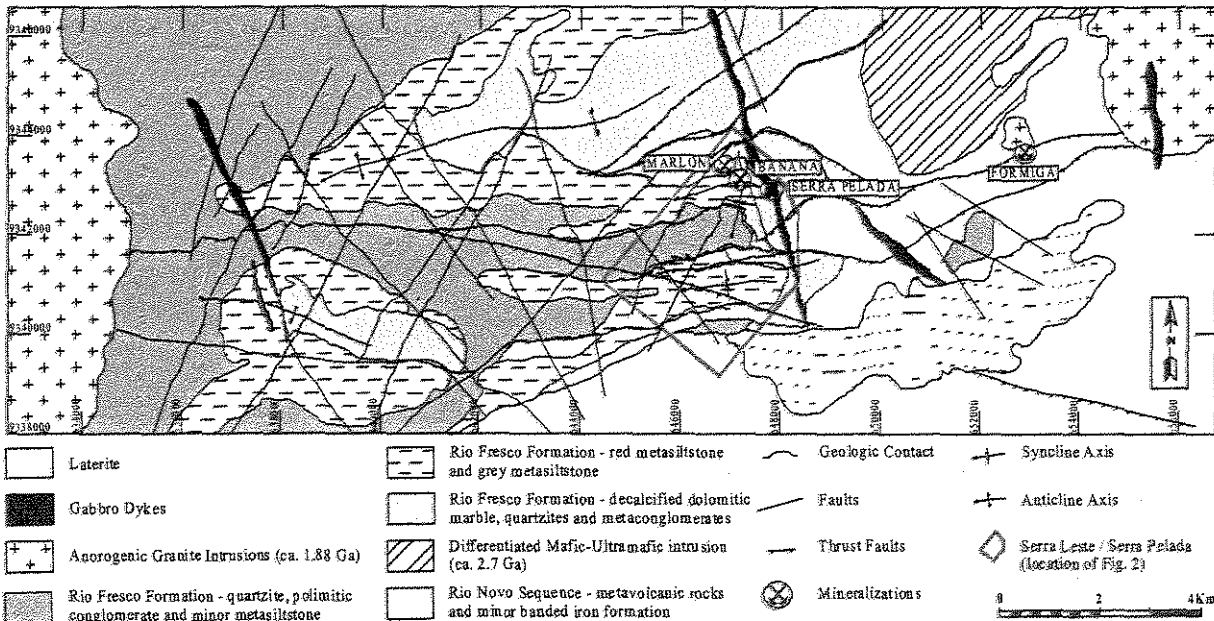
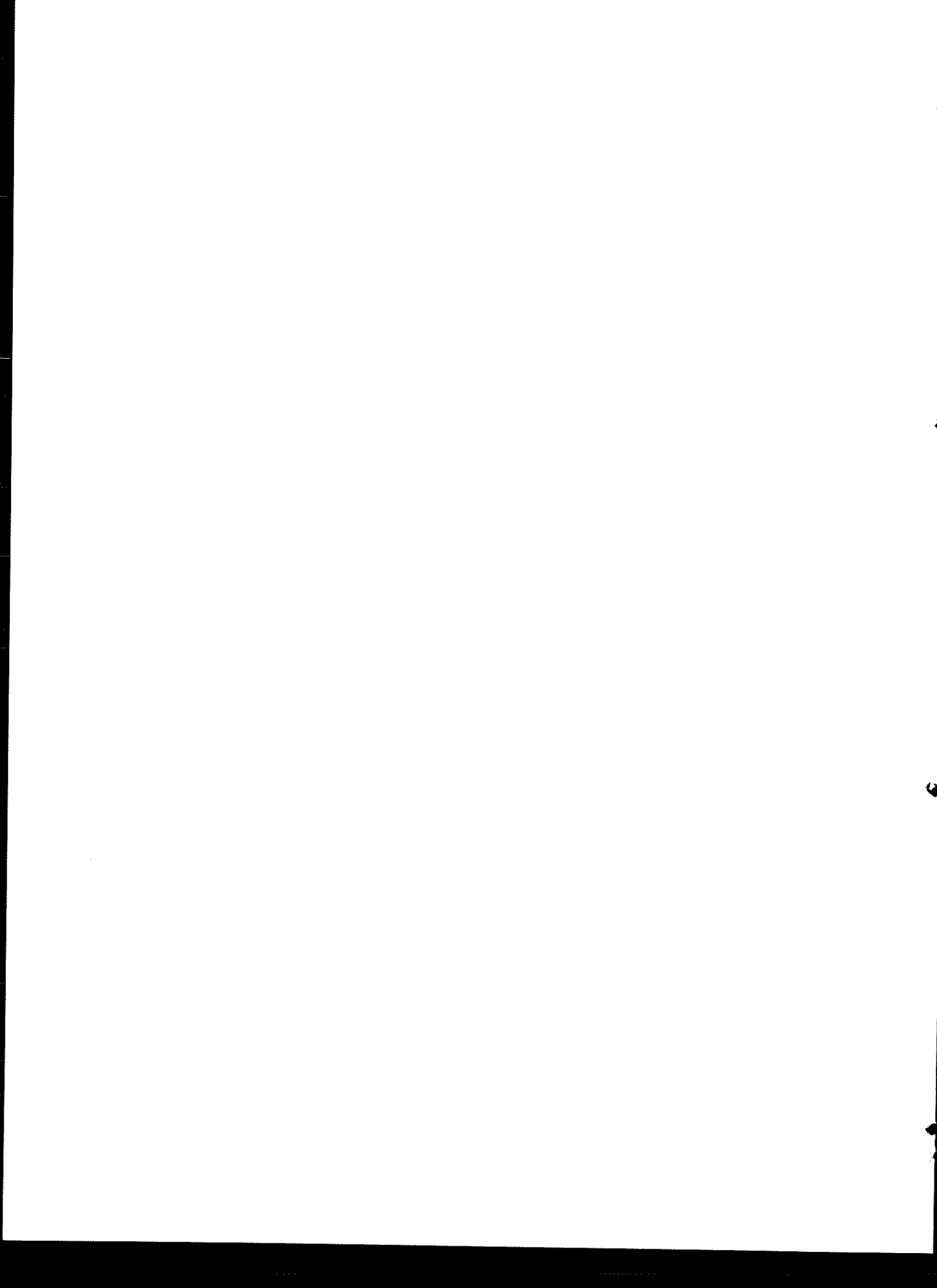


Figure 1-Simplified geological map of the eastern portion of the Carajás Region (modified from Docegeo 1999 unpublished).

1 - Instituto de Geociências, Universidade Estadual de Campinas, Cx. Postal 6152, 13083-970, Campinas, SP. fernando@ige.unicamp.br

2 - Companhia Vale do Rio Doce, Cx. Postal 51, Serra dos Carajás, 68516-000, Parauapebas, PA. claudio@cvrd.com.br, ccraivo@cvrd.com.br



metasedimentary rocks including metaconglomerate, metasandstone, metasiltstone and dolomitic marble of the Rio Fresco Formation (Hirata 1982).

Two distinct episodes of granitoid magmatism occur in the area: one of Proterozoic age, represented by the anorogenic Cigano Granite ( $1883 \pm 2$  Ma - Machado *et al.* 1991), and the other represented by small volume of dioritic and granodioritic plugs and dikes of uncertain age.

The Serra Leste Au-(Pd-Pt) mineralization is located at the eastern segment of the Cinzento strike-slip system. This regional E-W-trending, steeply dipping fault zone shows evidence of several episodes of movement since *ca.* 2.7 Ga (Pinheiro and Holdsworth 1997). The Rio Novo Sequence, the Rio Fresco Formation, as well as the Luanga Complex underwent folding and low-grade metamorphism due to reactivation of this strike-slip system (Suita and Nilson 1988, Pinheiro and Holdsworth 1995).

#### GEOLOGY OF SERRA LESTE

The Serra Leste mineralization is hosted by metasedimentary rocks of the Rio Fresco Formation,

which include the following units: metaconglomerate, metasandstone, dolomitic marble and metasiltstone (Fig. 2).

The structural evolution of Serra Leste includes two episodes of non-coaxial deformation. The earliest developed tight, recumbent, similar folds with axes plunging  $15-25^\circ$  southwestwards, to which a weak axial-planar foliation is related. A set of northeast and northwest subvertical fractures and faults overprint the folded structure and control the emplacement orientation of basic dikes.

**Clastic Metasedimentary Rocks** Metaconglomerate includes iron formation, quartzite and siltstone clasts, ranging from 3 mm up to 5 cm, set in a fine-grained and foliated quartz-sericite matrix. Metasandstones are poorly sorted and contain quartz grains and quartzite fragments, ranging from fine-grained to a locally conglomeratic nature. Manganese-bearing metasandstone beds occur locally within the sequence. Metasiltstone is characterized by very fine beds of quartz and sericite. The following varieties are mapped: carbonaceous metasiltstone, grey metasiltstone and red metasiltstone. The different colors reflect compositional variations related to the

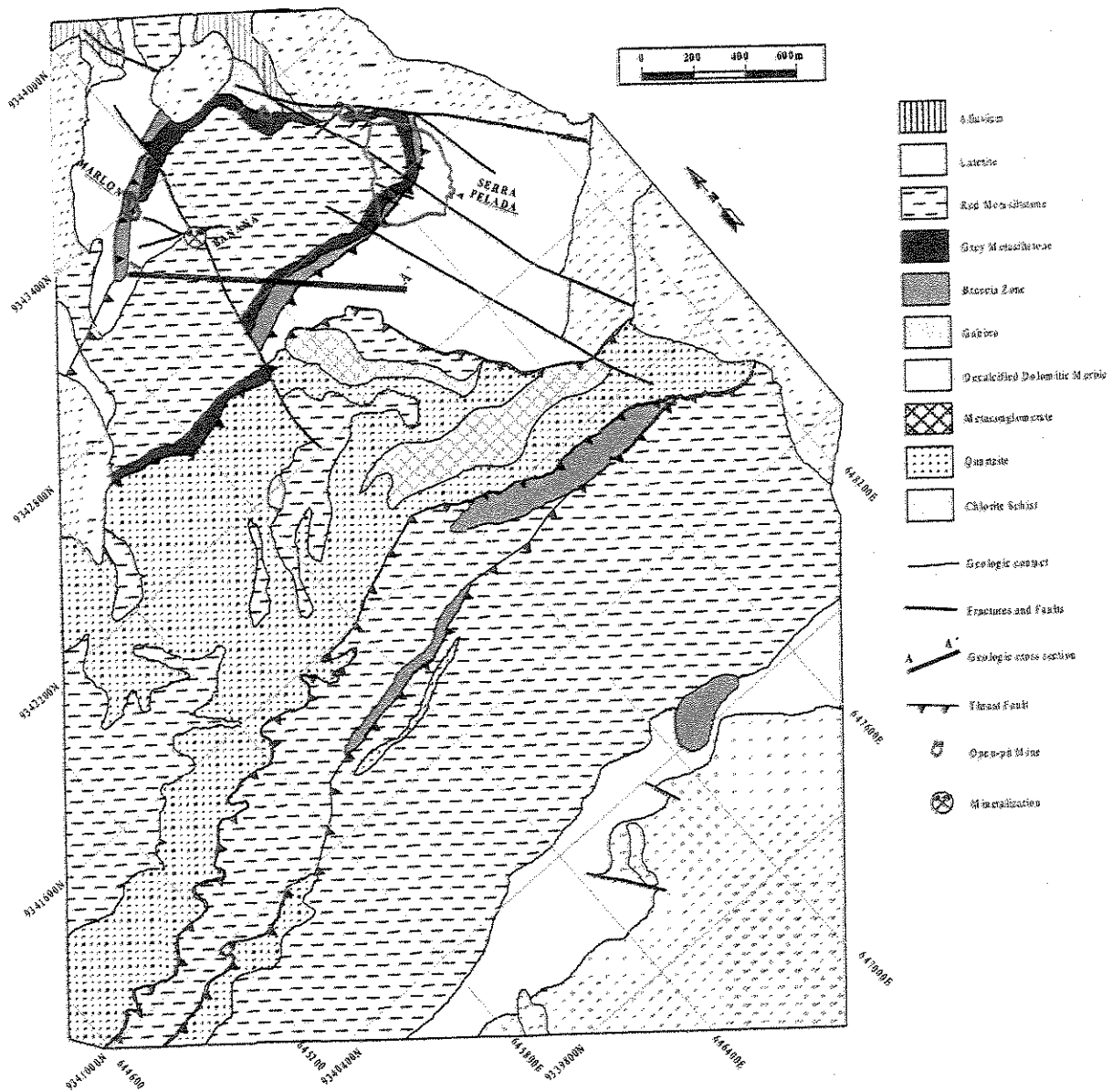


Figure 2-Geological map of the Serra Leste / Serra Pelada Au-(Pd-Pt) mineralization (modified from Docegeo 1995).

depositional environment. The red color reflects Fe-oxide enrichment, while gray and carbonaceous metasiltstones are related to varied proportions of amorphous carbon (2-10 wt%).

Metamorphic reactions of clastic metasediments are restricted to sericite formation. Tectonic fabric is defined by the orientation of sericite along the axial plane of folds in metaconglomerates and metasiltstones. Metasandstones exhibit weak recrystallization and, locally, the development of a granoblastic fabric.

In the vicinity of the orebodies, the metasiltstones are either brecciated or contain sets of veins with quartz + chlorite ± calcite ± tourmaline ± pyrite ± chalcopyrite which crosscut the foliation. These vein zones can evolve to breccias where angular metasiltstone fragments are welded by a hydrothermal matrix with same composition of the veins. Euhedral, poikiloblastic spessartine crystals are transgressive to foliation denoting post-tectonic thermal activity.

**Dolomitic Marble** Dolomitic marble includes rounded quartz grains (1-30 wt%), and rare iron formation and quartzite fragments in a matrix of granoblastic dolomite (20-85 wt%) and minor calcite (1-15 wt%), with variable amounts of actinolite (5-50 wt%), chlorite (1-20 wt%), biotite (1-20 wt%), talc (1-10 wt%) and rare diopside. Actinolite-calcite-rich marbles show randomly orientated actinolite crystals that are often altered to a mixture of calcite, talc and chlorite. Talc-chlorite-rich rocks are also enriched in calcite.

Chloritization is the most common and widespread alteration of the dolomitic marble. Actinolite, talc and biotite are altered to chlorite. Chlorite alteration is accompanied by the formation of xenomorphic and poikiloblastic sulfide minerals. Pyrrhotite occurs in equilibrium with pyrite, chalcopyrite and magnetite. Hydrothermal alteration also includes magnetite (up to 20 wt%) and muscovite (up to 25 wt%) enrichment. Magnetite is partially altered to hematite. Accessory hydrothermal minerals include tourmaline, titanite, allanite, epidote, monazite, apatite, molybdenite, galena and thorite.

**Dioritic Intrusion(s)** Several drill holes intercepted dioritic rocks at depths between 300-350 m. These rocks occur on the southwest border of the area and are inferred to underlie the mineralization. Country rock is the dolomitic marble, but neither the morphology nor the number of intrusions involved are yet known. These rocks exhibit a hypidiomorphic texture with andesine (~36 mol% An), actinolite and minor ilmenite. The igneous assemblage is hydrothermally altered to albite, sericite, quartz, chlorite, epidote, rutile, and carbonate minerals. Diorites are crosscut by a set of veins containing quartz, epidote, chlorite, sericite and sulfide minerals (pyrite, chalcopyrite and bornite).

**Supergene Alteration** At Serra Leste, weathering was responsible for the oxidation of clastic metasedimentary rocks and the leaching of dolomitic marble. The base of the oxidation profile, located at a depth of 300 m, is marked by a knife-edge limit between unaltered dolomitic marble and a loose sandy material, with the impregnation of iron and manganese oxide and hydroxide. Volume reduction, caused by decalcification of the dolomitic marble, developed collapse breccia generally enriched in supergenetic Mn-oxides. All orebodies at Serra Leste are intensely oxidized, and primary economic mineralization is yet unknown beyond the base of the oxidation profile.

**THE Au-(Pd-Pt) MINERALIZATION** The Serra Leste Au-(Pd-Pt) mineralization is located in the hinge zone of a recumbent syncline (Fig. 3). Dolomitic marble occurs at the base and is conformably overlain by metasiltstones. The morphology of the orebodies broadly follows the contact between dolomitic marble and the carbonaceous metasiltstone that seem to have controlled fluid discharge. The orebodies are surrounded by a silicification zone believed to be originated by the replacement of the dolomitic marble. The result is a 5- to 50-m-thick jasperoid composed of fine-grained quartz in association with traces of sericite, tourmaline, kaolinite, chlorite, hematite, chalcopyrite, and carbonate minerals.

The Au-(Pd-Pt) mineralization is hosted by fine-grained carbonaceous rocks mainly exhibiting isotropic fabric. Brecciated varieties with carbonaceous metasiltstone and minor silicified fragments are also common. The mineralogy is dominated by amorphous carbon (1-10 wt%), quartz (10-60 wt%), sericite (1-30 wt%), kaolinite (1-20 wt%), hematite (1-40 wt%), goethite (1-15 wt%) and Mn-oxides (1-15 wt%), with traces of tourmaline, carbonate

minerals, chlorite and magnetite.

Owing to the intense supergene oxidation, primary sulfide minerals are rare and are only recognized by SEM investigation. The dominant sulfide minerals are pyrite, chalcopyrite, arsenopyrite, covellite, bornite and galena. Ni-sulfides (millerite and pentlandite) and Ni-Co-(Cu)-sulfides (carrolite and siegenite) are responsible for an anomalous geochemical signature of the ore (Co up to 2000 ppm, Ni up to 1000 ppm and Cu up to 4000 ppm).

Palladium mineralization is related either to Au-Ag-Pd alloys (Au ~ 94 wt%; Ag ~ 3 wt%; Pd ~ 3 wt%) or to Pd-Hg-minerals (atheneite and potarite). Platinum minerals are rare and isoferroplatinum is the only identified phase. Gold mineralization is associated with alloys and native gold particles ranging from 4-60 mm in diameter. Supergene alteration played a decisive role in the gold mineralization. Oxidation increased gold fineness and grade, developing giant gold nuggets (up to 62 kg) most of which was recovered during the *garimpo* activity. Gold particles are 45% associated to gangue (mainly quartz and kaolinite), 44% to goethite and hematite, 8% to manganese oxides and 3% to carbonaceous material.

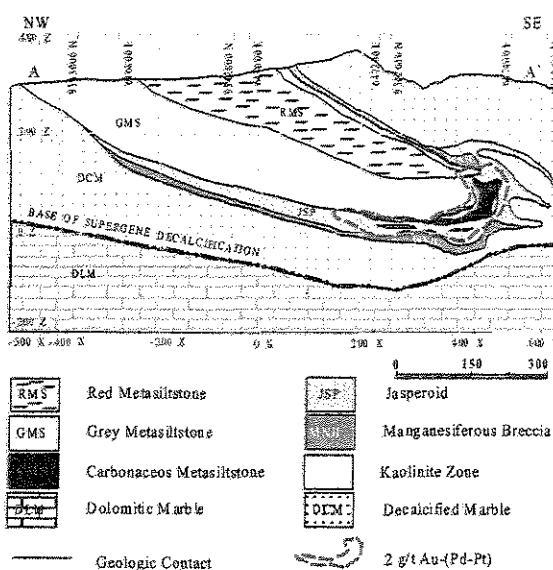


Figure 3-Geological cross section A-A' through the Serra Leste / Serra Pelada Au-(Pd-Pt) mineralization (see Fig. 2 for location).

## CONTACT METAMORPHISM AND HYDROTHERMAL ALTERATION

Prograde metamorphism of the dolomitic marble is determined by the reaction dolomite + quartz + H<sub>2</sub>O = actinolite + calcite + CO<sub>2</sub>. The equilibrium tremolite-calcite is stable below ~550°C for XCO<sub>2</sub> > 0.05, above which minerals react to form diopside (Tracy and Frost 1991). The widespread occurrence of the pair actinolite-calcite and the local association of diopside, indicate a minimum of 550°C for the peak metamorphic temperature. At equivalent temperatures, biotite, aluminum silicates and staurolite or cordierite would be expected in metasiltstones. However, the metasiltstones exhibit a very-low grade metamorphic assemblage and the rare garnet neoblasts are clearly post-tectonic and related to late hydrothermal activity. This thermal gradient is not consistent with the regional metamorphism, being better accounted for by a thermal-aureole hypothesis. Additional evidences for contact metamorphism include the presence of hydrothermally altered dioritic intrusion(s) and the mineralogical similarity of the dolomitic marble with other amphibole-rich magnetite skarns (Einaudi *et al.* 1981, Vidal *et al.* 1990).

Cooling of the aureole triggered the breakdown of actinolite in accordance with the reaction: tremolite (actinolite) + CO<sub>2</sub> + H<sub>2</sub>O = talc + calcite + quartz, at a temperature range of about 400-450°C (Tracy and Frost 1991). Later hydrothermal activity developed chlorite

alteration in association to sulfide precipitation in both dolomitic marble and diorite intrusion(s). Chlorite thermometry (Cathelineau 1988) indicates a thermal range between 230°C and 360°C. The pyrrhotite-pyrite-magnetite association, in the presence of chalcopyrite, denotes high  $f_{O_2}$  ( $\sim 10^{-30}$  to  $10^{-31}$ ) and moderate to high  $a_{SS}$  ( $\sim 10^{-1}$  to  $10^{-2}$ ) at 300°C (Mikucki and Ridley 1993). Late-stage evolution of the hydrothermal system developed hematite and minor bornite, indicating higher oxygen fugacity ( $>10^{-27}$ ) and lower sulfur activity ( $<10^{-3}$ ). These parameters are consistent with Au and Cu mobilization via Cl-complexes (Davidson and Large 1994). Cl-complexes are also efficient in transporting PGE, Hg and Ag in oxidized and acid hydrothermal solutions (Mountain and Wood 1988, Watkinson and Melling 1992).

**SUGGESTED GENETIC MODEL AND DISCUSSION** The Serra Leste Au-(Pd-Pt) mineralization is tentatively related to the hydrothermal alteration associated with the cooling of the diorite intrusion(s). The solubility of Au and PGE as Cl-complexes are of the same order of magnitude and drop rapidly with pH increase or  $f_{O_2}$  decrease (Mountain and Wood 1988). The carbonaceous metasiltstone possibly acted as a chemical barrier, triggering focused deposition of precious metals through a rapid decrease of oxidation conditions of the hydrothermal fluid. This process was possibly coupled with carbonate dissolution of dolomitic marble that triggered open-space-filling processes, developed an external jasperoid envelope around the orebodies and caused a pH increase. This depositional model is analogous to other sediment-hosted gold mineralizations (e.g. Berger and Bagby 1993) according to CVRD (1998) and Sillitoe (1998), although the metal content and mineralogical associations are quite distinct.

The source(s) of precious metals are as yet unknown. One can speculate that Au, Pd and Pt could have been scavenged from mafic-ultramafic rocks of the Rio Novo Sequence and/or from Luanga-type layered mafic-ultramafic intrusions. The dioritic intrusion(s) and the carbonaceous metasiltstone constitute additional potential for Au and PGE sources, respectively.

Except for the constraints derived from mineral equilibria, there is no direct data on the fluid. Thus, its source(s) and exact composition(s) are still to be established. However, the association with thorite and REE minerals, coupled with indirect evidence of a saline, oxidized and possibly acid fluid, suggest an intrusion-related model. The presence of the hydrothermally altered dioritic intrusion(s) and the contact-metamorphic aureole support this hypothesis.

The timing of mineralization is also unknown. The presence of shear zones within the diorite intrusion(s), together with the emplacement and brecciation transgressive with respect to regional foliation indicate that magmatism and hydrothermal activity took place in the latest stages of evolution of the Cinzento strike-slip system.

**Acknowledgments** The authors wish to thank the Companhia Vale do Rio Doce for authorizing the publication of their private data. We are also indebted to all the geologists of Rio Doce Geologia e Mineração S.A. (DOCEGEO) that took part in the Serra Pelada and Serra Leste Projects. Richard Sillitoe deserves a special vote of thanks for his comments that greatly improved our original ideas. We acknowledge the referees of RBG and also all the anonymous reviewers that enhanced our original manuscript. The first author is indebted to FAPESP (Fundação de Amparo à Pesquisa do Estado de São Paulo) for the grants #98/14401-5 and #99/03058-0.

## References

- Barton P.B. 1993. Problems and opportunities for mineral deposit models. In: R.V. Kirkham; W.D. Sinclair; R.I. Thorpe; J.M. Duke (eds) *Mineral Deposit Modeling*. Geological Association of Canada, Special Paper 40, 7-13.
- Berger B.R. & Bagby W.C. 1993. The geology and origin of Carlin-type gold deposits. In: R.P. Foster (ed) *Gold Metallogeny and Exploration*. London, Chapman & Hall, 210-248.
- Cathelineau M. 1988. Cation site occupancy in chlorites and illites as a function of temperature. *Clay Minerals*, 23:471-485.
- CVRD (Cia Vale do Rio Doce). 1998. I Workshop Sobre a Geologia de Serra Leste - Relatório. CVRD (internal report), 5p.
- Davidson G.J. & Large R.R. 1994. Gold metallogeny and the copper-gold association of Australian Proterozoic. *Mineralium Deposita*, 29:208-223.
- Diella V., Ferraro A., Girardi V.A.V. 1995. PGE and PGM in the Luanga mafic-ultramafic intrusion in Serra dos Carajás (Para State, Brazil). *Ore Geology Reviews*, 9:445-453.
- DOCEGEO (Rio Doce Geologia e Mineração S.A.). 1988. Província Mineral de Carajás. Litotestratigrafia e principais depósitos minerais. In: SBG, Congresso Brasileiro de Geologia, 35, Belém, Anexo aos Anais, 165p.
- DOCEGEO (Rio Doce Geologia e Mineração S.A.). 1995. Relatório de Etapa. Alvo Serra Leste, Belém, DOCEGEO (internal report), 150p.
- Einaudi M.T., Meinert L.D., Newberry R.J. 1981. Skarn deposits. *Economic Geology*, 75<sup>th</sup> Anniversary Volume: 317-391.
- Hirata W.K. 1982. Geologia Regional. In: SBG, Simpósio de Geologia da Amazônia, 1, Belém, Anexo aos Anais, 9-20.
- Machado N., Lindenmayer Z., Krogh T.E., Lindenmayer D. 1991. U-Pb geochronology of Archean magmatism and basement reactivation in the Carajás area, Amazon Shield, Brazil. *Precambrian Research*, 49:329-354.
- Meireles E.M. & Silva A.R.B. 1988. Depósito de ouro de Serra Pelada, Marabá, Pará. In: C. Schobbenhaus; C.E.S. Coelho (eds) *Principais Depósitos Minerais do Brasil, volume 3*. Brasília, DNPM/CVRD, 547-557.
- Mikucki E.J. & Ridley J.R. 1993. The hydrothermal fluids of Archean lode-gold deposits at different metamorphic grades: compositional constraints from ore and wallrock alteration assemblages. *Mineralium Deposita*, 28:469-481.
- Mountain B.W. & Wood S.A. 1988. Solubility and transport of platinum-group elements in hydrothermal solutions: thermodynamic and physical chemical constraints. In: H.M. Prichard; P.J. Potts; J.F.W. Bowles; S.J. Cribb (eds) *Geo-platinum 87*. London, Elsevier, 57-82.
- Pinheiro R.V.L. & Holdsworth R.E. 1995. Significado tectônico da clivagem transversa (transecting cleavage) em dobras na mina de Serra Pelada, Pará. *Boletim do Museu Paraense Emílio Goeldi, Série Ciências da Terra*, 7:289-308.
- Pinheiro R.V.L. & Holdsworth R.E. 1997. Reactivation of Archean strike-slip fault systems, Amazon region, Brazil. *Journal of the Geological Society*, 154:99-103.
- Sillitoe R.H. 1998. Geological model and exploration potential, Serra Leste Gold Deposit, Carajás Region, Brazil. CVRD (internal report), 15p.
- Suita M.T.F. & Nilson, A.A. 1988. Geologia do Complexo Mafico-Ultramafico Luanga (Província de Carajás, Pará) e das unidades encaixantes. In: SBG, Congresso Brasileiro de Geologia, 35, Belém, Anais, 6:2813-2823.
- Tassinari C.C.G. & Macambira M.J.B. 1999. Geochronological provinces of the Amazon Craton. *Episodes*, 22:174-182.
- Tracy R.J. & Frost B.R. 1991. Phase equilibria and thermobarometry of calcareous, ultramafic and mafic rocks, and iron formations. In: D.M. Kerrick (ed) *Contact Metamorphism*. Min. Soc. America, Reviews in Mineralogy, Volume 26, 207-290.
- Vidal C.E., Espinoza J.I., Sidder G.B., Mukasa S.B. 1990. Amphibolitic Cu-Fe skarn deposits in the Central Coast of Peru. *Economic Geology*, 85:1447-1461.
- Watkinson D.H. & Melling D.R. 1992. Hydrothermal origin of platinum-group mineralization in low-temperature copper sulfide-rich assemblages, Salt Chuck Intrusion, Alaska. *Economic Geology*, 87: 175-184.

Contribution IGC-075  
Received February 2, 2000  
Accepted for publication April 30, 2000

